

# **The planktic foraminiferal response to the Latest Danian Event (62.2 Ma)**

Von der Fakultät für Physik und Geowissenschaften,  
Institut für Geophysik und Geologie  
der Universität Leipzig

genehmigte

**D I S S E R T A T I O N**

zur Erlangung des akademischen Grades  
doctor rerum naturalium  
(Dr. rer. nat.)

vorgelegt von

Dipl. Geol. Sofie Luise Christiane Jehle,  
geboren am 27.07.1985 in VS-Villingen

Gutachter: PD Dr. A. Bornemann (BGR Hannover)

Prof. Dr. O. Friedrich (Universität Hannover)

Tag der Verleihung: 08.Juli 2019

“[...] plankton can do more than grow, sink or be consumed.”

Cullen, J.J., 1982. The Deep Chlorophyll Maximum - Comparing Vertical Profiles of Chlorophyll-A. Canadian Journal of Fisheries and Aquatic Sciences. 39 (5), 791-803. 10.1139/F82-108

## Bibliographische Beschreibung

Jehle, Sofie

The planktic foraminiferal response to the Latest Danian Event (62.2 Ma)

Universität Leipzig, Dissertation

182 Seiten, 298 Literaturangaben, 30 Abbildungen, 5 Tabellen im Text, 5 Anlagen

# Abstract

The Paleocene and early Eocene (~66–40 Ma) is characterised by a number of transient warming events, also named hyperthermals. A more recent candidate for a hyperthermal of Paleocene age is the Latest Danian Event (LDE, ~62.2 Ma). So far, the LDE was only poorly explored in few deep-sea records and Tethyan shelf settings. Planktic data characterizing the surface ocean were almost completely missing. In this thesis, it was studied whether the LDE satisfies the requirements for a hyperthermal and the impact on the planktic foraminifera fauna. Samples from three late Danian deep-sea cores (ODP Sites 1210 and 1262, IODP Site U1407) and one Tethyan shelf section (Qreiya 3, Egypt) were investigated in rather high resolution, which, for the first time, allowed to unravel the impact of the LDE, the evolution of the ocean structure and planktic foraminiferal species abundances on an almost global scale.  $\delta^{18}\text{O}$  paleothermometry revealed a temperature rise of 2–4°C affecting the entire water column in all three depth habitats (sea floor, subsurface and surface ocean) and a contemporary negative carbon isotope excursion of 0.6–0.9 ‰ indicates carbon cycle perturbations. Changes in the planktic foraminiferal assemblages indicate a global biotic response to the LDE.

# Referat

Das Paläozän und frühe Eozän (~66-40 Ma) sind durch mehrere kurzzeitigen (~200 kyr) Erwärmungsereignissen charakterisiert, auch als Hyperthermal-Ereignisse bekannt. Ein Kandidat für ein paläozänzeitliches Hyperthermal ist das Ober-Danium-Ereignis (Latest Danian Event, LDE, ~62,2 Ma), welches vor Beginn der vorliegenden Arbeit nur untergeordnet in Tiefsee-Sedimenten und Schelfablagerungen der Tethys untersucht wurde. Planktondaten die Hinweise auf Änderungen im Oberflächenwasser der Ozeane geben könnten fehlten nahezu vollständig. Im Rahmen dieser Dissertation wird untersucht, ob das LDE ein globales hyperthermales Ereignis darstellt und wie die planktische Foraminiferenfauna durch dieses Ereignis beeinflusst wurden. Drei Tiefseebohrkerne des Ober-Daniums (ODP Sites 1210 and 1262, IODP Site U1407) und einem Aufschluss vom tethyalen Schelf (Qreiya 3, Ägypten) wurden relativ hochauflösend untersucht. Es konnte zum ersten Mal auf globalem Niveau Erkenntnisse zu den Auswirkungen des LDEs, der Entwicklung der Ozeane und der Artenvergesellschaftung planktischer Foraminiferen gewonnen werden.  $\delta^{18}\text{O}$  Paläothermometrie zeigt eine Temperatur-Erhöhung von 2–4°C in allen untersuchten Wassertiefen der Ozeane zeitgleich zu einer negative Kohlestoff-Anomalie von 0.6–0.9 ‰, welches auf eine Störung des Kohlenstoffkreislaufs hinweist. Veränderungen in den Vergesellschaftungen der planktischen Foraminiferen zeigen eine globale Reaktion auf das LDE an.

# Erklärung

Hiermit bestätige ich, dass ich die vorliegende Arbeit selbständig verfasst und keine anderen als die angegebenen Hilfsmittel benutzt habe. Die Stellen der Arbeit, die dem Wortlaut oder dem Sinn nach anderen Werken (dazu zählen auch Internetquellen) entnommen sind, wurden unter Angabe der Quelle kenntlich gemacht.

Sämtliche Personen, welche mich bei Auswahl und Auswertung des Materials unterstützt haben, werden im Kapitel „Author information“ genannt. Ich versichere, dass außer den dort genannten Personen keine weiteren bei der geistigen Herstellung der vorliegenden Arbeit beteiligt waren und dass insbesondere nicht die Hilfe eines Promotionsberaters in Anspruch genommen wurde sowie dass keine weiteren Personen in meinem Auftrag weder mittelbar noch unmittelbar geldwerte Leistungen für Arbeiten erhalten haben, die im Zusammenhang mit dem Inhalt der vorliegenden Dissertation stehen.

Die vorliegende Arbeit wurde weder im Inland noch im Ausland in gleicher oder ähnlicher Form einer Prüfungsbehörde zum Zwecke einer Promotion oder eines ähnlichen Prüfungsverfahrens vorgelegt bzw. auch nicht in ihrer Gesamtheit veröffentlicht.

Hiermit erkenne ich die Promotionsordnung der Universität Leipzig, Fakultät für Physik und Geowissenschaften vom 24.08.2016 an.

Leipzig, den 01.02.2019

Sofie Jehle

# Acknowledgements

First, my great acknowledgements go to PD Dr. André Bornemann (Bundesanstalt für Geowissenschaften und Rohstoffe, Hannover) who planned and initiated the project and supervised and guided me patiently during my work and my time as a doctorate student. The project was planned together with Prof. Dr. Robert Speijer, University of Leuven who also contributed to fruitful and vivid discussions. I am very happy that they gave me the opportunity to work on this interesting topic. Prof. Dr. Werner Ehrmann (University of Leipzig, Institut für Geophysik und Geologie) has been my co-supervisor and I want to thank him very much for his support.

My work would have been impossible without the funding of the Deutsche Forschungsgemeinschaft (DFG) which paid my outcome, measurements and journeys during the three years. I am very grateful for the support, which made sampling, measuring and travel opportunities to exciting scientific events possible. I especially remember the rather expensive trips to the Urbino Summer School of Paleoclimate (2014, Italy) or the AGU Fall meeting in San Francisco (2015). The gain of knowledge was hopefully worth the money.

Many thanks go to the IODP for providing samples and data. I am grateful that I got access to the XRF core scanning facilities at the marum in Bremen and in particular to the patient introduction to the facility by Vera Luckies.

Many thanks go to the members of my examination committee (Prof. Dr. T. Brachert, Prof. Dr. W. Ehrmann, PD Dr. A. Bornemann) as well as the evaluators of this thesis (PD Dr. A. Bornemann, Prof. Dr. O. Friedrich).

I want to thank Prof. Dr. Maria Rose Petrizzo (University of Milano) for teaching me in planktic foraminifera taxonomy and gave me the opportunity for productive input and exchange to the beginning of my work. I happily remember the time at Università degli Studi di Milano, Dipartimento di Scienze della Terra “Ardito Desio”. Thank you for having me!

Sylvia Haeßner and Madlen Wild (University of Leipzig) gave me very kind help and advice on technical and bureaucratic issues. Dr. Stefan Krüger (University of Leipzig) proceeded mass spectrometry and explained me the results with great endurance. Lisa Petter, Michael Bernd, Claire Koch, Steven Nebel and Friederike Lägel helped me with my sample preparation. Many thanks go to Dr. Yvonne Milker for the course and explanations in statistics. Jörg Lenzner, Institute for Experimental Physic II, University of Leipzig, took some of the SEM pictures of the planktic foraminifera. Thank you, Mr. Lenzner! Some of the SEM pictures were taken at the Bundesanstalt für Geowissenschaften und Rohstoffe in Hannover, which is where I send my gratitude to as well.

My time as a doctorate student has had a faunal turnover like my sediment record in the composition of people in the institute. I am more than happy I spent my time with you: Sima Mousavi, Aron Böcker, Elshan Abdullayev, Martin Seidel, Sarah Beuscher, Yvonne Milker and Friederike Lägel.

I have had fruitful discussions and about topics of this thesis with friends outside of Leipzig: Thank you, Ulrike Baranowski, Patrick Zell, Philipp Munz and Tobias Hipp.

At the end of this period, I look back to many friends who brought me through tough times and didn't run away from work-related monologues. Also, they thankfully took me away to shorter and longer holidays, and I can't be happier that they didn't give up. Alena, Ecki, Jana, Anders, Carolin and Guy, Philipp and so many more friends from the climbing community. Anette, Ecki, Caro and Guy for the refreshing holidays in between. Thanks to my strong, lovely buddy Elpu, who carried and hosted me outdoors a lot. Your roaring sound will never leave my ears and whenever I smell a wet dog, tears rise into my eyes. I wish your servo-steering and your torboblower would not have been that expensive.

My greatest gratitude goes to my family for their loving emotional support and the parcels with cakes.

# Table of Contents

<b>BIBLIOGRAPHISCHE BESCHREIBUNG</b>	<b>I</b>
<b>ABSTRACT</b>	<b>II</b>
<b>REFERAT</b>	<b>II</b>
<b>ERKLÄRUNG</b>	<b>III</b>
<b>ACKNOWLEDGEMENTS</b>	<b>IV</b>
<b>TABLE OF CONTENTS</b>	<b>VI</b>
<b>LIST OF FIGURES</b>	<b>X</b>
<b>LIST OF TABLES</b>	<b>X</b>
<b>LIST OF ABBREVIATIONS AND ACRONYMS</b>	<b>XI</b>
<b>SCHRIFTENVERZEICHNIS / AUTHOR INFORMATION</b>	<b>XII</b>
<b>ZUSAMMENFASSUNG</b>	<b>XIV</b>
<b>SUMMARY</b>	<b>XVI</b>
<b>THESIS OUTLINE</b>	<b>XVIII</b>
<b>CHAPTER I: INTRODUCTION</b>	<b>1</b>
<b>1 Cenozoic climate</b>	<b>1</b>
1.1 Past climate variations as hints for understanding the recent climate change	1
1.2 Cenozoic trends: climate, fauna and continental drifts during Late Cretaceous and Early Paleocene	5
1.3 Transient warming events in the Paleogene	7
1.4 Paleocene-Eocene Thermal Maximum and consecutive Eocene events	7
1.5 Latest Danian Event	8
<b>2 Planktic foraminiferal ecology</b>	<b>11</b>
2.1 Historical notes on foraminiferal and paleoceanographic research	11
2.2 Cenozoic evolution of planktic foraminifera	11
2.3 Ecology and habitat of planktic foraminifera	13
2.4 Reproduction of planktic foraminifera	14
2.5 Photosymbiosis and stable isotope signal	14
<b>3 Paleoclimatic and paleoenvironmental proxies derived from planktic foraminifera</b>	<b>16</b>
3.1 Planktic foraminifera as paleoceanographic archive	16
3.2 Geochemical proxies	17
3.3 Planktic foraminifera assemblage proxies	19

<b>4</b>	<b>Origin of the studied sediment material and methods</b>	<b>19</b>
4.1	Method overview	19
4.2	Studied sites	20
4.2.1	Shatsky Rise	20
4.2.2	Walvis Ridge	21
4.2.3	Newfoundland	21
4.2.4	Qreiya	21
<b>5</b>	<b>Motivation and research questions</b>	<b>22</b>
 <b>CHAPTER II: THE IMPACT OF THE LATEST DANIAN EVENT ON PLANKTIC FORAMINIFERAL FAUNAS AT ODP SITE 1210 (SHATSKY RISE, PACIFIC OCEAN)</b>		<b>23</b>
<b>Abstract</b>		<b>23</b>
<b>1</b>	<b>Introduction</b>	<b>24</b>
1.1	Geological setting	27
1.2	Lithology	28
1.3	Stratigraphy	29
<b>2</b>	<b>Methods</b>	<b>30</b>
<b>3</b>	<b>Results</b>	<b>32</b>
3.1	Carbonate content and dissolution sensitive parameters	32
3.2	Foraminiferal stable isotopes ( $\delta^{13}\text{C}$ , $\delta^{18}\text{O}$ )	32
3.2.1	High resolution records of planktic and benthic foraminifera	32
3.2.2	Isotope results of selected planktic foraminifera species	33
3.3	Planktic foraminiferal assemblages	34
<b>4</b>	<b>Discussion</b>	<b>38</b>
4.1	Biostratigraphic implications	38
4.2	Carbonate preservation	38
4.3	Foraminiferal stable isotope data	40
4.4	Habitat implications of planktic foraminifera	41
4.5	Planktic foraminiferal assemblages	42
4.6	Paleoceanographic implications	44
<b>5</b>	<b>Conclusions</b>	<b>46</b>
<b>Acknowledgements</b>		<b>47</b>
 <b>CHAPTER III: PALEOCEANOGRAPHIC CHANGES ACROSS THE LATEST DANIAN EVENT IN THE SOUTH ATLANTIC OCEAN AND PLANKTIC FORAMINIFERAL RESPONSE</b>		<b>49</b>
<b>Abstract</b>		<b>49</b>
<b>1</b>	<b>Introduction</b>	<b>49</b>
<b>2</b>	<b>Material and Methods</b>	<b>51</b>
2.1	Geological setting and deposition	51
2.2	Stratigraphy	51
2.3	Methods	51
<b>3</b>	<b>Results</b>	<b>53</b>
3.1	Carbonate content and dissolution indicators	53
3.2	Foraminiferal stable isotopes ( $\delta^{13}\text{C}$ , $\delta^{18}\text{O}$ )	54
3.3	Planktic foraminiferal assemblages	55
3.4	Discussion: Carbonate dissolution and preservation of foraminiferal calcite	56



3.4.1	Carbonate preservation	56
3.4.2	Foraminiferal preservation	57
3.5	Stable isotope patterns during the LDE at Walvis Ridge	58
3.5.1	$\delta^{13}\text{C}$ response to the LDE	58
3.5.2	$\delta^{18}\text{O}$ response to the LDE	59
3.5.3	Implications on the stable isotope patterns for the LDE	59
3.6	Planktic foraminifera faunal changes	60
3.7	Comparison to Pacific ODP Site 1210	62
3.7.1	Paleogeography of ODP Sites 1210 and 1262	62
3.7.2	Geochemical data and preservation	63
3.7.3	Planktic foraminiferal faunal response to the LDE	64
<b>4</b>	<b>Conclusions</b>	<b>66</b>
	<b>Acknowledgments</b>	<b>67</b>
	<b>CHAPTER IV: MID-PALEOCENE PLANKTIC FORAMINIFERA BIOSTRATIGRAPHY – LESSONS FROM THE APPEARANCE OF <i>IGORINA ALBEARI</i> AND THE LATEST DANIAN EVENT</b>	<b>69</b>
	<b>Abstract</b>	<b>69</b>
<b>1</b>	<b>Introduction</b>	<b>69</b>
1.1	Mid-Paleocene magneto- and biostratigraphy	71
1.2	Taxonomic concepts	71
1.2.1	<i>Praemurica uncinata</i> (Bolli 1957) and <i>P. inconstans</i> (Subbotina 1953)	72
1.2.2	<i>Igorina</i> and <i>Igorina albeari</i> (Cushman and Bermudez 1949)	72
1.2.3	<i>Globanomalina pseudomenardii</i> (Bolli 1957)	73
<b>2</b>	<b>Material and Methods</b>	<b>74</b>
2.1	Studied sites and sections	74
2.1.1	ODP Site 1210 (Shatsky Rise, Pacific)	74
2.1.2	ODP Site 1262 (Walvis Ridge, South Atlantic)	74
2.1.3	IODP Site U1407 (Southeast Newfoundland Ridge, North Atlantic)	74
2.1.4	Gebel Qreiya 3 (Egypt)	75
2.2	Methods	75
<b>3</b>	<b>Chemo- and biostratigraphic results</b>	<b>75</b>
<b>4</b>	<b>Implications on stratigraphic definitions</b>	<b>76</b>
4.1	The LDE and the planktic foraminifera Subzone P3a/P3b	76
4.2	Planktic foraminifera Zone P4	81
<b>5</b>	<b>Conclusions and implications for the standard Paleocene planktic foraminifera zonation</b>	<b>81</b>
	<b>CHAPTER V: SYNTHESIS</b>	<b>85</b>
	<b>Characteristics of the Latest Danian Event</b>	<b>85</b>
<b>1</b>	<b>Research focus</b>	<b>85</b>
<b>2</b>	<b>The LDE negative carbon isotope excursion and temperature changes</b>	<b>85</b>
<b>3</b>	<b>Planktic foraminifera assemblages - a supplementary comparison</b>	<b>88</b>
<b>4</b>	<b>Biostratigraphic implications</b>	<b>90</b>
<b>5</b>	<b>Key results</b>	<b>91</b>

<b>REFERENCES</b>	<b>93</b>
<b>APPENDIX 1: TAXONOMIC NOTES</b>	<b>117</b>
<b>APPENDIX 2: DATA CHAPTER II</b>	<b>129</b>
<b>APPENDIX 3: DATA CHAPTER III</b>	<b>130</b>
<b>APPENDIX 4: DATA CHAPTER IV</b>	<b>131</b>
<b>APPENDIX 5: DATA CHAPTER V</b>	<b>132</b>
<b>CURRICULUM VITAE</b>	<b>I</b>

# List of Figures

Figure 1: Accelerating atmospheric CO <sub>2</sub> concentration 1720-2018	2
Figure 2: Monthly Global Ocean Temperature anomalies	2
Figure 3: Cenozoic (0-65 Ma) climate trends	6
Figure 4: Paleocene $\delta^{18}\text{O}$ and $\delta^{13}\text{C}$ developments	9
Figure 5: Biostratigraphic overview of the Paleogene	10
Figure 6: Model for oxygen/carbon variation in symbiotic and asymbiotic species,	16
Figure 7: Light microscope picture	17
Figure 8: Reconstructed paleo-map and observed sites	20
Figure 9: Stratigraphy, $\delta^{13}\text{C}$ and $\delta^{18}\text{O}$ measurements of benthic and planktic foraminifera on ODP Sites 1209	25
Figure 10: $\delta^{13}\text{C}$ and $\delta^{18}\text{O}$ of benthic (green), planktic subsurface (blue) and surface (red) foraminifera in comparison to XRF measured Fe counts for chemostratigraphic correlation	26
Figure 11: Pacific centered map of the Shatsky Rise	28
Figure 12: Sedimentary and other parameters of Site 1210	29
Figure 13: $\delta^{13}\text{C}$ – $\delta^{18}\text{O}$ plot of foraminiferal isotope measurements	34
Figure 14: Scanning electron microscope images of planktic foraminifera.	36
Figure 15: Species abundance and Fe XRF core scanning data for chemostratigraphic correlation.	37
Figure 16: $\delta^{13}\text{C}$ and $\delta^{18}\text{O}$ gradient and faunal development	43
Figure 17: Non-Metric multidimensional Scaling	44
Figure 18: Stratigraphy, XRF core scanning Fe intensities, stable isotopes and other sedimentary parameters of samples from the LDE at Site 1262	54
Figure 19: Species distribution of planktic foraminifera together with XRF core scanning	56
Figure 20: Non-metric multidimensional scaling	62
Figure 21: The $\delta^{13}\text{C}$ and $\delta^{18}\text{O}$ crossplots indicate the preferred depth habitat of different foraminiferal taxa	64
Figure 22: Comparison of key results from ODP Sites 1210 and 1262	66
Figure 23: Planktic foraminifera and calcareous nannoplankton biostratigraphic zones of the investigated sites	78
Figure 24: Biostratigraphy with quantitative data of marker species	80
Figure 25: Comparison of the planktic foraminifera zonation schemes	81
Figure 26: Scanning electron microscope pictures of <i>Praemurica inconstans</i>	83
Figure 27: Scanning electron microscope pictures of <i>Igorina albeari</i>	84
Figure 28: Scanning electron microscope pictures of <i>Globanomalina cf. pseudomenardii</i>	84
Figure 29: Comparison of the negative CIE (I) and the $\delta^{18}\text{O}$ (II) variations	87
Figure 30: Ternary diagram for site comparison in aspects of assemblage	89

# List of Tables

Table 1: Wall types of Early Paleocene trochospiral planktic foraminifera	12
Table 2: T-test p-values	33
Table 3: Overview planktic foraminiferal P3a/P3b Subzone boundary	79
Table 4: Compendious overview over $\delta^{13}\text{C}$ , $\delta^{18}\text{O}$ and $\Delta\text{T}$ peaks	86
Table 5: Mean percentages per artificial cluster	88

# List of abbreviations and acronyms

BFAR	Benthic foraminiferal accumulation rate (kyr per cm <sup>-2</sup> )
CCD	Calcite compensation depth
CCSF	Core composite depth below sea floor
CF	Coarse fraction
CIE	Carbon Isotope Excursion, here based on $\delta^{13}\text{C}$ measurements
DCM	Deep chlorophyll maximum
DSDP	Deep Sea Drilling Project (1968-1983)
ETM 2	Eocene Thermal Maximum 2 (also H1-event, 53.7 Ma)
ETM 3	Eocene Thermal Maximum 3 (also X-event, ~52 Ma)
FAD/ FcAD/ FrAD	first (common/ rare) appearance datum
GSSP	Global Stratotype Section and Point
IPPC	Intergovernmental Panel of Climate Change
IODP	Integrated Ocean Drilling Program (2003-2013), International Ocean Discovery Program (since 2013)
K-Pg	Cretaceous-Paleogene boundary at ~66 Ma
Ky, kyr	Kilo years, used for duration
LAD/LcAD/ LrAD	Last (common/rare) appearance datum
LDE, LDE1, LDE2	Latest Danian Event, divided into two phases, identified by two distinctly negative CIEs
Ma, Myr	Mega anni (10 <sup>6</sup> years, used for age), Million years (10 <sup>6</sup> years, duration)
mbsf	meters below sea floor
mbsl	meters below sea level
mcd	meters composite depth
NMDS	Non-metric multidimensional scaling
NOAA	National Ocean and Atmospheric Administration
ODP	Ocean Drilling Program (1983-2003)
%P	Percentage planktic foraminifera, relative to the total number of foraminifera
PETM	Paleocene Eocene Thermal Maximum (~56 Ma) a.k.a. ETM 1
PFAR	planktic foraminifera accumulation rate (individuals kyr per cm <sup>-2</sup> )
PFN	planktic foraminifera number (foraminifera/g sediment)
rmcd	revised meters composite depth
SEM	Scanning Electron Microscope
SENR	Southeast Newfoundland Ridge
SST	sea surface temperature
TOC	Total Organic Carbon
%wt	Weight percent

# Schriftenverzeichnis / Author information

## Chapter II (Kapitel II)

### **Publiziert als:**

Jehle S, Bornemann A, Deprez A, Speijer RP (2015): The Impact of the Latest Danian Event on Planktic Foraminiferal Faunas at ODP Site 1210 (Shatsky Rise, Pacific Ocean). PLoSONE10 (11): e0141644.doi:10.1371/journal.pone.0141644

### **Autoren:**

*Sofie Jehle\**, *André Bornemann*<sup>1,2</sup>, *Arne Deprez*<sup>3</sup>, *Robert P. Speijer*<sup>3</sup>

<sup>1</sup> Institut für Geophysik und Geologie, Universität Leipzig, Talstr. 35, 04103 Leipzig, Germany

<sup>2</sup> Bundesanstalt für Geowissenschaften und Rohstoffe, Stilleweg 2, 30655 Hannover, Germany

<sup>3</sup> Department of Earth and Environmental Sciences, KU Leuven, Celestijnenlaan 200E, 3001 Leuven/Heverlee, Belgium.

### **Beiträge der Autoren:**

Entwurf und Gestaltung der Experimente: André Bornemann, Sofie Jehle

Durchführung der Experimente: Sofie Jehle, Arne Deprez

Datenanalyse: Sofie Jehle

Textarbeit: Sofie Jehle, André Bornemann, Arne Deprez, and Robert P. Speijer

Statistische Analysen: Sofie Jehle, André Bornemann

## Chapter III (Kapitel III)

**Dieses Kapitel ist eingereicht und unter Revision zur Veröffentlichung (“under revision for publication”) im Fachmagazin “Palaeogeography, Palaeoclimatology, Palaeoecology” als:**

Paleoceanographic changes across the Latest Danian Event in the South Atlantic and the planktic foraminiferal response

### **Autoren:**

Sofie Jehle<sup>1</sup>, Anna Friederike Lägerl<sup>1</sup>, Arne Deprez<sup>3</sup>, Robert P. Speijer<sup>3</sup>, and André Bornemann<sup>2</sup>

### **Beiträge der Autoren:**

Entwurf und Gestaltung der Experimente: Sofie Jehle, André Bornemann

Durchführung der Experimente: Sofie Jehle, Anna Friederike Lägerl, Arne Deprez

Datenanalyse: Sofie Jehle

Textarbeit: Sofie Jehle, André Bornemann, Robert P. Speijer, Arne Deprez

Statistische Analysen: Sofie Jehle, André Bornemann

# Chapter IV (Kapitel IV)

**Titel:**

Mid-Paleocene planktic foraminifera biostratigraphy – lessons from the appearance of *Igorina albeari* and the Latest Danian Event

**Autoren:** Sofie Jehle, André Bornemann, Anna Friederike Lägél

**Status:** Unveröffentlichtes Manuskript

**Beiträge der Autoren:**

Entwurf und Gestaltung der Experimente: Sofie Jehle, André Bornemann

Durchführung der Experimente: Sofie Jehle, Anna Friederike Lägél, André Bornemann

Datenanalyse: Sofie Jehle

Textarbeit: Sofie Jehle, André Bornemann

Ein großer Teil der vorliegenden Arbeit wurde in enger Kooperation mit der Forschungsgruppe um Prof. Dr. Robert P. Speijer at Department of Earth and Environmental Sciences, KU Leuven, Belgien erarbeitet. Sediment Material von Walvis Ridge ODP Site 1262 was wurde zum Teil im labor bearbeitet durch Dr. Arne Deprez, SENR IODP Site U1407 durch Mr. Rik Van Bael. Die benthischen Foraminiferen *Nuttallides truempyi* und *N. umbonifera* von Shatsky Rise ODP Site 1210 und Walvis Ridge Site 1262 wurden zur geochemnischen Analyse von  $\delta^{13}\text{C}$  und  $\delta^{18}\text{O}$  teilweise gepickt von Dr. Arne Deprez.

Most of the data for this thesis was gained in close cooperation with the research group of Prof. Dr. Robert P. Speijer at Department of Earth and Environmental Sciences, KU Leuven, Belgium. Walvis Ridge ODP Site 1262 sediment material was partly processed by Dr. Arne Deprez, SENR IODP Site U1407 by Mr. Rik Van Bael. Benthic foraminifera *Nuttallides truempyi* and *N. umbonifera* of Shatsky Rise ODP Site 1210 and Walvis Ridge Site 1262 were partly picked for  $\delta^{13}\text{C}$  and  $\delta^{18}\text{O}$  geochemistry by Dr. Arne Deprez.

# Zusammenfassung

Das Paläozän und Eozän (~66-34 Ma) stellen eine besondere Zeit für Veränderungen in der Evolution des globalen Klimas und des marinen Lebens dar. Während der letzten Jahrzehnte konnten verschiedene, einschneidende Klimaereignisse aus dieser Zeitspanne identifiziert werden. Davon wurden einige erst in der letzten Zeit verstärkt erforscht, darunter unter größter Beachtung die Auswirkungen des Paläozän-Eozän Temperatur-Maximum (PETM, ~56 Ma). Ein neuerer und bislang weniger erforschter Kandidat für ein kurzes (~200 kyr) Paläozänes Erwärmungsereignis (Hyperthermal-Ereignis) ist das Ober-Danium-Ereignis (Latest Danian Event, LDE, ~62,2 Ma), welches eine ~2°C Ozeanbodenerwärmung während einer übergeordneten langfristigen Abkühlung aufweist. Darüber hinaus ist das LDE durch eine 0,7–1,6 ‰ negative Kohlenstoff-Isotopen-Anomalie (carbon isotope excursion, CIE) charakterisiert. Diese negative Kohlenstoff-Isotopen-Auslenkung stellt die negativsten Werte für das gesamte Paläozän dar und deutet damit auf eine bedeutsame Phase im globalen Kohlenstoff-Kreislauf hin.

Foraminiferen bieten einen beispiellosen Einblick in paläozeanographische und paläoklimatische Bedingungen und erzeugen möglicherweise die bestbekanntesten geochemischen und biotischen Aufzeichnungen für prä-Pleistozäne Paläozeanographie. Sie werden als besonders gut verwendbare Anzeiger für die hier bedachten Forschungsfragen der Rekonstruktion paläozänen marinen Lebens während eines Hyperthermal-Ereignisses gesehen. Ihre Kalkschalen weisen ein hohes Fossilisationspotential auf und stellen nach der sedimentären Einbettung wertvolle und fundierte Informationen bereit. Foraminiferen leben sowohl im Oberflächenwasser als auch auf oder im Ozeanboden, wo sie unterschiedliche geochemische und biologische Signale aufzeichnen. Globale Klimaereignisse, die im Paläozän einen Einfluss auf marines Leben hatten, wurden häufig über Untersuchungen an Tiefsee-Sedimenten und Foraminiferen-Schalenresten nachgewiesen.

Vor Beginn der vorliegenden Arbeit waren die Tiefsee-Sedimente des späten Daniums kaum erforscht. Hochauflösende biotische Daten, besonders hinsichtlich der Reaktion planktischer Foraminiferen und damit der oberen Wasserschichten, fehlten. Das Ereignis wurde zum ersten Mal anhand von negativen Kohlenstoffisotopen-Anomalien entdeckt und nachgewiesen an verschiedenen Untersuchungsstandorten in Ägypten, im baskischen Zumaia (Spanien) und in den Tiefseesedimenten von Shatsky Rise im Pazifischen Ozean (ODP Site 1209). Niedrig auflösende Daten planktischer Foraminiferen aus den Tethys-Gebieten in Zumaia und Ägypten wiesen bereits auf biotische Reaktionen auf das Event hin. In der Vergangenheit wurde das Ereignis biostratigraphisch nahe der P3a/P3b Subzonen-Grenze für planktische Foraminiferen verortet. Zwei auffällige Auslenkungen in XRF-gemessenem Eisengehalt und in der magnetischen Suszeptibilität können zur Korrelation mit Orbitalzyklen und damit zur astrochronologischen Datierung genutzt werden. Daher wird von einer Dauer von ~200 kyr ausgegangen. Das LDE fand während einer Phase hoher Ozean-Spreizungsraten und vulkanischen Entgasungen südöstlich von Grönland statt.

Im Rahmen der vorliegenden Arbeit werden zum ersten Mal Ergebnisse aus Untersuchungen planktischer Foraminiferen aus verschiedenen Tiefsee-Kernen (Shatsky Rise ODP Site 1210, Walvis Ridge ODP Site 1262, Newfoundland IODP Site U1407) und von einem Aufschluss auf den tethyalen Schelf (Qreiya 3, Ägypten) des Ober-Daniums in relativ hoher Auflösung gezeigt. Diese stellen detaillierte Informationen über die Entwicklungen der Vergesellschaftungen von planktischen Foraminiferen, einen nahezu globalen Einblick in Ozean-Strukturen sowie die Existenz und die Auswirkungen des LDEs bereit.

Es wurde untersucht, ob das LDE die erforderlichen Merkmale für ein kurzzeitiges paläozänes Erwärmungsereignisses erfüllt. Zur Temperaturrekonstruktion wurde  $\delta^{18}\text{O}$ -Paläothermometrie aus Gesamt-Karbonat sowie aus benthischen und planktischen Kalkschalen der drei Hauptbereiche der Ozean-Wassersäule (Ozeanboden, aphotische Suboberfläche und lichtdurchflutete Wasseroberfläche) genutzt und dabei eine Erwärmung von 2–4°C ermittelt.

Eine negative Kohlenstoff-Isotopen-Anomalie von 0,6–0,9 ‰ zeitgleich zur Erwärmung wurde an allen untersuchten Lokationen ermittelt, was auf Störungen im Kohlenstoff-Kreislauf im offenen Ozean hinweist. Der Verlauf mit der Doppel-Spitze impliziert eine zweiphasige Entwicklung ohne vollständige Erholung dazwischen.

Veränderungen in der Faunenzusammensetzung zeigen biotische Reaktion auf die Paläoumweltänderungen wie z.B. erhöhte Temperaturen, Änderungen im Nährstoffangebot oder der Wasserdichte während des LDEs. Dadurch, dass manche Arten lichtabhängig aufgrund ihrer Photosymbionten-Aktivität sind, weist die An- oder Abwesenheit auf Änderungen in der vertikalen Ozeanstruktur oder Wasserschichtung hin. Die Fauna der planktischen Foraminiferen reagierte unterschiedlich in den verschiedenen Ozeanbecken.

Einige der beobachteten Faunenänderungen lassen auf einen direkten Einfluss des LDEs vermuten, während andererseits der Faunenwechsel sich schon deutlich vor dem LDE angebahnt haben könnte. Beispielsweise wurde der biostratigraphische Anzeiger für P3a/P3b Subzone *Igorina albeari* an sämtlichen Untersuchungsstandorten bis zu ~400 kyr früher angetroffen als in der bisherigen Literatur vermerkt, wird aber erst im LDE häufig, während die Gattung *Praemurica* vor dem Ereignis häufiger wird, aber während des LDEs ausstirbt.



## Summary

The Paleocene to Eocene (~66-34 Ma) represents an important time interval for changes in global climate and evolution of marine life. Over the last decades, a number of past climate events of the Paleocene and Eocene have been identified. Several Paleogene events, often named so-called hyperthermals (transient warming events with a duration of ~ 100 to 200 kyr), were more recently explored, of which the Paleocene-Eocene Thermal Maximum (PETM, ~56 Ma) has had most recognition and impact. A new and sparsely investigated candidate for a Paleocene hyperthermal is the Latest Danian Event (LDE, 62.2 Ma), which shows a ~2°C bottom water temperature rise and a ~0.7–1.6‰ negative carbon isotope excursion (CIE). The negative CIE represents the most negative values for the entire Paleocene and therefore hints towards remarkable changes in the global carbon cycle.

Foraminifera offer an unprecedented window into paleoceanographic and paleoclimatic conditions and putatively produce the best-known geochemical and biotic record for pre-Pleistocene paleoceanography, which is why they are seen as the most applicable proxies to answer the herein considered research questions on the reconstruction of a Paleocene warming event. Their calcareous tests bear a high fossilization potential and provide valid information after deposition. Foraminifera live in the surface ocean and on or in the sea floor, where they collect different geochemical and biological signals, which tell us about the past oceanographic and climatic conditions. Global climatic events, which had effects on the marine life were often proved by the analysis of deep-sea sediments and foraminiferal test residuals. Before this thesis project started, the late Danian deep-sea records were only poorly studied. High-resolution assemblage data of planktic foraminifera, and with that, information about the marine upper water layers were largely missing. The studied LDE was first detected and proved on negative  $\delta^{13}\text{C}$  shifts at various sites in Egypt and Zumaia (Spain) and at Shatsky Rise in the Pacific Ocean (ODP Site 1209). Low-resolution planktic foraminiferal data from Zumaia and Egypt already hint towards substantial biotic reactions to the LDE. The biostratigraphic position of the LDE is classically pinpointed close to the P3a/P3b Subzonal boundary. A duration of ~200 kyrs for the LDE was suggested based on astrochronological tuning of two distinct peaks of Fe XRF core scanning data and magnetic susceptibility. The LDE took place during an interval of very high ocean spreading rates and volcanic outgassing at the SE Greenland margin. For the first time, planktic foraminifera from different Late Danian deep-sea cores (Shatsky Rise ODP Site 1210, Walvis Ridge ODP Site 1262, Newfoundland Ridge IODP Site U1407) and one Tethyan shelf section (Qreiya 3) were investigated at rather high resolution. This allowed for unravelling of evolutionary trends in planktic foraminifera and an almost global view into the ocean structure as well as the existence and impact of the LDE.

Within the scope of this thesis it was intended to test whether the LDE satisfies the requirements for a further Paleocene transient warming event.  $\delta^{18}\text{O}$  paleothermometry as derived from benthic and planktic foraminiferal carbonate was primarily used to reconstruct temperature changes at the sea floor as well as in the surface mixed layer and of subsurface water masses. In all three habitats a temperature rise of 2–4°C was recorded.

A negative CIE of 0.6–0.9 ‰ was measured at all sites contemporary to the temperature rise, indicating perturbations of the carbon cycle in the open ocean. The double-peak implies a two-phase character of the event without complete recovery in between.

Changes in the planktic foraminiferal assemblages show a biotic response to environmental perturbations like temperature increase, nutrient availability or water density change during the LDE. As some species are light dependent due to their photosymbiotic activity, the abundance of certain species hints towards changes in of the vertical ocean structure or water stratification. Planktic foraminiferal fauna assemblage data show different reactions in each ocean basin.

However, some of the observed changes suggest a direct response to the environmental changes associated with the LDE, whereas other shifts already commenced well before the event. *Igorina albeari*, for instance, is the index species for the base of planktic foraminiferal subzonal boundary and occurs according to the results of this thesis up to 400 kyrs earlier than documented in the literature but became abundant during the event. By contrast, the genus *Praemurica* declines in abundances before the LDE and became extinct right at its onset.

# Thesis outline

After a general introduction into paleoenvironmental developments of the Paleocene and the use of planktic foraminifera as climate proxies (**Chapter I**), the impact of the LDE on planktic foraminifera in the Pacific Ocean at Shatsky Rise Site 1210 is described and discussed (**Chapter II**). The chapter is published in PLOS ONE, Jehle et al. (2015) and, for the first time, unravels a temperature rise in the upper water column as well as the complexity of enhanced stratification of the upper water layers connected to the LDE and its consequences for planktic foraminiferal assemblages.

In **Chapter III**, paleoceanographic changes in the southern Atlantic Ocean are analysed and compared to Pacific Site 1210 data. Like in **Ch. II**, planktic foraminifera are investigated on faunal assemblage and  $\delta^{13}\text{C}$  and  $\delta^{18}\text{O}$  test geochemistry. Results were compared to previous data from Shatsky Rise Site 1210 as larger differences in the geochemical and faunal reaction to the event were revealed. The chapter was submitted (October 2018) to “Palaeogeography, Palaeoclimatology, Palaeoecology” and is now under revision for publication.

**Chapter IV** sheds light onto ambiguities around the biostratigraphic index species for the P3b base *Igorina albeari* and suggests biostratigraphic adjustments. Results from ODP Sites 1210 and 1262 of earlier research are supplemented by data from Newfoundland Ridge Site U1407 (North Atlantic Ocean) and Qreiya 3 (Egypt). The structure of this chapter is designed for a later publication.

**Chapter V** aims at a general conclusion and summary. Key results are summed up and new, unpublished data of species assemblages of IODP Site U1407 and Qreiya 3 (Egypt) are compared to data of the ODP Sites 1210 and 1262.



# Chapter I: Introduction

## 1 Cenozoic climate

### 1.1 Past climate variations as hints for understanding the recent climate change

Climate conferences as well as national and international political debates like the UN climate conferences exhibit broadly-based risen awareness for our society's position in front of the obligation to solve problems of climate change, the warming process and a future warmer planet. For the last 20 years, knowledge about the anthropogenic impact onto global climate has substantially improved (e.g. Williams et al., 2007; Davis and Caldeira, 2010) and started to gain more attention on a political level within the scope of science-politics-interface-meetings like the Intergovernmental Panel on Climate Change (IPCC; Houghton et al., 2001; Masson-Delmotte et al., 2013; Allen et al., 2018, Figure 1, Figure 2).

Due to the complexity of climate systems, the relationship between climate and atmospheric CO<sub>2</sub> is still under debate, but the close feedback between the two is uncontroversial. The greenhouse gas effect is a natural phenomenon, which is evidently strongly accelerated by human activities, especially since the beginning of the industrialisation. It has been stated and is known to be common sense that the globally averaged net effect of human activities since 1750 has, with very high confidence, lead to global warming by emitting atmospheric greenhouse gasses like CO<sub>2</sub>, CH<sub>4</sub> or N<sub>2</sub>O (Alley et al., 2007, Masson-Delmotte et al., 2013; Allen et al., 2018). Greenhouse gases have played an important role during past glacial-interglacial cycles, even if other drivers were present as well. This makes paleoclimatic research a highly beneficial source for projections towards future global warming.

Within the last years, many new climate-change-related records were reached or broken:

A recent NOAA report has shown that 2016 was a year for the record books as it was the warmest year since the beginning of human weather records, the Arctic sea ice had its smallest annual maximum extent for the second year in a row and reached its second smallest minimum extend on record, tied with 2007 (Blunden and Arndt, 2017). For the first time in the past 800.000 years, the annual CO<sub>2</sub> concentration in the atmosphere surpassed the 400-ppm-landmark by 2.9 ppm (Figure 1). With an increase of 3.5 ppm since 2015 it is also the largest annual increase ever measured. The CO<sub>2</sub> concentration has been below that for the last 650,000 years (e.g. Blunden and Arndt, 2017; Allen et al., 2018).

2017 was the third-warmest year since the beginning of recordings and the warmest non-El-Nino-influenced year, according to land- and ocean-based weather stations (NOAA, Global weather record, 2018<sup>1</sup>; Blunden and Arndt, 2018).

In Germany, April 2018 has been the warmest since the beginning of records: average global land and ocean surface temperatures for January to March 2018 was 0.74°C above the 20<sup>th</sup>

---

<sup>1</sup> <https://www.ncdc.noaa.gov/sotc/global/2018/03/supplemental/page-1> (July 2018)

century average of 12.3°C, which is the sixth highest global land and ocean temperature for January to March in the long-term record of 1880–2018, however, 0.43°C cooler than the record of 2016<sup>1</sup>. The period April to July 2018 shows temperature-wise and with very low amount of precipitation the highest anomaly for these months since 1881 (Imbery et al., 2018).

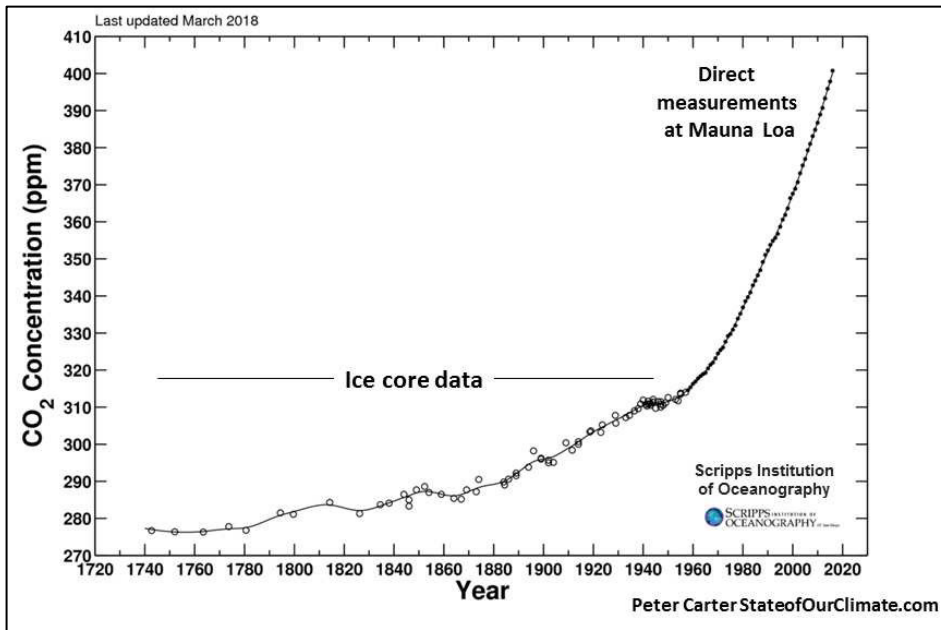


Figure 1: Accelerating atmospheric CO<sub>2</sub> concentration 1720-2018. A merged Ice-core record is shown from Scripps Institution of Oceanography. CO<sub>2</sub> increases in concentrations of carbon dioxide coinciding with the start of the Industrial Revolution in about 1820. Graph by Peter Carter, stateofourclimate.com, based on data from the NOAA Paleoclimatology and Earth System Research Laboratory. Antarctic ice core data before 1958 is from Law Dome Glacier, younger data is from seasonally detrended arithmetic average of air measurements from Mauna Loa and the South Pole Observatory.

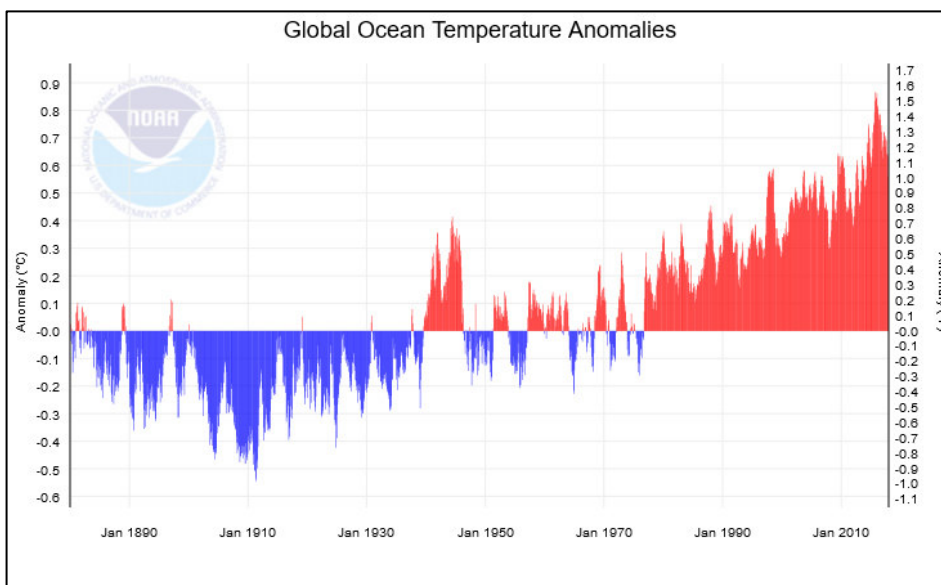


Figure 2: Monthly Global Ocean Temperature anomalies since 1890, plotted by NOAA Global Time Series<sup>2</sup>.

<sup>2</sup> <https://www.ncdc.noaa.gov/cag/global/time-series> (Dec 2018)

One indicator for increasing temperatures (Figure 2) is the sea-level rise, which is influenced by both melted ice sheets as well as by expansion of warmer water. Coastal tidal gauge records measured a sea-level rise of ~230 mm between 1870 and 2013 (CISRO<sup>3</sup>), satellite sea-level observations data from the NASA Goddard Space Flight Center show a sea-level rise of 86 mm between January 1993 to July 2018 and a recent rate of 3.2 mm per year<sup>4</sup>. The Antarctic ice-extension got an all-time low in both spring 2017 and 2018 (National Sea and Ice Data Center NSIDC, University of Colorado<sup>5</sup>).

The modern global climate change has already had significant impact on ecosystems, such as: alterations of global circulation like monsoon patterns and strength (e.g. Turner and Annamalai, 2012), El Niño/ENSO forcing (e.g. Trenberth and Hoar, 1997), thawing of permafrost (e.g. Hipp et al., 2012) as well as melting of arctic polar ice caps and mountain glaciers, which leads to devastation of fertile river deltas, landslide, desertification, enhanced occurrence of heat waves, cyclones, coastline rise and loss of land. Within temperate regions, slightly higher temperatures in combination with higher precipitation rates are sometimes beneficial for agricultural growth rates, but in the Mediterranean region (notably: Provence Alpes-Côte d’Azur, France; Blunden et al., 2018) devastating droughts have become common already. Resulting from higher temperature, forced losses in bio- and ethnodiversity, strongly limited access to drinking water and enhanced migration of entire human and animal populations are only some already observed examples, (e.g. Gobiet et al., 2014; Rosenzweig et al., 2014; Molinos et al., 2016).

After the passing of a certain threshold or tipping point, global warming works as a trigger for even more warming (Steffen et al., 2018). The exact amount of warming for this tipping point is not finally numbered, however, ecologic and economic benefits from a 1.5°C limited warming instead of 2.0°C were shown within the IPCC Special Report 2018<sup>6</sup> and discussed at the COP24 (Conference of the Parties to the United Nations Framework Convention on Climate Change) in Katowice, Poland, Dec 2018.

Marine ecosystems are covering ~70 % of the Earth’s surface. River deltas and coral reefs are especially endangered marine habitats that are called “hotspots of species diversity” or “rainforests of the ocean”. The sudden temperature-induced stress-reaction coral bleaching can lead to the death of a coral stock (e.g. Donner, 2009; Pandolfi et al., 2011). Symbionts are leaving the hosts as a reaction to changes in temperatures or light or nutrient availability. Due to photosymbiosis and sessile lifestyle, corals are very water-level dependent (e.g. Eakin et al., 2009). This issue was also found on climate-induced stressed larger benthic foraminifera (e.g. Schmidt et al., 2011). The Oceans play an especially important role as a heat distributor and CO<sub>2</sub> sink. This function is reduced with increasing temperatures. Due to inertia of mass, the temperature rise in the open ocean is slower, but impacts are lasting longer. Because of its size and the large number of possible influencers, the open ocean is a very complex system, so that reactions to climate change and its harms are less investigated than within terrestrial habitats and coastline areas. Some stressors to the marine ecosystems are amplified by climate change,

---

<sup>3</sup> <https://research.csiro.au/slrwavescoast/sea-level/sea-level-changes/> (Oct 2018)

<sup>4</sup> [Climate.nasa.gov](https://climate.nasa.gov)

<sup>5</sup> <http://nsidc.org/arcticseaicenews/charctic-interactive-sea-ice-graph/> (Oct 2018)

<sup>6</sup> IPCC 2018 *Global Warming of 1.5°C. Special Report*

which are: acidification, which inhibits the calcification processes of e. g. unicellulars like coccolithophores or foraminifera. Secondary effects of warmed water are: enhanced stratification and therefore less oxygenated deeper water, increased metabolic rates and variations in solubility constants, salinity variations or eutrophication by e.g. enhanced precipitation which is washing fertilizer into the marine habitats. The ecosystems are under most extreme pressure in a situation of quick changes of many parameters and not all organisms are able to adapt quickly enough. If certain tolerance thresholds are passed, entire ecosystems can be destroyed by self-accelerating processes (Bopp et al., 2013). Following a global temperature rise, ecosystems are known to be re-organized and affected the most at the base of the food-web, e.g. primary producers, which are more prone to environmental stress. Since 1880, the global surface temperature has increased by  $\sim 1^\circ\text{C}$  (NASA's Goddard Institute for Space Studies GISS<sup>7</sup>), which is almost 1,000 times faster than during the PETM (Paleocene-Eocene Thermal Maximum,  $\sim 56$  Ma). It is well explored that the temperature rise during the PETM has driven many species to extinction, especially benthic parts of the marine ecosystem (e.g. Bralower, 2002; Speijer et al., 2012; Norris et al., 2013).

The detailed knowledge of catastrophic events, short-term perturbations and their effects on living organisms in the past is crucial to better estimate future impacts and threats due to ongoing climate change (e.g. Bowen et al., 2006). There are no exact analogies for future climate change, but paleoclimatology shows some testpieces for deeper understanding of the systems. Past global warming events show possible analogies for future global warming (Pörtner et al., 2014). Past climate changes are mostly reconstructed over data derived from geological phenomena by analogy and are therefore to be interpreted within the limits of the measurable record. As we neither can nor want to wait for the results of the real-time experiment of global warming, we are very much in need for knowledge of the impacts of older, probably comparable developments.

One of the most important results of paleoclimatic research is the fact that climate change can have a very fast development, like proved by  $\delta^{18}\text{O}$  paleothermometry in Greenland-icecores of the Dansgaard-Oeschger-events, Heinrich Events or the Little Ice Age. During Dansgaard-Oeschger-Events, temperature changes of  $4\text{-}5^\circ\text{C}$  within 30-40 years occurred several times, caused by freshwater-inflow into the ocean (e.g. Burns et al., 2003; Rahmstorf, 2003; Bond et al., 2013). Comparable scenarios occurred with the Heinrich Events. These events have in common to drastically change marine salinity and carbon cycles, leading to diversity loss in foraminifera (Bond et al., 2013). During these dramatic temperature jumps, oceanic circulation changed a lot in the tropics and subtropics, deep water formation stopped, and the development was not uniform within Northern and Southern hemisphere. Climate modelling like General Circulation Models (GCM, e.g. Barron and Peterson, 1991) are powerful tools to simulate effects of greenhouse gas emissions (see for overview: Randal et al., 2007), nevertheless, we might especially be interested in long-term paleo-records which are the hardest to simulate with existing instruments. Models, in all their complexity, remain imperfect, reduced and are constantly in need for validation by observation data of past climate proxies (Markwick, 2007). Qualitative paleoclimate data will improve the accuracy of the models and the predictions of

---

<sup>7</sup> <https://climate.nasa.gov/vital-signs/global-temperature/> (Oct 2018)



the future climate. For instance, it is to keep in mind that Cenozoic climate, especially during the PETM, has had different conditions than today, like presumably ice-free poles, higher global mean temperatures and a higher greenhouse gas concentration (e.g. Zachos et al., 2008). Slightly different paleogeography lead to other ocean circulation patterns. Both fields, proxy data and modelling, did benefit a lot from each others in the recent years (Markwick, 2007; Williams et al, 2007; Kirtland Turner and Ridgwell, 2016).

## 1.2 Cenozoic trends: climate, fauna and continental drifts during Late Cretaceous and Early Paleocene

The Paleocene was preceded by the very warm Cretaceous (145.0–66.0 Ma, Figure 3), which ended with a catastrophic incident at the K/Pg-boundary (~66 Ma). The Cretaceous geographic poles are considered as largely ice-free and many continental areas were flooded by numerous epicontinental seaways and basins (e.g. Barron et al., 1991; Herman and Spicer, 1996). The period is characterized by several larger tectonic movements, like the separation of India and Madagascar from Gondwana, Australia from Antarctica, Afro-Arabia from South-America and first extension between North-America and Eurasia, starting from 120 Ma (Hay et al., 1999; Hart, 2007; Markwick, 2007). The Tethys Ocean in the subtropical zone transported warm equatorial water of the Pacific to the area where the Mediterranean Sea is located today. Through the entire Cretaceous, the pole-to-equator temperature gradient and, as a consequence, the ocean circulation was presumably less effective than today (Huber et al., 1995; Tripathi and Elderfield, 2005; Sluijs et al., 2006), leading to low-oxygenized conditions in deeper layers and episodic development of black shale deposits (Arthur, 1979; Summerhayes, 1981; Brumsack, 2006). Flourishing nannofossil, dinoflagellate and diatom populations built up huge chalk banks and planktic foraminifera evolved a very high diversity (e.g. Keller, 1988; Premoli Silva and Sliter, 1999).

The age was terminated by the Chixulub impact, where supposedly a 10 km sized asteroid caused a crater of roughly 180 km in diameter and harmed most ecosystems severely. About 66–75 % of all species did not recover (D'Hondt et al., 2005; Coxall et al., 2006; Gulick et al., 2016). The Deccan Trap volcanism in India produced large flood basalts and is seen as an additional influence to the asteroid impact scenario (e.g. Courtillot et al., 1986; Schulte et al., 2010).

During the Paleogene, mammals developed into the vacant niches on the continents: Placentalia were much superior to Marsupialia and replaced them on many continents. Within plants, angiosperm Magnoliophyta started to dominate and grasslands became more resistant with silicate frameworks and the new C4 metabolism. Modern Teleostei and marine mammals replaced extinct Ichthyosaurs and other inhabitants of the marine realm. Continental drifts placed Antarctica at the South Pole where the ice formation lead to global sea-level drops exposing more continental areas and letting the Tethys-Ocean disappear. India collided with Eurasia, causing the orogenesis of the Himalayans.

Photosymbiotic planktic foraminifera were among the highly affected taxa of the K-Pg mass extinction. It is assumed that only three species survived which formed the base for the evolution of modern foraminifera (D'Hondt and Zachos 1998; Houston and Huber, 1998; Norris, 1998).

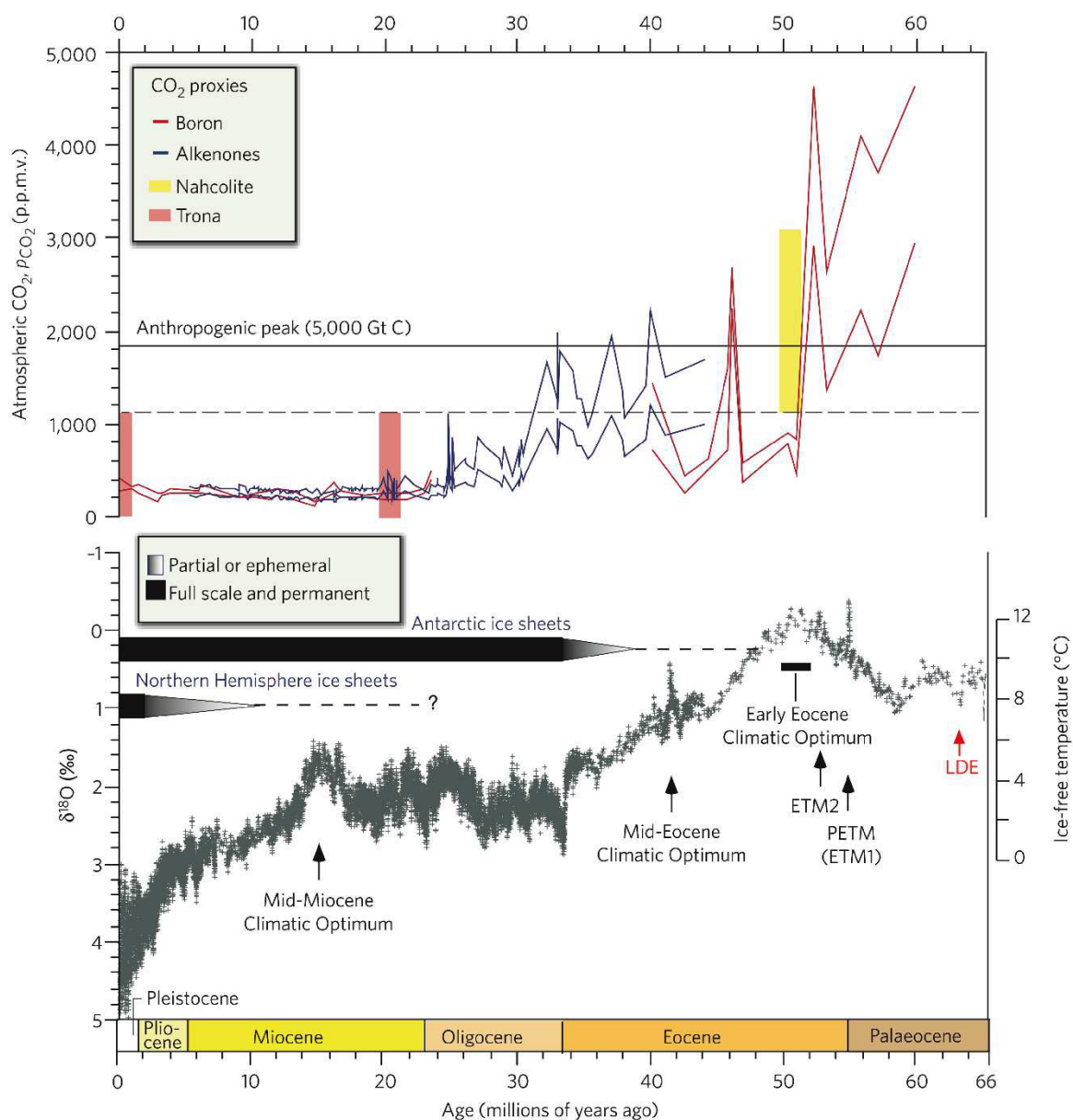


Figure 3: Cenozoic (0-65 Ma) climate trends, climatic and biotic events in conjunction with  $\delta^{18}\text{O}$ ,  $\delta^{13}\text{C}$  isotope measurements, amended from Zachos et al., 2008. Here, several marine and lacustrine proxy records were compiled. The  $\delta^{18}\text{O}$ ,  $\delta^{13}\text{C}$  curves are based on Deep Sea Drilling Project and Ocean Drilling Programm sites. Please note that the age calibration is not in line with newer, orbitally tuned versions and the LDE-data density was low to the time this graphic was being established. The LDE was pinpointed to an absolute age of 62.2 Ma (Dinarès-Turell et al., 2014).

### 1.3 Transient warming events in the Paleogene

Hyperthermal events, also named transient warming events (200 kyrs), are superimposed on already warm climate and accompanied and putatively triggered by a massive CO<sub>2</sub> release. The CO<sub>2</sub>-warming coupling has been part of bigger discussions (e.g. Zachos et al., 2008). The hyperthermal events are identified by several characteristics: (1) major perturbations of the global carbon cycle, reflected in the negative Carbon Isotope Excursions (CIE,  $\delta^{13}\text{C}$  variation) in e.g. inorganic and biogenic carbon of calcific tests of benthic and/or planktic foraminifera; (2) short-term climate warming; (3) extreme biotic response like faunal turnovers and (4) the uplift of the calcite compensation depth (CCD), mostly on a global scale (e.g. Zachos et al., 2005). The most important energy source which influences the earth's climate is the sun, which is controlled by Milancovic's cycles precession (19, 22 and 24 kyr), obliquity (41 kyr) and eccentricity (95, 125 and 400 kyr). These cycles were often connected to transient warming events. Temperature distribution is influenced by marine circulation as well as the continent-ocean location and proportion, which are attributed to the albedo effect.

### 1.4 Paleocene-Eocene Thermal Maximum and consecutive Eocene events

The PETM was the most devastating and ecologically influencing event after the K-Pg mass extinction and it was therefore investigated on numerous terrestrial and marine sites, most likely in each and every marine and terrestrial habitat (e. g. Norris, 1996; Agnini et al., 2007; Bowen et al., 2008; Birch et al., 2012; Monechi et al., 2012). It is beyond the scope of this thesis to give a comprehensive overview and to mention all the important work. Some main issues should be mentioned in order to set the impact into perspective and to compare it to the LDE.

The most recognizable characteristics of the PETM are:

- a negative  $\delta^{13}\text{C}$  for 170 ky of 1 to 5 ‰ (Röhl et al., 2007; Sluijs et al., 2007a, b; see Figure 3),
- a decrease in benthic foraminifera and bulk sediment  $\delta^{18}\text{O}$  by >1 ‰, implicating a bottom water warming of up to 5°C (Kennett and Stott, 1991; Thomas and Shackleton, 1996; Dunkley Jones et al., 2013),
- a shallowing of the lysocline and CCD linked to ocean acidification (Zachos et al., 2005),

a major benthic foraminifera extinction of 35–50 % of in bathyal and abyssal sites as well as a faunal turnover of calcareous nannoplankton communities on shallow shelf areas and in the deep sea (e.g. Kelly et al., 1996; Thomas, 2003; Bralower, 2002; Speijer et al., 1995; Stassen, 2012). It was suggested that it was probably not that much of an extinction but more of a migration and origination event (Speijer et al., 2012). The event was linked to enhanced atmospheric CO<sub>2</sub> and other greenhouse gasses in the atmosphere. Concluding reasons for the PETM are still under debate (Sluijs et al., 2007) as there seems to be no clear evidence for the source of the supposedly enormous Carbon input resulting in the remarkable global warming.

One largely accepted explanation is an extremely high climate sensitivity to CO<sub>2</sub> so that the needed amount of greenhouse gas would have been lower than for a comparable scenario like the recent-day climate change (Pagani et al., 2006). A non-singular trigger as the cause of late Paleocene and early Eocene events was implied (Sluijs et al., 2007) in parallel with the theory of massive volcanic outgassing at the North Atlantic Igneous Provinces (Gutjahr et al., 2017).

Similar Eocene events, including the PETM (a.k.a. ETM1), the Eocene Thermal Maximum 2 (ETM2, 53.5 Ma; Sluijs et al., 2009) and ETM3 (52.0 Ma; Röhl et al., 2005), indicate concurrence of the events to orbital forcing as these transient events started during short (100 kyr) and long-term (405 kyr) eccentricity maxima, according to spectral analysis of magnetic susceptibility and colour reflectance records from Walvis Ridge (Lourens et al., 2005; Röhl et al., 2007). It was argued that eccentricity maxima were superimposed on other trends and lead to passing of certain thresholds, resulting in climate change (Sluijs et al., 2007). However, a clear linkage is questioned (Stap et al., 2010), mainly because it was found that PETM and ETM2 do not exactly correspond to maxima in long-term eccentricity cycles. This leaves us with the realization that mechanisms of orbital forcing are more complicated due to uncertainties in available astronomical computations for that time (Lourens et al., 2005; Sluijs et al., 2007). The question is not only important for the PETM but also for preceding and consecutive events of Paleocene and Eocene age, like the Latest Danian Event.

## 1.5 Latest Danian Event

The Latest Danian Event (62.18 Ma; Bornemann et al., 2009; Westerhold et al., 2011; Jehle et al., 2015, Ch. II) represents the onset of the Paleocene Carbon Isotope Maximum (PCIM), culminating during the C25n/C25r transition (e.g. Shackleton et al., 1984). Due to its stratigraphic position, the LDE is also known as Top Chron 27n event (Westerhold et al., 2008, 2011). It had an estimated background level of ~300–500 ppm atmospheric CO<sub>2</sub> (Masson-Delmotte, 2013) and took place during a general cooling trend, beginning at ~63.0 Ma (Figure 3, Figure 4; Westerhold et al., 2011).

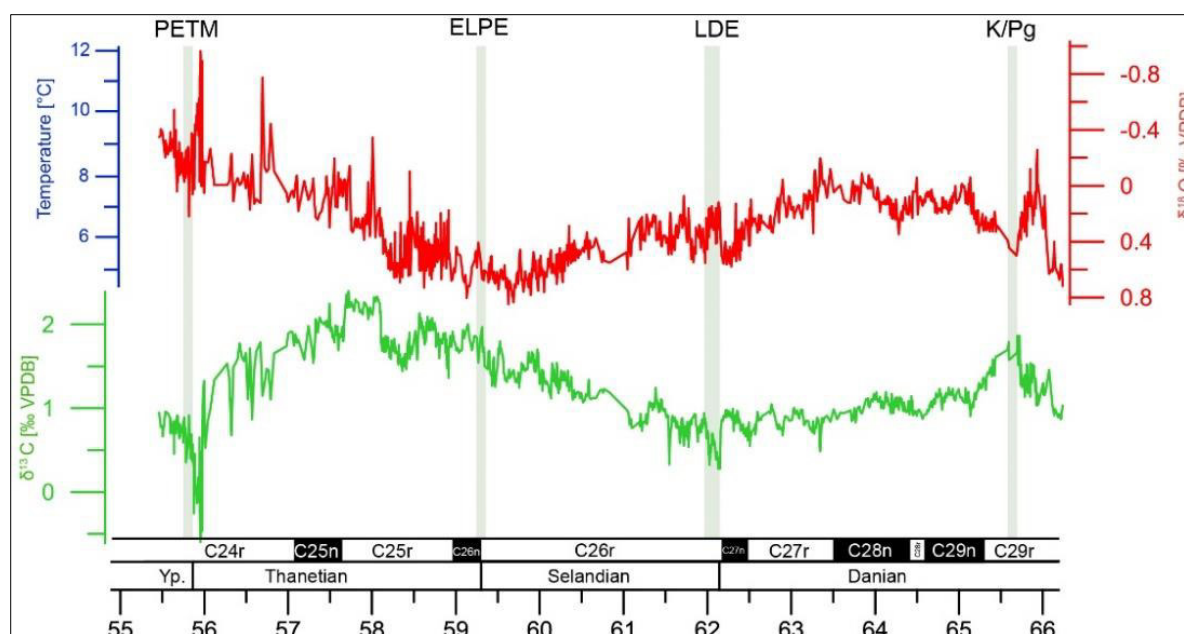


Figure 4: Paleocene  $\delta^{18}\text{O}$  and  $\delta^{13}\text{C}$  developments, amended from Westerhold et al., 2011 (age calibration option 2). The LDE warming takes place during a long-term cooling trend, which started  $\sim 63.5$  Ma. Please note that the age calibration is not in line with the newer age calibration by Dinarès-Turell et al. (2014). The graph shows a very long  $\delta^{18}\text{O}$  and  $\delta^{13}\text{C}$  record from benthic foraminiferal carbonate from Shatsky Rise ODP Site 1209, Pacific Ocean

The LDE was globally identified by a characteristic double peak in magnetic susceptibility and XRF Fe data (Westerhold et al., 2008, 2011) which correspond to the short eccentricity cycles 38 and 39. Both magnetic susceptibility and XRF Fe signals are supposedly caused by lowered carbonate input in relation to higher clay concentration. A lower carbonate content was detected in several deep-sea sediments, enhanced terrestrial deposition can be ruled out due to the open ocean positions of each site. Increased export production decreased a second time during late LDE and the decline of  $\text{CaCO}_3$  indicates a shoaling of CCD/lysocline and corrosive water in the Northern Atlantic (Yamaguchi et al., 2017).

The LDE is characterized by a negative CIE of 0.7–1.6 ‰ in several investigated sites, such as shelf sections on benthic foraminifera test data from Egypt (Bornemann et al., 2009) or Caravaca, Spain (Alegret et al., 2016), bulk rock data from Zumaia (Schmitz et al., 2011), deep sea *Nuttallides truempyi* data from Wombat Plateau ODP Site 761B (Quillévére et al., 2002) or Shatsky Rise 1209 and 1210 (Westerhold et al., 2008, 2011, Jehle et al., 2015, Deprez et al., 2017) and Walvis Ridge Site 1262 (Monechi et al., 2013; Deprez et al., 2017). There is no complete CIE recovery between the two phases. Investigations on nannofossils at the Zumaia GSSP site revealed a five-meter acme of *Braarudosphaera bigelowii* contemporary to a 3.5 ‰ negative CIE of the LDE, together with a highly increased pentolith abundance, hinting towards increased fragmentation (Criscione et al., 2017). Cyclostratigraphic age calibration pinpoints the onset of the event to an absolute age of 62.2 Ma (Westerhold et al., 2011; Dinarès-Turell et al., 2012).

There are two biostratigraphic systems for the temporal identification used in parallel, derived from planktic foraminifera and from nannofossils (Figure 5). Therefore, the LDE is supposedly positioned slightly above the planktic foraminiferal P3a/P3b boundary, which is defined by the

FAD of *Igorina albeari* and the lowermost NTp7B nannofossil zone (Sprong et al. 2009; Varol, 1989). New investigations rise doubt in the exact FAD, which would shift the boundary towards an older age, see for discussions Chapter IV.

Period	Standard Chronostratigraphy		Geomagnetic Polarity	Planktonic Foraminifers Sub-Tropical Zone	Calcareous Nannofossils	
	Epoch	Age/Stage				
Paleogene	Eocene	Ypresian		E3 E2 E1 P5	NP10 NP9	
		Thanetian		C24		
				C25	P4	NP8 NP7 NP6
	Paleocene	Selandian		C26	P3 LDE	NP5
		Danian		C27	P2	NP4
				C28	P1	NP3
				C29	Pa P0 <i>Plummerita hantkeninoides</i>	NP2 NP1
	Cretaceous	Late	Maastrichtian		C30	<i>Pseudoguembelina hariaensis</i> CC26

Figure 5: Biostratigraphic overview of the Paleogene, adapted from time scale creator<sup>8</sup>. The orange area indicates the LDE.

A short-term warming phase in the upper ocean layers with  $\sim 2\text{--}3^\circ\text{C}$  and  $\sim 2^\circ\text{C}$  on the sea floor with a duration of  $\sim 0.2$  Ma was interpreted from a negative  $\delta^{18}\text{O}$  signal at Shatsky Rise Sites 1209 and 1210, Wombat Plateau 761B (Quillévére et al., 2002; Westerhold et al., 2011, Jehle et al., 2015), and Walvis Ridge ODP Site 1262 (Ch. III). The warming was superimposed on a long-term cooling after  $\sim 63.0$  Ma or Top Chron 28n and initiated a warming trend towards the PETM (Westerhold et al., 2011). However, no evidence of warming was detected in the  $\delta^{18}\text{O}$  in ostracode carbonate from Sidi Nasseur (Tunisia, Bornemann et al., 2012). Regarding  $\delta^{13}\text{C}$  and  $\delta^{18}\text{O}$  values, the LDE might be similar in duration like PETM, but smaller in magnitude, suggesting similar operating processes (Westerhold et al., 2011). Biotic reactions on the event in terms of faunal changes were observed on planktic foraminifera (Guasti, 2005; Jehle et al., 2015), within benthic foraminifera in dysoxic shelf settings (Sprong et al., 2011, 2012; Schulte et al., 2013) but also on mammals (Clyde et al., 2008) and calcareous nannofossils (Fuqua et al., 2008; Monechi et al., 2012). Benthic foraminiferal response at Walvis Ridge Site 1262 reflect enhanced food supply during LDE1 and a decreased during LDE2, which is compatible with the development of U1407 (Deprez et al., 2017; Yamaguchi et al., 2017). At Newfoundland IODP Site U1407, changes in ostracod faunal taxonomic composition and diversity were seen minor during LDE1, together with high export productivity as indicated by benthic ostracod numbers and NMDS. Taxonomic diversity loss, low  $\text{CaCO}_3$  and alternated

<sup>8</sup> <https://engineering.purdue.edu/Stratigraphy/tscreator/index/index.php>, Gradstein et al., 2012

export productivity is shown during LDE2. Benthic ostracods show partly similar developments to the PETM in terms of e.g. biotic response and CCD shoaling, but show no signs for extinction (Yamaguchi et al., 2017).

## 2 Planktic foraminiferal ecology

### 2.1 Historical notes on foraminiferal and paleoceanographic research

A connection between plankton species assemblages, their global distribution and climatic developments was identified as early as the 19<sup>th</sup> century (Murray, 1897; Schott, 1935; Arrhenius, 1950). In retrospective, these studies can be considered as the birth of paleoceanography. Emiliani (1954) proved for the first time with the help of geochemical analysis that different species calcify at different water depths. The first paleo-ecological transfer function for the reconstruction of terrestrial and atmospheric states from data like temperature, distribution of water masses, salinity etc. was extraordinarily salient (Imbrie and Kipp, 1971) and lead to the pioneering project for an overall reconstruction of the terrestrial and marine surface of the ice-aged Earth at the time of the Last Glacial Maximum (CLIMAP, 1976).

### 2.2 Cenozoic evolution of planktic foraminifera

For the classification of Cenozoic planktic foraminifera, the primary criterion on genus level is the wall structure, which is seen as a fundamental higher-level taxonomic character of modern foraminifera (e.g. Hemleben et al., 1989; Olsson et al., 1992; Sen Gupta, 2002). The end-Cretaceous mass extinction (K-Pg; ~66 Ma ago) was not only devastating for many marine vertebrates but also invertebrates including unicellular phyto- and zooplankton taxa (Sheehan et al., 1996). Planktic foraminifera decreased to almost extinction. It assumed that only three species survived the catastrophe and started on a rapid evolution therefrom.

The most likely ancestors of later planktic foraminifera are: (1) the triserial *Guembelitra cretacea* (Cushman 1933, LrAD P1b), which gave rise to the microperforate group as well as (2) the trochospiral *Hedbergella monmouthensis* (Olsson et al., 1999, LrAD P0) as a first member of the normal perforate smooth-walled group *Globanomalina*. It is built up by a finely perforate wall with short, minute spines constitute the species according to the first description (Olsson 1960). (3) The third survivor would be *Hedbergella holmdelensis* with a finely perforate, delicately hispid wall (Olsson et al., 1999).

Since sediment rework is of issue in lower Danian sections (namely: Atlantic DSDP Site 384, Indian DSDP 213/ODP 758 and Pacific ODP 465; Berggren and Norris, 1997), the survivorship of other Cretaceous taxa than *Guembelitra* sl. and *Hedbergella* is difficult to prove. Most observations are based on the presumption of little if no sediment displacement involved.

Cladistic and stratophenetic phylogenies suggest that all Paleocene trochospiral foraminifera are monophyletic, which implies that the three mentioned major lineages diverged in the

earliest Danian from the triserial *Hedbergella* Brönniman and Brown (1958; Berggren and Norris, 1997; Quillévéré and Norris, 2003). It gave rise to the normal perforate smooth-walled nonspinose *Globanomalina* Haque (1956; Banner, 1989) and later to the cancellate non-spinose group *Eoglobigerina* Morozova 1959 and *Parasubbotina* Olsson et al., 1992 (Tabelle 1).

Table 1: Wall types of Early Paleocene trochospiral planktic foraminifera (e. g. Olsson et al., 1999)

Wall type	Genus and description	pore size
microperforate	Guembeltriida	< 1 $\mu\text{m}$
Normal perforate, smooth-walled, nonspinose	<i>Globanomalina</i> Haque, 1956	> 1–8 $\mu\text{m}$
normal perforate, cancellate, nonspinose	<i>Praemurica</i> characterized by subparallel longer ridges connected by shorter ridges which originate from coalescing pustules (Soldan et al., 2011)	
normal perforate, cancellate, spinose	<i>Eoglobigerina</i> , <i>Subbotina</i> , and <i>Parasubbotina</i> characterised by regular ridges similar to <i>Globigerinoides</i> Cushman 1927 (Soldan et al., 2011)	

After the K-Pg extinction, a burst of diversification developed towards full diversification after only a few million years (Corfield and Shackleton, 1988; Olsson et al., 1999). At deep-sea site ODP Site 528 (Li and Keller, 1998) within only 300 kyrs, 18 new species and 8 new genera came to light. At Pacific Site 577 it was discovered that *Praemurica uncinata* and its descendant morozovellids started on diversification before final  $\delta^{13}\text{C}$  recovery after K-Pg.

Two new genera, *Praemurica* (typified by *Globigerina taurica* Morozova 1961) and *Parasubbotina* (typified by *Globigerina pseudobulloides* Plummer 1926) were established for the newly recognized cancellate nonspinose group. The genus of the cancellate spinose groups was first described in the Danian (Berggren and Norris, 1997). During the Early Paleogene (planktic foraminifera biostratigraphic zones P0–P2), some more wall texture groups developed from these species (Olsson et al., 1992). In the mid Paleocene, the muricate non-spinose wall was developed as a new wall texture type, characterized by short pointed pustules in terms of muricae or pseudospinae and layered wall structures formed during ontogeny. Pseudospinae are located mostly all over the test or concentrated at the umbilicus. *Morozovella* split up into two lineages: (1) completely muricate walls (*M. apantesma* – *M. aequa*) and (2) muricae concentrated on peripheral parts of the test (*M. angulata* – *M. velascoensis*; Berggren and Norris, 1997).

*Praemurica* is a paraphyletic genus in transition between *Globanomalina*, *Morozovella* and *Igorina*. The praemuricate wall structure seems to be an intermediate form between the muricate and the cancellate non-spinose.



The LDE takes place at the end of the second post-extinction recovery phase from the K-Pg event during a phase of rapid rising planktic foraminiferal diversification (Coxall et al., 2006). ~4 Ma after the event, diversity returned to almost pre-K-Pg-extinction levels. Due to striking similarities in the shapes of the curves, it seems as if the recovery of planktic foraminifera was closely linked to recovery of marine carbon cycling. Evolutionary diversification was especially high amongst *Morozovella* and later by *Igorina* and *Acarinina* (Coxall et al., 2006). The abrupt radiation of Morozovellids into vacant morphospace after K-Pg points to radically changed and/or vacated niches and happened with such a rapidity that it is seen as example of punctuated equilibrium (Kelly et al., 1996).

## 2.3 Ecology and habitat of planktic foraminifera

Planktic foraminifera are single-cell organism, living in a calcite test, which covers most of the organelles of the eukaryote. Cytoplasm outside of the test is a network of long rhizopodia, which serves to collect food particles and transport them into the test through aperture and pores. Planktic foraminifera are not able to control their floating direction, but they can maintain the optimal depth by varying buoyancy with their so-called fibrillary bodies. As far as it is understood, this is accomplished by low-density metabolites or osmolytes (Hemleben et al., 1989; Boyd and Gradmann, 2002). Certain species are observed to be concentrated at a similar water depth, which hints towards the existence of such a vertical positioning control system. The water depth is of high importance for cycles of reproduction (Schiebel and Hemleben, 2005).

The calcareous walls provide much information on the paleoenvironment as extracted by geochemical analysis, which, in turn, gives hints towards the paleoenvironment. While benthic foraminifera reflect the infaunal and epifaunal living conditions on the sea floor, planktic foraminifera mostly cover 200–300 m and with some exceptions the deeper water layers of the upper water with a free-floating existence. They present various trophic behaviours between omnivore, herbivore with phytoplankton like diatoms and dinoflagellates and carnivore with zooplankton like copepods or ciliates (Hemleben et al., 1989). Photosymbiosis with harbouring intracellular algae is a common trophic behaviour of the photic area and is of particular advantage in oligotrophic zones with low nutrient and food but high light availability (e.g. Bijma et al., 1992). Living planktic foraminifera are grouped into five assemblages corresponding to the temperature zones of the world's oceans: tropical, subtropical, temperate, subpolar and polar provinces (Bradshaw, 1957; Bé and Tolderlund, 1971). The distribution of these zones during the Paleogene might have differed since the global temperature gradient was presumably lower than today. However, paleogeographic studies (Boersma and Premoli Silva 1983; 1991) suggest that such zones already existed in the Paleogene. Depth stratification became more established during the Paleocene, leading to a significant diversification, possibly fuelled by photosymbiosis (Quillévéré and Norris, 2003).

Maximum diversity within foraminifera and calcareous nannoplankton in the modern ocean can be found in tropical oligotrophic ocean gyres, as there, the vertical stratification of surface water is very strong, with a thickness variation in both thermocline and mixed layer, influenced by latitude and annual cycle of surface wind. The mixed layer and the upper thermocline are

the most densely populated, while living plankton is more or less absent at depths below 1,000 m (Vincent and Berger, 1981; Kucera, 2007). The thermocline can be found below the upper mixed layer of the surface ocean and becomes apparent in a rapid temperature change towards deeper water in shape of a thin layer. It can, but does not have to, lay within the photic zone and can vary within latitude and annual surface wind patterns (Quillévére and Norris, 2003). A study on the distribution of living foraminifera found a very narrow range of average living depth (ALD) of < 50 m for some photosymbiotic species. Subsurface dwellers showed an ALD of > 100 m (Rebotim et al., 2017).

## 2.4 Reproduction of planktic foraminifera

Planktic foraminifera might practise exclusively sexual reproduction, while benthic foraminifera show a more complex life cycle with a multistep sexual and asexual reproduction. For planktic foraminifera, biflagellated isogametes are produced inside the cytoplasm and released species-specifically synchronized in time and space, often in pace with the lunar cycle. This specific accumulation is probably one reason for the foraminifera's preferences for deeper waters instead of shelf areas (Hemleben, 1989; Schmuker, 2000). After the fusion of gametes, the growth of tests is accomplished by addition of chambers, formed by the external rhizopodian network. The empty adult test sinks to the sea floor (details in Hemleben, 1989; Schiebel and Hemleben, 2005; Kucera et al., 2007).

It is almost impossible to determine juvenile tests to the species level; therefore, assemblage census is usually based on larger sizes (> 125µm). It has been under debate whether the ontogenetic stages might be linked to changes in trophic behaviour and hosting symbionts (e.g. Shackleton et al., 1985; Norris, 1996).

## 2.5 Photosymbiosis and stable isotope signal

Planktic foraminifera, which live in the photic zone often inhabit phytoplanktic symbionts (dinoflagellate or chrysophycophyte algae). Such a relationship is beneficial in warm oligotrophic water with sparse nutrient availability but plenty of light: the foraminifera in its calcite shell gains extra energy from the symbiont, which in turn benefits from shelter and protection. The distinctive isotope signature allows to identify whether or not tests hosted photosymbiotic algae and can be used as a valid proxy (Norris, 1996). The photosymbiotic activity of Paleocene species was assumed by analogy with modern foraminifera (Quillévére et al., 2002).

Typical proofs for a photosymbiotic nutrition are:

1.  $\delta^{13}\text{C}$  values are most positive compared to coexisting species due to preferred uptake of  $^{12}\text{C}$  of the symbiont, leading to  $^{13}\text{C}$  enrichment in the host, used for calcification. In addition, the  $\delta^{18}\text{C}$  signal is algae-induced species-specific (dinoflagellates, chrysophytes) as dinoflagellate symbionts show much more positive  $\delta^{18}\text{C}$  values than chrysophyte hosts (Hemleben et al., 1989). Then, the surface water environment of photosymbiotic foraminifera might be locally enriched in positive  $\delta^{18}\text{C}$  due to their metabolism (Spero and DeNiro, 1987).

2. Due to warmer surface water temperatures  $\delta^{18}\text{O}$  are the more negative than any coexisting species within one sample.  $\delta^{18}\text{O}$  values in photosymbiotic foraminifera are very low in consequence of the warmer surface water signal than within asymbiotic planktic foraminifera. There is no correlation between  $\delta^{18}\text{O}$  and increasing size in photosymbiotic planktic foraminifera, presumably because of a light-obliged life through all stages (Norris, 1996; Berggren and Norris, 1997).

The rather high  $\delta^{13}\text{C}$ /low  $\delta^{18}\text{O}$  signature is explained with the fact that the main calcification phase (adolescence and adult stages) took place in a photosymbiotic niche in upper, light flooded water columns.

Further indications are

3. a flat relationship between size and  $\delta^{18}\text{O}$ . Also, a very negative  $\delta^{18}\text{O}$  hints towards the surface ocean (Norris, 1996);
4. a positive correlation between increased  $\delta^{13}\text{C}$  and test size, related to higher algae activity and enhanced density of symbionts with bigger sizes (Spero and Lea, 1993), called the metabolic effect (D'Hondt and Zachos, 1993; Figure 6). Symbiont bearing foraminifera tend to build up larger tests to maximize the symbiont density (Spero and DeNiro, 1987);
5. a large range of  $\delta^{13}\text{C}$  values (Berggren and Norris 1997).

Some living foraminifera are facultatively symbiont-bearing and it is assumed, that photosymbiotic species have a juvenile asymbiotic trophic behaviour (e.g. Shackleton et al., 1985), which makes the interpretation of the  $\delta^{18}\text{C}$  signal more complicated. Many species seem to vary in their depth or even climatic habitat over their life cycles (Emiliani 1954; Shackleton et al. 1985; Berger et al. 1978; Douglas and Savin 1978; Corfield and Cartlidge 1991; Spero et al, 2003).

Based on the assumption that smaller tests represent juvenile ontogenetic stages with a putatively non-photosymbiotic nutrition, only tests with a diameter of  $> 150 \mu\text{m}$  (sieve separation) are used for measurements for environmental interpretations so that this metabolic effect and the supposedly enhanced kinetic fragmentation might be avoided. The fractionation effect is decreased by a lower growth rate within larger tests. There might be a link between carbon uptake and photosymbiosis in the slope of the  $\delta^{13}\text{C}$ /size curve that could reflect an increased dependency on photosymbiosis during the Early Paleocene (e.g. Kelly et al., 1996; Spero et al., 1997). Evolution of photosymbiosis in planktic foraminifera likely took a step forward during the main radiation of Paleogene planktic foraminifera at the transition between *Praemurica* and *Morozovella* (Norris, 1996; Quillévéré and Norris, 2003). It is accepted that photosymbiosis was already developed in *Praemurica inconstans* and improved in the succeeding *Acarinina*, *Igorina* and *Morozovella* (Birch et al., 2012). By interpretation of isotope signals it was concluded that the general establishment happened 0.9 Ma before the transition between *P. inconstans* and *P. uncinata*. The evolutionary transition from *Praemurica* to *Morozovella* took place during planktic foraminifera zone P2 and might have involved the evolution of the symbiotic ecology (Norris, 1996). The LDE possibly might have been a trigger for optimization of photosymbiosis between dinoflagellates and planktic foraminifera, one of

the major innovations in the ecology of Paleocene planktic foraminifera. This development was reflected in shelf areas (Sprong et al., 2009) but also on the open ocean on a global scale (Jehle et al., 2015). High sampling resolution data from Shatsky Rise Site 1210 shows evidence for photosymbiotic activity in *P. uncinata*, *P. praecursoria* and *P. inconstans*, *Morozovella angulata*, *M. velascoensis*, *M. conicotruncata*, *Igorina albeari* and probably in *Acarinina strabocella* due to their isotope signature (Jehle et al., 2015). The results confirm the presumed metabolic strategies of each species and henceforth give indications towards changes in the symbiont activity during the LDE, confirmed by  $\delta^{13}\text{C}$  and  $\delta^{18}\text{O}$  measurements. Different results were interpreted as linked to different depth habitats and test sizes. Morozovellids mostly reflect the photic zone, whereas *Igorina* and *Praemurica* possibly lived in slightly deeper depths or have had other reasons for the diverging signal. The taxa are very different in size, so that the signal for the small *Igorina* might result from lower symbiont numbers, which would leave a less positive  $\delta^{13}\text{C}$  residuum. The by far larger *Praemurica* might have used a different, less evolved and less effective photosymbiotic metabolism (Quillévére et al., 2001).

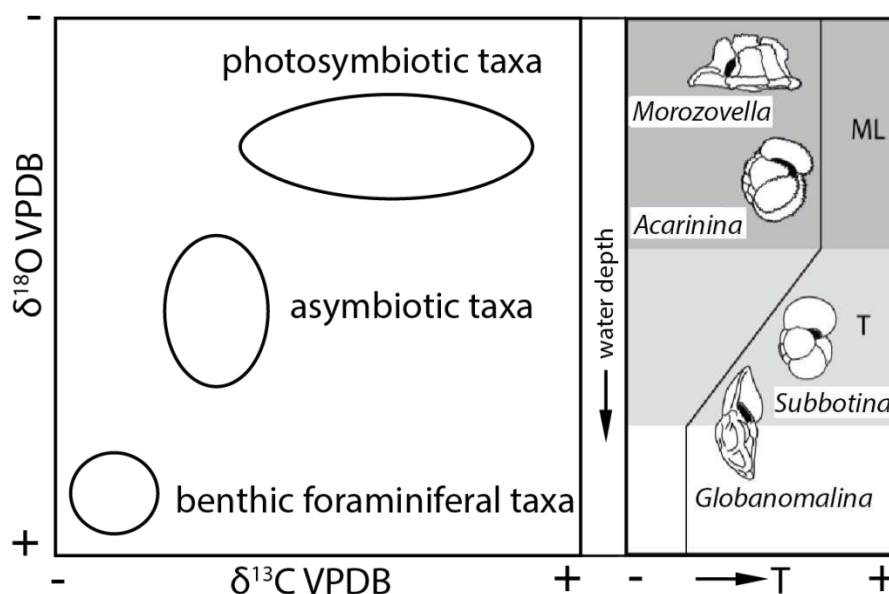


Figure 6: Model for oxygen/carbon variation in symbiotic and asymbiotic species, altered after Norris, 1996 (left). Typical habitats for various planktic foraminiferal species at the D/S transition (61.3–60.9 Ma). ML: Mixed layer, T: Thermocline, depth sizes are not to scale. Adapted from Quillévére and Norris, 2003 (right).

### 3 Paleoclimatic and paleoenvironmental proxies derived from planktic foraminifera

#### 3.1 Planktic foraminifera as paleoceanographic archive

All proxies are linked to the habitat and life cycle of the individual species and must be interpreted separately. Lyell (1837) found empirical use of assemblage data for climate proxies from plants and animals as early as 1830, his principles were applied in consecutive studies for three key assumptions: for (1), climatic factors limit the (co-) occurrences of taxa, (2) taxa evolve climate-related characteristics (e.g. leaf shape), and (3) climatic conditions cause

relative frequency variations in taxa. Applied to foraminiferal assemblages, these methods are spread over into taxonomical and morphological reviews (Vaughan, 2007).

Planktic foraminifera (Figure 7) are among the most important proxies or, in other words, signal carriers in paleoceanographic reconstruction (Pearson, 2012). They are often used for reconstructing paleoceanographic conditions as they archive the chemical and physical conditions under which tests were calcified. The high production, short life-cycle, their usually very well preservation in oceanic sediments, the long fossil record into Jurassic times, opportunistic lifestyle and morphological diversity have made foraminifera a very well-used assemblage and geochemical proxy. The existence of a water column distribution leading to different depth habitats of planktic foraminiferal species is crucial for the understanding of the geochemical record. Influential varying parameters, induced from vertical distribution patterns, which form and control niches, are light intensity, water temperature, food, nutrient and oxygen availability, as well as predation. This, in turn, is reflected in the calcified test. The interpretation of proxies concerning foraminiferal environmental niches is mainly based on spatial and temporal changes in abundance of species or assemblage composition. The usefulness of planktic foraminifera as a recorder of the past oceanic situation depends on insight and understanding of the preferred living conditions (Kucera et al, 2007).

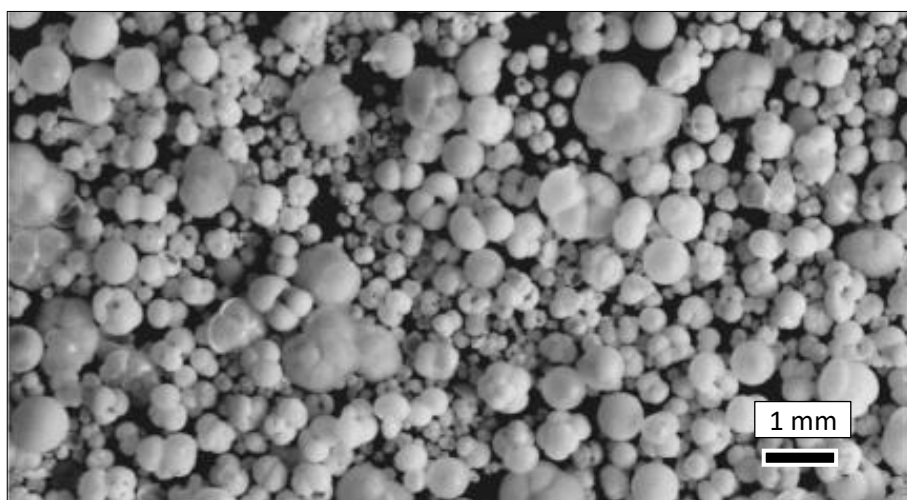


Figure 7: Light microscope picture of the > 63 µm fraction residue from a recent tropical deep-sea sediment sample cycle, dominated by planktic foraminifera. Picture taken by Wilfried Rönfeld (Universität Tübingen), amended from Kucera, 2005.

## 3.2 Geochemical proxies

The importance of foraminiferal calcite as a geochemical recorder has been acknowledged since the 1950ies (Emiliani et al., 1955). There, the first quantitative Pleistocene temperature record based on a  $\delta^{18}\text{O}$  paleothermometer was published. Isotope fractionation or Rayleigh-distillation is a widely-used tool for paleoreconstruction. The operating principles are more thoroughly discussed in e.g. Kendall and Caldwell (1998). Our reconstruction is mainly based on  $\delta^{18}\text{O}$  and  $\delta^{13}\text{C}$  compositions (eq. (I) and (II)) which were derived from calcified benthic and planktic foraminiferal tests. In general, light isotopes are preferably deprived from the pool, so that the remaining product becomes relatively heavier.

$$\delta^{18}\text{O} = \left( \frac{\frac{^{16}\text{O}}{^{18}\text{O}}_{\text{sample}}}{\frac{^{16}\text{O}}{^{18}\text{O}}_{\text{standard}}} - 1 \right) \times 1,000 \text{ ‰} \quad (\text{eq. I})$$

The preferred uptake of light  $^{16}\text{O}$  leads to an enrichment of  $^{18}\text{O}$  in the residing pool, therefore the warmer the temperature, the more fractionation happens, leading to isotopically heavier remaining water. A decrease in  $\delta^{18}\text{O}$  is interpreted as a relative increase in temperature. Besides temperature, other factors influencing the  $\delta^{18}\text{O}$  in the test carbonate include ice volume, salinity, diagenesis and dissolution as well as vital effects. In fact,  $\delta^{18}\text{O}$  data from foraminifera is very applicable for the reconstruction of the global ice volume as well as for the paleotemperature (e.g. Shackleton et al., 1985; Pearson, 2012). Following the calculations of Erez and Luz (1983), in tropical to temperate zones the change of 0.25 ‰ in  $\delta^{18}\text{O}$  corresponds to 1°C change in global sea temperature. Since ice-free poles during the Paleocene were assumed, the ocean was estimated to be 0.9 ‰ lighter than today in terms of  $\delta^{18}\text{O}$  (ice-effect, Shackleton and Kennett, 1975; Shackleton et al., 1985).

The ratio between heavy and light Carbon isotopes ( $\delta^{13}\text{C}$ , eq. (II)) is species-specific and depends on the individual growth rate in foraminiferal tests.

$$\delta^{13}\text{C} = \left( \frac{\frac{^{12}\text{C}}{^{13}\text{C}}_{\text{sample}}}{\frac{^{12}\text{C}}{^{13}\text{C}}_{\text{standard}}} - 1 \right) \times 1,000 \text{ ‰} \quad (\text{eq. II})$$

$\delta^{13}\text{C}$  is controlled by and, hence, a proxy for biochemical fractionation via production and respiration of organic matter, as well as physical fractionation within  $\text{CO}_2$  exchange at the seawater-atmosphere interface and temperature (e.g. Emrich et al., 1970; Hoefs, 1997). A negative carbon isotope excursion (CIE) allows to gather information about short- and long-term developments in nutrient sources, productivity rates, changes in the global carbon pump, deep water circulation or production, connected to burial and oxidation of organic matter and further to get information about addition of carbon from sources such as volcanism or methane release.

During photosynthesis, the lighter  $^{12}\text{C}$  is preferably incorporated by phytosymbionts, which leads to a relative enrichment of the heavier  $^{13}\text{C}$  in the residing carbon pool of the surface oceans and a continuously decreasing gradient of  $\delta^{13}\text{C}$  in the upper 1,000 m of the upper ocean layers (e.g. Krookpnik, 1985). Sinking and flowing water masses accumulate respired  $^{12}\text{C}$ -rich  $\text{CO}_2$ , which is remineralized from settling organic matter. Therefore, younger water (younger last contact to the surface ocean) generally has a higher  $\delta^{13}\text{C}$  level than deep water with longer last contact to the surface or to other sources of  $^{12}\text{C}$ .

The paired combination of  $\delta^{13}\text{C}$  and  $\delta^{18}\text{O}$  (Figure 6) allows us to derive information about the habitat of species (e.g. Wefer and Berger, 1991; Huber et. al., 1995; Norris and Wilson, 1998), salinity, paleo-temperature, habitat depth, water energy or the paleocirculation of oceans (Henderson, 2002). Like depicted below (Figure 6) and mentioned above (Chapter 2.5), low temperature (low/heavy  $\delta^{18}\text{O}$ ) and low/light  $\delta^{13}\text{C}$  indicate deeper living asymbiotic planktic foraminifera. The signal is vice versa for surface dwelling photosymbiotic foraminifera: higher

temperatures (lighter  $\delta^{18}\text{O}$ ) and heavier  $\delta^{13}\text{C}$  is typical within the ocean surface water. These signatures are incorporated during the main calcification phase.

### 3.3 Planktic foraminifera assemblage proxies

Proxies derived from planktic foraminifera is a mature field of science (Kucera et al., 2005). Physical properties used for proxies are assemblage counts and census data, which characterize ecosystems, or presence/absence data, which is used for biostratigraphy. Biometric measurements on individual specimens offer insights into ecology, whereas surveys on the taphonomic record are signals for the embedding situation and sea floor chemistry.

Physical property proxies can be obtained in general relatively easily and with high precision (Kucera et al., 2007). Foraminiferal proxies are often based on ecologically significant indicator species. Each indicator species has the need or preference for a certain ocean depth for their reproduction cycle (e.g. *G. truncaloinoides*, Schiebel and Hemleben, 2005), upwelling systems (*G. bulloides*, Sen Gupta, 2002) or cold-water temperatures (*Neogloboquadrina pachyderma*, e.g. Sen Gupta, 2002). These proxies are not easy to be transferred to deep time like the Paleocene, but some indicator species are detected. Absolute values of assemblage proxy signals are often avoided; however, relative qualitative interpretations tend to be strong enough for Paleocene predictions.

## 4 Origin of the studied sediment material and methods

### 4.1 Method overview

All samples were taken from deep-sea sites, drilled by the Ocean Drilling Program (ODP) and the Integrated Ocean Drilling Program (IODP) between 1988 and 2012.

The samples were processed following standard treatment. Methods are outlined in each chapter (Ch. II–IV) in higher detail. Generally, the sediment was investigated in aspects of:

- XRF core scanning (published and own data), planktic and benthic foraminifera assemblage count data,
- geochemistry:  $\delta^{13}\text{C}$  and  $\delta^{18}\text{O}$  bulk stable isotopes as well as shell  $\delta^{13}\text{C}$  and  $\delta^{18}\text{O}$  of benthic and planktic surface as well as planktic subsurface dwellers,
- $\text{CaCO}_3$  content, TOC and TC,
- Scanning Electron Microscope (SEM) pictures.

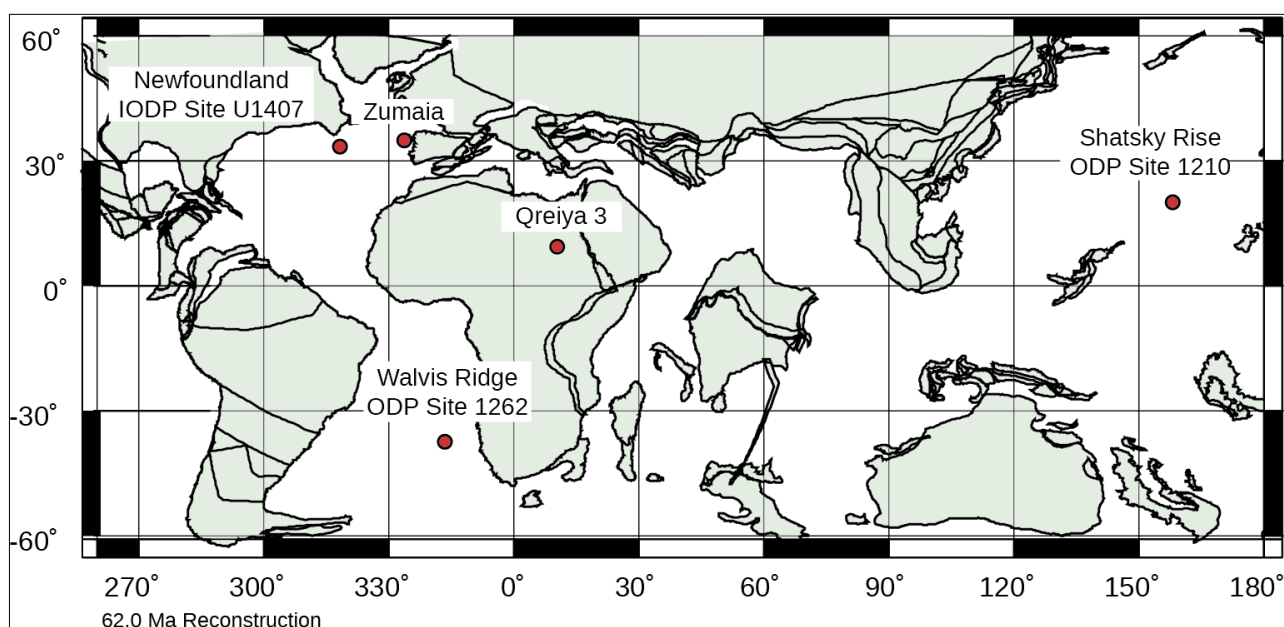


Figure 8: Reconstructed paleo-map and observed sites, generated by: <http://www.odsn.de/odsn/services/paleomap/paleomap.html> (Hay et al., 1999).

## 4.2 Studied sites

### 4.2.1 Shatsky Rise

Sediment from ODP Site 1210 (32° 13.41 N, 158° 15.564 E; Figure 8) was drilled in 2,573 mbsl (meters below sea-level) in 2001. Paleodepth is estimated to ~2,000-2,500 mbsl based on benthic foraminiferal assemblages (Bralower et al., 2002; Dutton et al., 2005; Deprez et al., 2017). The site is located on the southern part of the Shatsky Rise Plateau which was formed during Late Jurassic and Early Cretaceous (149–135 Ma) as large igneous province, situated on a triple-junction in the Pacific Ocean (Bralower et al., 2002). During Cretaceous and Paleogene, it was positioned close to the equator (paleolatitude: ~24° N, Torsvik et al., 2012; van Hirsbergen et al., 2015) and shifted in north-western direction with changing velocities. The study interval at ODP Hole 1210A covers 5.1 meters of core 23H sections 1–4 (231.4–236.6 rmcd, revised meters composite depth, Westerhold et al., 2005). Two prominent dark brown horizons are intercalated into the monotonous calcareous ooze sequence representing the Latest Danian Event (233.4–234.6 rmcd). The key interval is about 0.5 m thick. Below the first event bed at 243.4 rmcd, the colour is darker and turns much lighter above the LDE. Sample resolution is up to 1.5 cm in the key interval.



### 4.2.2 Walvis Ridge

ODP Site 1262 (position today: 27° 11.15'S, 1° 34.62'E, 4,755 mbsl drilling depth; Figure 8) had a Paleocene latitude of ~37° S (Zachos et al., 2004; Kent and Irving, 2010) in the Angola Basin, where sediments were deposited at a paleodepth of estimated ~3,300 mbsl, based on a thermal subsidence model and benthic foraminiferal assemblages (Zachos et al., 2004). This site is situated in the transition from the Angola Basin to the Walvis Ridge. Walvis Ridge is a ~3,000 km long volcanic mountain chain in South-West to North-East direction and elevates up to 200 mbsl from a deep-sea depth of ~5,000 m. Paleocene sediments are predominantly composed of calcareous nannofossil ooze with cyclic variations in sediment lightness and geochemistry, representing a response to orbital forcing (Westerhold et al., 2008).

Samples of Leg 208, Site 1262 were taken from hole C in core sections 10, 2-4 (169.75–174.75 mbsf) and from hole B in core sections 20 1-7 (172.7–181.15 mbsf) in 2 to 50 cm steps with highest resolution around the LDE.

### 4.2.3 Newfoundland

South Eastern Newfoundland Ridge Site U 1407 (SENR) cores were drilled in 3,073 mbsl at 41°25.50'N, 49°48.80'W (Figure 8). The estimated paleodepth is ~1,800 m (Norris et al., 2014) at paleolatitude of ~36°N (Torsvik et al., 2012; van Hirsbergen et al., 2015). It is located at the south eastern crest of Newfoundland Ridge, ~650 km off the Newfoundland coastline. The ridge is part of a transform margin, formed during the opening of the northern Atlantic Ocean, therefore the south eastern part consists as a fracture zone in the oceanic crust (Le Pichon et al., 1977). During Barremian to Aptian ages (~130–115 Ma), the crest was supposedly not covered by water and subsided thereafter as confirmed by reef-like structures (Tucholke and Vogt, 1979). White nannofossil chalk with foraminifera built up the sediments of the Early Paleocene. Due to redistribution by currents the sediment shows some local erosion and irregular, non-connected distribution.

Samples were taken at Bremen Core repository with 0.1–0.93 m spacing from cores 1407 C 20 3-4 (179.39–180.32 CSF-A) and 1407 A 22 3-5 (176.9–181.7 CSF-A), again, highest sample density is around the event.

### 4.2.4 Qreiya

Site Gebel Qreiya 3 is located close to the southern tip of Gebel Qreiya (26°27.702'N, 33°1.905'E (Figure 8), covering a lower Danian to Ypresian succession with a total thickness of ~100 m. The water paleodepth was estimated to 150–250 m (Bornemann et al., 2009; Sprong et al., 2011) and the paleolatitude of ~9°N (Torsvik et al., 2012). The area is part of the Eastern Desert and of the southern Tethyan shelf. The regional Paleocene section is known as Esna shales and has a uniform lithology of greenish-grey shale. Lithostratigraphically the beds are part of the Dakhla Formation, which consists of monotonous brownish to grey marls and shales and intercalated thin marly limestone beds (Said, 1990).

Samples for assemblage data were taken with 0.15–1.20 m spacing.

## 5 Motivation and research questions

For the first time, late Danian planktic foraminifera from different marine settings were studied in high resolution and allow for unravelling detailed trends of planktic foraminiferal evolution and the upper ocean structure during that time.

The primary focus was to test the hypothesis whether the LDE represents a Paleocene transient warming event of global extent in different marine habitats and to which extend biotic responses of planktic foraminifera took place. Before this study started, the LDE was scarcely understood in deep-sea settings regarding planktic foraminifera and the temperature evolution of the surface ocean.

As hyperthermal events are identified by temperature change, negative CIE and biotic reactions, this work addressed the following questions and issues:

- (1) Did the LDE affect both the sea floor and the surface ocean? This was tested by comparing  $\delta^{18}\text{O}$  and  $\delta^{13}\text{C}$  of planktic (surface and subsurface taxa) and benthic foraminifera.
- (2)  $\delta^{18}\text{O}$  of benthic and planktic foraminiferal carbonate during the LDE interval was used as a paleothermometer. By analysing foraminiferal test carbonate from the surface and subsurface ocean as well as the sea floor, temperature changes of the three main habitats of the open ocean were explored.
- (3) A negative CIE ( $\delta^{13}\text{C}$ ) in foraminiferal carbonate was measured for unravelling environmental perturbations in the open ocean and to identify habitat and trophic behaviours of certain species and changes therein.
- (4) How did planktic foraminifera faunas respond to warming and accompanied environmental perturbations during the LDE? Samples were analysed on assemblage composition with occurrence, abundance and disappearance of species in order to reconstruct changes under the prevailing Paleocene conditions. The analysis of planktic foraminifera from different water depths offer insights into the variation within habitats.
- (5) Different deep-sea sites show spatially diverse reactions to the LDE. In order to investigate the global importance of the LDE, planktic foraminiferal assemblages were analysed from three deep-sea cores (Shatsky Rise, Walvis Ridge and Newfoundland Ridge) covering different ocean basins as well as the Tethyan shelf (Qreiya 3, Egypt).
- (6) Ambiguities in the age calibration of the biostratigraphic marker *Igorina albeari* were found during the assemblage analysis of ODP Sites 1210 and 1262. The species was found in up to ~400 ky older sediment than expected. As the the stratigraphic position of the LDE was classically defined by the P3a/P3b planktic foraminifera Subzone boundary, this observation might have an impact on the standard mid-Paleocene biostratigraphic zonation scheme.
- (7) Finally, it was intended to evaluate whether the observed biotic changes represent a short-term impact, i.e. a direct response to the LDE or a long-term phenomenon.

## Chapter II: The impact of the Latest Danian Event on planktic foraminiferal faunas at ODP Site 1210 (Shatsky Rise, Pacific Ocean)

Published as:

Jehle, S., Bornemann, A., Deprez, A. and Speijer, R.P., 2015. The Impact of the Latest Danian Event on Planktic Foraminiferal Faunas at ODP Site 1210 (Shatsky Rise, Pacific Ocean). PLoS ONE. 10 (11), e0141644

### Abstract

The marine ecosystem has been severely disturbed by several transient paleo-environmental events (<200 kyr duration) during the early Paleogene, of which the Paleocene-Eocene Thermal Maximum (PETM, ~56 Ma) was the most prominent. Over the last decade a number of similar events of Paleocene and Eocene age have been discovered. However, relatively little attention has been paid to pre-PETM events, such as the “Latest Danian Event” (“LDE”, ~62.18 Ma), specifically from an open ocean perspective. Here we present new foraminiferal isotope ( $\delta^{13}\text{C}$ ,  $\delta^{18}\text{O}$ ) and faunal data from Ocean Drilling Program (ODP) Site 1210 at Shatsky Rise (Pacific Ocean) in order to reconstruct the prevailing paleoceanographic conditions. The studied five-meter-thick succession covers ~900 kyr and includes the 200-kyr-lasting LDE. All groups – surface dwelling, subsurface dwelling and benthic foraminifera – show a negative  $\delta^{13}\text{C}$  excursion of >0.6 ‰, similar in magnitude to the one previously reported from neighboring Site 1209 for benthic foraminifera.  $\delta^{18}\text{O}$ -

inferred warming by 1.6 to 2.8°C (0.4–0.7‰  $\delta^{18}\text{O}$  measured on benthic and planktic foraminiferal tests) of the entire water column accompanies the negative  $\delta^{13}\text{C}$  excursion. A well stratified upper ocean directly before and during the LDE is proposed based on the stable isotope gradients between surface and subsurface dwellers. The gradient is less well developed, but still enhanced after the event. Isotope data are supplemented by comprehensive planktic foraminiferal faunal analyses revealing a dominance of *Morozovella* species together with *Parasubbotina* species. Subsurface-dwelling *Parasubbotina* shows high abundances during the LDE tracing changes in the strength of the isotope gradients and, thus, may indicate optimal living conditions within a well stratified surface ocean for this taxon. In addition, distinct faunal changes are reported like the disappearance of *Praemurica* species right at the base of the LDE and the continuous replacement of *M. praeangulata* with *M. angulata* across the LDE.

# 1 Introduction

Over the past two decades, a series of short-term warming events (<200 kyr) have been documented for the early Palaeogene (c. 66–48 Ma, e. g. Lourens et al., 2005; Zachos et al., 2008; Sexton et al., 2011). Many of these events have in common that they are associated with abrupt perturbations of the global carbon cycle as reflected in the  $\delta^{13}\text{C}$  of inorganic and biogenic carbonates as well as of terrestrial and marine organic matter, an accompanying temperature rise and extreme biotic responses. The most prominent of these events is the Paleocene-Eocene Thermal Maximum (PETM; 56 Ma; e. g., (Kennett and Stott, 1991; Sluijs et al., 2007). This event is characterized by (a) a short-lived 170–230 kyr lasting, negative  $\delta^{13}\text{C}$  excursion (CIE) between 1 and 5 ‰ (e. g. Röhl et al., 2007; McInerny and Wing, 2011), (b) global warming of several degrees as indicated by temperature-sensitive proxies like  $\delta^{18}\text{O}$ , Mg/Ca or TEX<sub>86</sub> (Sluijs et al., 2007), (c) a drop of CaCO<sub>3</sub> in deep-sea sediments and a shallowing of the lysocline/CCD probably due to ocean acidification (Zachos et al., 2005), and (d) a major extinction of deep-sea benthic foraminifera and changes in organic dinoflagellate, larger foraminifera, ostracoda and calcareous plankton communities (e. g. Kelly et al., 1996; Crouch et al., 2001; Bralower, 2002; Thomas, 2003; Speijer et al., 2012). The strong negative CIE indicates that the amount of isotopically light carbon added to the global carbon cycle, possibly derived from methane hydrates, is to some extent comparable to the present day input of carbon to the atmosphere through combustion of fossil fuels. Thus, the PETM is sometimes considered as a deep-time analogue to rapid climate change as is expected for the near future (e. g. Zachos et al., 2008; Ridgwell and Schmidt, 2010; Masson-Delmotte, 2013).

Recent studies have revealed that the PETM may not have been a single event. Similar events of Paleocene age are the Dan-C2 Event (65.2 Ma ago, Quillévéré et al., 2008), the Latest Danian Event (LDE) or Top Chron C27n Event (62.18 Ma, e. g. Bornemann et al., 2009; Westerhold et al., 2011; Dinares-Turell et al., 2012; 2014), and the Mid- Paleocene Biotic Event (MPBE, 58.9 Ma, e. g. Petrizzo, 2005; Bernaola et al., 2007).

The LDE is characterized by a prominent negative  $\delta^{13}\text{C}$  excursion of at least 0.7 ‰ in different marine settings like the southern Tethyan shelf (Egypt, Bornemann et al., 2009), the northern Tethys (Bjala, Bulgaria, Dinares-Turell et al., 2012), the eastern North Atlantic (Zumaia, Spain; Dinares-Turell et al., 2010), and the Pacific Ocean (Westerhold et al., 2011). Moreover, the LDE is identified by the most negative  $\delta^{13}\text{C}$  values for the entire Paleocene, thus, representing an extreme position in the secular changes of the global carbon cycle (Westerhold et al., 2011, Figure 9). Similar to other Paleogene hyperthermals the negative  $\delta^{13}\text{C}$  excursion might be attributed to the addition of huge amounts of  $^{13}\text{C}$  depleted carbon to ocean and atmosphere. Accompanied warming might be explained either by the possibility of high atmosphere greenhouse gas concentrations similar to the PETM or increased insolation due to the orbital constellation (PC<sub>40510</sub>; Dinares-Turell et al., 2014) during the upper Chron C27n. Further, the LDE falls within a time interval with an increase of oceanic spreading rates and volcanic activity along the SE Greenland margin (Speijer et al., 2003; Westerhold et al., 2008).

In various Ocean Drilling Program (ODP) cores this event is marked by two prominent peaks in Fe intensities based on XRF core scanning (Figure 9) and magnetic susceptibility. According to orbital tuning the two LDE peaks correspond to two short eccentricity cycles suggesting a total duration of 190–200 kyr (Westerhold et al., 2008; Dinares-Turell et al., 2012; Figure 9).

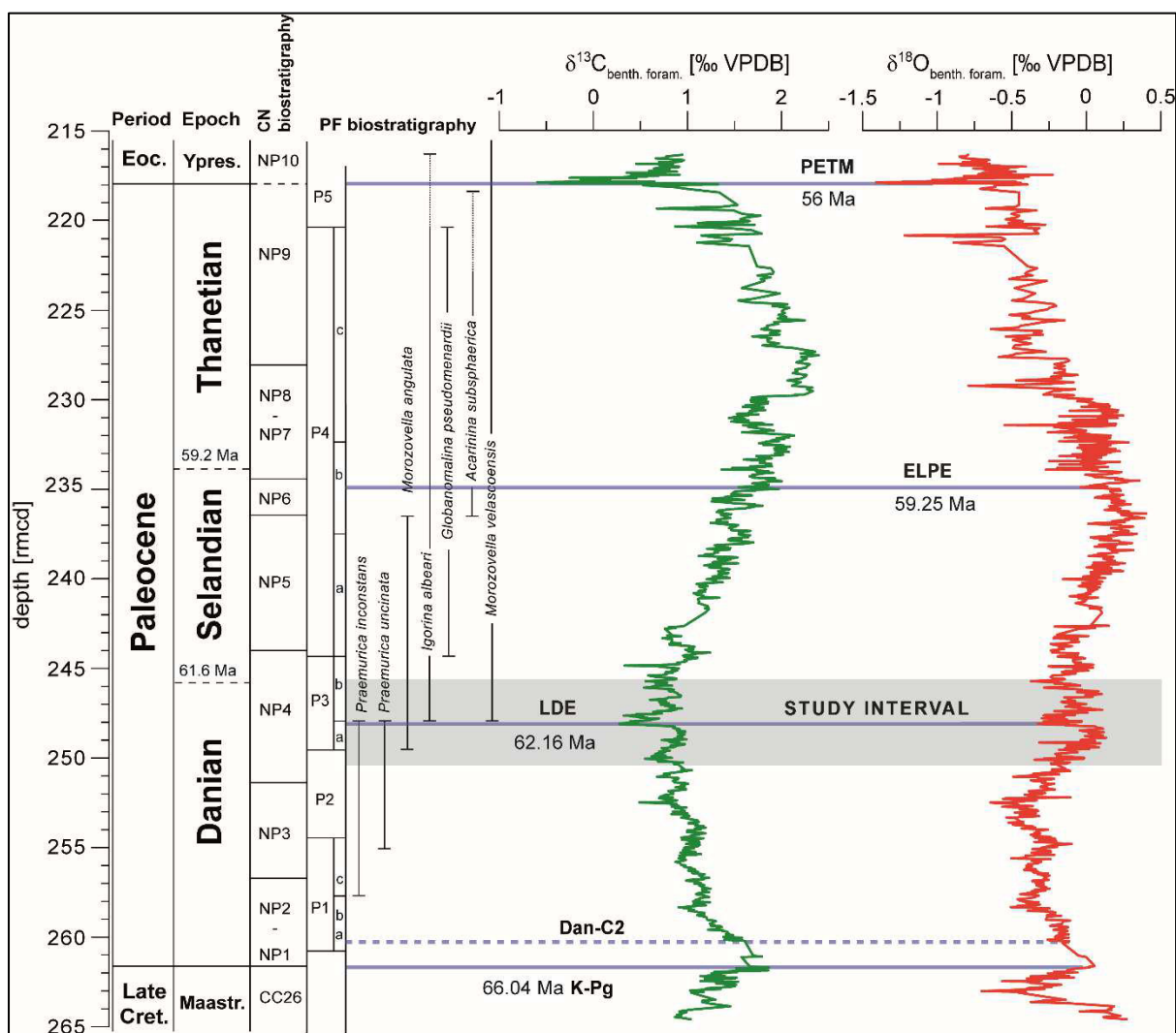


Figure 9: Stratigraphy,  $\delta^{13}\text{C}$  and  $\delta^{18}\text{O}$  measurements of benthic and planktic foraminifera on ODP Site 1209:  $\delta^{13}\text{C}$  (green) and  $\delta^{18}\text{O}$  (red) in a long-term benthic *Nuttallides truempyi* record (plotted against rmcd after Westerhold et al. (2011)). Period, epoch, Calcareo nannofossil, polarity chron, age and Planktic foraminifera biostratigraphy are from Petrizzo et al. (2005) and Westerhold et al. (2011), isotope data are adopted from Westerhold et al. (2011). Absolute ages given are based on (GTS 2012, Dinares-Turell et al., 2012).

Due to the supra-regional nature of the LDE, the associated paleoenvironmental changes (e. g. oligotaxitic benthic foraminiferal assemblages, poor oxygenation of the seafloor on the Southern Tethyan shelf) that resemble those of the PETM (Speijer, 2003; Bornemann et al., 2009; Shulte et al., 2013) and benthic foraminiferal  $\delta^{18}\text{O}$  data from nearby ODP Site 1209 (Westerhold et al., 2011) suggesting a bottom-water temperature rise of  $\sim 2^\circ\text{C}$  (Figure 9), it has been hypothesized that the LDE might represent a Paleocene hyperthermal. In addition, biotic changes are associated with the LDE interval. Similar to the PETM at the C27n–C26r transition major turnovers of land mammals have been observed in China and North America (Clyde et

al., 2008; 2010). In the marine realm the LDE coincides with an interval of major diversification events in calcareous plankton groups suggesting re-organization of the surface oceans ecosystem. This also includes the evolutionary changes of the muricate *Acarinina* and *Morozovella* lineages in planktic foraminifera (e. g. Kelly et al., 1996; Quillévére et al., 2002), and a major radiation event of fasciculithids (e. g. Fuqua et al. 2008; Aubry et al.; 2012; Monechi et al., 2013). However, all these studies are based on rather long-term records with a limited temporal resolution. So far, no detailed planktic foraminiferal data are available for the LDE from the deep-sea. Here we present the first high-resolution planktic foraminiferal faunal data across this event from ODP Site 1210 (Shatsky Rise).

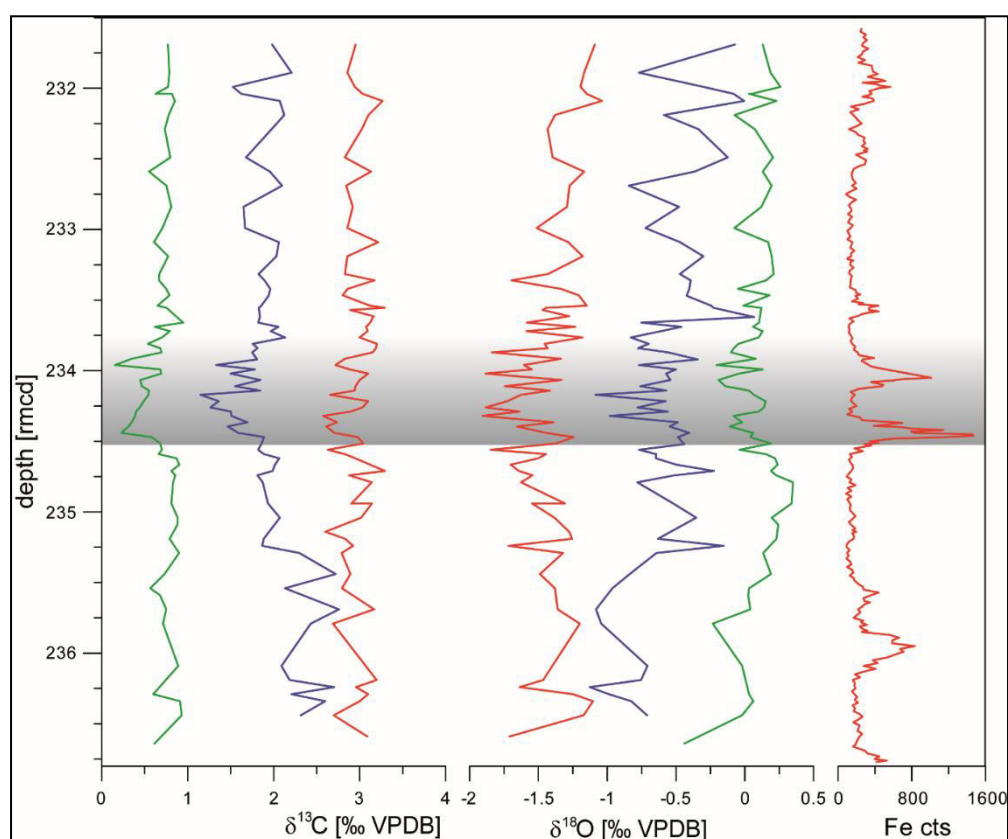


Figure 10:  $\delta^{13}\text{C}$  and  $\delta^{18}\text{O}$  of benthic (green), planktic subsurface (blue) and surface (red) foraminifera in comparison to XRF measured Fe counts for chemostratigraphic correlation. The LDE is marked in grey.

Since planktic foraminifera are an important component of the marine food web as primary or secondary consumers they are highly sensitive to paleoceanographic changes and should respond to environmental perturbations (e. g. Kucera and Schönfeld, 2007).

In this paper we investigate for the first time changes in the community structure of planktic foraminiferal assemblages as a response to environmental changes during the LDE. Further, we test the hypothesis whether the LDE represents a transient warming event by analyzing  $\delta^{18}\text{O}$  and  $\delta^{13}\text{C}$  of benthic and planktic foraminifera, in order to gain insight into the evolution of the vertical ocean structure and other paleoenvironmental parameters. We further assess the degree of  $\text{CaCO}_3$  dissolution related to the LDE by analyzing the sedimentary  $\text{CaCO}_3$  content, percentage planktic foraminifera (%P), coarse fraction, and employ a planktic foraminiferal fragmentation index.

## 1.1 Geological setting

Shatsky Rise Plateau is a large igneous province situated on a triple-junction in the Pacific Ocean, formed in Late Jurassic to Early Cretaceous times (149–135 Ma; Sager, 2005; see Figure 11). The plateau was then located close to the equator and drifted to the Northwest with changing velocities during the Cretaceous and the Paleogene. Shatsky Rise possibly crossed the equator during the Maastrichtian. Rates of subsidence and drifting were faster during the Jurassic–Cretaceous boundary interval and slowed down with time (Bralower, 2002).

ODP Leg 198 Site 1210 (lat: 32.2235°N, long: 158.2594°W) is situated on the southern part of the Shatsky Rise Plateau and was drilled in 2001 at a water depth of 2573 mbsl (meters below sea level). Paleodepth has been estimated as upper abyssal to lower bathyal (Bralower, 2002). Neighboring ODP Site 1209 likely rose from a paleodepth of ~2500 mbsl to 2387 mbsl today (Dutton et al., 2005), which suggests ~2700 m as paleodepth for Site 1210 assuming a uniform uplift of the plateau (Larson et al., 1992).

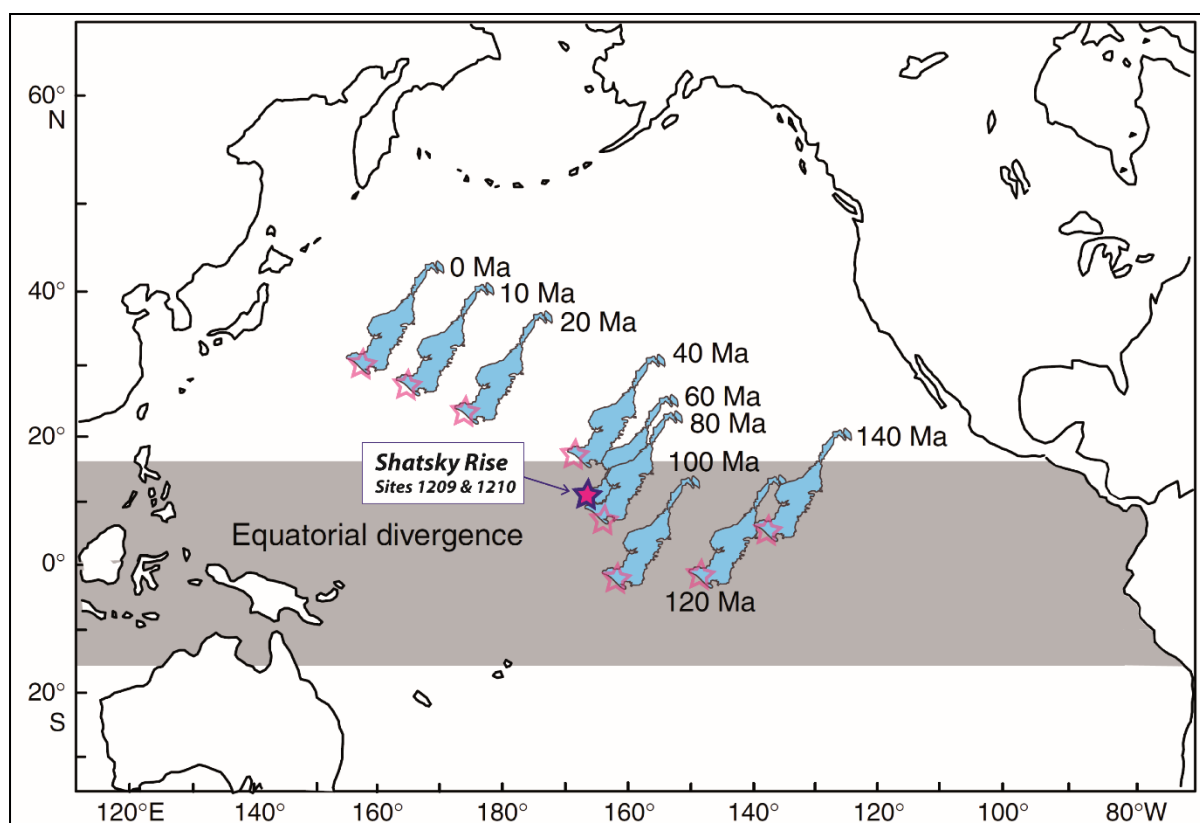


Figure 11: Pacific centered map of the Shatsky Rise (amended after Bralower et al. (2002)). ODP Sites 1209 and 1210 are marked by purple stars. Due to plate tectonic movements, the Shatsky Rise Plateau shifted north-westwards over the last 140 Myr. The blue framed star shows the studied site during the middle Paleocene (~60 Ma).

## 1.2 Lithology

The more than 100-m-thick sedimentary succession of Paleogene age (base Paleocene to early Oligocene) at Site 1210 shows in general higher carbonate values and offers shades of orange and yellowish brown nannofossil ooze, nannofossil ooze with clay and minor amounts of clay with nannofossil ooze (Figure 12). A remarkable similarity in the lithologic record between Sites 1209 and 1210 seems to be evident (Bralower et al., 2002). The study interval at ODP Hole 1210A covers 5.1 meters of core 23H sections 1–4 (231.4–236.6 rmcd, revised meters composite depth, Westerhold et al., 2005). Two prominent dark brown horizons are intercalated into the monotonous calcareous ooze sequence representing the Latest Danian Event (233.4–234.6 rmcd). This key interval is about 0.5 m thick. Below the first event bed at 243.4 rmcd the color is darker and it becomes much lighter above the LDE. In addition to these two prominent layers, three less pronounced darker beds are intercalated into this succession (at ~236 rmcd, at ~233.6 rmcd right above the LDE, and at 232 rmcd below it; Figure 12).



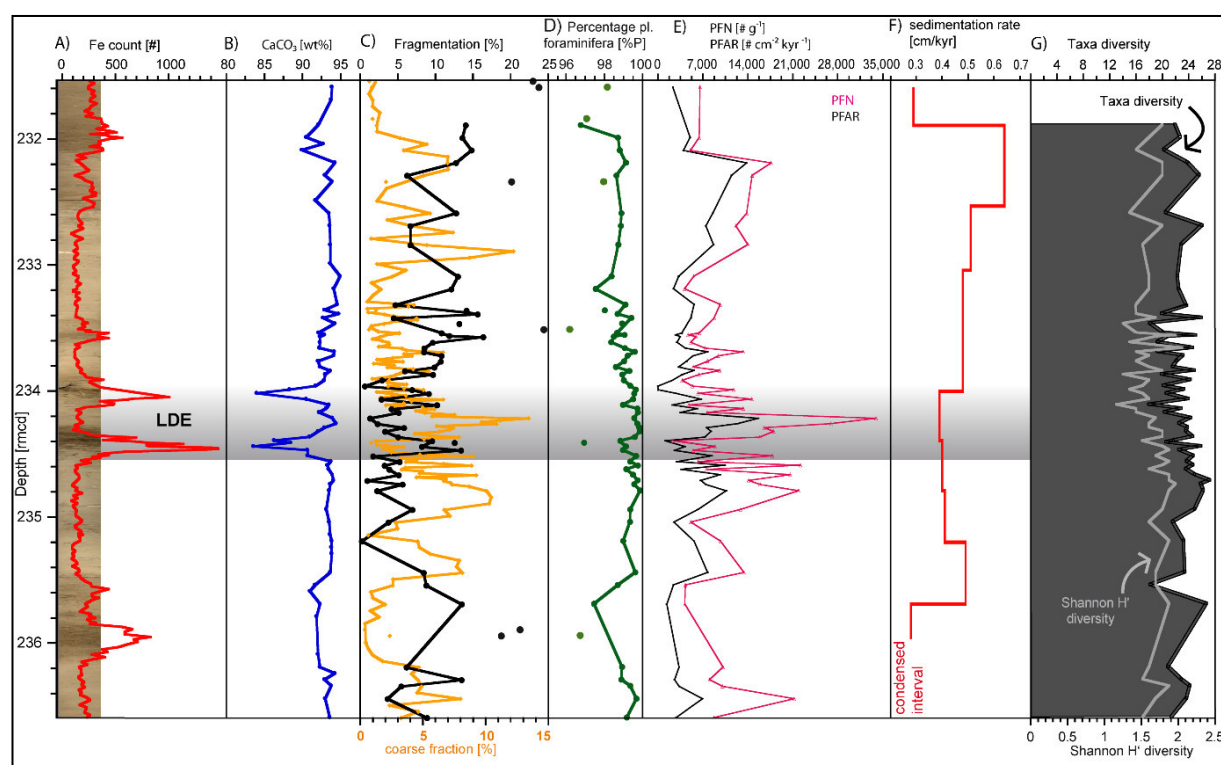


Figure 12: Sedimentary and other parameters of Site 1210. The LDE is marked in grey. **A)** Biostratigraphy and Fe XRF core scanning data overlying the sediment core photo. The two main peaks mark the LDE and are used for stratigraphic correlation. The LDE interval covering the XRF Fe peaks are marked by a blue bar. The misfit between XRF core scanning Fe peaks and lithology is most likely an artifact of core expansion in storage. **B)**  $\text{CaCO}_3$  data. **C)** Coarse fraction (orange) and fragmentation (black) show opposing trends. **D)** Percentage of planktic foraminifera [%P] (green) shows only little variation below 100% with minima close to Fe maxima. For **C)** and **D)**: Data points marked as single symbols represent samples that have been excluded from faunal assemblage analyses due to potential diagenetic alteration. **E)** The amount of planktic foraminifera per g sediment (PFN [#  $\text{g}^{-1}$ ], pink) has a minimum close to the first LDE peak and a maximum shortly thereafter, however, the variability of planktic foraminiferal accumulation rates (PFAR, black, [#  $\text{cm}^{-2} \text{kyr}^{-1}$ ]) is much lower than the absolute abundance of planktic foraminifera per gram sediment. **F)** Sedimentation rate according to Westerhold et al. (2008) based on the presented cyclostratigraphy therein. **G)** Simple diversity (grey) and Shannon  $H'$  diversity (black line with a dark grayish background) both indicate a slight decrease during the LDE interval.

### 1.3 Stratigraphy

Synonymously to the Latest Danian Event (LDE, Bornemann et al., 2009) the term “Top Chron C27n Event” is often used (Westerhold et al., 2011; Dinares-Turell et al., 2010; Westerhold et al., 2008) indicating the magnetostratigraphic position of this event as observed at stratigraphically well-calibrated ODP Site 1262 (Walvis Ridge; Westerhold et al., 2008) and Zumaia (Spain; Dinares-Turell et al., 2010; 2012). The latter represents the Global Stratotype Section and Point (GSSP) for both base and top of the Selandian Stage (Schmitz et al., 2011). However, no reliable magnetostratigraphy exists for the study interval at Site 1210, but supra-regional chemo- and cyclostratigraphic correlation supports the same stratigraphic position of the LDE at Sites 1209 and 1210 (Westerhold et al., 2008). In many deep-sea sections the LDE is characterized by two distinct peaks in magnetic susceptibility and Fe XRF core scanning data, which are paralleled by a prominent ( $\sim 0.7\%$ ) negative CIE in benthic foraminifera

(Petrizzo et al., 2005; Westerhold et al., 2011). The two prominent Fe peaks of the LDE have also been observed at ODP Site 1210 (Figure 10, Figure 12). The very similar pattern in XRF measurements allows to apply the astronomically-tuned 1209 age model to Site 1210 (Westerhold et al., 2008).

Recent studies propose that the LDE coincides with 405 kyr-precession cycle 10 (Dinares-Turell et al., 2014; Hilgen et al., 2015). Based on such a correlation we infer that the study interval covers ~900 kyr and pinpoint the largest and lowest LDE Fe peak at 234.45 rncd to an absolute age of 62.18 Ma, just before the Danian-Selandian boundary at 61.61 Ma as suggested by Dinares-Turell et al. (2014) and Vandenberghe et al. (2012). Biostratigraphically, the LDE is positioned with its lowest XRF Fe peak close to the P3a–P3b planktic foraminiferal subzonal boundary and within the NTp7B and NP4 nannofossil zones (Dittert et al., 2009).

## 2 Methods

Seventy-three samples were taken at a resolution of 2 to 15 cm with the highest resolution across the assumed LDE. All samples were approved and provided by the International Ocean Discovery Program (IODP) Gulf Coast Repository (College Station, Texas, USA). No further specific permissions were required for the studied location. The performed study did not involve endangered or protected species. Sample material is stored at the geological collections of the Institute for Geophysics and Geology, University of Leipzig.

The samples were studied with respect to  $\delta^{13}\text{C}$  and  $\delta^{18}\text{O}$  of planktic and benthic foraminifera,  $\text{CaCO}_3$  content, planktic foraminiferal assemblages, percentage of planktic foraminifera and other parameters like fragmentation, coarse fraction, absolute abundances per gram sediment (planktic foraminiferal number, PFN). In addition, planktic foraminiferal accumulation rates (PFAR) have been calculated using the published age model (Westerhold et al., 2008) and shipboard dry bulk density data (Bralower, 2002).

Sediment samples were oven-dried at 40°C for at least 48 hours. The sediment was weighed and soaked in tap water. In some samples, the sediment disintegrated within a few minutes and was processed immediately. Samples were washed through a 63- $\mu\text{m}$ -mesh sieve, transferred onto filtering paper with deionized water and a splash of acetone, and then gently dried for at least 48 hours at 40° C.

Coarse fraction is calculated by:

$$\text{CF} = ((\text{dry weight of residuum } >63\mu\text{m}) / (\text{dry weight of total sample})) \times 100 [\%] \text{ (eq. III)}$$

Percentages of planktic foraminifera (%P) were counted from the >63  $\mu\text{m}$  sieve size fraction and are primarily used to assess dissolution intervals since planktic foraminifera are more prone to dissolution than benthic foraminifera (e. g. Dittert et al., 1999). For faunal analysis, the >125  $\mu\text{m}$  fraction was split into proportions containing 300–600 planktic specimens with a microsplitter and identified under a Zeiss Stemi 2000-C binocular microscope at 50 $\times$  magnification. Planktic foraminiferal taxonomy follows Berggren and Norris (1997) and Olsson et al. (1999).

The fragmentation index was calculated as follows, counting tests larger than half as complete tests and tests smaller than half as fragments in the >125 µm size fraction (Erez and Luz, 1983):

$$F = (\text{no. of fragments}) / (\text{no. of fragments} + \text{no. of complete tests}) \times 100 [\%] \quad (\text{eq. IV})$$

Absolute abundances of planktic foraminifera (PFN, [# g<sup>-1</sup>]) were calculated using dry weight of the sample, number of counted specimens (>125µm) and the applied split-factor. Planktic foraminifera accumulation rate (PFAR) was calculated by dry density (DBD; Bralower, 2002) multiplied with linear sedimentation rate (LSR) as well as abundance per g (PFN):

$$\text{PFAR} = \text{DBD} \times \text{LSR} \times \text{PFN} \quad [\# \text{ cm}^{-2} \text{ kyr}^{-1}] \quad (\text{eq. V})$$

The diversity of planktic foraminiferal assemblages was characterized by species richness (S) and Shannon heterogeneity (H'). The latter one was calculated by using an information function (Shannon and Weaver, 1949) as follows:

$$H' = - \sum_{i=1}^k p_i \times \ln p_i \quad (\text{eq. VI})$$

with  $p_i$  as the proportion of individuals belonging to the  $i^{\text{th}}$  species in the dataset of interest.

For  $\delta^{13}\text{C}$  and  $\delta^{18}\text{O}$  measurements 3 to 7 specimens were reacted with 100% phosphoric acid at 75°C using a Kiel IV online carbonate preparation line connected to a MAT 253 mass spectrometer. Reproducibility was checked by replicate analysis of laboratory standards and was better than 0.05 ‰ and 0.06 ‰ for  $\delta^{13}\text{C}$  and  $\delta^{18}\text{O}$ , respectively. Planktic specimens were picked from the 250–355 µm size fraction. Where this did not yield sufficient material for the analysis, 180–250 µm was used additionally. Benthic foraminifera were mostly picked from 125–180 µm.

We generated stable isotope ( $\delta^{13}\text{C}$ ,  $\delta^{18}\text{O}$ ) records of the best preserved planktic and benthic foraminifera. Bottom water conditions were estimated from analyses of epibenthic *Nuttallides truempyi* and in some samples barren of *N. truempyi*, *N. umbonifera* or *N. truempyi/umbonifera* was used. A t-test was performed on  $\delta^{13}\text{C}$  and  $\delta^{18}\text{O}$  of benthic, subsurface- and surface-dwelling foraminifera comparing the isotope values before, during and after the LDE. Subsurface conditions are inferred from analyses of *Parasubbotina pseudobulloides/variospira* and *P. varianta*, while surface water conditions were determined using *Morozovella angulata*. Further multiple-test measurements were carried out on *Igorina albeari*, *M. velascoensis* and *M. conicotruncata*, *Globanomalina chapmani*, *G. imitata* and *Acarinina strabocella*, *Praemurica praecursoria*, *Pr. uncinata* and *Pr. inconstans* in order to better constrain their depth habitat. Relative temperature changes were estimated based on the calibration equation of Erez and Luz (1983). Calcium carbonate values are derived from measurements carried out with an Elementar III (VARIO Corp.) CNS analyzer.

For the statistical analysis, we used the relative abundances of all samples that have not been excluded due to a potential preservational bias (n=59), see explanation below. In order to analyze changes in the assemblage composition non-metric multidimensional scaling (NMDS) was applied, which is one of the most widely used ordination techniques and one of the most robust unconstrained ordination methods in community ecology (e. g. Jiang et al., 2010; Schneider et al., 2013). We used the “vegan package” for R to run ecological multivariate

statistics. Environmental vectors as represented by the  $\delta^{13}\text{C}$  and  $\delta^{18}\text{O}$  of benthic, subsurface- and surface-dwelling foraminifera, and sedimentary  $\text{CaCO}_3$  have been fitted onto the NMDS ordination. For this the ‘envfit’ function of the vegan package was used in order to test if the vector projections correlate with the gained faunal patterns.

## 3 Results

### 3.1 Carbonate content and dissolution sensitive parameters

$\text{CaCO}_3$  values range from ~84 to 95 wt%, with minima within the two LDE beds with values around 84 wt%. The background values (~94 wt%) are rather uniform (Figure 12). Other carbonate dissolution sensitive parameters (Figure 12) are coarse fraction (CF), fragmentation of planktic species (%F), percentages of planktic species (%P), absolute abundance of planktic foraminifera (>125  $\mu\text{m}$ ) per gram sediment (expressed as planktic foraminifera number, PFN), connected to planktic foraminifera accumulation rate (PFAR, [ $\# \text{cm}^{-2} \text{kyr}^{-1}$ ]), and diversity.

CF percentages vary between 1 and 14% below the LDE, displays three peaks or outliers of 7 to 11% and a minimum at 234.4 rmcd. The fragmentation index (%F) ranges between 0 and 24%, and shows a reversed trend to CF with a maximum of 18% coinciding with the position of the minimum in CF (Figure 12).

PFN (Figure 12) increases to ~34,000  $\# \text{g}^{-1}$  between the lowest and second LDE peak, which is also the highest value within the study interval. A strong minimum is visible concurrent with the lowest LDE iron peak. The background signal varies between 4,000 and 20,000 specimens. PFAR (Figure 12) ranges from 1,115 to 15,612  $\# \text{cm}^{-2} \text{kyr}^{-1}$  and is much smoother than PFN pointing to less substantial variations in the numbers of planktic foraminiferal tests. No significant correspondence to the LDE has been observed there.

Percentages of planktic foraminifera (%P, >63  $\mu\text{m}$ , Figure 10) vary between 96.5 and 100% with three distinct minima: (1) below the LDE (~235.7 rmcd), (2) within the lowest LDE peak (~234.4 rmcd), and (3) at the top of the study interval (~231.9 rmcd). Apart from the drop in one sample within the lowest LDE peak, %P is rather constant with ~ 98.5–99.5% across the entire LDE interval.

Simple diversity (S) varies between 13 and 23 species per sample (Figure 12), Shannon diversity ( $H'$ ) ranges from 1.64–2.47 with an average of 2.08. The lowest diversity for both scales is found at the beginning of the second LDE Fe peak and stays low until 233.5 rmcd after the LDE. Diversity mean is slightly higher before than after the event by 0.1 (2.16 before, 2.09 during and 2.06 after the LDE).

### 3.2 Foraminiferal stable isotopes ( $\delta^{13}\text{C}$ , $\delta^{18}\text{O}$ )

#### 3.2.1 High resolution records of planktic and benthic foraminifera

All three groups, surface dwelling (*Morozovella angulata*, *M. praeangulata*), subsurface dwelling (*Parasubbotina pseudobulloides*, *P. varianta*) and benthic foraminifera (*Nuttallides*

truempyi, *N. umbonifera*, *N. umbonifera-truempyi* intermediate) show negative excursions for both  $\delta^{13}\text{C}$  and  $\delta^{18}\text{O}$  of different amplitudes at the lowest LDE peak (Figure 10).

Species-specific measurements on surface dwelling taxa (*Morozovella angulata*, *M. praeangulata*) range from 2.55 to 3.3 ‰ for  $\delta^{13}\text{C}$  and from -1.9 to -1.2 ‰ for  $\delta^{18}\text{O}$  (Figure 10, Figure 13). Subsurface dwellers (*Parasubbotina pseudobulloides*, *P. varianta*) display values between 1 and 3 ‰ for  $\delta^{13}\text{C}$  and between -1.1 and -0.4 ‰ for  $\delta^{18}\text{O}$ , while  $\delta^{13}\text{C}$  and  $\delta^{18}\text{O}$  values of benthic foraminifera are of 0.2 to 0.9 ‰ and -0.1 to 0.35 ‰, respectively.

At the base of the lowest LDE peak,  $\delta^{13}\text{C}$  drops in planktic surface dwellers by  $\sim 0.7$  ‰ (3.25–2.55 ‰), whereas subsurface ones decrease by  $\sim 0.9$  ‰ (2.1 to 1.2 ‰) and benthic by  $\sim 0.6$  ‰ (0.8–0.2 ‰; Figure 9). Accordingly, a negative carbon isotope excursion (CIE) coincides with the lowest LDE Fe peak. For surface dwelling taxa,  $\delta^{18}\text{O}$  decreases by  $\sim 0.6$  ‰ (-1.3 to -1.9 ‰), at the subsurface ocean by  $\sim 0.5$  ‰ (-0.5 to -1 ‰) and on the sea-floor (benthic foraminifera) by  $\sim 0.4$  ‰ (0.3 to -0.1 ‰; Figure 9).  $\delta^{18}\text{O}$  and  $\delta^{13}\text{C}$  show partly significant differences between before, during and after the event as tested by the two-sided t-test (Table 2, t-test). The development for the  $\delta^{13}\text{C}$ -record is generally more significant than for  $\delta^{18}\text{O}$  except from *M. angulata*, which varies within a smaller range.  $\delta^{18}\text{O}$  shows no or low significant difference for *P. pseudobulloides* and *N. truempyi* between below the event and during the LDE. The t-test results of *P. pseudobulloides* might be influenced by the wide scatter of isotope values influencing the mean, which is compared in the analysis. Same sample segments for the intervals before, during and after the LDE were used for the NMDS analysis.

Table 2: T-test p-values. Numbers marked in bold indicate numbers that are significant on the 95% confidence limit.

	<i>M. angulata</i>		<i>P. pseudobulloides/</i> <i>variospira</i>		<i>N. truempyi</i>	
	Post-event vs. LDE	LDE vs. Pre-event	Post-event vs. LDE	LDE vs. Pre-event	Post-event vs. LDE	LDE vs. Pre-event
N	23/20	20/25	23/20	20/25	26/21	21/24
p-values T-test $\delta^{13}\text{C}$	0.07128	0.54873	<b>0.00020459</b>	<b>4.3639E-07</b>	<b>1.3505E-07</b>	<b>9.523E-08</b>
p-values T-test $\delta^{18}\text{O}$	<b>9.7945E-06</b>	<b>0.03424</b>	<b>0.0003105</b>	0.37363	<b>0.0046499</b>	0.099652

### 3.2.2 Isotope results of selected planktic foraminifera species

$\delta^{13}\text{C}$  and  $\delta^{18}\text{O}$  values of *M. occlusa* are similar to coexisting *M. velascoensis* and *Acarinina mckannai*. *Morozovella velascoensis* and *M. conicotruncata* generally appear in the same range as *M. angulata*, but both with higher  $\delta^{18}\text{O}$  values. *Morozovella velascoensis* values are close to *M. angulata* while *M. conicotruncata* shows a different course for  $\delta^{13}\text{C}$  towards heavier values after the LDE CIE.

*Acarinina strabocella*, measured on only four samples, show lower  $\delta^{18}\text{O}$  before than after the LDE and higher  $\delta^{13}\text{C}$  before than after it. Measurements on *Praemurica inconstans* and *P. praecursoria* show low  $\delta^{18}\text{O}$  values compared to results of *P. uncinata*. *Igorina albeari* reveals values between those of surface and subsurface dwellers but slightly closer to the surface ones (Figure 13). The temporal course continuously parallels *M. angulata* with lower  $\delta^{13}\text{C}$  and higher  $\delta^{18}\text{O}$ .

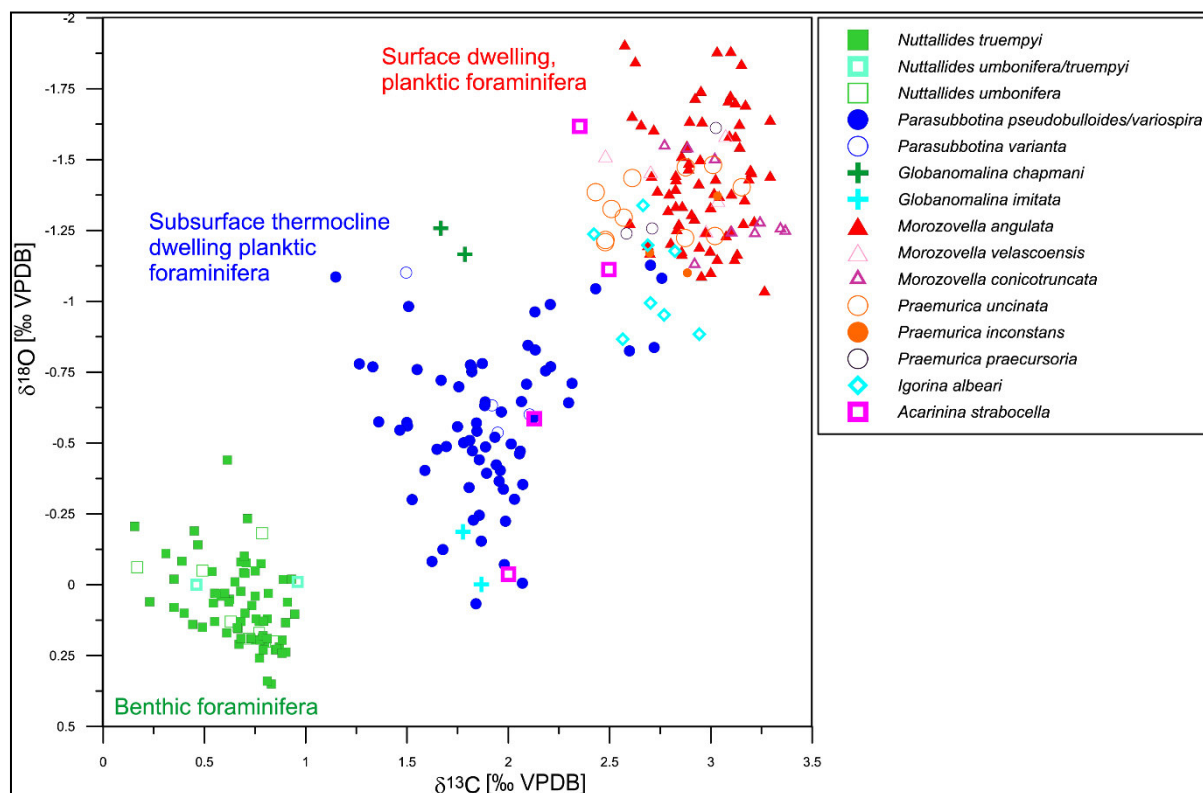


Figure 13:  $\delta^{13}\text{C}$ – $\delta^{18}\text{O}$  plot of foraminiferal isotope measurements. Distinct clusters separate epibenthic (*Nuttallides truempyi*, *N. umbonifera* and intermediate form), planktic subsurface (e. g. *Parasubbotina pseudobulloides/variospira*, *P. varianta*) and surface dwelling taxa (e. g. *Morozovella angulata*). Besides these, isotopic signatures of other taxa were measured to better understand their depth-habitat and paleoecology.

### 3.3 Planktic foraminiferal assemblages

Planktic foraminiferal faunas (Figure 14, Figure 15) are dominated by nine taxa that make up ~86% of the total assemblage. Here they are described in the stratigraphic order of their abundance maxima:

*Praemurica uncinata* is quite common (c. 26% at 236.6 and 235.4 rmcd) before the LDE, but virtually disappears at the base of the LDE. A similar trend is observed for the less abundant *P. inconstans* and *P. praecursoria*. *Morozovella praeangulata* has a strongly muricate peripheral margin which is rounder than that of *M. angulata*, but *M. praeangulata* has in general a similar appearance (Kelly et al, 1999; Olsson et al., 1999). *Morozovella praeangulata* decreases steadily from 35 to 10% abundance below the LDE and shows a massive break-down around the first LDE horizon at 234.5 rmcd. *Igorina pusilla* has its main peak with 24.5% before the LDE (235.2 rmcd) to decrease at the LDE onset. The abundance of *I. pusilla* oscillates strongly, as does *I. albeari*. It decreases from 15% (234.8 rmcd) to about 2% and

almost disappears shortly thereafter, displaying a similar course as *M. praeangulata*. *Morozovella conicotruncata* shows a constant rise (up to 5 %) between 236.5 to 234.8 rmcd. Its abundance drops to 0.8% just below the LDE and oscillates between 1 and 8% at 234.4 to 233.5 rmcd. Abundances above the LDE vary between 1 and 5% with one exception at 8.7%. *Morozovella angulata* increases steadily from 2 to 40% over the study interval with peaks of 52% above the second LDE horizon at 233.5 rmcd. A few specimens of *Globanomalina chapmani* appear below 235.5 rmcd. The abundance rises to 5% right below the LDE and strongly decreases afterward with varying abundances of less than 3%. In this study *Parasubbotina variospira* and *P. pseudobulloides* have been lumped together for assemblage counting due to an inconsistent taxonomic definition and a similar morphology. They have a slight variation in trochospiral chamber arrangements with a wider umbilicus of *P. variospira* without a distinct threshold between both species (Olsson et al. 1999). Abundance patterns of *Parasubbotina pseudobulloides/variospira* present a belly-shaped tipping 26% (234.2 rmcd) with 5 to 10% below and above the LDE. *Morozovella apantesma* only appears in small numbers but throughout the entire study area. Peaks are at 234.5 rmcd which rises just before and with the lowest LDE peak and at 233.4 rmcd above the event with a maximum of 6%. *Igorina albeari* is the marker species for the subzone P3b (Berggren et al., 1995; 2005) and occurs throughout the entire study interval, which implies that the base of P3b is well below the LDE at Shatsky Rise. It starts with an abundance of 0.2–6%, to rise with the onset of the LDE at 243.5 rmcd to 14.8%. *Subbotina* spp. shows a slight increase before the LDE with a maximum of 9% to decrease during the event down to 3–5% and recover afterwards to ~12%. Relative abundance of *P. varianta* varies between 2 and 4% with a maximum during the LDE. Highest values of ~12% are observed directly above the LDE. *Morozovella occlusa* is distinguished from *M. acutispira* by its lower number of chambers in the final whorl (generally four to six, maximum eight in *M. occlusa*; eleven to twelve in *M. acutispira*). *Morozovella occlusa* is suggested to be closely related to *M. angulata* (Corfield and Granlund 1968; Olsson et al., 1999). *Morozovella acutispira* appears for the first time at 235 rmcd below the LDE to slowly rise in abundance to up to 4 % and above it abundance rises to 7%. A similar trend is shown by *M. occlusa* as values rise above 5% 15 cm below the LDE peaks at 235 rmcd for the first time. During the LDE, it has its highest abundance in the upper part with 11% (234 rmcd) and low numbers at the top of the LDE (233.5 rmcd) after which this taxon visibly increases in abundance from 5% (few samples) to 25% (233.4 rmcd and upwards). Results from multivariate statistics (NMDS) of the faunal data are discussed in section 4.5.



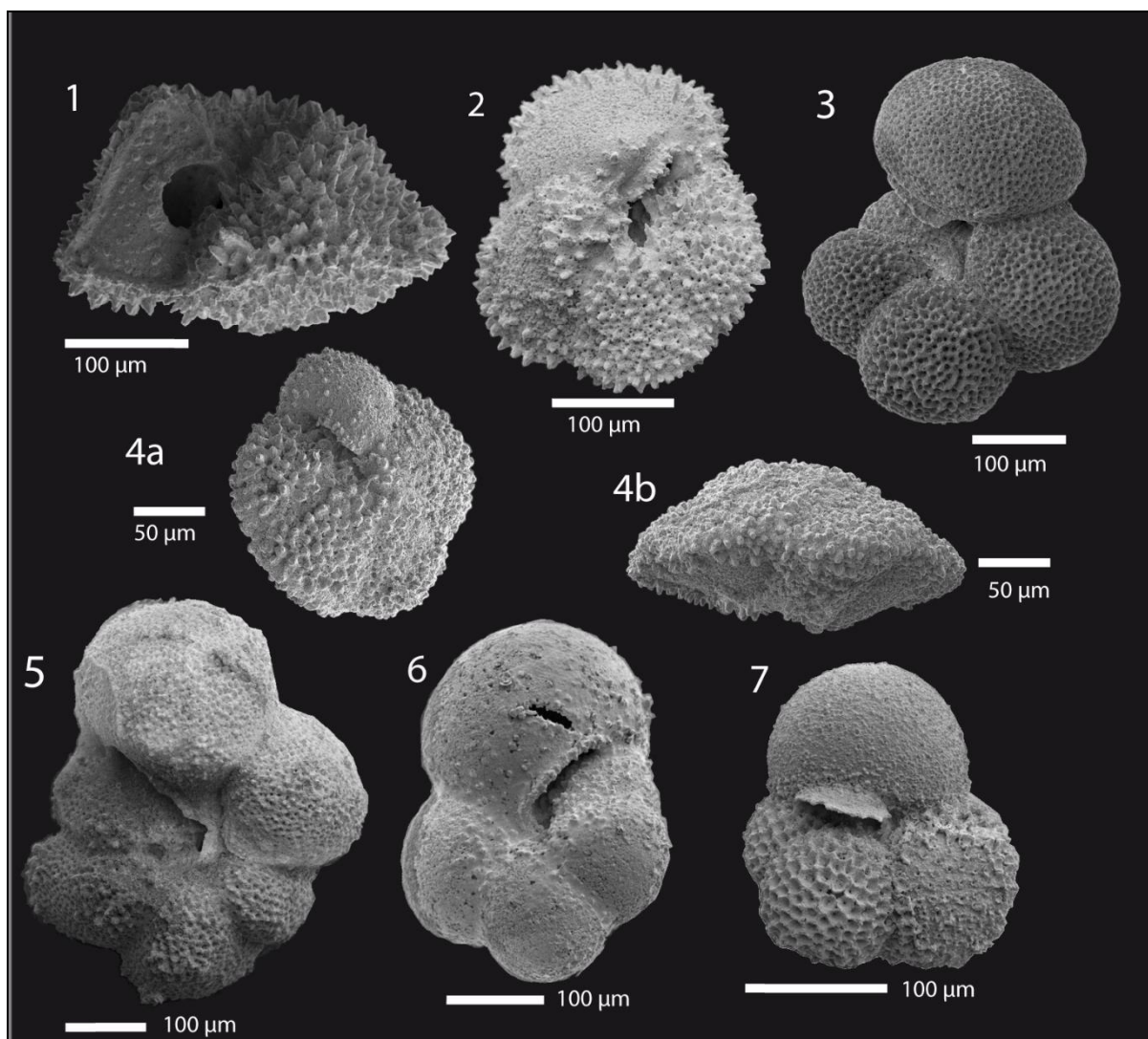


Figure 14: Scanning electron microscope images of planktic foraminifera. 1: *Morozovella angulata*, lateral view (Sample 1210A-23-3, 0-1.5 cm); 2: *Morozovella aequa*, umbilical view (1210A-23-3, 37.5–39 cm); 3: *Parasubbotina variospira*, umbilical (1210A-23-3, 30-31. (1210A-23-3, 30-31.5 cm); **4a+4b**: *Igorina albeari* umbilical/lateral (1210A-23-1, 90–92 cm); **5**: *Praemurica uncinata*, umbilical (1210A-23-3, 52.5-54 cm); **6**: *Globanomalina chapmani*, umbilical (1210A-23-1, 85–87 cm); **7**: *Subbotina triangularis*, umbilical (1210A-23-3, 52.5–54 cm).



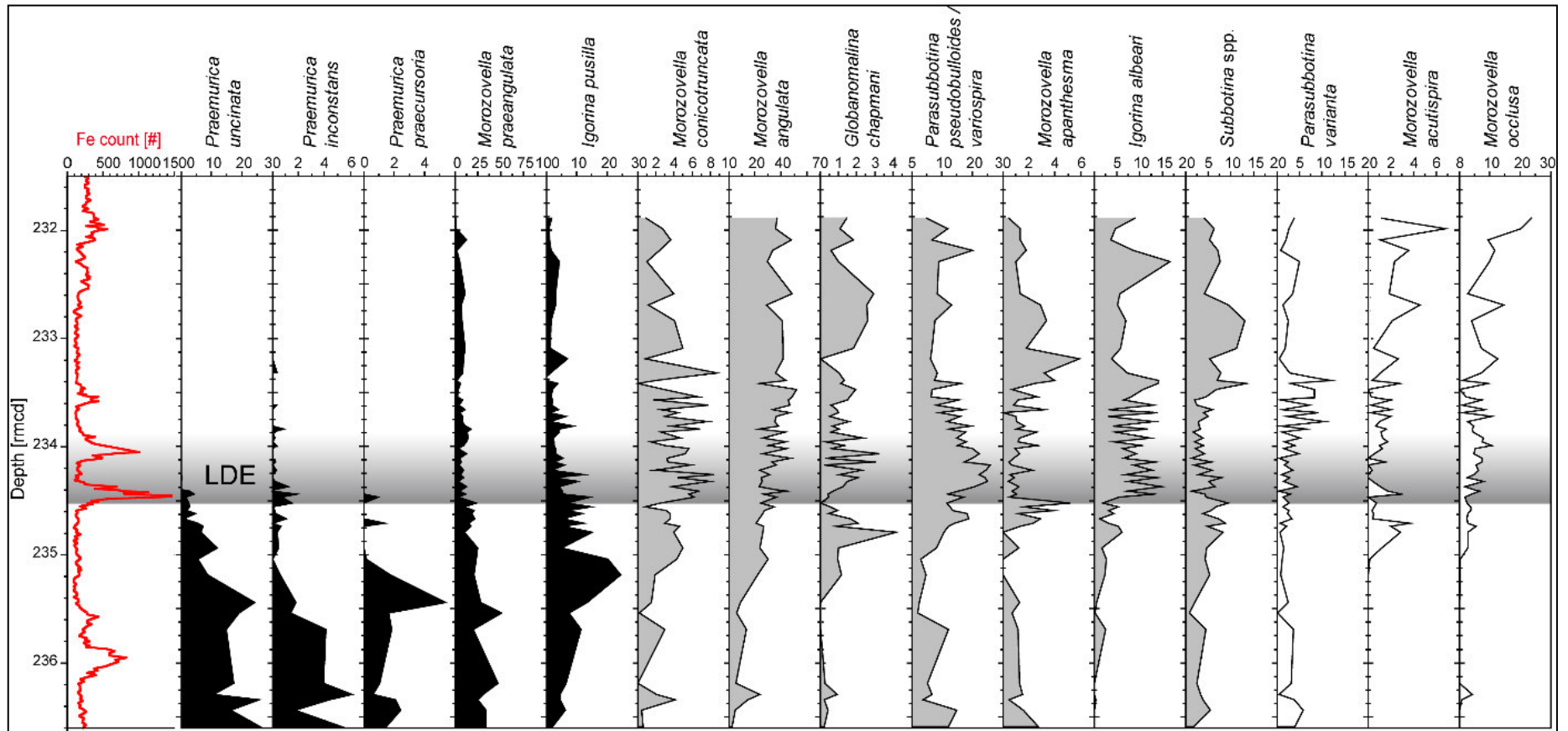


Figure 15: Species abundance and Fe XRF core scanning data for chemostratigraphic correlation. Species abundance data in %, sorted according to the stratigraphic order of their abundance maxima. The LDE is marked in grey

## 4 Discussion

### 4.1 Biostratigraphic implications

According to planktic foraminifera biostratigraphy the LDE has to date usually been placed at or just above the P3a–P3b subzone boundary (Bornemann et al., 2009; Westerhold et al., 2011; Sprong et al., 2009) as defined by the first appearance datum of *Igorina albeari* (Berggren et al., 1995; Wade et al., 2011), however, there is still a discrepancy in the definition on this taxon (e. g. Arenillas et al., 2008; Sprong et al., 2009; Soldan et al., 2011). *Igorina albeari* might have closely related species, as determined by Soldan et al. (2011), but here we strictly follow the taxonomic description given by (Olsson et al., 1999). Results from our study suggest that *I. albeari* (sensu Sprong et al., 2009) already appears consistently at least 400 kyr below the LDE (Figure 15). Thus, we suggest that at Shatsky Rise the first common abundance of *I. albeari* marks the onset of the LDE at 234.4 rmcD rather than a simple first (rare) occurrence. Therefore, the P3a–P3b boundary is suggested to be well below the LDE. Based on this early occurrence at Shatsky Rise we tentatively propose that this species may have evolved from *I. pusilla* in the Pacific and appears later in other ocean basins. *G. pseudomenardii* (defining the base of Zone P4) was observed in rare abundances at a lower stratigraphic position than expected and may have, thus, possibly been overseen in other biostratigraphic studies or alternatively appears earlier in the Pacific Ocean. Further, specimens with slight morphological differences to *G. pseudomenardii* were found and named *G. cf. pseudomenardii* as they do not allow for an unequivocal identification of this species. However, these findings need to be confirmed at other deep-sea sites.

### 4.2 Carbonate preservation

Changes in foraminiferal test preservation due to species-specific dissolution susceptibility can alter the assemblage composition and, thus, bias the ecological and environmental interpretation of faunal data (e. g., Berger, 1970; Pearson et al., 2001; Petrizzo, 2007; Nguyen et al., 2011). Moreover, dissolution, but specifically recrystallization can cause changes in the geochemical composition of foraminiferal calcite.

In this study we assessed a potential preservational bias of the faunal data by using, in addition to visual criteria, a combined approach comprising coarse fraction data (CF, >63 µm), absolute abundances of planktic foraminifera (PFN, >125 µm), %P (>63 µm), planktic foraminiferal fragmentation (%F, >125µm) and diversity changes (Figure 12). Eight samples were excluded from further interpretations based on this approach using a threshold of 18% for the fragmentation index since these high values are also accompanied by low values of both %P and CF and a lower planktic foraminiferal diversity pointing to a diagenetically controlled bias of the faunal composition (Figure 12). For comparison, planktic foraminiferal fragmentation during the PETM interval in Shatsky Rise Hole 1209B (Petrizzo et al., 2008) displays background values of 10–20% and rise to a maximum of 45% during the PETM.

Visual observations of planktic foraminiferal assemblages reveal a general good preservation in nearly all samples. Foraminiferal tests are unfilled, primary features like pores, keel structures and openings are usually well developed as is evident from SEM images (Figure 14).

Apparent dissolution features on tests such as missing chambers or broken walls have rarely been observed, but many specimens show indications of recrystallization, which is not surprising with background CaCO<sub>3</sub> values of >90 wt%. The intervals with lower CaCO<sub>3</sub> like the LDE beds contain relatively high abundances of dissolution-sensitive *Igorina albeari* (Petruzzo, 2007; Nguyen et al., 2011). This shows that these samples are not significantly altered by dissolution. The brownish event beds of the LDE display slightly lower values of ~84 wt% CaCO<sub>3</sub> (Figure 12).

Coarse fraction (CF) shows similar patterns to Site 1209, where the CF generally follows short-eccentricity cycles (Westerhold et al., 2011). The highest CF peak occurs between the lowest and second LDE Fe peaks while minima correspond to each of these. Since the >63 µm fraction consists almost exclusively of planktic foraminifera due to the absence of sand-sized terrigenous input in the central Pacific and negligible abundances of radiolarians, changes in the coarse fraction are predominantly controlled by planktic foraminiferal productivity, test fragmentation or CaCO<sub>3</sub> dissolution. High intensities in Fe XRF core scanning in combination with low CF are suggested to be a further indication for enhanced dissolution at 232.00, 234.00, 234.40 and 235.95 rncd (Figure 12).

While planktic assemblages, PFN and fragmentation were both from >125 µm size fraction, %P was analyzed on >63 µm. Using this size fraction probably leads to a higher amplitude of changes than expected for the >125 µm fraction for two reasons: (1) the smaller size fraction usually contains plenty of juveniles and more fragile taxa and therefore will be first fragmented, and (2) dissolution susceptibility is strongly species-dependent (Erez and Luz, 1983; Nguyen et al., 2011). Fragmentation of planktic foraminifera is widely used as an indicator for CaCO<sub>3</sub> dissolution (Dittert, 2000). Planktic foraminiferal tests are usually more prone to dissolution or recrystallization than most benthic ones (e. g. Berger, 1970; Dittert et al., 1999). General dissolution rankings of late Paleocene and early Eocene planktic foraminifera from Shatsky Rise and Allison Guyot (Nguyen et al., 2011) are inferred from laboratory experiments where the genus *Igorina* is considered to be more prone to dissolution than *Acarinina*, *Morozovella* and most *Subbotina*. In this study, the species *I. pusilla* and *I. tadjikistanensis* show a high dissolution-sensitivity. Opposed to that, faunal dominance of *Igorina* species was observed (Petruzzo, 2005; Bernaola et al., 2007) during the Early Late Paleocene Event (ELPE, 58.9 Ma; Petruzzo, 2005) which is partly seen as a dissolution event (Petruzzo, 2005). It might imply that *Igorina* truly flourished during the ELPE and the species might still be prone to dissolution.

Sedimentation rates (SR; Figure 12) of Site 1210 (adapted from astronomical tuning; Westerhold et al., 2008) show variations between 0.28 and 0.64 cm kyr<sup>-1</sup> with an average of 0.44 cm kyr<sup>-1</sup> during the short-eccentricity cycles (Pc<sub>100</sub> 34 – 44). Due to the lack of terrestrial hinterland at Site 1210 the main sediment material originates from carbonate microfossils, whereas radiolarians as well as terrigenous dust and clays are only minor contributors to the sediment. Assuming a constant pelagic carbonate factory during the study interval the SR may reflect changes in the rates of carbonate dissolution (Figure 12) as is also suggested by the anti-correlation to short-eccentricity derived SR. The SR is lowest at the lowest and uppermost part of the studied interval with values between 0.2 and 0.35 cm kyr<sup>-1</sup> (Westerhold et al., 2008). Values are slightly decreasing during the LDE, which can point to a lower carbonate supply or increased dissolution, or both. This fact might be related to a lysocline shoaling during the LDE as observed during the PETM (Zachos et al., 2005), and is supported by the dark event horizons,

high XRF Fe counts and lower carbonate content. Planktic foraminiferal accumulation rate (PFAR) which also considers the sedimentation rates shows only minor changes that can be clearly attributed to the LDE (Figure 12).

Furthermore, the good correlation ( $R^2 = 0.59$ ,  $N=67$ ,  $p<0.001$ , our data) between planktic proportion and fragmentation is considered as a useful indicator for carbonate dissolution (Hancock and Dickens, 2006). The simultaneous trends of fragmentation increase and planktic proportion decrease (Figure 12) might therefore be also connected to lysocline variations. However, the overall correlation is with  $R^2= 0.77$  somewhat lower than in Hancock and Dickens (2006) from neighboring ODP sites over the entire Paleocene. Between 61.33–63 Ma, their  $R^2$  is even 0.965 ( $N=5$ ,  $p<0.001$ , calculated from published data Hancock and Dickens, 2006), which most likely results from a particularly small sample quantity. Based on this approach we assume that carbonate dissolution as a consequence of a lysocline rise during the LDE at Site 1210 might be minor compared to the ELPE and PETM.

To conclude, we suggest that the diagenetic alteration in terms of dissolution of the sample material is limited in the LDE. %P never drops below 95.5% and fragmentation never reaches values above 17% in the selected samples. This suggests only minor changes due to dissolution. Recrystallized tests are assumed to break much easier which might have also lead to enhanced fragmentation rates (Pearson et al., 2014).

### 4.3 Foraminiferal stable isotope data

Test alteration due to secondary overprint is characterized by two successive stages after calcification: early diagenesis and diagenesis after burial (e. g. Stap et al., 2010). It is well known that diagenetic alteration of foraminiferal calcite has an influence on  $\delta^{13}\text{C}$  and  $\delta^{18}\text{O}$  values, specifically if recrystallization and precipitation of diagenetic calcite is involved (D'Hondt and Zachos; 1993 Killingley, 1983; Pearson et al., 2001). While  $\delta^{13}\text{C}$  of recrystallized planktic foraminifera from deep-sea cores shows usually similar values to unaltered calcite (Pearson et al., 2001),  $\delta^{18}\text{O}$  tends to increase due to the bottom-water signal recorded by precipitated secondary calcite during early diagenesis (Schrag et al., 1995; Pearson et al., 2001). Previous studies suggest that absolute  $\delta^{18}\text{O}$  values are biased by recrystallization, whereas trends and amplitude of changes are largely preserved (Pearson et al., 2001; Sexton et al., 2006). Calcite recrystallization would therefore rather damp the interpreted temperature change than amplifying it. It is further proposed that benthic foraminifera are probably less affected by diagenesis, therefore  $\delta^{18}\text{O}$  paleothermometry remains a valuable benchmark (Pearson et al., 2001).

Even after picking the visually best preserved specimens for stable isotope analyses we cannot fully rule out recrystallization. Thus, we consider  $\delta^{13}\text{C}$  to be largely unaltered, whereas absolute  $\delta^{18}\text{O}$  values might have slightly changed, but we assume that the relative warming related to the LDE represents a primary signal as explained above. The reason for the generally noisier  $\delta^{18}\text{O}$  signal might be (1) the higher hydrographic variability of surface water masses compared to the deep-sea, (2) the fact that planktic foraminifera are more prone to diagenetic alteration specifically of absolute values of  $\delta^{18}\text{O}$ , or, most likely, a combination of both.

Benthic foraminiferal isotope data from Site 1210 are similar to those of Site 1209 (Westerhold et al., 2011). However, the benthic foraminiferal  $\delta^{13}\text{C}$  excursion at the base of the LDE is better developed at Site 1210 (Figure 10). The CIE consists of a rather sharp base and an asymmetry that resembles the typical shape of the PETM CIE and contrasts the symmetric  $\delta^{13}\text{C}$  pattern known from early Eocene hyperthermal events like the ETM-2 or the MECO (e. g. Norris, 1996; Stap et al., 2010). This shape may suggest a rapid injection of isotopically light carbon to the ocean as a trigger mechanism for the LDE and/or  $\text{CaCO}_3$  dissolution at the base of the LDE CIE (e. g. Norris, 1996; Zachos et al., 2008). In contrast to ODP Site 1209 no clear double peak for  $\delta^{13}\text{C}$  and  $\delta^{18}\text{O}$  is visible at Site 1210 and also no third peak (Westerhold et al., 2011).

If we attribute our benthic foraminiferal  $\delta^{18}\text{O}$  shift to temperature, this results in a temperature increase of  $\sim 1.6^\circ\text{C}$  at the base of the LDE respectively the lowest LDE peak. Our subsurface planktic foraminiferal data would correspond to a temperature shift of  $\sim 2.4^\circ\text{C}$  (0.6 ‰) and planktic surface data to  $2.8^\circ\text{C}$  (0.7 ‰). The non-uniform warming of the ocean could have led to water layers characterized by different temperatures, intensifying a temperature-driven upper ocean stratification.

#### 4.4 Habitat implications of planktic foraminifera

The  $\delta^{13}\text{C}$  and  $\delta^{18}\text{O}$  record of benthic and planktic foraminifera display the typical inter-specific offset between benthic foraminifera showing the heaviest  $\delta^{18}\text{O}$  and lightest  $\delta^{13}\text{C}$  values, subsurface-dwellers with intermediate values for both isotope species, and surface-dwellers with the lightest values for  $\delta^{18}\text{O}$  and the most positive ones for  $\delta^{13}\text{C}$  (Figure 10, Figure 13). The apparent differences between surface dwelling and benthic foraminifera of nearly 2 ‰ for  $\delta^{13}\text{C}$  and 1.0 to 1.5 ‰  $\delta^{18}\text{O}$  point towards a generally well-stratified water column as can be expected for the subtropical central Pacific.  $\delta^{13}\text{C}$  in photosymbiotic foraminifera tests are generally enriched in  $^{13}\text{C}$  in comparison to asymbiotic living species due to the symbionts' preferred  $^{12}\text{C}$  consumption (e. g. D'Hondt et al., 1994).  $\delta^{18}\text{O}$  is somewhat more negative in photosymbiotic species than in asymbiotic subsurface dwelling ones (Berggren and Norris, 1997: 0.86 ‰ more negative on average, N= 70). In addition to the planktic species *M. angulata* and *P. pseudobulloides/variospira*, which represent surface and subsurface habitats, several other species were analyzed to better characterize their depth habitat and to better interpret general community changes (Figure 12). Data of *M. velascoensis* imply a preference for the same environmental conditions as *M. angulata* and *M. praeangulata* as they are within the same isotope range. *Igorina* tends to have more positive  $\delta^{18}\text{O}$  values than *Morozovella*, hinting towards an occurrence during slightly cooler seasons or deeper waters than the latter one (Berggren and Norris, 1997). The signal might be influenced by a smaller average test size within the used grain size range and therefore less symbionts compared to the bigger *Morozovella* test, causing a more positive  $\delta^{18}\text{O}$  (e. g. Shackleton et al., 1985; Pearson et al., 1993). The lower  $\delta^{13}\text{C}$  values for *I. albeari* might also suggest a less intense photosymbiotic activity as proposed for other igorinids, e. g. *I. broedermanni* (D'Hondt et al., 1994; Pearson et al., 1993; Guastiet al., 2006).

Due to low abundance only few specimens were measured for *Globanomalina imitata* and *Acarinina strabocella*. *Globanomalina imitata*, analyzed in two samples above the LDE shows values of  $\delta^{13}\text{C}$  (c. 1.8 ‰) and  $\delta^{18}\text{O}$  (c. -0.1 ‰) within the range of subsurface dwelling

*P. pseudobulloides/variospira*. Therefore, a subsurface habitat is assumed for *G. imitata*. *Globanomalina chapmani* and *G. cf. pseudomenardii* show lower  $\delta^{18}\text{O}$  (c. -1.2 ‰), which is interpreted as higher habitat temperatures than *P. pseudobulloides*. *Acarinina strabocella* shows more ambiguous results: The  $\delta^{13}\text{C}$  signal of all four measurement points are closely spaced within 0.5 ‰ (2–2.5 ‰), yet the  $\delta^{18}\text{O}$  signal strongly varies (0–1.7 ‰). Therefore two samples suggest a surface ocean, photosymbiont-bearing habitat as proposed from other studies (D'Hondt et al., 1994), whereas the two other samples suggest a non-photosymbiont thermocline habitat.

## 4.5 Planktic foraminiferal assemblages

*Praemurica uncinata*, *P. inconstans* and *P. praecursoria* show similar patterns in abundance concerning their disappearance at the lowest LDE peak (Figure 15). This suggests that this group is seriously affected by LDE-related environmental changes like carbon cycle perturbation and temperature and was less competitive compared to *Morozovella* species inhabiting a similar ecological niche. The disappearance of *Praemurica* close to this stratigraphic level has previously also been documented successions from the Tethys Ocean (e. g. Steurbaut et al., 2008). A similar faunal shift has been documented for the latest Danian in the northeastern Atlantic (Ortiz et al., 1996), however, the LDE itself has not been identified in these successions.

The LDE at Site 1210 marks a permanent decrease in *M. praeangulata* and a simultaneous increase in *M. angulata* (Figure 15), suggesting better ecological adaptation to LDE and post-LDE surface conditions for *M. angulata* compared to its precursor. Above the LDE, surface water conditions favored the prevalence of *Morozovella*. Most *Morozovella* species show a long-term trend to higher relative abundances and seem to be more adapted to warm and stratified oligotrophic surface water.

Thermocline dwelling *P. pseudobulloides/variospira* was a highly successful species during the LDE as highest relative and absolute abundance were found between the two LDE peaks suggesting that *Parasubbotina* benefited from oceanic changes accompanying the LDE (Figure 15). The rise to higher abundances starts together with the onset of the negative CIE which again hints towards an environment enriched in nutrients in form of digestible particles as preferred by subsurface dwellers. However, directly above the LDE *Parasubbotina* was again less successful in exploiting a niche in the thermocline. The closely related *Subbotina* spp. is rather rare in the late Danian which does not allow for a detailed ecological interpretation.

A low-resolution study in the Tethys Ocean (Steurbaut et al., 2008) at three shelf locations in Tunisia over the P2–P3b time period comprises slightly different results from ours. There, *Praemurica* spp., *Subbotina* spp. and *Parasubbotina* spp. are slightly more or equally abundant than *Morozovella* spp. In Tunisia, *Subbotina* spp. was notably more abundant than *Parasubbotina* spp. (Steurbaut et al., 2008). This is not the case in our study, where *Morozovella* is by far most abundant, followed by *Parasubbotina*, *Igorina*, *Subbotina* and *Praemurica*. However, these differences in assemblage composition might be largely attributed to the fact that these localities are situated on the North African continental margin at much shallower paleodepths (outer neritic to upper bathyal).

NMDS ordination (Figure 17) reveals a development of our paleocommunity (Figure 15) during the investigated interval by projecting the ranking of relationships between species and samples as well as environmental proxies like  $\delta^{13}\text{C}$  and  $\delta^{18}\text{O}$  into two dimensions. A distance of the samples between before, during and after the event is apparent, specifically along NMDS axis 1 (Figure 17). The fauna during and above the LDE shows a close connection, whereas pre-LDE samples differ from the later faunal communities, seen by scores as well as distances in the scatter plot. Post-LDE samples appear to be relatively homogeneous in their assemblages and reflected by the constantly very low NMDS axis 1 scores after the LDE. Subsurface  $\delta^{13}\text{C}$  and  $\delta^{18}\text{O}$  (*P. pseudobulloides*/*variospira*) strongly correspond to NMDS axis 1 but even more striking are similarities to the  $\delta^{13}\text{C}$  and  $\delta^{18}\text{O}$  offset gradient as discussed in higher detail below.

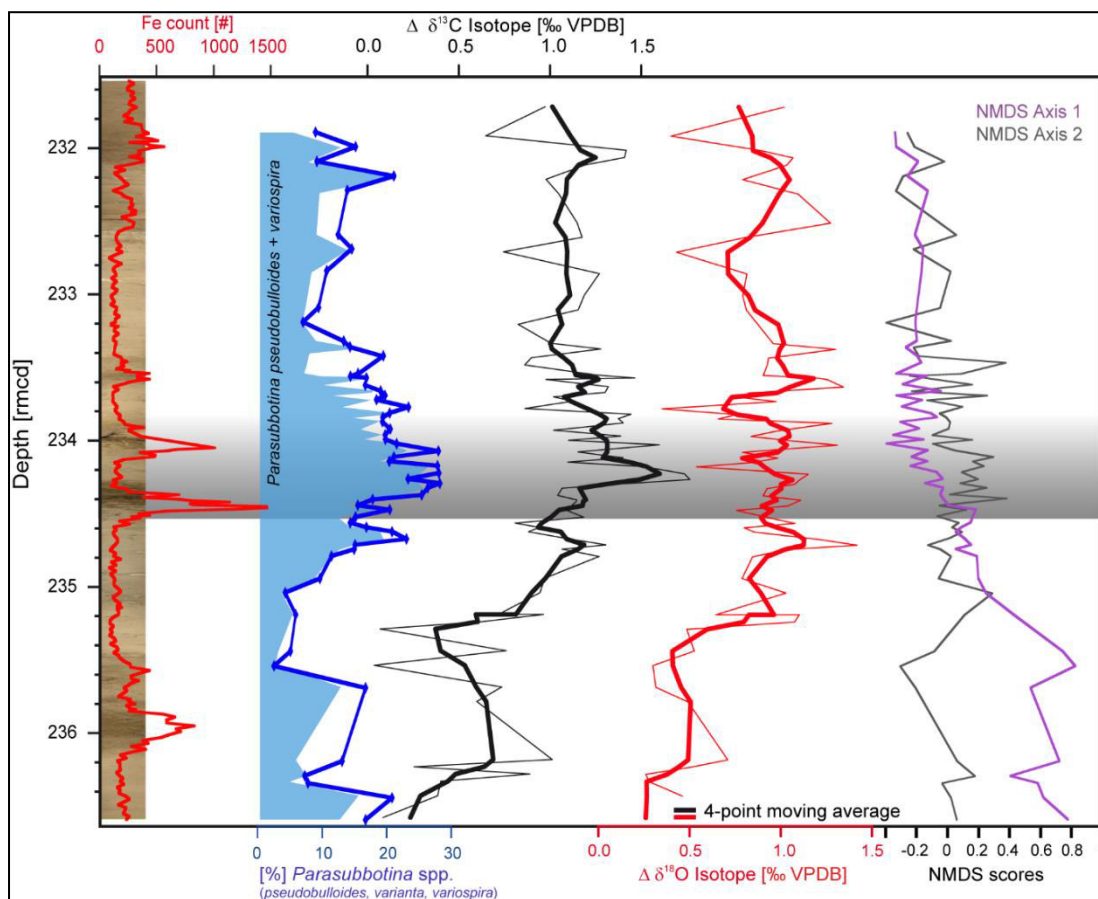


Figure 16:  $\delta^{13}\text{C}$  and  $\delta^{18}\text{O}$  gradient and faunal development. Gradient of  $\delta^{13}\text{C}$  and  $\delta^{18}\text{O}$  signals calculated by planktic surface minus subsurface dwelling foraminifera, expressed as  $\Delta\delta^{18}\text{O}$  and  $\Delta\delta^{13}\text{C}$ . A four-point moving average has been applied. The core photo and the XRF core scanning Fe counts serve for stratigraphic correlation. In addition, results from non-metric multidimensional scaling (NMDS) as a statistical measure of the faunal composition are shown (see also Fig. 9). The LDE is marked in grey.





and seem to have benefited from a more stratified upper water column during the LDE. A potential scenario explaining the abundance changes of *Parasubbotina* might be a thermocline shallowing and an accompanied development of a deep chlorophyll maximum (DCM). A DCM is a feature of highly stratified open oceans and is often either seasonally formed or part of a permanent gyre system (Rohling and Gieskes, 1989; Huisman et al., 2006) when the thermocline, or more generally speaking the pycnocline, is positioned well within the euphotic zone. In such a setting the surface mixed layer is usually characterized by oligotrophic conditions, and nutrients are trapped right below the pycnocline. This allows for the development of a DCM between the pycnocline and the base of the euphotic zone. Due to consumption of nutrients by the deep-phytoplankton community the nutricline lies at the base of the DCM (Castradori, 1993). A comparable scenario has been proposed for the formation of Mediterranean Sea sapropels during the Late Quaternary. Here, enhanced stratification occurs during warm phases due to salinity and temperature changes in favor of stagnation and low oxygen conditions at the sea floor (Emeis et al., 2003, Rohling et al., 2006). However, other studies attribute the lack of vertical mixing and deep water ventilation in the Mediterranean Sea to increased density stratification caused by freshwater inflow (e. g. Rohling et al., 2006).

Directly above the second LDE peak light-dependant surface dwellers (*I. albeari*, *M. angulata* and *M. conicotruncata*) show higher abundances while thermocline layer inhabitants decline, probably resulting from a return to conditions similar to the pre-event stratified upper ocean.

At Shatsky Rise unequal warming of the different water masses during the LDE, with stronger warming of the surface mixed layer may have enhanced stratification of the upper water masses. Both  $\delta^{13}\text{C}$  and  $\delta^{18}\text{O}$  data suggest a stronger surface to subsurface gradient from slightly below the LDE upwards (Figure 16). The  $\delta^{13}\text{C}$  gradient is more pronounced than the  $\delta^{18}\text{O}$  one and parallels the relative abundance of the subsurface-dweller *Parasubbotina*. The difference in the offset between before and after the LDE makes c. 0.8 ‰ for  $\delta^{13}\text{C}$  and c. 0.6 ‰ ( $\cong$  c. 2.4 °C) for  $\delta^{18}\text{O}$  on average. Both  $\delta^{13}\text{C}$  and  $\delta^{18}\text{O}$  gradients are rising by 0.5 ‰ 20 cm below the LDE and remain higher after the event than before. Above the LDE at 233.7 mcd a slight reduction of these gradients took place. The  $\delta^{13}\text{C}$  gradient is largely controlled by the signature of *P. pseudobulloides/variopira* whereas surface dwelling foraminifera show more stable values (Figure 10, Figure 13). The  $\delta^{18}\text{O}$  offset gradient is more balanced and not controlled by one habitat alone but might be interpreted as a stronger temperature increase of the surface ocean whereas thermocline waters are influenced by somewhat cooler and/or more saline waters.

Due to the co-variation between the  $\delta^{13}\text{C}$  isotope gradient and the relative abundance pattern of *P. pseudobulloides/variopira* as well as the importance of the *Parasubbotina*  $\delta^{13}\text{C}$  in the NDMS we presume that *P. pseudobulloides/variopira* took advantage of the well stratified ocean accompanied by the formation of a prominent DCM, and, thus, high nutrient availability in subsurface waters as well as less competitive pressure due to the disappearance of aforementioned species.

Alternatively, the long-term trend of an increasing gradient strength with a weaker gradient below and the observed variability above the LDE might be also partly owing to the Paleocene paleogeographic position of Shatsky Rise on the northern rim of the equatorial divergence zone (Figure 11). Intervals with a weaker gradient might indicate periods of enhanced upwelling. Since the gradient did not fully recover to pre-LDE levels in our record, we, further, tentatively

speculate that Shatsky Rise passed a certain threshold inhibiting or reducing vertical mixing by leaving the equatorial upwelling zone due to its plate tectonic movement (Larson et al; 1992).

Finally, the timing of the faunal change in relation to the LDE is crucial for understanding the planktic foraminiferal faunal response to the LDE. From the isotope depth gradients and  $\delta^{18}\text{O}$  data as well as the NMDS axis 1 scores it is apparent that substantial changes in the fauna, but also in the oceanographic conditions commenced  $\sim 170$  ky before the LDE onset ( $\sim 0.7$  m below Figure 16, Figure 17). However, a second step in these changes corresponds to the short-term negative  $\delta^{13}\text{C}$  excursion during the LDE. Our data indicate long-term ocean warming and, thus, stratification started well before the LDE, but culminated during the LDE interval. This let us conclude that both long-term and transient environmental changes associated with the LDE had a strong control on the assemblage composition of planktic foraminifera (Figure 15)

## 5 Conclusions

- (I) High-resolution analysis of planktic foraminiferal assemblages and foraminiferal  $\delta^{13}\text{C}$  and  $\delta^{18}\text{O}$  provide new insights into the prevailing paleoceanographic conditions and planktic foraminiferal responses to the Latest Danian Event at Shatsky Rise: Some dissolution is apparent from the studied samples of the LDE at ODP Site 1210 (Shatsky Rise) during the LDE Fe peaks, and also recrystallization might be an issue in some intervals of the carbonate-rich intervals before and after the LDE. Eight samples were excluded from the faunal analysis for this reason.
- (II) A significant negative CIE of 0.7 ‰ in surface, 0.9 ‰ in subsurface dwellers and 0.6 ‰ in benthic foraminifera was observed, identifying the LDE together with the two prominent Fe peaks.
- (III) The entire water column has been warmed by  $\sim 1.6\text{--}2.8^\circ\text{C}$  (0.4 ‰ benthic, 0.6 ‰ subsurface and 0.7 ‰ surface dwellers) during the LDE at Shatsky Rise, but started  $\sim 170$  ky below the LDE onset. This decrease in  $^{18}\text{O}$  supports the idea that this event might represent a Paleocene hyperthermal, albeit temperature variability is generally of a similar magnitude throughout the latest Danian. However, this is the only warming phase that is accompanied by a negative CIE in the mid-Paleocene.
- (IV) The isotope gradients between surface and subsurface dwellers point towards an enhanced stratification of the upper water column just below the LDE, strongly enhanced during it and less but still enhanced above. This change in the gradient is accompanied by abundance changes of the subsurface dwelling *Parasubbotina pseudobulloides/variospira* probably linked to the development of a deep-chlorophyll maximum under well-stratified conditions. Above the LDE, symbiont-bearing surface dwellers (*Morozovella*) become more successful after they might have developed more effective photosymbiosis strategies.
- (V) We observed major changes in the faunal assemblages specifically in photosymbiont-bearing taxa like the abrupt virtual disappearance of *Praemurica* within the first LDE peak and the gradual evolution of new *Morozovella* taxa.

- (VI) Multivariate statistics indicate rather distinct faunal communities below, during and above the event. The results clearly show that faunal changes started more than ~170 kyr before the LDE similar to the isotope depth gradients and temperature changes.
- (VII) The first appearance datum (FAD) of *Igorina albeari* is dated well below (>400 kyr) the onset of the LDE, and not at the LDE (or directly below) as proposed in other studies.

## Acknowledgements

We greatly appreciate help with taxonomic determinations by Maria Rose Petrizzo (University of Milan, Italy). Lisa Petter (University of Leipzig) is thanked for the help with micropaleontological sample preparation. We further thank Stefan Krüger (University of Leipzig) very much for the stable isotope measurements. The manuscript benefited from constructive reviews of Eduardo Koutsoukos and an anonymous reviewer.

We acknowledge support from the Universität Leipzig within the program of Open Access Publishing.



# Chapter III: Paleoceanographic changes across the Latest Danian Event in the South Atlantic Ocean and planktic foraminiferal response

Sofie Jehle<sup>1</sup>, André Bornemann<sup>2</sup>, Anna Friederike Lägerl<sup>1</sup>, Arne Deprez<sup>3</sup> and Robert P. Speijer<sup>3</sup>

<sup>1</sup>Institut für Geophysik und Geologie, Universität Leipzig, Germany

<sup>2</sup>Bundesanstalt für Geowissenschaften und Rohstoffe, Hannover, Germany

<sup>3</sup>Department of Earth and Environmental Sciences, KU Leuven, Belgium

## Abstract

A number of short warming events occurred during Paleocene and Eocene, of which the “Paleocene-Eocene Thermal Maximum” (PETM, 56 Ma) is the most severe and most investigated event. The less known “Latest Danian Event” (LDE) at 62.2 Ma represents a 200 ky-lasting warming phase superimposed on a long-term cooling trend after the Early Paleocene. South Atlantic ODP Site 1262 data, covering ~1 myr, indicate a warming of the entire water column by 1.5–2.6°C, accompanying a prominent negative carbon isotope excursion (~0.9–1.1 ‰) and a long-term re-organization of the planktic foraminiferal fauna associated with the LDE. This study unravels a different paleoceanographic evolution of the upper

ocean structure compared to results from Pacific ODP Site 1210. Unlike the Pacific, the Atlantic site lacks an apparent change of stratification as well as an overall dominance of thermocline dwelling planktic foraminifera species and a low abundance of surface dwelling photosymbiotic foraminifera. Within the LDE, indications for a slightly enhanced stratification of the upper water column and transient warming was indicated when surface dwelling planktic foraminifera became temporarily more abundant. The long-term evolution in planktic foraminifera with the disappearance of *Praemurica* at the LDE onset and a contemporaneous rise in *Morozovella* is similar to the trends reported from Shatsky Rise ODP Site 1210.

**Keywords:** Paleocene, hyperthermal event, Latest Danian Event, negative CIE, planktic foraminifera assemblage, surface ocean stratification

## 1 Introduction

The early Paleogene is known for significant climate and carbon cycle perturbations (e.g. Kennett and Stott, 1991; Lourens et al., 2005; Zachos et al., 2008; Littler et al., 2014). It is characterized by a long-term global bottom water cooling trend between 66 and ~59 Ma by ~3°C, followed by a long-term temperature rise by ~4–5°C culminating at the Early Eocene Climatic Optimum (EECO, ~53 Ma; Zachos et al., 1994, 2008; Westerhold et al., 2011). These million-year-scale cooling and warming trends of Paleocene and Eocene are interrupted by several short-term warming events of 100–200 ky duration (e.g., Kennett and Stott, 1991, Lourens et al., 2005; Quillévéré et al., 2008; Zachos et al., 2008; Westerhold et al., 2011). The

warming events, also named hyperthermals, are accompanied by negative carbon isotope excursions (negative CIEs), indicating the injection of isotopically light carbon into the ocean-atmosphere system, and severe biotic responses such as extinctions and turnovers (e.g. Crouch et al., 2001; Lourens et al., 2005; Bernaola et al., 2007; Zachos et al., 2010).

The best studied and most severe hyperthermal event is the Paleocene-Eocene Thermal Maximum (PETM, ~56 Ma) with a duration of 170–220 ky (e.g. Kennett and Stott, 1991; Röhl et al., 2007). Characteristics of this event are: a negative CIE of at least -2.5 ‰, ocean warming by up to 6–7°C (Zachos et al., 2008) for the bottom water, and up to 10°C for the surface ocean (Sluijs et al., 2007), a drop in calcium carbonate (wt% CaCO<sub>3</sub>) in deep-sea records, most likely due to lysocline shallowing as a consequence of ocean acidification (e.g. Zachos et al., 2005), a major extinction of deep-sea benthic foraminifera and assemblage changes in many other marine microfossil groups (e.g. Kelly et al., 1996; Crouch et al., 2001; Bralower, 2002; Thomas, 2003; Speijer et al., 2012; Yamaguchi and Norris, 2015).

Several similar events, albeit of smaller magnitude, were reported from the Paleocene and Eocene, like the “Latest Danian Event” (LDE = Top C27n Event, 62.2 Ma, Bornemann et al., 2009, Dinarès-Turell et al., 2012). So far, the LDE was described from the margins of the Tethys Ocean in Egypt (Speijer, 2003; Bornemann et al., 2009; Sprong et al., 2011), NW-Tunisia (Guasti, 2005; Sprong et al., 2013), Bjala in Bulgaria (Dinarès-Turell et al., 2012) and Caravaca, Spain (Alegret et al., 2016). The LDE also was unequivocally identified in the North Atlantic (Zumaia, Spain, e.g. Dinarès-Turell et al., 2012, 2014; off Newfoundland, Yamaguchi et al., 2017), the South Atlantic (Ocean Drilling Program ODP Site 1262; Westerhold et al., 2008; Monechi et al., 2013; Deprez et al., 2017a), and the Pacific at Shatsky Rise ODP Sites 1209 and 1210 (Westerhold et al., 2011; Jehle et al., 2015). Faunal changes amongst planktic foraminifera (Guasti, 2005; Jehle et al., 2015), mammals (Clyde et al., 2008) and calcareous nannofossils (Fuqua et al., 2008; Monechi et al., 2012) were observed as well as within benthic foraminifera in dysoxic shelf settings (Sprong et al., 2011, 2012; Schulte et al., 2013).

At several sites in the Pacific and South Atlantic, the LDE was identified by two remarkable XRF core scanning Fe peaks and decreasing CaCO<sub>3</sub> values, indicated as LDE1 and LDE2 beds (Westerhold et al., 2008, 2011; Deprez et al., 2017a). A 1.6–2°C ocean floor warming was derived from benthic foraminifera  $\delta^{18}\text{O}$  variations (Westerhold et al., 2011; Jehle et al., 2015; Deprez et al. 2017a, 2017b) and 2.8°C from planktic surface-dwelling foraminifera (Jehle et al., 2015). Enhanced stratification of the upper water column at Shatsky Rise (ODP Site 1210) during the LDE was proposed, based on apparent isotope gradients ( $\delta^{18}\text{O}$ ,  $\delta^{13}\text{C}$ ) between surface and subsurface planktic foraminifera and an assemblage shift from high abundances of surface dwelling to subsurface dwelling planktic foraminifera. Both observed changes started ~170 ky prior to the LDE. This increase in stratification was explained by the development of a Deep Chlorophyll Maximum formed under a permanent gyre system leading to high abundances of subsurface dwelling foraminifera, benefiting from high nutrient levels below this layer. Furthermore, the extinction of *Praemurica* species and the rise of morozovellids occurred simultaneously with the onset of the LDE (Jehle et al., 2015). For this study, we analysed planktic foraminifera across the transient warming of the LDE from the South Atlantic deep-sea ODP Site 1262 in order to evaluate the impact of the event on the composition of planktic foraminiferal assemblages and to link this to paleoenvironmental changes as inferred from stable isotopes ( $\delta^{18}\text{O}$ ,  $\delta^{13}\text{C}$ ) of planktic and benthic foraminifera carbonate. Our new data

provide insight into the upper ocean structure of the South Atlantic across the LDE. Further, we compare our results with those of Pacific ODP Site 1210 (Jehle et al., 2015) to obtain more general patterns of paleooceanographic and paleoclimatic evolution based on planktic foraminifera across this event.

## 2 Material and Methods

### 2.1 Geological setting and deposition

ODP Site 1262 is positioned at the transition from the Angola Basin to Walvis Ridge (27°11.15'S, 1°34.62'E, 4755 mbsl, metres below sea level). During the Paleocene, the Site was situated at a latitude of ~37°S (Zachos et al., 2004; van Hinsbergen et al., 2015). Walvis Ridge is a ~3000 km long SW-NE trending aseismic ridge and reaches up to 200 mbsl from an abyssal depth of ~5000 m. Paleocene sediments were deposited at a paleodepth of ~3300 mbsl (Zachos et al., 2005) and are predominantly composed of calcareous nannofossil ooze, though more clayey and ash-rich in the deeper parts. Cyclic changes in magnetic susceptibility, also visible in colour variation, reflect orbital forcing (Westerhold et al., 2008).

### 2.2 Stratigraphy

Site 1262 holds a continuous record between the Cretaceous-Paleogene boundary and PETM (Westerhold et al., 2008). The LDE is biostratigraphically positioned within the basal part of the planktic foraminifera Subzone P3b (Wade et al., 2011; see Figure 18A) and the upper part of calcareous nannofossil Zone NP4 (Wade et al., 2011). The first radiation of fasciculiths/*Lithoptychius* is pinpointed close to the base of the LDE (Monechi et al., 2012, 2013). Magnetostratigraphically, the LDE is situated in the topmost part of C27n and the basal part of C26r. Accordingly it was also referred to as “Top C27n Event” (Westerhold et al., 2008; Dinarès-Turell et al., 2012, 2014).

Age control of Site 1262 is based on magnetostratigraphy and astrochronology (solution 2 of Westerhold et al., 2008). The onset of the LDE is at 62.18 Ma (Dinarès-Turell et al., 2014), the total duration of the LDE is about 200 ky and the investigated interval spans ~950 ky. TC27n was also pinpointed to 62.2 Ma in Zumaia, (Dinarès-Turell et al., 2014). Maxima of short-eccentricity cycles 38 (195.3 mcd, metres composite depth) and 39 (194.6 mcd) correspond to the two XRF Fe peaks during long eccentricity cycle Pc<sub>405</sub>10 (Dinarès-Turell et al., 2014). Site 1262 was stratigraphically correlated to ODP Sites 1209 and 1210 (Westerhold et al., 2008) as well as to Zumaia, Spain (Dinarès-Turell et al., 2014). The latter represents the Global boundary Stratotype Section and Point (GSSP) for the base of the Selandian Stage (Schmitz et al., 2011).

### 2.3 Methods

Nine meters of core (189.5 mcd–198.48 mcd) were sampled at a 2.5–45 cm spacing with highest sample density across the LDE. Sediment samples were washed over a 63 µm sieve and oven dried at 50°C for at least 48 hours.

Wt% CaCO<sub>3</sub> and coarse fraction (%CF) were measured on 84 and 86 samples, respectively, planktic foraminiferal fragmentation (%Fp), planktic foraminiferal number (PFN), planktic foraminiferal accumulation rate (PFAR) and planktic proportion (%P) as well as the faunal composition were analysed on 40 samples (Figure 18).  $\delta^{18}\text{O}$  and  $\delta^{13}\text{C}$  were measured on *Morozovella angulata*, *M. praeangulata* (surface dwelling planktic foraminifera), *Parasubbotina pseudobulloides*, *P. variospira* (planktic subsurface dwellers) and *Nuttallides truempyi* (benthic foraminifera) to provide data for the different habitats of the surface ocean, subsurface thermocline and the deep-sea. For  $\delta^{18}\text{O}$  and  $\delta^{13}\text{C}$  measurements, *P. pseudobulloides* and *P. variospira* were lumped together due to their rather similar morphology (see for discussion Jehle et al., 2015) and extremely similar values. For each data point, 3–6 planktic specimens were picked from 250–355  $\mu\text{m}$  size, however, in samples without quantitatively sufficient material, specimens of the 180–250  $\mu\text{m}$  fraction were added. Benthic foraminifera (Deprez et al., 2017a) were selected from the 125–180  $\mu\text{m}$  fraction only with 5–7 specimens. The specimens were reacted with 100 % phosphoric acid at 75°C using a Kiel IV online carbonate preparation line connected to a MAT 253 mass spectrometer. Machine reproducibility was checked by replicate analysis of laboratory standards, which was better than 0.03 ‰ and 0.1 ‰ for  $\delta^{13}\text{C}$  and  $\delta^{18}\text{O}$ , respectively. CaCO<sub>3</sub> values were analysed with a LECO CS 230 analyser at the BGR, Hannover. Coarse fraction was calculated by:

$$\%CF = ((\text{dry weight of residue [g]} > 63\mu\text{m}) / (\text{dry weight of total sample [g]})) \times 100 [\%] \quad (\text{eq. VII}).$$

Planktic foraminiferal fragmentation (%Fp) was counted in the >125  $\mu\text{m}$  size fraction during species quantification. Specimens with less than 50 % preserved were considered as a test fragment and %Fp was calculated by:

$$\%Fp = (\text{no. of fragments}) / (\text{no. of fragments} + \text{no. of complete tests}) \times 100 [\%] \quad (\text{eq. VIII})$$

PFN is the number of planktic foraminifera per gram dry unwashed sediment. For PFAR, the age model of Westerhold et al. (2008), expressed in linear sedimentation rate (*LSR*, [ $\text{cm kyr}^{-1}$ ]) between each short-term eccentricity maximum, and shipboard dry bulk density (*DBD*, [ $\text{g cc}^{-1}$ ]) data were linearly interpolated and multiplied with PFN.

$$PFAR = DBD \times LSR \times PFN \quad [\# \text{ cm}^{-2} \text{ kyr}^{-1}] \quad (\text{eq. VIII}).$$

40 samples were analysed for planktic foraminiferal assemblage composition under a Zeiss Stemi 2000-C binocular with 100 × magnification. Planktic foraminifera were counted from sample splits which yield between 300 and 400 specimens in the >125  $\mu\text{m}$  size fraction (Figure 19). It is very error-prone to determine juvenile tests to the species level; therefore assemblage census is usually based on larger sizes (> 125 $\mu\text{m}$ ). The ontogenetic stages might be linked to changes in trophic behaviour and hosting symbionts (e.g. Shackleton et al., 1985; Norris, 1996). Species identification follows almost exclusively Berggren and Norris (1997) and Olsson et al. (1999).



The diversity of planktic foraminiferal assemblages was characterized by species richness (S), Shannon heterogeneity (H', Shannon and Weaver, 1949) and evenness:

$$\text{Shannon heterogeneity: } H' = - \sum_{i=1}^S p_i \ln p_i \quad (\text{eq. X})$$

$$\text{Evenness: } E = H'/H_{\max}, H_{\max} = \ln(S) \quad (\text{XI})$$

$p_i$  as the proportion of individuals belonging to the  $i^{\text{th}}$  species in the dataset of interest,

heterogeneity is  $0 \leq H' \leq \ln S$ ,

Evenness is  $0 \leq E \leq 1.0$ .

We used the “vegan package” for R for the statistical analysis of the non-metric multidimensional scaling (NMDS, Figure 20) with Bray-Curtis distance measure and  $\text{CaCO}_3$  as well as  $\delta^{18}\text{O}$  and  $\delta^{13}\text{C}$  of all three foraminifera groups. Relative abundance of all samples with paired  $\text{CaCO}_3$ ,  $\delta^{18}\text{O}$  and  $\delta^{13}\text{C}$  results were used. All species with a relative abundance  $>2\%$  in at least one sample were included.

## 3 Results

### 3.1 Carbonate content and dissolution indicators

Background  $\text{CaCO}_3$  values (Figure 18 B) range between  $\sim 80$  and  $86\text{ wt } \%$ , with two distinct minima of  $69$  and  $71\text{ wt } \%$  corresponding to LDE1 ( $195.4\text{ mcd}$ ) and LDE2 ( $194.5\text{ mcd}$ ).

Coarse fraction ( $\%CF$ , Figure 18 C) data show background values of  $3\text{--}4\%$  below the LDE and a minimum of  $0.6\%$  at the onset of LDE1, from where it rises up to  $8\%$  from LDE2 to the upper part of the record, where it drops to  $2\%$ . Fragmentation of planktic foraminifera ( $\%Fp$ ,  $>125\text{ }\mu\text{m}$ ; Figure 18 D) shows maxima ( $\sim 15\%$ ) at the base of the sequence together with the lowest  $\%CF$  during the onset of LDE1, relative to background values of  $4\text{--}5\%$ .

The sedimentation rate (SR, Figure 18 E) varies between  $0.82$  and  $0.88\text{ cm kyr}^{-1}$  and, considering the uncertainties of this calculation, is seen as constant. Planktic foraminiferal numbers (PFN,  $>63\text{ }\mu\text{m}$  [ $\# \text{ g}^{-1}$ ]; Figure 18 F) decrease at the onset of LDE1, subsequently rise to peak values within LDE2 and show a long-term decrease after the LDE. PFN ranges between  $15,000$  and  $219,000\text{ g}^{-1}$ . PFAR ( $>63\text{ }\mu\text{m}$ ) ranges between  $\sim 17,000$  and  $250,000\text{ cm}^{-2}\text{ kyr}^{-1}$  with a similar trend like PFN. The percentage of planktic foraminifera,  $\%P$  ( $>63\text{ }\mu\text{m}$  fraction; Figure 18G) shows a decrease to  $97.9\%$  during LDE1 compared to a background of  $>99\%$ . The overall shape of the curve is similar to  $\%CF$ .

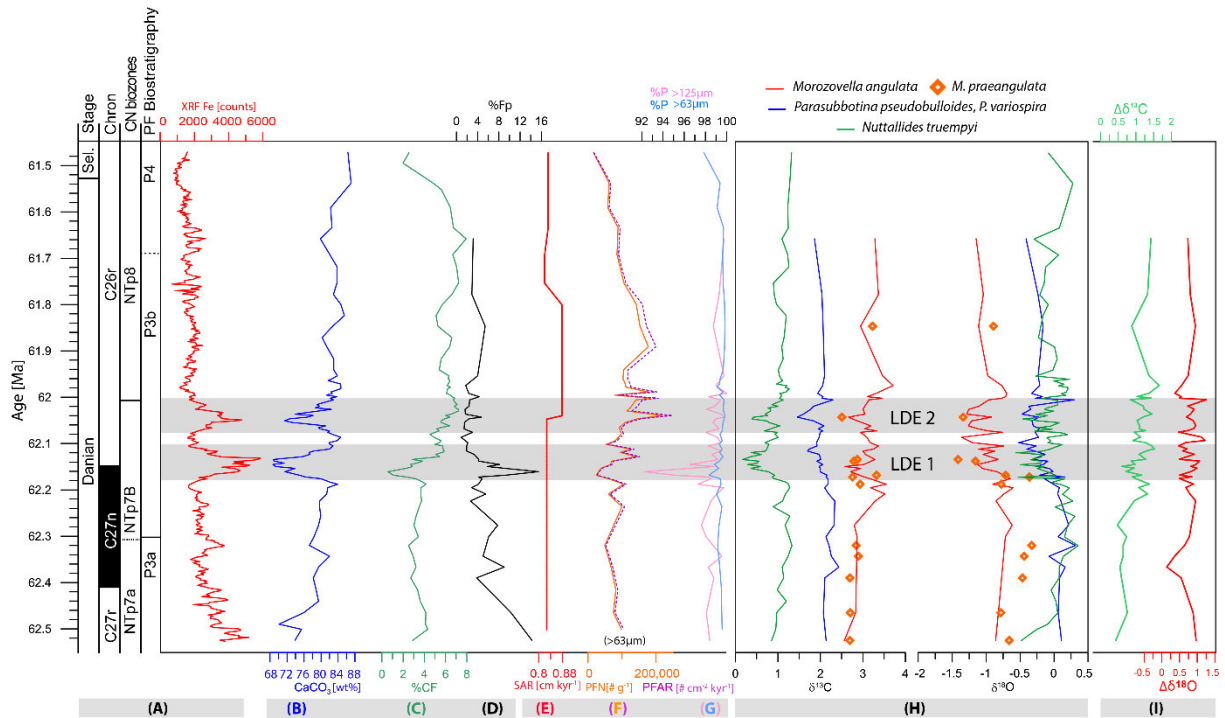


Figure 18: Stratigraphy, XRF core scanning Fe intensities, stable isotopes and other sedimentary parameters of samples from the LDE at Site 1262. (A) Stratigraphy, including magnetostratigraphy and biostratigraphy, adapted from Monechi et al. (2013). characteristic Fe intensities (Westerhold et al., 2008) during the LDE are used for stratigraphic correlation. Sedimentary parameters are (B) carbonate (wt% CaCO<sub>3</sub>) measurements, with (C) coarse fraction (%CF), (D) planktic foraminifera fragmentation index (%Fp) >125µm, (E) sedimentation rate (SR, Westerhold et al., 2008, used for planktic foraminifera accumulation rate (PFAR)), (F) planktic foraminifera number (PFN) with PFAR and (G) the planktic foraminifera proportion (%P) in two different size fractions (>63µm, >125µm). (H) shows δ<sup>13</sup>C and δ<sup>18</sup>O records of benthic (*Nuttallides truempyi*), planktic subsurface (*P. pseudobulloides* and *P. variospira*) and planktic surface dwellers (*M. praeangulata* and *M. angulata*) and (I) Δδ<sup>13</sup>C and Δδ<sup>18</sup>O gradients of surface to subsurface isotope values.

### 3.2 Foraminiferal stable isotopes (δ<sup>13</sup>C, δ<sup>18</sup>O)

δ<sup>13</sup>C of benthic foraminifera (*Nuttallides truempyi*) varies around 1.0 ‰ and displays two negative excursions (up to -0.9 ‰) contemporary to the Fe XRF core scanning peaks (Figure 18 A, H; Deprez et al., 2017a). δ<sup>13</sup>C values of subsurface dwelling *Parasubbotina pseudobulloides* and *P. variospira* show a slightly decreasing trend of -0.6 ‰ (2.3 to 1.7 ‰) within LDE1 and a sharper, more negative excursion of -0.8 ‰ (2.2 to 1.4 ‰) during LDE2. Surface dwelling *Morozovella angulata* shows a -1.1 ‰ excursion (3.7 to 2.6 ‰) and, thus, a more distinct response than *P. pseudobulloides* and *P. variospira* to the LDE. However, the variability in *M. angulata* is generally very high and may thus overestimate the amplitude. The positive excursion just below and above LDE1 show amplitudes of comparable heights to the negative CIEs.

The δ<sup>18</sup>O values of *N. truempyi* show a high variability with two distinct negative excursions (up to -0.8 ‰) within the LDE. *Parasubbotina pseudobulloides* and *P. variospira* yield values between -0.7 and 0.2 ‰ and display a negative long-term trend from below LDE1. δ<sup>18</sup>O of *M. angulata* decreases by -0.7 ‰ (-0.6 to -1.3 ‰) and rises directly above LDE2 to -0.7 ‰ before it slowly decreases to a steady level of -0.9 ‰. Surface and subsurface species display a rather similar curve, whereas the benthic record shows a pattern with distinctly negative peaks in

LDE1 and LDE2, resembling the negative excursions in the XRF Fe counts. The  $\delta^{13}\text{C}$  gradient between surface and subsurface slightly increases below LDE1 (+0.3 ‰), but there is no clear trend for  $\Delta\delta^{18}\text{O}$  (Figure 18 I).

### 3.3 Planktic foraminiferal assemblages

Planktic foraminiferal diversity remains relatively constant during the study interval. Shannon H' diversity varies between 2.2 and 2.6 and species richness (S) between 14 and 27 species. Both parameters show maxima during LDE1 and LDE2 and a high variability between the two phases (Figure 19).

The ten most abundant species cover 92 % of all planktic foraminifera tests. Subsurface dwelling *Parasubbotina* and *Subbotina* make up almost 70 %, whereas surface dwelling *Morozovella* show an average abundance of 11 % (Figure 19). Species can be grouped according to their abundance and appearance (Figure 19): (1) species with highest abundances below the LDE, (2) species present with minor variations throughout the record or with slightly enhanced abundances during the LDE and (3) species with appearance or high abundances above the LDE. Group (1) covers *Praemurica inconstans* and *P. uncinata* as they initially compose 4 % and 24 % of the assemblage and disappear just below or during the LDE, and *M. praeangulata* with a comparable pattern, starting with up to 17 % below the LDE.

Group (2) contains *Globanomalina ehrenbergi* with one peak of 4 % between LDE1 and LDE2, *Globanomalina imitata* varies between 0 and 5 % and is most common below the LDE. *Globanomalina chapmani* ranges from 1.5–10 %, *Parasubbotina varianta* appears between 7 and 18 % without distinct maxima, *Subbotina triloculinoides* occurs abundantly with peak values of 22 % just before the onset and after the termination of the LDE. *Subbotina cancellata* ranges from 10–21 % with a long-term decrease through the record. *Subbotina velascoensis* shows its highest abundance (7 %) below the LDE. *Parasubbotina pseudobulloides* shows a decreasing trend during our record from 9–2%. *Parasubbotina variospira* shows a similar pattern with peak values below the LDE (25 %). *Igorina pusilla* reaches highest abundances of up to 10 % during the LDE interval.

Generally higher abundances above the LDE (group 3) were observed for *M. conicotruncata*, *I. albeari* and *M. angulata*. *Morozovella conicotruncata* peaks (11 %) above the LDE, *I. albeari* shows peak abundances (12 %) during LDE1 and LDE2. *Morozovella angulata* initially also shows peak levels up to 12 % within LDE1 and LDE2 but becomes even more abundant (20 %) towards the top of the record.

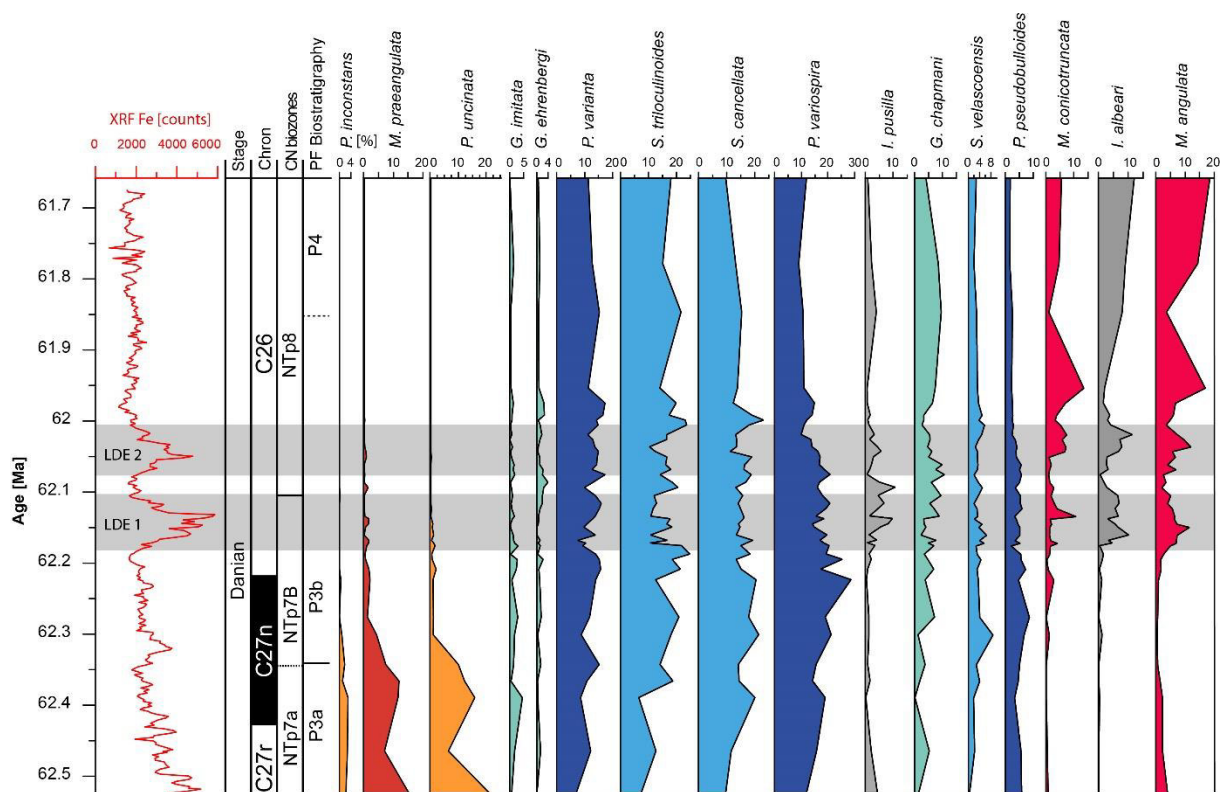


Figure 19: Species distribution of planktic foraminifera together with XRF core scanning Fe intensities (Westerhold et al., 2008) and (bio-) stratigraphy. Species are coloured according to their habitats: surface mixed layer in red, subsurface thermocline in blue and green and Igorina albeari and I. pusilla in grey. The taxa also make three groups by their appearances, which is (1) appearance mostly below the LDE, (2) appearance over the entire record or enhanced during the LDE and (3) appearance mostly after the LDE.

### 3.4 Discussion: Carbonate dissolution and preservation of foraminiferal calcite

#### 3.4.1 Carbonate preservation

Deep-sea carbonate dissolution is predominantly controlled by depth changes of the lysocline/calcite compensation depth (CCD) as well as by oxidation of organic carbon. Dissolution causes enhanced test fragmentation of planktic foraminifera (%Fp: e.g. Berger, 1970; Dittert et al., 1999), which are up to three times more dissolution-susceptible than benthics (Berger, 1973). Consequently, carbonate dissolution leads not only to increased %Fp and lower CaCO<sub>3</sub>, but also to lower %CF, %P, PFN and PFAR.

As indicated, carbonate background values are rather constant throughout the studied succession, whereas the LDE beds display CaCO<sub>3</sub> minima. CaCO<sub>3</sub> drops by 14 wt% (83–69 %) within LDE1 (195.4 mcd), and by 13 wt% (84–71 %) within LDE2 (194.5 mcd). We consider carbonate dissolution to be more severe during LDE1 than during LDE2 due to higher %Fp and lower %CF (Figure 18D) concurrent to lower values of %P, PFN and PFAR during LDE1. For LDE2, we speculate that other processes were involved such as enhanced dilution by clay or a decline of carbonate production. Enhanced dilution is assumed due to an accompanied increase in the sedimentation rate, starting during LDE2 (Figure 18 E). However, absolute abundances of planktic foraminifera are rather constant (Figure 18 F), but changes within numbers of calcareous nannofossils were not taken into account. As the second benthic negative CIE (194.5 mcd) is smaller than the first peak, the amount of carbon injected into the ocean-

atmosphere system might have been below the threshold for a substantial lysocline rise during LDE2. Clay-enriched horizons were also documented at the base of the entire LDE from deep-sea successions at Shatsky Rise (Westerhold et al., 2008, 2011; Jehle et al., 2015).

### 3.4.2 Foraminiferal preservation

Good preservation of foraminiferal carbonate is key for both reliable geochemical analyses and assemblage counts. Mechanisms controlling test preservation include dissolution, bacterial activity and recrystallization or overgrowth (e.g. Hancock et al., 2007; Nguyen et al., 2011). Foraminifera largely precipitate their carbonate from ambient seawater (e.g. Erez and Luz, 1983), and are, thus, considered to be excellent carriers of past seawater geochemistry signals. However, the geochemical composition of their calcite might be altered by diagenesis and recrystallization during and after burial (e.g. Stap et al., 2010; Edgar et al., 2013).  $\delta^{13}\text{C}$  tends to be less influenced by diagenetic alterations while the effect on  $\delta^{18}\text{O}$  is more substantial (Killingley, 1983; D'Hondt and Zachos, 1993; Pearson et al., 2001).

Light microscope observations of planktic foraminifera in Paleocene samples of Site 1262 reveal sparse overgrowth, but an overall moderate to good preservation (Birch et al., 2012 and observations of the current work). Slight yellow stains on the tests make them appear less white than seen in other Paleocene sequences like Shatsky Rise Site 1210 (Jehle et al., 2015). Specimens are free from infillings, show a milky, coarsely textured surface through light microscopy and indicate recrystallization under the SEM (Birch et al., 2012). It seems to be a typical, somewhat “frosty” preservation in deep-sea carbonate oozes (Pearson et al., 2001; Sexton et al., 2006). This state of planktic foraminiferal preservation usually leads to heavier  $\delta^{18}\text{O}$  values, since the calcite carries an additional bottom water isotope signature due to recrystallization, and therefore reconstructed paleo-temperatures are lower than for unaltered tests (Pearson et al., 2001; Sexton et al., 2006; Edgar et al., 2015). For the more strongly built benthic foraminifera, the impact of recrystallization on both  $\delta^{13}\text{C}$  and  $\delta^{18}\text{O}$  is considered to be much less severe than for planktic foraminifera (Edgar et al., 2013; Voigt et al., 2016).

In contrast to earlier studies (e.g. Thomas et al., 1999; Raffi and Bernardi, 2008), we suspect that diagenetic alteration has played a substantial role at Site 1262 for the planktic  $\delta^{18}\text{O}$  signal. Besides ultrastructural observations by SEM (Birch et al., 2012), this is supported by the negligible vertical temperature gradient between  $\delta^{18}\text{O}$  values of surface, subsurface and benthic dwellers and the complete lack of a  $\delta^{18}\text{O}$  gradient between subsurface and benthic environment (Figure 18 I). The temperature difference between surface ocean and seafloor of only  $\sim 6.5^\circ\text{C}$  is unrealistically low. For comparison, the vertical temperature gradient at Pacific Shatsky Rise Site 1210 was estimated to be  $\sim 9^\circ\text{C}$  during the LDE (Jehle et al., 2015) and up to  $15^\circ\text{C}$  at the tropical or equatorial North Pacific Ocean (Shatsky Rise Site 1209, Allison Guyot Site 865) during Late Paleocene, PETM and Early Eocene (Tripathi and Elderfield, 2005). In certain intervals the subsurface dwellers have even lower  $\delta^{18}\text{O}$  values than the benthics (Figure 18 H, 195.05–195.98 rmcd). This would not be the case in well-preserved foraminiferal assemblages, even if we would consider the unlikely existence of warm saline bottom waters. Based on visually indicated recrystallization and overgrowth in these intervals (Birch et al., 2012), we conclude that surface and subsurface planktic foraminiferal tests were recrystallized during early burial, which shifted the recorded  $\delta^{18}\text{O}$  towards more positive values. Nevertheless,

assuming a more or less homogeneous diagenetic overprint during the studied interval, the relative  $\delta^{18}\text{O}$  changes might still represent the original trends (Sexton et al., 2006), with a modified magnitude of change.

Furthermore, species-specific dissolution susceptibility can change the assemblage composition (e.g. Berger, 1970; Pearson et al., 2001; Petrizzo, 2007; Nguyen et al. 2011; Nguyen and Speijer, 2014) and consequently bias the interpretation of faunal data. As some species are more dissolution susceptible than others, the planktic foraminiferal assemblage composition could, to some extent, be biased by carbonate dissolution. Dissolution and fragmentation occurs during settling, sedimentation or shortly after burial. As a consequence, the assemblage composition would shift to lower relative abundances of dissolution-susceptible taxa such as *Igorina* spp. and subsequently higher relative abundances of thick-walled *Acarinina* or *Morozovella* species (Petrizzo et al., 2008; Nguyen et al., 2011). However, both aforementioned taxa are not very abundant in the studied samples while *Igorina* spp. is present in moderate numbers and flourishes during the LDE. The species might prefer a warmer environment; therefore, the very high production rate might cover dissolution to some extent. Further indicators for partial dissolution are supposedly a combination of low relative abundance and increased fragmentation of *Subbotina* spp., low %P rate and PFN (e.g. Nguyen et al., 2009). Altogether, in contrast to the stable isotope signal, the planktic foraminiferal composition has presumably not been substantially affected by dissolution during or before sedimentation.

### 3.5 Stable isotope patterns during the LDE at Walvis Ridge

In addition to literature data (Berggren and Norris, 1997; Olsson et al., 1999), the habitats of planktic foraminifera taxa were inferred from  $\delta^{13}\text{C}$  and  $\delta^{18}\text{O}$  values. We distinguished between (photosymbiotic) surface dwelling and subsurface dwelling, thermocline species (e.g. Shackleton et al., 1985; Norris, 1996; Birch et al., 2012). Studied photosymbiont-bearing taxa are *M. angulata*, *M. praeangulata*, *P. uncinata* and *P. incontans*, while non-photosymbiotic are *P. variospira* and *P. pseudobulloides*. For the benthic habitat, *N. truempyi* was used.

#### 3.5.1 $\delta^{13}\text{C}$ response to the LDE

The surface water signal is influenced by primary productivity and subsidence of  $^{12}\text{C}$ -enriched organic particles to the seafloor, causing a carbon depth gradient. Due to preferred uptake of  $^{12}\text{C}$  by symbiotic algae, photosymbiotic foraminiferal tests are  $^{13}\text{C}$  enriched relative to ambient seawater and to deeper dwelling foraminifera without photosymbionts (e.g. Shackleton et al., 1985; Spero et al., 1991; Rohling and Cooke, 2003). Hence,  $\delta^{13}\text{C}$  of seawater and foraminifera is depth-dependent.

Even though the  $\sim 1\text{‰}$  CIE in planktic surface dwellers is quite large and distinct during the LDE, it also has a steady state below the LDE until  $\sim 62.25$  Ma with about the same values as the peak and shows a quick positive excursion just below the event. For surface dwelling foraminifera, possible reasons might be (a) varying photosymbiotic activity or (b) surface ocean currents. Suboptimal living conditions might have led to smaller tests, inhabiting less algae symbionts (Schmidt et al., 2004). The average  $\delta^{13}\text{C}$  values are more positive above the LDE

than below, suggesting either a higher photosymbiotic activity for *M. angulata* than for *M. praeangulata*, or, more likely, they follow the secular trend to heavier  $\delta^{13}\text{C}$  values above the LDE probably due to higher primary productivity and slightly more oxygenated surface water after the LDE.

The surface- to subsurface  $\delta^{13}\text{C}$  gradient ( $\Delta\delta^{13}\text{C}$ ) displays a rather constant offset (Figure 18 I). Enhanced stratification as observed at Shatsky Rise (Jehle et al., 2015) is not visible here. The  $\delta^{13}\text{C}$  value was probably very uniform in the different water layers due to a higher mixing rate and ocean currents, or because of diagenetic overprint, even though  $\delta^{13}\text{C}$  is normally less affected.

### 3.5.2 $\delta^{18}\text{O}$ response to the LDE

Temperature is an important factor controlling  $\delta^{18}\text{O}$  of foraminiferal calcite due to equilibrium fractionation between seawater and calcite. Because of their shallower habitat,  $\delta^{18}\text{O}$  values are lower in photosymbiotic planktic foraminifera than in their non-symbiotic relatives. Changes in salinity, carbonate ion concentration or pH as well as waxing and waning of continental ice sheets (e.g. Shackleton, 1967; Railsback et al., 1989; Spero et al., 1997) are additional factors to influence foraminiferal  $\delta^{18}\text{O}$ . The ice-effect is not taken into consideration as the early Paleogene is generally suspected as an ice-free period (e.g. Zachos et al., 1994).

During the LDE,  $\delta^{18}\text{O}$  records suggest a temperature rise of  $\sim 2.0^\circ\text{C}$  (0.5 ‰) at the seafloor (*N. truempyi*),  $\sim 1.5^\circ\text{C}$  (0.35 ‰) in the thermocline (*P. variospira* and *P. pseudobulloides*) and  $\sim 2.6^\circ\text{C}$  (0.6 ‰) in surface water (*M. angulata*). This ocean warming is supported by the faunal data, which show an abundance increase of warm-water, low-latitude taxa such as *Morozovella*.

### 3.5.3 Implications on the stable isotope patterns for the LDE

The negative CIEs associated with the LDE could be explained by various scenarios as proposed for the PETM (e.g., Dickens et al., 1997). For the PETM, one scenario considers a sudden and massive release of methane from the seafloor, probably triggered by circulation changes in the deep ocean (Tripathi and Elderfield, 2005; Nunes and Norris, 2006) or large-scale continental slope failure (e.g. Katz et al., 2001). This methane was rapidly oxidized to  $\text{CO}_2$ , contributing to stronger greenhouse forcing. On the other hand, the destabilization of methane hydrates was seen as unlikely to be the sole source as the reservoir at the end of the Paleocene was probably not sufficient (e.g. Buffet and Archer, 2004; Kirtland Turner and Ridgwell, 2016), whereas the magnitude of warming and changes in the CCD are compatible with much greater carbon masses. Therefore, additional carbon sources were suggested, such as volcanic outgassing or thermal decomposition of organic matter or oxidation of terrestrial and marine organic carbon (Pagani et al., 2006; Dickens, 2011; DeConto et al., 2012; Gutjahr et al., 2017).

For the LDE, most of these explanations suggest amplifications by increased insolation due to temporal coincidence with short-term eccentricity maxima (Westerhold et al., 2008) contributing to global warming. In addition, the oxidation of a massive amount of organic carbon or enhanced  $\text{CO}_2$  content in the ocean-atmosphere system due to intense volcanic activity in the North Atlantic Igneous Province or southeastern Greenland margin (Sinton and

Duncan, 1998; Pedersen et al., 2002; Larsen et al., 2016) may have played an important role. At the same time, and probably linked to that volcanic activity, the South Atlantic spreading rate shows a major deceleration at the Danian-Selandian boundary from ~17 to ~14 km myr<sup>-1</sup>.

However, as the LDE is more comparable to ETM2 with regard to orbital pacing and magnitude than to the PETM, similar causes have been inferred for these two events (Deprez et al., 2017a, 2017b). As for the LDE, Eocene short-term hyperthermals like ETM2 and ETM3 mostly coincide with eccentricity maxima. Moreover, orbital pacing might have triggered changes in ocean ventilation, leading to oxidation of dissolved organic matter during transient Eocene warming events (Sexton et al., 2011; Stap et al., 2009). This idea has also been put forward by Dinarès-Turell et al. (2012) to explain the LDE negative CIEs as a form of interaction between orbital cycles and volcanism.

### 3.6 Planktic foraminifera faunal changes

Surface mixed layer foraminifera were abundant below the LDE with a maximal abundance of *Praemurica uncinata*, *P. inconstans* (together up to 24 %) and *M. praeangulata* (up to 15 %). A turnover of photosymbiont-bearing taxa is well documented by the disappearance of the genus *Praemurica*, the long-term decline of *M. praeangulata* and the parallel emergence of other taxa (e.g. *Igorina albeari*, *Morozovella* spp.) with the onset of the LDE. The disappearance of *Praemurica* and decline of *M. praeangulata* started ~170 ky before the event and received a final push with the LDE onset. The surface ocean assemblage changed from a praemuricate to a muricate fauna as observed at other sites (Norris, 1996; Guasti et al., 2006; Jehle et al., 2015). Other than *P. uncinata* and *P. inconstans*, *M. praeangulata* survived the LDE, albeit with decreasing abundances. The replacement of *Praemurica* by *Morozovella* likely had competitive reasons, since both genera are photosymbiotic surface dwellers and inhabited a similar ecological niche (Norris, 1996; Birch et al., 2012). They have probably coexisted and competed at the same time in biogeographical sympatry. The transition of a *Praemurica*- to *Morozovella*-dominated surface ocean fauna took place around the first occurrence of *Igorina albeari* (=P3a/P3b Subzone boundary), whereas the final disappearance of *Praemurica* coincides with LDE1. In addition, the planktic turnover is characterised by the rise of *I. albeari* and *M. conicotruncata*.

$\delta^{18}\text{O}$  indicates slightly lower calcification temperatures for *Praemurica* than for *M. angulata* and *M. praeangulata*, suggesting either a somewhat deeper habitat or alternatively a flourishing of *Praemurica* during a colder season. *Morozovella praeangulata* is considered to have a closer relationship to *Praemurica* than the other morozovellid species (e.g. Berggren and Norris, 1997; Olsson et al., 1999). The ecological preferences of *M. praeangulata* as inferred from  $\delta^{13}\text{C}$  suggest a similar photosymbiotic activity like *M. angulata* (Figure 18 H).

Absolute and relative abundances of *M. angulata* increased within the LDE beds (Figure 19), suggesting a relative benefit from temperature rise and paleoenvironmental changes. This development is compatible with a characterization as a warm water taxon showing higher numbers in the (sub-)tropical oceans (e.g. Quillévéré and Norris, 2003). Similar to *M. angulata*, *I. albeari* showed enhanced abundances in both LDE beds, while *I. pusilla* only increased during LDE1. Therefore, *I. albeari* might have had a higher temperature sensitivity than



*I. pusilla*, *Morozovella* and *Igorina* probably lived in different niches and were not direct competitors as the latter lived in slightly deeper water than *Morozovella* (e.g. Norris, 1996; Berggren and Norris, 1997; Pearson et al., 2001; Jehle et al., 2015). In contrast to *I. albeari*, which became more abundant towards the top of the record, *I. pusilla* then declined and might have had different ecological optima in terms of nutrient availability, temperature, water depth or flourishing during a somewhat colder season than *I. albeari*.

Over the long run, surface dwellers (*M. angulata*, *M. conicotruncata*) show a relative increase at the expense of *Parasubbotina* as also supported by absolute numbers. The change starts at the LDE onset and can be linked to the observed LDE warming and the gradual replacement of *Praemurica* by *Morozovella*.

Thermocline dwellers (*Parasubbotina* spp., *Subbotina* spp.) make up 46–86 % of all species (~70 % in average). Absolute abundance (cf. Appendix) of *Subbotina* and *Parasubbotina* show slightly enhanced numbers of *S. cancellata*, *S. triloculinoidea* and *P. variospira* during the LDE beds, however, as a short-term response only. We conclude that the thermocline habitat was constantly unstable and, thus, favourable for the two subsurface genera.

The above given interpretations are supported by non-metric dimensional scaling (NMDS). The strongest separation is between the samples below 196.63 mcd (before 62.30 Ma) by ~0.3 dissimilarity measure in the NMDS axis 1 (Figure 20) and the samples during LDE1. Assemblage changes as demonstrated by the NMDS are expressed by two main sample groups, separating the samples “below the LDE” from those “during” and “above”. The samples during and above the LDE show a very similar faunal assemblage opposed to the samples below the event. The start of major, but gradual changes are observed ~160 ky before the LDE (196.98 mcd at 62.34 Ma) as expressed by NMDS axis 1 loadings (Figure 20), possibly caused by a decrease and subsequent disappearance of praemuricate species and the introduction of *I. albeari* and new *Morozovella* species.

Based on stable isotope and faunal data, the paleooceanographic scenario for Site 1262 might reflect a development from a “temperate” system to a more “subtropical” one, in which the zonal boundary shifted southwards during the LDE warmings. The subtropical system is generally warmer, more stable and better stratified, causing improved living conditions for surface dwelling photosymbiont-bearing foraminifera. Before the LDE, photosymbiotic species were rare, which can be explained by enhanced deep mixing of the upper water column. As surface dwellers mostly declined between the two LDE peaks and show higher abundances during both event levels, the somewhat colder and less stratified conditions in between probably inhibited proliferation. After the LDE, the situation became somewhat more favourable for photosymbiotic taxa, supporting a slightly better stratified upper ocean as indicated by the enhanced stable isotope gradients ( $\Delta$ ) and improved living conditions for subsurface taxa (Berggren and Norris, 1997; Figure 19, Figure 20).

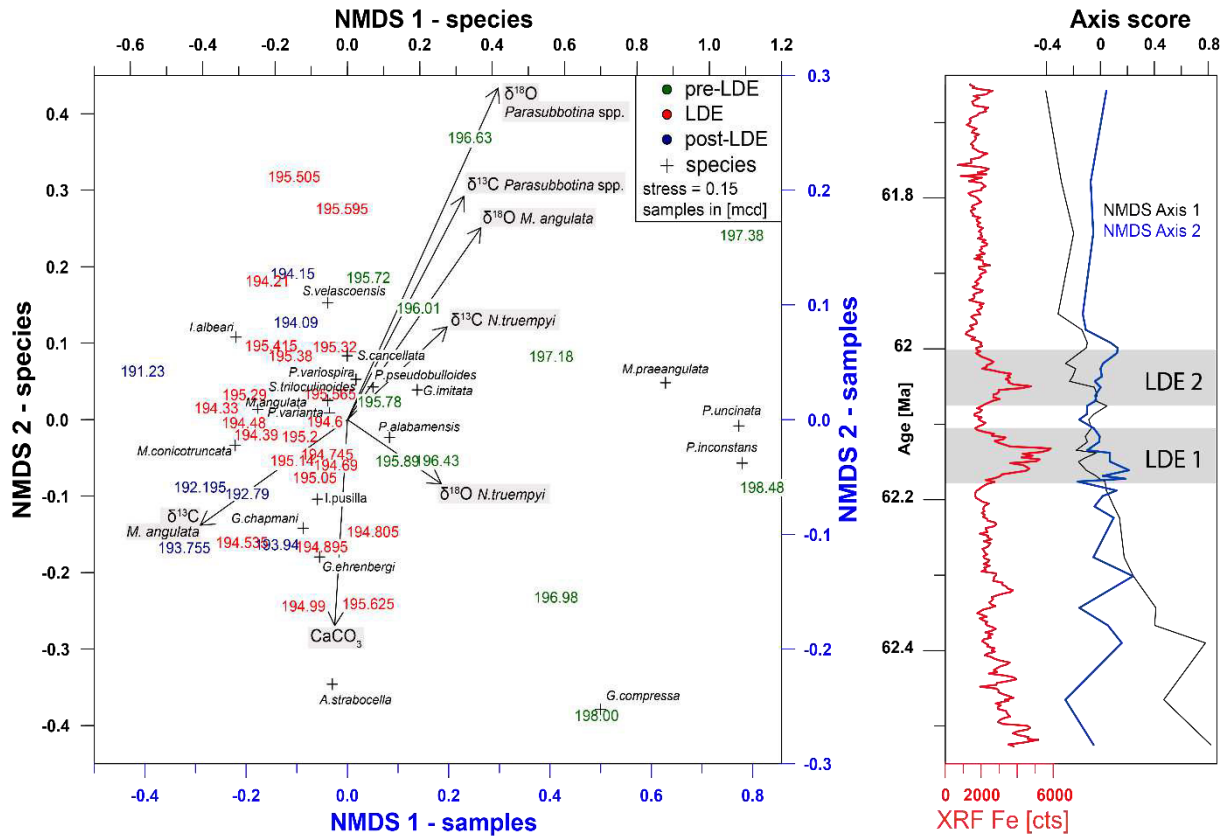


Figure 20: Non-metric multidimensional scaling. Left panel: Results of NMDS (stress=0.15, Bray-Curtis distances) offer relative similarities and differences of the planktic foraminifera communities (species level) between the event stages (color-coded as indicated). Species are marked with cross symbols. Numbers of depth indicate the sample. Pre-LDE assemblages stand out from the rest of the record.

Vectors are considered to represent ecological control of the distribution and belong to the “species” coordinate system. Environmental parameters should be considered in aspects of direction, length again is arbitrarily scaled and should be compared in relation to each other (Hammer and Harper, 2012). Significant at the 95 % level are  $\delta^{13}\text{C}$  and  $\delta^{18}\text{O}$  of *Parasubbotina uncinata*, *P. inconstans* and *M. angulata*. Right panel: Loadings of NMDS Axis 1 and 2, as well as the XRF core scanning Fe variations (Westerhold et al., 2008) are shown.

### 3.7 Comparison to Pacific ODP Site 1210

#### 3.7.1 Paleogeography of ODP Sites 1210 and 1262

The opening of the South Atlantic Ocean started in the Early Cretaceous (Pérez-Díaz and Eagles, 2017), and so, the ocean was narrower in the Paleocene and more restricted than today, causing a different ocean current system compared to the recent South Atlantic. The Walvis Ridge Paleocene paleoceanographic reconstructions suggest strong vertical surface water mixing in the South Atlantic from south to north along the African coastline (e.g. Haq, 1981; Pak and Miller, 1992).

ODP Site 1210 (Shatsky Rise) was located at a subtropical paleolatitude of  $\sim 24^\circ\text{N}$  (van Hinsbergen et al., 2015) and an estimated paleodepth of about 2700 m (Site 1262:  $\sim 3300$  m). The plateau was positioned much closer to the equator than today and was, thus, subjected to higher insolation and a different circulation pattern from today (Bralower et al., 2002).

### 3.7.2 Geochemical data and preservation

Like for Site 1262, two distinct XRF core scanning Fe peaks identify the LDE horizons at Site 1210 (195.3 mcd, LDE1, and 194.6 mcd, LDE2). These Fe peaks serve as a key tool for stratigraphic correlation between the two sites (Westerhold et al., 2008).

The average wt%  $\text{CaCO}_3$  content is high at both sites, but at Site 1210 with 84–95 % much higher than at Site 1262 (68–86 %). Both show two negative peaks contemporary to the event horizons. Both Sites 1262 and 1210 as well as 1209 (Westerhold et al., 2011) show two negative benthic CIEs, which are  $\sim 100$  ky apart from each other, supporting the idea of a two-phase event coinciding with two short eccentricity maxima (Westerhold et al., 2008; Dinares-Turell et al., 2014) and Fe XRF peaks. A two-phase scenario was identified at several deep-sea sites (ODP Sites 1001, 1209, 1210, 1262, U1407; Westerhold et al. 2008; Jehle et al., 2015; Deprez et al., 2017a and b; Yamaguchi et al., 2017). At Site 1210, benthic foraminifera show a by 0.4 ‰ minor excursion of both  $\delta^{18}\text{O}$  and  $\delta^{13}\text{C}$  compared to Site 1262, indicating (a) slightly higher deep-water temperatures at 1210, which is plausible due to a shallower water depth, or (b) lighter  $\delta^{13}\text{C}$  might result from aged water masses, transported from other ocean areas (e.g. Kroopnick, 1979; Quillévéré et al., 2002). As the Southern Ocean was an important place for deep-water formation (Pak and Miller, 1992, Kroopnick, 1980), the transport of bottom water masses to the central Pacific was longer than to the South Atlantic.

From comparing dissolution sensitive parameters of Site 1210 (Jehle et al., 2015) with Site 1262 such as CF, %PF or %Fp, we conclude more intense carbonate dissolution for Site 1262, like previously observed in the early Eocene (Stap et al., 2009). At both sites, LDE1 was more influenced by carbonate dissolution than LDE2. Slightly enhanced carbonate dissolution, caused by a lysocline/CCD rise, is assumed for LDE1, whereas terrigenous dilution could be more possible during LDE2 at Site 1262 than at Site 1210. Hints for that scenario are a stronger  $\text{CaCO}_3$  drop, increased %Fp, low %CF and low %P, PFN and PFAR during LDE1 compared to a smaller  $\text{CaCO}_3$  drop and a lack of these characteristic changes during LDE2 (Figure 18).

In addition to that, recrystallization is higher at Walvis Ridge than at Shatsky Rise. This view is supported by a strongly muted temperature difference between planktic and benthic foraminifera at Site 1262. At Site 1210, the largest  $\delta^{18}\text{O}$  temperature gradient ( $\Delta$ ) is  $\sim 9^\circ\text{C}$ , which is already rather low and probably overprinted by early diagenesis. At Site 1262, however, this difference makes up only  $\sim 6.5^\circ\text{C}$ , strongly suggesting an overprint of the pelagic signal through early diagenesis at the colder seafloor. Recrystallization of planktic foraminiferal calcite dampened the  $\delta^{18}\text{O}$  warming signal (Pearson et al., 2001; Sexton et al., 2006; Jehle et al., 2015).

Jehle et al. (2015) observed at Shatsky Rise 1210 a rising gradient before and during the LDE, suggesting enhanced stratification of upper water masses, a change which is accompanied by higher abundance of thermocline dwelling *Parasubbotina*. It was proposed that a Deep

Chlorophyll Maximum was developed under well-stratified conditions during and after the LDE.

Comparing the  $\delta^{13}\text{C}/\delta^{18}\text{O}$  crossplots of the two sites, divergent signatures in the different habitats become apparent (Figure 21).  $\delta^{13}\text{C}$  results of surface dwelling *M. angulata* and *Praemurica* species are within the same range, but surface  $\delta^{18}\text{O}$  values distinctly differ with higher values at Site 1210. Due to the tropical to subtropical setting at Site 1210, the observed  $\delta^{18}\text{O}$  values seem realistic, although the different signals between the depth habitats might be reduced by stronger diagenetic alteration at Site 1262. Site 1262 subsurface dwellers isotope data cover a narrower range suggesting that (a) the thermocline habitat has been more stable through time in the South Atlantic or (b) diagenetic alterations made the signal more even.

Both sites show a wider spread in the  $\delta^{18}\text{O}$  surface signal than in  $\delta^{13}\text{C}$  and shows again the likelihood of biased 1262 results by poor preservation as indicated by a lack of  $\Delta\delta^{18}\text{O}$  variation. These findings support our assumption that early diagenetic dissolution and recrystallization did probably not influence much the benthic foraminiferal  $\delta^{13}\text{C}$  and  $\delta^{18}\text{O}$  signals (Edgar et al., 2013; Voigt et al., 20156), but had a substantial impact on planktic foraminifera  $\delta^{18}\text{O}$  (e.g. Pearson et al., 2001).

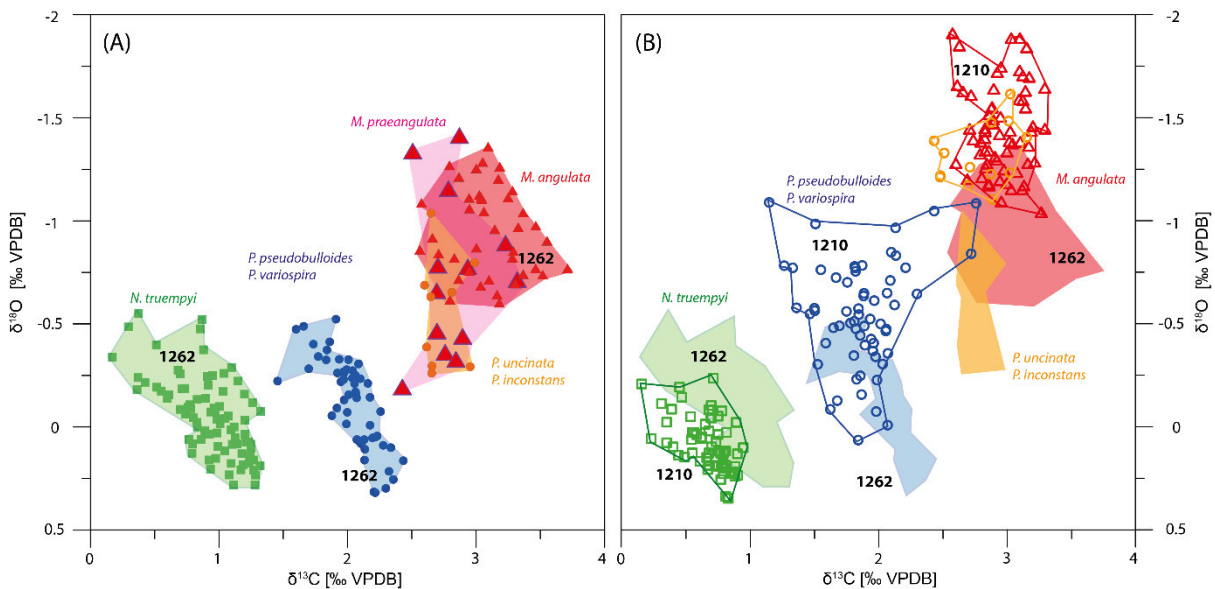


Figure 21: The  $\delta^{13}\text{C}$  and  $\delta^{18}\text{O}$  crossplots indicate the preferred depth habitat of different foraminiferal taxa. In green: benthic foraminifera; blue: planktic subsurface foraminifera; red small triangles, dark red large triangles with blue frame (only 1262) as well as orange circles: planktic surface dwelling foraminifera.

(A)  $\delta^{13}\text{C}$  and  $\delta^{18}\text{O}$  crossplot of Site 1262. (B)  $\delta^{13}\text{C}$  and  $\delta^{18}\text{O}$  crossplot in a comparison between Sites 1262 (shaded areas) and Site 1210 (Shatsky Rise: open areas and symbols).

### 3.7.3 Planktic foraminiferal faunal response to the LDE

Both diversity (Shannon  $H'$ ) and evenness (Figure 22) are generally higher at Walvis Ridge Site 1262 and show increased values at the onset of the LDE, in contrast to consistently lower parameter values at Shatsky Rise Site 1210 during the LDE. The diversity increase at the LDE onset is probably related to the introduction of several new *Morozovella* species right after the LDE potentially triggered by the warming associated with this event. The increase of Shannon

H' and species richness at Walvis Ridge with the onset of the LDE might have also led to a more even distribution among taxa.

A striking similarity of the two sites is the pre-LDE shift in the assemblage starting 170–200 ky before the LDE negative CIE shift as indicated by an increase in *Morozovella angulata* and a contemporary decrease in *Praemurica uncinata*, *P. inconstans* and *M. praeangulata*. This prominent change represents a slow shift from praemuricate to muricate species, where *M. praeangulata* was replaced by *M. angulata* and *Praemurica* disappeared, starting each at ~62.35 Ma. As the development started before the event, the negative CIE and temperature change could be reactions to ecological changes.

The most apparent compositional difference between the South Atlantic (Site 1262) and the Pacific (Site 1210) across the LDE is the dominance of subsurface dwellers at Site 1262 (79.9 % in average), whereas photosymbiotic planktic foraminifera are much more abundant at Site 1210 (74.9 % in average). Possible reasons for this are (a) the paleolatitude, as 1210 is situated closer to the equator and 1262 in a subtropical to temperate zone, which yield the highest diversity in modern oceans (e.g. Berger and Parker, 1970; Rutherford et al., 1999; Quillévéré and Norris, 2003), or (b) a closed-sum-effect, causing a bias due to much higher production of *Parasubbotina* and *Subbotina* at 1262, diluting the less abundant surface-dwelling taxa, even though the total production of surface dwellers was unchanged. At Pacific Shatsky Rise Site 1210, environmental conditions resulting from a permanent gyre system might have been beneficial for higher abundances of surface dwellers (e.g. Ortiz et al., 1995; Birch et al., 2013). There are other, more subtle differences between the faunal assemblages of the two sites, hinting towards the described scenario: At 1262, some surface water species vary highly in abundance, whilst subsurface species show more steady numbers during the LDE. This suggests that the surface ocean might have been more affected by environmental changes like enhanced vertical mixing and weaker stratification in contrast to the rather stable situation at Site 1210. The South Atlantic subsurface assemblage composition in turn seems to be more stable with less species variation compared to the Pacific fauna and less influenced by the environmental changes accompanying the LDE, even though the position of the thermocline was putatively shallower and seasonally more stirred up than in the tropical central Pacific. As outlined, at 1262 the abundance of subsurface dwellers was three times higher than surface specimens. A shoaling thermocline can indicate upwelling or high turbulence from deeper waters (Cullen, 1982; Herbland and Voituirez, 1979) resulting in higher abundances of subsurface dwellers. This fits well with the virtual lack of stratification at 1262 as indicated by the rather constant  $\Delta\delta^{13}\text{C}$  offset.

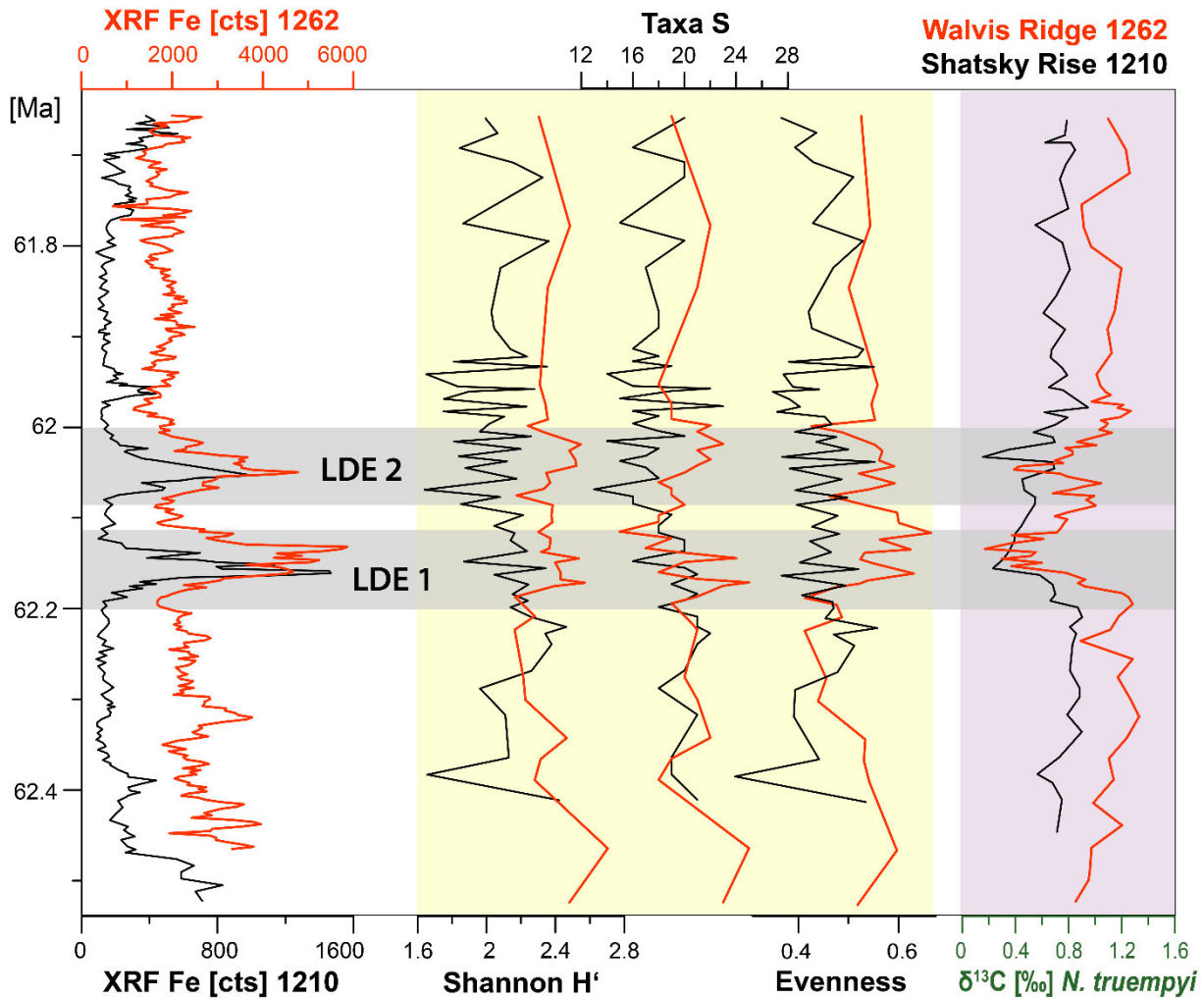


Figure 22: Comparison of key results from ODP Sites 1210 and 1262: Shannon H', simple diversity, evenness and benthic foraminifera  $\delta^{13}\text{C}$

## 4 Conclusions

Key results for the LDE at Walvis Ridge ODP Site 1262 are:

- Both LDE beds are characterized by a substantial  $\text{CaCO}_3$  drop of 15–17 wt%, of which LDE1 shows indications of dissolution, probably related to lysocline shallowing, and LDE2 is interpreted as a result of terrigenous dilution. Both LDE beds are characterized by a substantial  $\text{CaCO}_3$  drop of 15–17 wt%, of which LDE1 shows indications of dissolution, probably related to lysocline shallowing and LDE2 is interpreted as a result of terrigenous dilution.
- Two distinctly negative CIEs of about 0.9 ‰ are apparent in benthic (*Nuttallides truempyi*) and planktic photosymbiotic surface foraminifera (*Morozovella angulata*), however, the thermocline subsurface planktic foraminifera (*Parasubbotina variospira/pseudobulloides*)  $\delta^{13}\text{C}$  peak during LDE1 is only poorly developed.

- Ocean warming as reflected by  $\delta^{18}\text{O}$  is rather uniform between the different habitats with 1.5–2.6°C. A low temperature difference between the surface ocean and the seafloor as well as a lack of gradient between the subsurface and benthic foraminifera  $\delta^{18}\text{O}$ , we suggest a substantial impact of recrystallization of planktic foraminiferal calcite.
- Subsurface dwelling foraminifera are very dominant and decrease slightly over the studied interval in relative abundance. Surface-dwelling warm-water *Morozovella* and *Igorina* significantly rise in their abundances within the LDE and become generally more abundant after the event hinting towards a shift of the geographical zones from temperate to subtropical.

A comparison between ODP Site 1262 and Shatsky Rise ODP Site 1210 (Jehle et al., 2015) revealed a number of striking similarities and differences:

- Surface dwelling planktic and benthic foraminifera species show a stronger  $\delta^{13}\text{C}$  response to the LDE by up to 0.4 ‰ at Site 1262.
- Diagenetic alteration of planktic foraminiferal tests is more pronounced at Site 1262.
- At both sites, ecological changes like a decrease of *Praemurica* occur about 160 kyrs before the LDE. Further, both sites show the extinction of *Praemurica* at the base of the LDE, followed by a long-term rise in *Morozovella* abundance.
- Planktic foraminiferal assemblages of Site 1262 are dominated by subsurface taxa such as *Subbotina* and *Parasubbotina*, whereas warm surface water indicating *Morozovella* taxa are dominant in the Pacific (Site 1210). Overall assemblage changes within the event are stronger at Shatsky Rise Site 1210, probably due to stronger ecological changes like the development of a DCM.

## Acknowledgments

This work used samples provided by the Integrated Ocean Drilling Program and was supported by the Deutsche Forschungsgemeinschaft to AB [grant numbers BO2505/8-1, EH 89/20] and the KU Leuven Research Fund to RPS. Stefan Krüger (Univ. Leipzig) is thanked for stable isotope measurements.

Supplementary data will be provided on Pangaea.de, Data Publisher for Earth & Environmental Science.





# Chapter IV: Mid-Paleocene planktic foraminifera biostratigraphy – lessons from the appearance of *Igorina albeari* and the Latest Danian Event

## Abstract

Over the last decade, the refinement of Paleocene stratigraphy due to improved astrochronological tuning, magnetostratigraphy and high-resolution  $\delta^{13}\text{C}$  chemostratigraphy combined with biostratigraphy allowed for the precise dating of several short-termed warming events such as the Latest Danian Event (LDE, ~62.2 Ma). This in turn gave the opportunity to evaluate the exact timing of appearances and disappearances of zonal marker species at different sites in relation to well-defined carbon cycle changes.

Here, we present new biostratigraphic data from IODP Site U1407 (Newfoundland), and the Tethyan shelf section Gebel Qreiya 3

(Egypt), which are compared to contemporary intervals from ODP Sites 1210 (Shatsky Rise, Pacific Ocean) and 1262 (Walvis Ridge, South Atlantic). Each record covers a ~1 My interval around the LDE which has been dated to the P3a/P3b planktic foraminiferal Subzone boundary as defined by the first appearance datum of the planktic foraminifera *Igorina albeari*. However, our data reveals a first appearance of this taxon up to 400 ky before the LDE, and a diachrony of up to 250 ky among the studied sites. The last appearance datum of the genus *Praemurica* coincides with the onset of the LDE and seems to represent a much more reliable marker than *I. albeari*.

**Keywords:** Planktic foraminifera Subzone boundary P3a/P3b, biostratigraphy, chemostratigraphy.

## 1 Introduction

Planktic foraminifera are widely used as biostratigraphic tools and represent - besides calcareous nannofossils - to be the most important group for the biostratigraphy of Cenozoic pelagic carbonates. First regional biostratigraphic schemes for the Cenozoic era were developed in the 1940s (e.g. Cushman and Stainforth, 1945) and were rapidly improved thanks to the need of high resolution dating in hydrocarbon exploration (e.g. Bolli, 1957; Berggren, 1969; Blow, 1979; Berggren and Miller, 1988; Berggren et al., 1995; Premoli Silva and Bolli 1973; Stainforth et al. 1975; Tourmakine and Luterbacher, 1985; Berggren and Norris, 1997; Berggren and Pearson, 2005). The Deep Sea Drilling Project (DSDP) and its successors, the Ocean Drilling Program (ODP), the Integrated Ocean Drilling Program and International Ocean Discovery Program (both IODP) have substantially contributed to untangling the regional zones and arranging the puzzle pieces to a global picture towards a standard plankton stratigraphic scheme (Wade et al., 2011). Biostratigraphic zones are based on planktic foraminifera and calcareous nannofossils, allowing, in combination with magneto- and chemostratigraphy, for a better link of regional schemes with global chronostratigraphy.

The  $\delta^{13}\text{C}$  chemostratigraphy of the Paleocene and early Eocene is punctuated by several short-lived negative carbon isotope excursions (CIEs) of up to  $-4\text{‰}$ , interpreted as a result of the injection of isotopically light carbon into the ocean-atmosphere system (e. g. Zachos et al., 2008), which are accompanied by a temperature rise. Global  $\delta^{13}\text{C}$  shifts are not only a very robust proxy for the determination of paleoenvironmental perturbations, but also for global chemo- and biostratigraphic correlation (Saltzman and Thomas, 2012). The late Danian comprises with the Latest Danian Event (LDE,  $\sim 62.2\text{ Ma}$ ) an exceptionally negative CIE of  $\sim 1\text{‰}$  (Bornemann et al., 2009; Westerhold et al., 2011; Jehle et al., 2015; Deprez et al., 2017a, b), representing the most negative  $\delta^{13}\text{C}$  for the entire Paleocene (Westerhold et al., 2011).

Magnetostratigraphically the LDE is positioned at the top of Chron C27n with a duration of  $\sim 200\text{ kyrs}$  (Westerhold et al., 2008, 2011; Dinarès-Turell et al., 2012, 2014). In the deep sea, the LDE is additionally marked by two positive Fe XRF core scanning as well as magnetic susceptibility shifts, contemporary to the two negative CIEs. The LDE is seen as a two-phase event with no complete recovery and therefore divided into LDE1 (lower) and LDE2 (upper phase, see also Deprez et al., 2017).

The mid-Paleocene interval still largely lacks high-resolution biostratigraphic planktic data. This is probably due to the fact the Paleocene stage is sandwiched by two very intensively studied key intervals in Earth history - the Cretaceous-Paleogene (K-Pg, 66 Ma) boundary and the Paleocene-Eocene thermal maximum (PETM, 56 Ma), which might have led to a scientific negligence of the interval in-between. Biostratigraphically the LDE has often been placed at the base of planktic foraminifera Subzone P3b (Bornemann et al., 2009), which is defined by the first appearance datum (FAD) of *Igorina albeari* (Olsson et al., 1999). The identification of *I. albeari* is complicated by different taxonomic concepts for this taxon (see Sprong et al., 2009; Soldan et al., 2013). The taxon concept in this work is based on Olsson et al. (1999) and includes *Igorina laevigata* as widely accepted by others. According to Soldan et al. (2013) *I. laevigata* has an earlier FAD than *I. albeari* and might therefore contribute to the current P3a/P3b Subzone boundary discussion. Recent studies suggest larger uncertainties in the biostratigraphic position of the FAD of *I. albeari*, as low numbers of *I. albeari* were identified well below the LDE (Jehle et al., 2015). This relatively rare and small taxon might have been overlooked before.

In this study, three deep-sea sediment records from ODP Sites 1210 and 1262, IODP Site U1407 and the Tethyan shelf Site Qreiya 3 (Figure 8) were investigated biostratigraphically using planktic foraminifera over a  $\sim 1\text{ My}$  lasting interval. We focused on the stratigraphic appearance of the following planktic foraminiferal marker species: *Igorina albeari*, *Praemurica uncinata*, *Praemurica inconstans* and *Globanomalina pseudomenardii*. New planktic foraminiferal assemblage data of Site U1407 (Newfoundland) are published here for the first time. High-resolution  $\delta^{13}\text{C}$  chemostratigraphy is used as a marker for a globally synchronous stratigraphy contemporary to the biostratigraphic investigation.

## 1.1 Mid-Paleocene magneto- and biostratigraphy

Magnetostratigraphy is a powerful and well-used tool for global age correlation, based on reversals of Earth's magnetic field which are recorded by natural remanent magnetisation (NRM) in ferromagnetic material, iron-containing sediment in this case (e.g. Lund and Karlin, 1990; King and Channel, 1991). Astrochronological calibrations combine magnetostratigraphy and plankton biostratigraphy with investigations on lithological cyclicity as well as chemostratigraphy. The integrated use of this combination provides a very reliable stratigraphic framework for age control (e.g. Dinarès-Turell et al., 2007; Westerhold et al., 2008).

The herein studied interval of the late Danian and basal Selandian covers magnetochrons C27n to C25r (Cande and Kent, 1995; Wade et al., 2011, Vandenberghe et al., 2012). The planktic foraminiferal P2/P3 Zonal boundary was put close to the C27r-C27n transition, the P3a/P3b as well as P3b/P4 boundaries are classically located within C26n (Wade et al., 2011; Vandenberghe et al., 2012). Based on data from Zumaia (Spain), Bajala (Bulgaria) and ODP Site 1262 (Walvis Ridge), the LDE was positioned at the top of magnetochron C27n and is therefore also known as “Top Chron 27n” event (Dinarès-Turell et al., 2010, 2012; Westerhold et al., 2008).

Planktic foraminifera Zone P3 is defined as *Morozovella angulata* – *Globanomalina pseudomenardii* Interval Zone (Berggren et al., 1997) and as the interval between the consecutive FADs of the two species. Later, P3 was renamed to *Morozovella angulata* FAD Zone by Berggren and Pearson (2005). It is embraced by the Zone P2 below (*Praemurica uncinata* – *Morozovella angulata* Zone, Berggren et al., 1995) and Zone P4 above (*Globanomalina pseudomenardii* Taxon-range Zone, Bolli, 1957).

Planktic foraminifera Zone P3 is subdivided into Subzones P3a and P3b (Berggren and Norris, 1997): Subzone P3a is defined as *Igorina pusilla* partial-range subzone (Berggren and Pearson, 2005; Petrizzo, 2005). Due to higher abundance, *M. angulata* is the denominative taxon for the base of P3a instead of *I. pusilla* (Berggren et al., 1995).

The base of Subzone P3b, which is formerly known as *Igorina albeari* – *Globanomalina* (cf.) *pseudomenardii* Subzone (Berggren and Norris, 1997; Berggren and Pearson, 2005), is defined as the interval between the FADs of *I. albeari* and *G.* (cf.) *pseudomenardii* (Berggren and Norris, 1997). The latter in turn defines the base of planktic foraminifera Zone P4. As a secondary marker *Morozovella velascoensis* is accepted in case of low numbers of *G.* (cf.) *pseudomenardii* (e.g., Blow, 1979; Toumarkine and Luterbacher, 1985), since the FAD of *G.* (cf.) *pseudomenardii* is under debate and might appear earlier or even at the same time as *I. albeari* (e.g. Olsson et al., 1999; Sprong et al., 2009; Jehle et al., 2015).

## 1.2 Taxonomic concepts

In general, taxa defining biostratigraphical (Sub-)Zones are ideally defined by a short life-span, high evolutionary rates, a wide geographical distribution, high abundance and a clear morphological definition in addition to a high preservation potential (Berggren et al., 1995; Berggren and Pearson, 2005; Wade et al., 2011). We briefly summarize the taxonomic concepts of index species of the mid-Paleocene.

### 1.2.1 *Praemurica uncinata* (Bolli 1957) and *P. inconstans* (Subbotina 1953)

*Praemurica uncinata* is characterised as nonspinose, weakly cancellate, elongate-oval, planoconvex to moderately high spired and lobulated with 5–8 chambers in the last whorl, sometimes loosely coiled. Sutures are radial and depressed on the umbilical side, on the spiral side incised and strongly recurved with typical trapezoidal-shaped chambers. The axial periphery is subangular and non-carinate but with rugose muricae along the peripheral margin at the early chambers of the last whorl. Typically, the umbilicus is narrow and deep, bordered by weakly developed circumbilical shoulder formed by raised perumbilical chamber extensions. The aperture appears as narrow interiomarginal with an umbilical-extraumbilical arch extending to a peripheral margin (Olsson et al., 1999).

According to Berggren et al. (1999) *Praemurica inconstans* ranges from the base of the P1c Subzone to near to the base of P3a. The species' last appearance datum (LAD) is slightly after the last appearance of *P. uncinata*. *Praemurica inconstans* was described as non-spinose, subcircular to broadly elongate-oval, moderately lobulate, 5–7 chambered, cancellate test. The peripheral margin is rounded to weakly subangular, chambers in early whorls are tightly coiled and final whorl is rapidly expanding. The sutures are radial and straight to weakly curved in early forms but more strongly curved and weakly incised in more advanced forms. The aperture is an interiomarginal, umbilical-extraumbilical slit with distinctly lipped rim.

One of several morphotypes of *P. inconstans* is *P. praecursoria* with a similar FAD and LAD in lower specimen abundance and more chambers in the last whorl (Plate 1, Figure 14). Both are not used as biostratigraphic index species.

### 1.2.2 *Igorina* and *Igorina albeari* (Cushman and Bermudez 1949)

*Igorina*, like *Acarinina*, is considered to be a sister group of *Morozovella* and both are originally characterized by small, globular taxa with a wall texture described as “muricate funnel-pores”. *Igorina* has a tight coiling and develops numerous umbilically inflated chambers in the final whorl with varying spiral heights amongst the species (Berggren et al., 1997). Further, the genus *Igorina* (Davidzon, 1976) is described as:

“...bilaterally convex. Equatorial outline round, slightly undulate. Axial outline takes the form of a bilateral cone with variable vertex angles. Chambers on spiral side alate, on umbilical side triangular. Umbilicus small or absent. Aperture a slit at the base of the septal surface of the last chamber. Surface of chambers smooth or almost uniformly covered with small spines” (transl. from Russian, Berggren and Norris, 1997).

The genus *Igorina* comprises three (Olsson et al., 1999) to nine species to date (Soldan et al., 2013) and ranges from Subzone P3a (FAD, mid-Paleocene) to Zone P11 (LAD, Early Eocene). Phylogenetic relationships, based on morphology, define *I. pusilla* to be the first representative of genus *Igorina* (Soldan et al., 2011).

The current species identification follows Olsson et al. (1999).

*Igorina albeari* has a stratigraphic range from the P3a/P3b boundary to P4. The species concept is still issue of debates (e.g. Olsson et al., 1999; Soldan et al., 2013; and others). The concept

of Soldan et al. (2011, 2013) includes nine taxa: *I. pusilla*, *I. trichotrocha*, *I. tadjikistanensis*, *I. convexa*, *I. albeari*, *I. laevigata*, *I. lodoensis*, *I. broedermanni* and *I. anapetes*. Even though the nine-species-concept has been proved eligibility, the broader definition with three Paleogene *Igorina* species only seems to be more applicable, in which *I. albeari* includes *I. laevigata*, *I. convexa* and *I. “trichotrocha”* (Soldan et al., 2011). The *I. albeari* definition of Olsson et al. (1999), supplemented with Berggren and Norris (1997) descriptions applies for the specimens of this work (Plate 2, Figure 27).

Diagnostic characters of *Igorina albeari* are a moderately to strongly biconvex test which is essentially circular, cancellate and pustulose with 6–8 chambers in the last whorl. Intercameral sutures on the umbilical side are radial to weakly recurved and yield triangular-shaped chambers. On the spiral side, limbations are strongly recurved and distinctly exhibiting, in particular between the last 3–4 chambers, which are trapezoidal-shaped. The peripheral margin is distinctly carinate, notably the very last chamber. The aperture has a low interiomarginal, umbilical-extraumbilical arch extending towards – but not to – the peripheral margin (Olsson et al., 1999). A consistent species definition includes an incipient keel, identifiable by the flattening of the last chambers and a fusion of muricae on the peripheral margin (Sprong et al., 2009). In comparison, both  $\delta^{13}\text{C}$  and  $\delta^{18}\text{O}$  of *I. albeari* are more negative than *Acarinina* and *Morozovella*, and more positive than *Subbotina* and *Globanomalina* (Olsson et al., 1999). The isotope data points to a photosymbiotic live style and either a habitat slightly deeper than *Morozovella* or flourishing during a somewhat cooler season. In addition, the smaller tests limit the number of phytoplanktic hosts which would result to lower symbiont density and the impression of less photosymbiotic activity. The global distribution is limited to tropical to subtropical regions or low latitudes in general (Olsson et al., 1999).

### 1.2.3 *Globanomalina pseudomenardii* (Bolli 1957)

*Globanomalina* (cf.) *pseudomenardii* (Plate 3, Figure 28) defines the top of planktic foraminifera Zone P3 and is the index species for the total range Zone P4 (Berggren et al., 1995). The current biostratigraphic scale (Berggren and Pearson, 2005) considers the species as subzone marker for P4a (FAD) and P4c (LAD).

The species is rather large (350–600  $\mu\text{m}$ ), the biconvex test is characterized by a distinct keel and a sharply angled axial periphery with a narrow periphery with 5–6 chambers in the ultimate whorl. The chambers rapidly increase in size and the intercameral sutures are depressed and weakly curved on the umbilical side. The peripheral margin is strongly compressed and the keel is very distinct, especially on the last chambers. The wall has a smooth, finely perforate surface, the umbilicus is narrow and shallow. The aperture has a low, interiomarginal umbilical-extraumbilical arch with a thin lip (Berggren and Norris, 1997).  $\delta^{13}\text{C}$  and  $\delta^{18}\text{O}$  signatures are comparable to *Parasubbotina varianta* and *Subbotina velascoensis*, species which are well known for an asymbiotic subsurface lifestyle (Olsson et al., 1999).

Due to struggles in identification, the here found tests are named *Globanomalina* cf. *pseudomenardii*. There seems to exist an intermediate form which is slightly resembling *G. chapmani* and makes species identification sensu stricto ambitious. The possibly intermediate species has the required outer shape and size in general, a distinct apex in the centre of the spire, a smooth band at the keel, but the keel itself is slightly less sharp-edged than

described and pictured earlier in Berggren and Norris (1997) or Olsson et al., (1999). Still, it seems difficult to draw the line and it would be better to avoid the establishment of an intermediate form.

## 2 Material and Methods

### 2.1 Studied sites and sections

#### 2.1.1 ODP Site 1210 (Shatsky Rise, Pacific)

ODP Site 1210 is located at 32°13.41'N, 158°15.56'W (Figure 8) and was drilled in 2,573 mbsl. The site is situated on a plateau, formed during Late Jurassic and Early Cretaceous (149–135 Ma) as a large igneous province, situated on a triple-junction in the Pacific Ocean (Bralower et al, 2002). Sediment was deposited on the southern part of the Shatsky Rise Plateau at a lower bathyal paleo-water depth of ~2,700 mbsl (Petruzzo et al., 2005) and a paleolatitude of ~24°N (Torsvik et al., 2012; van Hirsbergen et al., 2015).

The drilled sediments consist of nannofossil ooze, ooze with clay and occasionally clay with ooze (Bralower et al., 2002). Two prominent dark brown horizons intercalate into the monotonous calcareous ooze sequence representing the prominent negative CIE (233.4–234.6 rmcd, Bralower et al., 2002). Below the first event bed at 243.4 rmcd, the colour is darker and turns much lighter above the LDE.

The age control is based on astrochronological investigations in combination with magneto- and biostratigraphy on ODP Site 1209 record (Westerhold et al., 2008). Results for the current time frame were transferred to Site 1210.

#### 2.1.2 ODP Site 1262 (Walvis Ridge, South Atlantic)

ODP Site 1262 (27°11.15'S, 1°34.62'E, 4,755 mbsl, meters below sea level, Figure 8) had a Paleocene latitude of ~37°S (Zachos et al., 2004; Kent & Irving, 2010), sediments were deposited at a paleo water depth of ~3,300 mbsl (Zachos et al., 2004). The site is situated in the transition from the Angola Basin to the Walvis Ridge. Paleocene sediments are predominantly composed of calcareous nannofossil ooze with cyclic variations in sediment lightness and geochemistry, representing a response to orbital forcing (Westerhold et al., 2008). The age control of Walvis Ridge 1262 is based on astronomical tuning and supplemented by calcareous nannofossils and magnetostratigraphy (Agnini et al., 2007; Westerhold et al., 2008; Aubry et al., 2012; Monechi et al., 2012, 2013).

#### 2.1.3 IODP Site U1407 (Southeast Newfoundland Ridge, North Atlantic)

Southeast Newfoundland Ridge Site U1407 (SENR U1407) was drilled at 3,073 mbsl and is located at 41°25.50'N, 49°48.80'W (Figure 8). The estimated paleodepth is ~1,800 m (Norris et al., 2014) and paleolatitude 33.40 N (Torsvik et al., 2012; van Hirsbergen et al., 2015). It is situated at the crest of the south eastern Newfoundland Ridge with a distance of ~650 km to the Newfoundland coastline. White nannofossil chalk with foraminifera built up the sediments of

the Early Paleocene, together with layers of laminated claystone with nannofossils, zeolithic claystone with organic material as well as chert and radiolarian sand. Calcareous nannofossil in combination with XRF Fe data as well as magnetic susceptibility and bulk carbon isotopes are the base for the age calibration (Yamaguchi et al, 2017).

#### 2.1.4 Gebel Qreiya 3 (Egypt)

Site Gebel Qreiya 3 (named Qreya 3 from hereon) is located near the southern tip of Gebel Qreiya (26°27.702'N, 33°1.905'E, Figure 8) covering a lower Danian to Ypresian succession with a total thickness of ~100 m. The water paleodepth was estimated to 150–250 m (Bornemann et al., 2009; Sprong et al., 2011) and the paleolatitude of ~9.4°N (Torsvik et al., 2012). The area is part of the Eastern Desert and of the southern Tethyan shelf. The regional Paleocene section is known as Esna shales and has a uniform lithology of greenish-grey shale. Lithostratigraphically the beds are part of the Dakhla Formation, which consists of monotonous brownish to grey marls and shales and intercalated thin marly limestone beds (Said, 1990). The event layer close to the P3a/P3b boundary has been identified to represent the LDE (Bornemann et al., 2009; Sprong et al., 2011).

The age control is based on planktic foraminifera and nannofossil biostratigraphy (Steurbaut and Sztrakos, 2008; Sprong et al., 2009).

## 2.2 Methods

The sediment was carefully washed on a 63 µm sieve and dried at 40°–50°C for at least 48 hours. Foraminifera were picked and identified under a Zeiss Stemi 2000 light microscope with 50 × magnification. Taxonomy largely follows Berggren and Norris (1997) and Olsson et al. (1999), if not stated otherwise. Scanning electron microscope images were performed at BGR in Hannover (FEI Sirion 200).

First rare appearance datums (FrAD) are defined as the appearance datum of the species in low numbers, here below 3% and as a first common appearance datum (FcAD), the species has to show more than 3% abundance. The same counts for the last common (LcAD) and the last rare appearance datum (LrAD).

For  $\delta^{13}\text{C}$  measurements, 3–7 specimens of bulk grained sediment were reacted with 100% phosphoric acid at 75°C using a Kiel IV online carbonate preparation line connected to a MAT 253 mass spectrometer at the facility of University of Leipzig. Bulk data of Newfoundland Site U1407 was measured with a Kiel III online carbonate preparation line connected to a ThermoFinnigan 252 mass spectrometer at the University of Erlangen (Geo-Zentrum Nordbayern). Replicate measurements for  $\delta^{13}\text{C}$  were always better than 0.1 ‰.

## 3 Chemo- and biostratigraphic results

All deep-sea sites show a negative CIE with the characteristic double peak associated to the contemporary LDE horizons on either bulk or benthic foraminiferal carbonate (Figure 23, Figure 24), whereas this feature is less concise or not apparent in the onshore successions of

Gebel Qreiya (Egypt, Bornemann et al., 2009), Zumaia and Caravaca (both Spain, Schmitz et al., 1997; Dinarès-Turell et al., 2014; Alegret et al., 2016). This might result from enhanced bioturbation or sediment relocation in shelf settings or diagenetic alteration. Moreover, the sample resolution is higher amongst the investigated deep-sea sites than at Qreiya 3, Caravaca and Zumaia. The negative CIEs peaks are between -0.6 ‰ (ODP Site 1210: 234.5 mcd, 234.0 mcd) and -0.9 ‰ (ODP Site 1262: 195.3 mcd, 194.5 mcd; Qreiya 3: 8.3 m) on benthic foraminiferal carbonate. Bulk carbonate of U1407 peaks with 0.9 ‰ at 210.2 CCSF [m].

At ODP Site 1210, *Igorina albeari* has a first rare appearance (FrAD) at ~ 236.34 mcd and a first common appearance datum (FcAD) from 234.79 mcd on (Figure 18, Figure 19, Table 1) as opposed to earlier studies where the species had a later FAD (~234.2 mcd, Petrizzo, 2005) which goes in line with our FcAD. *Praemurica* species become very rare at 234.4 mcd and have their last rare appearance (LrAD) at ~232.8 mcd. *Globanomalina* (cf.) *pseudomenardii* appears for the first time at 234.5 mcd and stays below 2 % (Jehle et al., 2015).

At Site 1262, the FrAD of *I. albeari* is at 197.0 mcd, the FcAD at 195.6 mcd just below the LDE1 onset. *Praemurica uncinata* and *P. inconstans* are abundant before 196.6 mcd and the last rare appearance (LrAD) is at 195.3 mcd. *Globanomalina* (cf.) *pseudomenardii* appear for the first time at 193.6 mcd and never go above 2 % abundance (Chapter III, Figure 23, Figure 24).

At IODP Site U1407 *I. albeari* shows a FrAD at 211.9 m CCSF, which continuously turns into a FcAD at 211.125 m. The LcAD of *P. uncinata* at 211.85 m and *P. inconstans* at 211.2 m CCSF both turn into a LrAD at 210.7 m CCSF. *Globanomalina* (cf.) *pseudomenardii* rarely occurs for the first time at 209.0 m CCSF, but stays below 2% abundance (Figure 18, Figure 19).

Data from Qreiya 3 show the FrAD of *I. albeari* at 5.05 m and FcAD at 8.50 m. *Praemurica uncinata* disappears at 8.35 m and *P. inconstans* at 8.50 m, the LcAD of *P. uncinata* is at 7.50 m. *Globanomalina* (cf.) *pseudomenardii* does not appear within the observed record (Figure 23, Figure 24).

## 4 Implications on stratigraphic definitions

### 4.1 The LDE and the planktic foraminifera Subzone P3a/P3b

The synchronous negative CIEs are accompanied by the first radiation of fasciculithids, which is documented close to the base of the LDE1 CIE at Shatsky Rise Site 1210, Walvis Ridge Site 1262 and SENR U1407 (e.g. Aubry et al., 2012; Monechi et al., 2012). The identification at several deep-sea sites indicates that this transient carbon cycle perturbation is a synchronous, global event, which can be used as a chemostratigraphic age tie point. Earlier studies on this time interval suggested that the LDE coincides with the planktic foraminifera subzone boundary P3a/P3b as indicated by *Igorina albeari* (e.g., Sprong et al., 2009; Bornemann et al., 2009; Westerhold et al., 2008, 2011; Alegret et al., 2016). Earlier high-resolution studies (Jehle et al., 2015; Chs. II and III) show that *I. albeari* appears well below the LDE at several sites. One reason for this deviation is probably because the fact that the mid-Paleocene was largely



neglected by micropaleontological studies until now and only checked for low-resolution shipboard biostratigraphy (one sample per 9-m-core).

At the GSSP reference section Zumaia, *I. albeari* appears above the LDE (Figure 23; Schmitz et al., 2011), which is possibly the result from either a non-global species distribution, lower sample resolution, poor preservation or different taxonomic concepts (e.g. Olsson et al., 1999; Sprong et al. 2009; Soldan et al., 2013).

For Shatsky Rise Site 1209, a close neighbour to Site 1210, the P3a/P3b Subzone boundary mid-point is set at ~61.77 Ma (Westerhold et al., 2011). However, at Site 1210, *I. albeari* was found at  $62.5 \pm 0.13$  Ma ( $235.95 \pm 0.25$  rmcd) or in a very low number even at  $62.73 \pm 0.03$  Ma ( $236.4 \pm 0.04$  rmcd) which puts the P3a/P3b boundary at least to a 0.63 Ma older place than at Site 1209 (Table 3).

The FrAD of *I. albeari* at Walvis Ridge occurs at  $62.36 \pm 0.02$  Ma and a FcAD at  $62.19 \pm 0.013$  Ma (according to La14, Dinarès-Turell et al., 2014).

At Site 1210, *I. albeari* occurs 2 m below the LDE onset, and at Site 1262 ~1.5 m. For these two sites, this equals to about 0.35 kyrs at 1210 and 0.21 kyr at 1262 according to the La14 astrochronological timescale (Dinarès-Turell et al., 2014).

At IODP Site U1407, the FrAD of *I. albeari* is at  $211.81 \pm 0.04$  m CCSF, which is about 1.0 m below the negative CIE of LDE1 at 62.18 Ma (Yamaguchi et al., 2017). The FAD of *I. albeari* falls together with the first radiation of fasciculithids. The age control for U1407 is aligned to biostratigraphic tie points as taken from Norris et al. (2014), however, there exists no complete age calibration yet.

The P3a/P3b Subzone boundary has been discussed and shifted downwards before at sections in Egypt based on samples containing *I. albeari* in small numbers below the LDE (Sprong et al., 2009). At Qreiya 3, we found the FrAD of the P3a/P3b boundary marker ~3 m below the LDE, but the FcAD fits well with the LDE onset as well as with the decrease of *Praemurica* spp. At Gebel Qreiya 3 (Bornemann et al., 2009) and in Tunisia (Guasti, 2005) the co-occurrence of the LDE and the P3a/P3b Subzone boundary might result from a hiatus around the LDE or above since sediments are channel deposits (Bornemann et al., 2009).

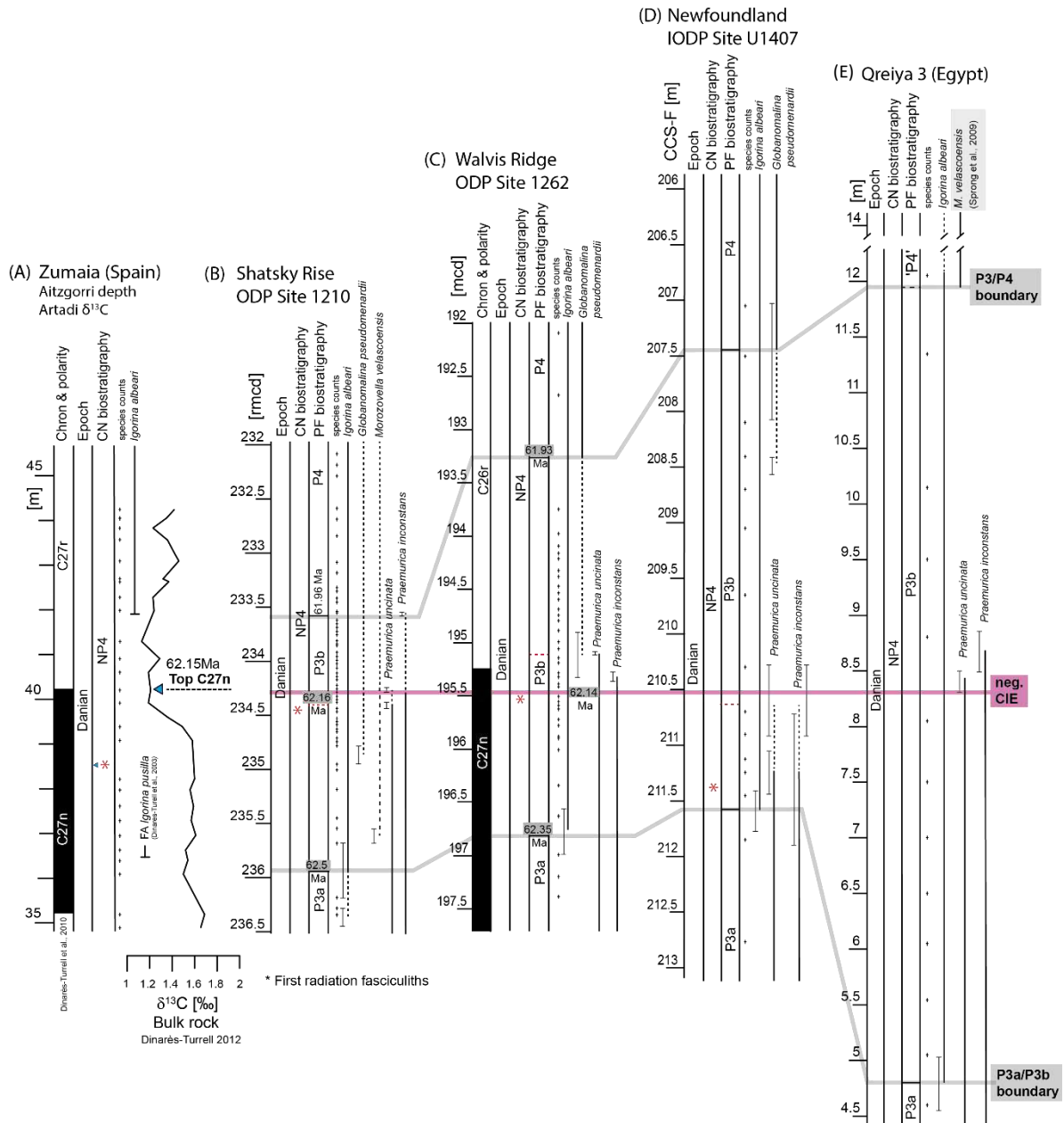


Figure 23: Planktic foraminifera and calcareous nannoplankton biostratigraphic zones of the investigated sites. Crosses indicate sample positions. Planktic foraminifera zones of Zumaia are not shown, because of major taxonomic uncertainties and disagreements in all other studies. PF zones are supplemented by FADs and LADs of marker species. Dashed lines within the species appearance mark the first rare appearance datum (FrAD) before the first common appearance datum (FcAD). The pale red line marks the position of the negative CIE, representing the onset of the LDE, in grey the FAD of *Globanomalina* (cf.) *pseudomenardii*. The red asterisk marks the stratigraphic position of the first radiation of fasciculithids (Monechi et al., 2013; Yamaguchi et al., 2017). The red dashed line in **B**, **C** and **D**: proposed P3a/P3b Subzone due to LAD of *Praemurica uncinata*. **A**: Zumaia-Aitzgorri, after Dinarès-Turell et al. (2014), GSSP Site Zumaia-Aitzgorri is supplemented by bulk  $\delta^{13}\text{C}$  data (Dinarès-Turell et al., 2012) and magnetostratigraphic zones; **B**: Shatsky Rise ODP Site 1210, Jehle et al. (2015), Westerhold et al. (2008); **C**: Walvis Ridge Site ODP 1262, Jehle et al., submitted. NP zones by Monechi et al., (2013). **D**: Newfoundland Site IODP U1407; nannofossil radiation and LDE are positioned according to Yamaguchi et al., 2017; **E**: Qreiya 3. As these Qreiya 3 samples do not cover P4, data was taken from Sprong et al, 2009, where *M. velascoensis* was used for the approximation of the P4 onset.

Overall, the LADs of the *Praemurica* lineage give a more consistent picture. In standard biostratigraphy, the LAD of *P. uncinata* takes place within the lower part of P3a, but our new data implies notable abundance towards the P3a/P3b boundary with *Praemurica inconstans* and *P. uncinata*. At all sites (Sites 1210, 1262, U1407, Qreiya 3), these two species disappear almost synchronously right after the LDE1 carbon isotope excursion. It is interesting that at the three deep sea sites *Praemurica* decreases in abundance about 150 kyr below the LDE and only few species were consistently observed in samples between this decline and the LDE onset. This was not observed at Qreiya 3. A synchronous disappearance of *Praemurica* spp. agrees with observations of Guasti (2005) from southern Tethyan shelf of Tunisia or from ODP Site 761B at Wombat Plateau, where *Praemurica* disappears close to TC27n. The largely synchronous LAD of *Praemurica* in three different ocean basins and in both deep sea and shelf settings might be a more reliable boundary marker than the FAD of *I. albeari*.

Table 3: Overview planktic foraminiferal P3a/P3b Subzone boundary

	P3a/P3b Subzone boundary literature	Radiation fasciculiths	FAD <i>Igorina albeari</i> this study FrAD/FcAD	Suggested P3a/P3b Subzone boundary this study, based on LcAD, LrAD <i>Praemurica uncinata</i> , <i>P. inconstans</i>
Shatsky Rise Site 1210	61.77 Ma *	234.4 rmc	236.39 ± 0.05 rmc (62.73 ± 0.03 Ma) / 234.95 ± 0.26 rmc (62.5 ± 0.13 Ma)	234.4 ± 0.007 rmc (62.14 ± 0.002 Ma)
Walvis Ridge Site 1262	-	195.4 mcd 62.14 Ma	196.8 ± 0.18 mcd (62.36 ± 0.02 Ma) / 195.6 ± 0.15 mcd (62.2 ± 0.013 Ma)	195.3±0.02 mcd (62.15±0.001 Ma) 196.8 ± 0.18 mcd (62.38 ± 0.02 Ma)
SENR U1407	-	211.4 m (CCSF)	211.81 ± 0.04 m / 211.18 ± 0.05 m (CCSF)	210.5 ± 0.02 m (CCSF)
Qreiya 3	8 m		4.825 ± 0.23 m / 8.425 ± 0.075 m	8.65 ± 0.15 m

\* transferred from ODP Site 1209, Westerhold et al., 2009

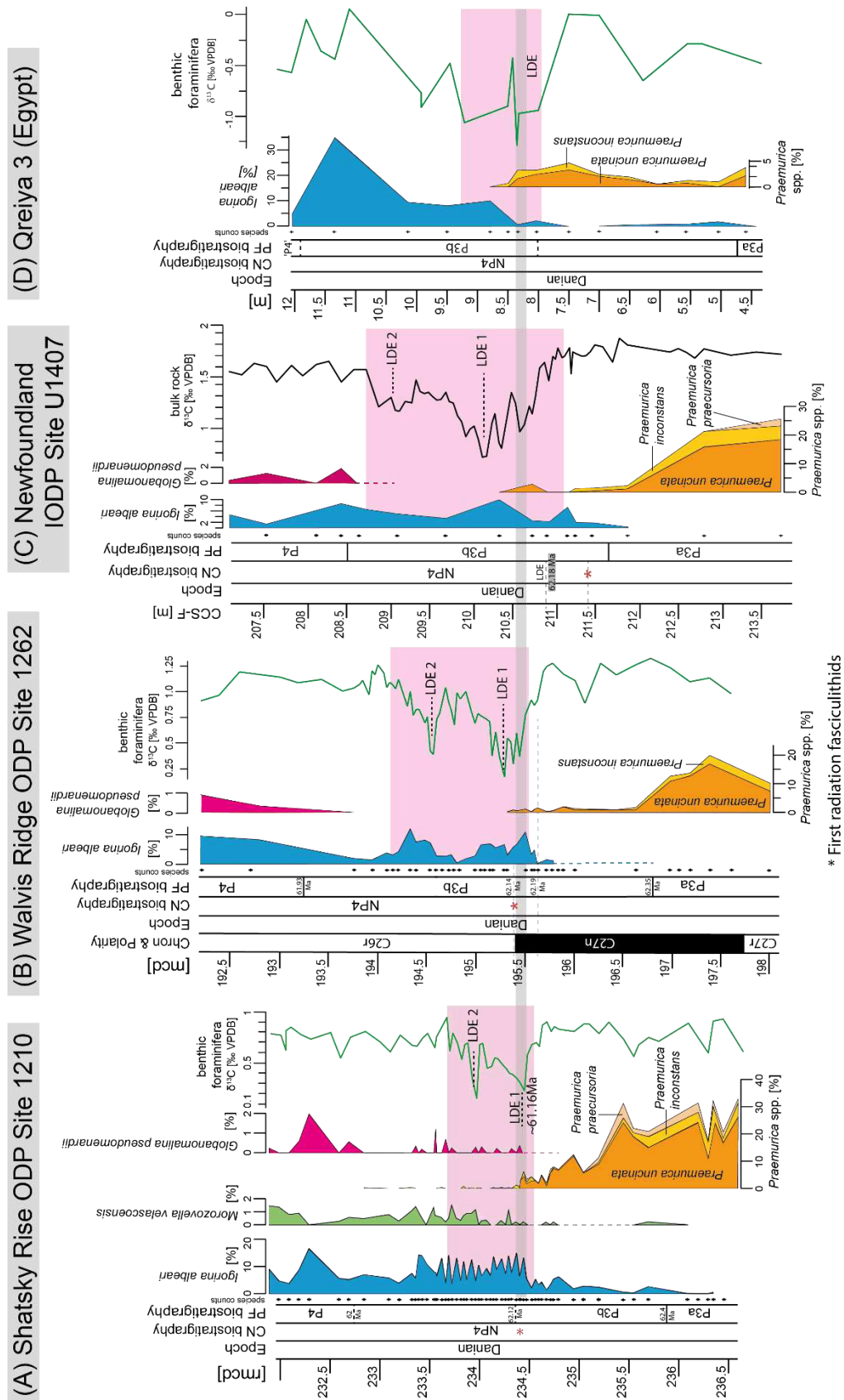


Figure 24: Biostratigraphy with quantitative data of marker species *Igorina albeari*, *Praemurica uncinata* and *P. inconstans* and *Morozovella velascoensis* (Shatsky Rise) as well as *Globanomalina* (cf.) *pseudomenardii*.  $\delta^{13}\text{C}$  shows the negative carbon isotope excursions of the LDE (62.15 Ma). The added red asterisk marks the first radiation of fasciculithids. (A) Shatsky Rise Site 1210: the dashed P3a/P3b boundary is transferred from Shatsky Rise Site 1209 (Westerhold et al., 2011); (B) Walvis Ridge Site 1262 with foraminiferal  $\delta^{13}\text{C}$  each, showing two CIEs; (C) Newfoundland Site U1407 shows one CIE in bulk  $\delta^{13}\text{C}$ ; (D) Qreiya 3: the dashed P3a/P3b as well as the P3b/P4 boundaries are from Sprong et al. (2009).



Due to our new data, both the P3a/P3b Subzone boundary and the base of Zone P4 might benefit from the establishment of other marker species and surely more high resolution biostratigraphic data.

The P3a/P3b boundary is defined by the FAD of *Igorina albeari* and has been correlated to the Latest Danian Event onset (~62.18 Ma). Results from deep sea (IODP Sites 1210, 1262 and U1407) show consistently earlier rare appearances of the index taxon below the designated P3b Subzone base and an abundance increase with the LDE onset. The situation is similar but less clear at Tethyan shelf Site Qreiya 3.

We were able to show that the use of *I. albeari* is suboptimal when working at a reasonable high resolution: Even if the FAD of *I. albeari* approximates the LDE, the appearance is diachronous by up to 250 kyrs within other observed sites.

As a more reliable alternative we herein propose the LAD of the planktic foraminifera *Praemurica uncinata* and *P. inconstans* for the P3a/P3b Subzone boundary. The synchronicity of the documented LADs is not only indicated by  $\delta^{13}\text{C}$  chemostratigraphy, but also by the first radiation of fasciculithids (calcareous nannofossils).

This study also covers the FAD of *Globanomalina cf. pseudomenardii*, which appeared earlier than suggested in the literature. The observed diachronic appearance appears somewhat suboptimal as a marker for the base of planktic foraminiferal biozone P4, too. There might be either a much earlier P3b/P4 Subzone boundary or an alternative marker species.



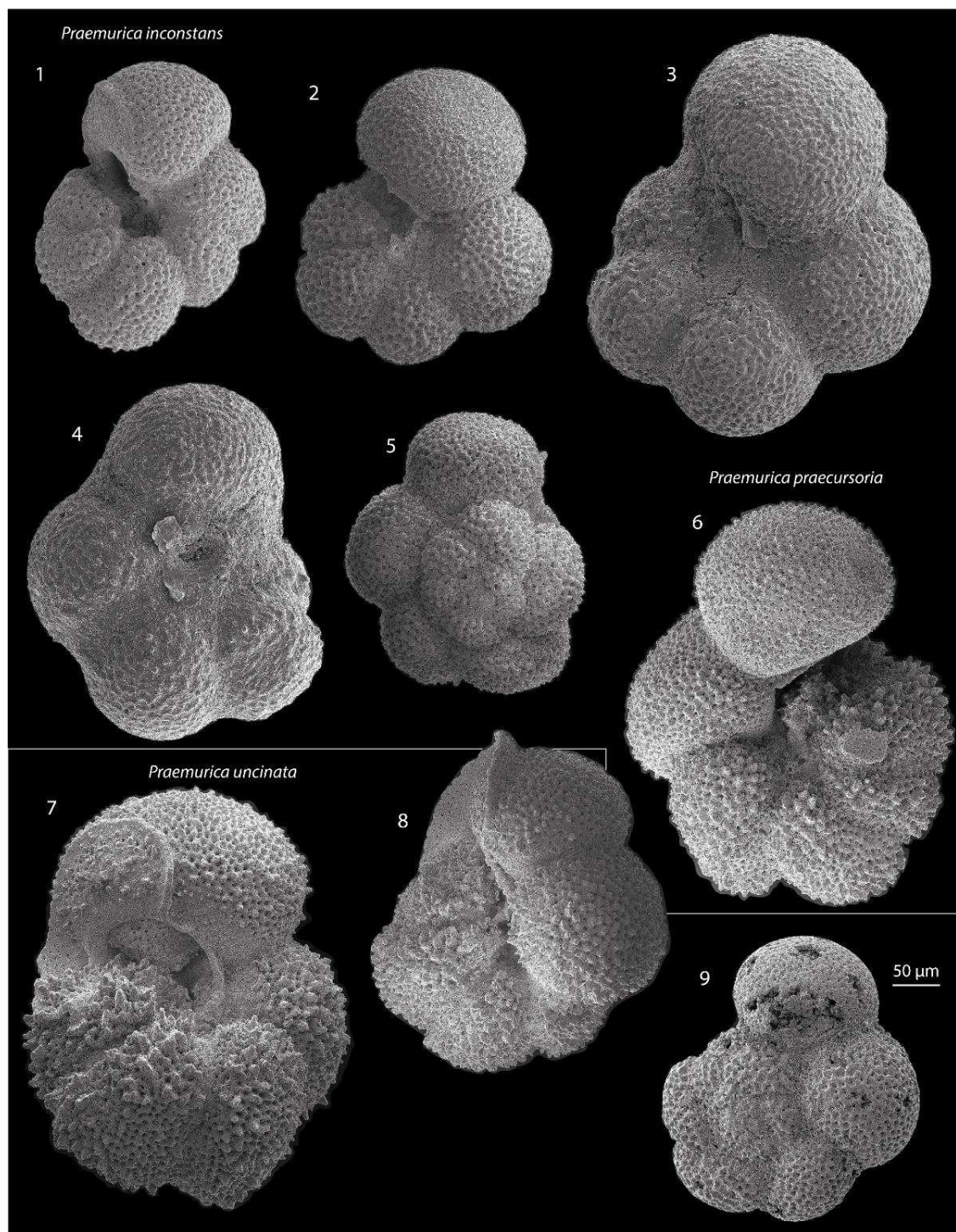


Figure 26: Scanning electron microscope pictures of *Praemurica inconstans* umbilical (1-4) and spiral side (5); 6: *Praemurica praecursoria* (umbilical side); *Praemurica uncinata* spiral (7, 8) and umbilical side (9).

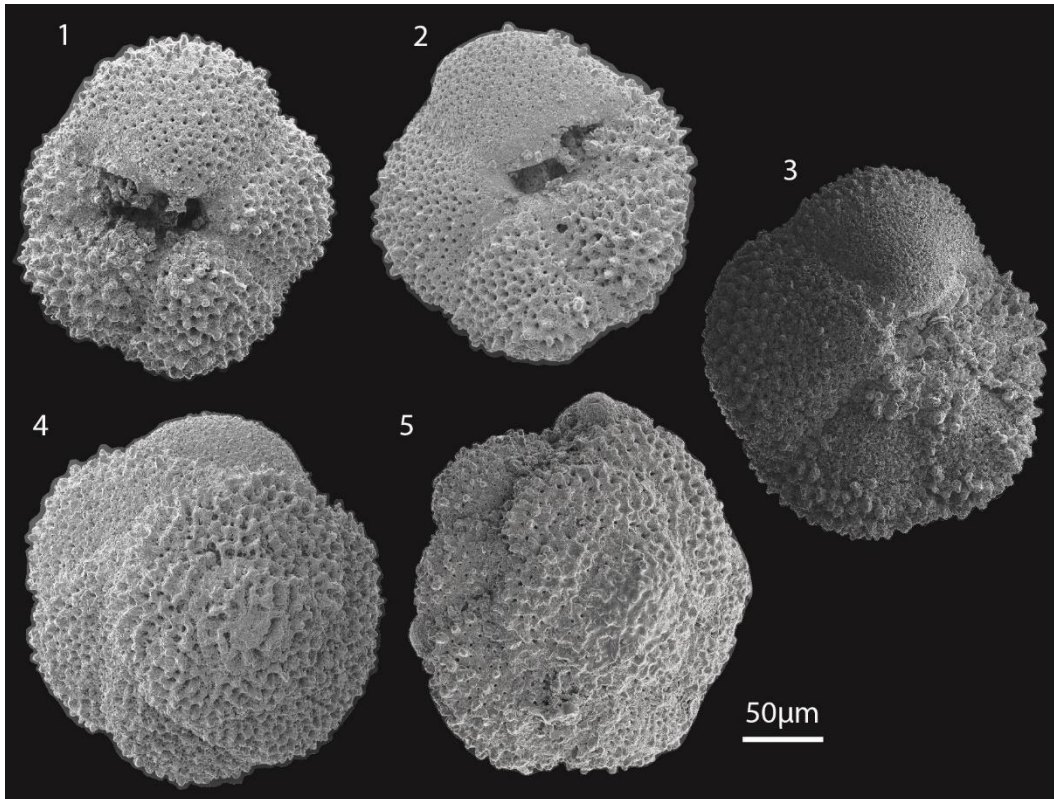


Figure 27: Scanning electron microscope pictures of *Igorina albeari* in umbilical (1-3) and spiral view (4-5)

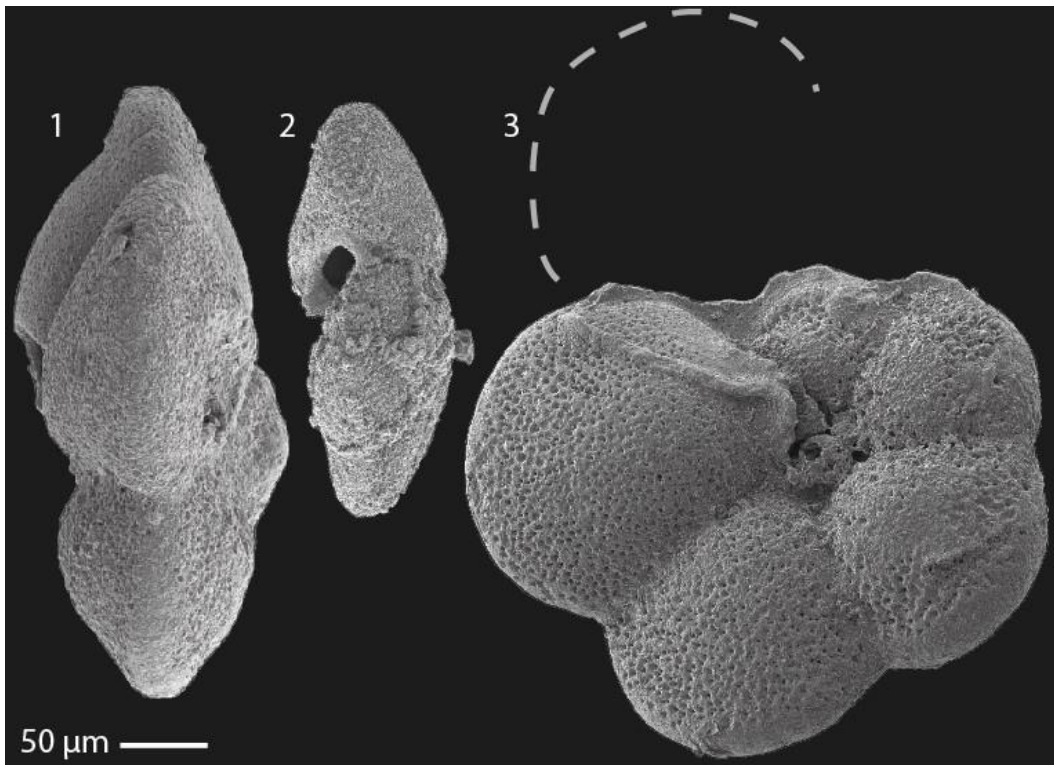


Figure 28: Scanning electron microscope pictures of *Globanomalina cf. pseudomenardii* in lateral (1, 2) and umbilical (3) view. As the tests are very fragile, not many are conserved in piece, therefore the last chamber was sketched



# Chapter V: Synthesis

## Characteristics of the Latest Danian Event

### 1 Research focus

Within the scope of this thesis, the Latest Danian Event (LDE) was investigated on samples from three deep-sea sites (Shatsky Rise, Walvis Ridge, Newfoundland) and one Tethyan shelf section (Qreiya 3, Egypt). The data is covering four ocean basins (North Atlantic, South Atlantic, Pacific Ocean, Tethys Ocean) on planktic foraminiferal assemblages,  $\delta^{13}\text{C}$  and  $\delta^{18}\text{O}$  of planktic and benthic foraminifera and other sedimentary parameters like carbonate content or total organic carbon. Shatsky Rise ODP Sites 1210 (Ch. II and III) and 1262 (Ch. III) and IODP Site U1407 (South East Newfoundland Ridge, SENR, Ch. IV) and Qreiya 3 (Egypt, Ch. IV).

This thesis presents the first high-resolution study on late Danian planktic foraminifera from different water depths and offers detailed insights into variations within habitats and the different impacts to the LDE. It was of interest to find out how environmental changes associated with the LDE influenced the living conditions of the climatically and environmentally sensitive planktic foraminifera. More specifically, the focus was on planktic foraminiferal assemblage changes and  $\delta^{13}\text{C}$ -,  $\delta^{18}\text{O}$ -excursions in the calcific tests for paleoenvironmental reconstruction and if it can be seen as a mostly supraregional or even global event.

### 2 The LDE negative carbon isotope excursion and temperature changes

Besides the well-explored PETM, other Paleocene and Eocene hyperthermal events were identified by their negative CIE and temperature anomalies, often in pace with orbital cycles and accompanied by ocean acidification and biotic changes. In comparison, the  $\delta^{13}\text{C}$  and  $\delta^{18}\text{O}$  results of the LDE strongly resemble those of the Eocene H2-event (=ETM2, ~54 Ma, e. g. Stap et al., 2010) as well as the Dan-C2-Event (~65.2 Ma; Coccioni et al., 2012). Other events like the PETM or the ETM2 resulted in higher  $\delta^{13}\text{C}$  and  $\delta^{18}\text{O}$  excursions.

A negative CIE has been unambiguously proved in benthic foraminifera at all investigated sites. Amplitudes of all LDE-related peaks are shown in Table 4 and Figure 29. At Shatsky Rise, the negative CIE within subsurface planktic foraminifera is very sharp, while the surface water signal was rather inconclusive or absent. A much clearer picture was found at Walvis Ridge for surface signals in both event beds, however, the subsurface signal is poorly developed during LDE1 but shows an excursion during LDE2. The negative CIE at SENR was derived from bulk rock and shows a larger excursion during LDE1 than during LDE2.

These findings prove that the LDE was not restricted to the sea floor or to certain ocean basins but, as proposed, on a supraregional scale. As revealed before, all main marine habitats were

influenced, including Tethyan areas like Zumaia and Caravaca in Spain or Bjala in Bulgaria (e. g. Arenillas et al., 2008; Dinarès-Turell et al., 2010, 2012; Storme et al., 2014).

Table 4: Compendious overview over  $\delta^{13}\text{C}$ ,  $\delta^{18}\text{O}$  and  $\Delta\text{T}$  peaks during LDE as measured on own data

		Shatsky Rise ODP Site 1210	Walvis Ridge ODP Site 1262	SENR IODP Site U1407
$\delta^{13}\text{C}$	benthic ( <i>N. truempyi</i> )	0.6 ‰	0.9 ‰	-
	Subsurface planktic ( <i>P. variospira</i> , <i>P. pseudobulloides</i> )	0.7 ‰	No clear peak	-
	Surface planktic ( <i>M. angulata</i> )	0.9 ‰	0.9 ‰	-
	bulk	-	-	1.0 ‰
$\delta^{18}\text{O}$ $\Delta\text{T}$	benthic ( <i>N. truempyi</i> )	(0.4 ‰) 1.6°C	(0.5 ‰) 2.0°C	-
	Subsurface planktic ( <i>P. variospira</i> , <i>P. pseudobulloides</i> )	(0.6 ‰) 2.4°C	(0.35 ‰) 1.4°C	-
	Surface planktic ( <i>M. angulata</i> )	(0.7 ‰) 2.8°C	(0.6 ‰) 2.4°C	-
	bulk	-	-	(0.75 ‰) 3°C
<u>Remarks</u>				
SENR: South East Newfoundland Ridge				
* data adopted from Bornemann et al. (2009)				
** some additional samples were used for P/B-ratio				

Potential causes for the negative CIE are the injection of isotopically light carbon into the ocean-atmosphere system by volcanic outgassing at the south-eastern Greenland margin (Sinton and Duncan, 1998), increased ocean spreading rates were proposed, while it also coincides with orbital forcing (e. g. Westerhold et al., 2008; Zachos et al., 2008).

The different  $\delta^{18}\text{O}$  results (Table 4, Figure 29) within the ocean sites are interpreted by oceanographic settings and connected to that, threshold-passing oceanographic developments at Shatsky Rise 1210 and not at Walvis Ridge 1262 or alternately by different test preservation. The suspicious signal of the smaller temperature rise in subsurface waters than at the sea floor is interpreted and discussed in Ch. III. SENR bulk rock data shows a -0.75 ‰ shift in  $\delta^{18}\text{O}$  which is interpreted as a  $\sim 3^\circ\text{C}$  warming in the North Atlantic Ocean for the entire water column.

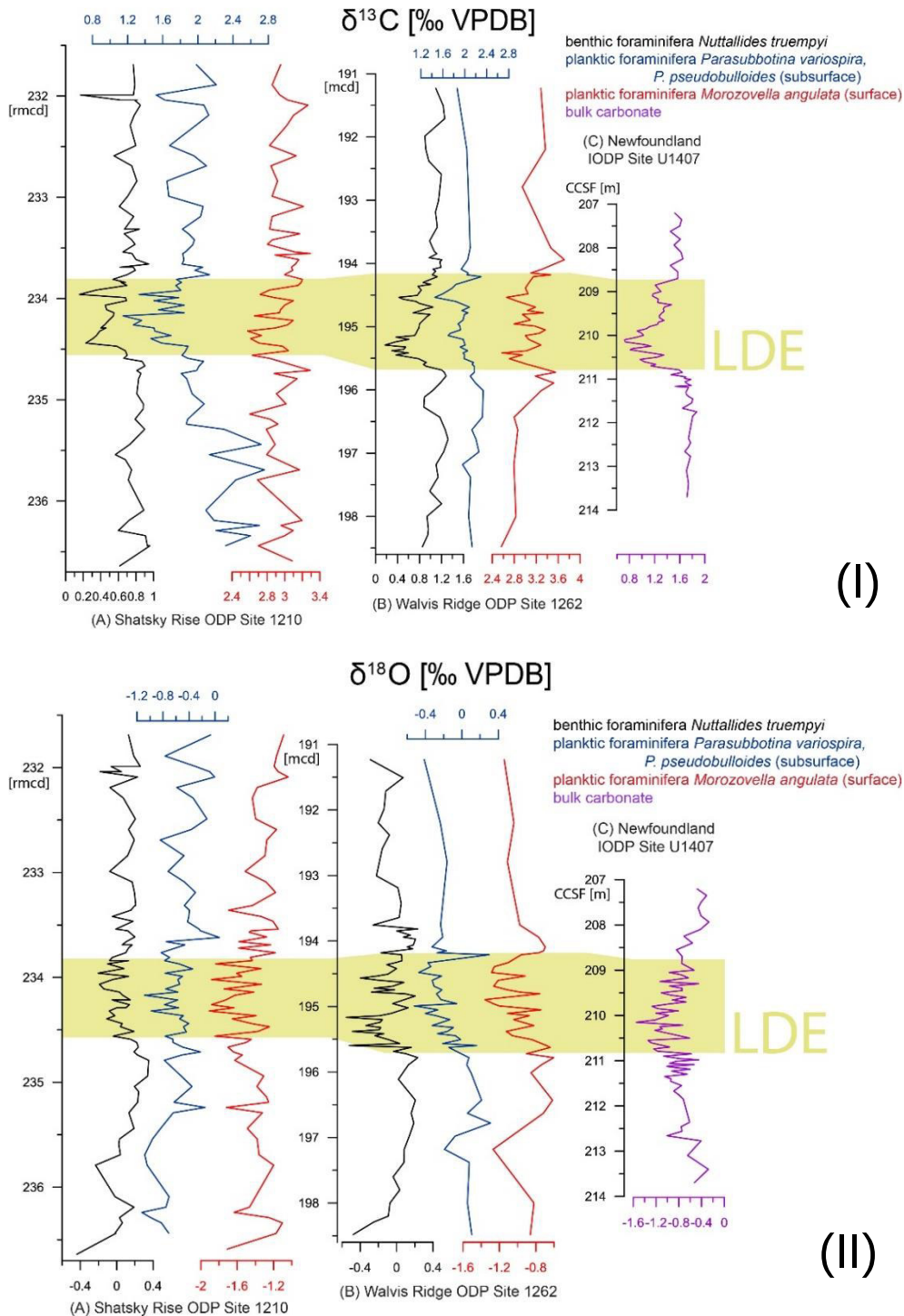


Figure 29: Comparison of the negative CIE (I) and the  $\delta^{18}\text{O}$  (II) variations at Shatsky Rise, Walvis Ridge and Newfoundland. Please note that the sites are not synchronized in this graphic. (A) and (B) show data from on benthic, surface as well as subsurface planktic foraminifera test carbonate, at SENR (C) bulk carbonate was analysed in the mass spectrometer and therefore represents the entire water column.

### 3 Planktic foraminifera assemblages - a supplementary comparison

In contrast to the muted benthic foraminiferal biotic response (Deprez et al., 2017), the planktic community has been substantially influenced by the LDE as documented by planktic foraminifera and calcareous nannofossil (e.g. the rise of fasciculiths). As discussed and proved for ODP Sites 1210 and 1262 (chapters II and III), the composition of the planktic foraminiferal assemblages changed over the observed time span. To gain a more comprehensive overview on planktic foraminifera assemblage changes, samples from SENR IODP Site U1407 and Tethyan shelf site Qreiya 3 (Egypt) were analysed in the same way as samples from ODP Sites 1210 and 1262 (see also Chapter IV).

The new assemblage data is added to a ternary diagram in order to display differences and similarities between the four sites. The species data was divided into three artificial clusters, which had the highest abundance before (1) during (2) or after (3) the LDE (Table 5).

(1) Pre-event cluster: *Praemurica uncinata*, *P. inconstans*, *P. praecursoria* and *Morozovella praeangulata*.

(2) LDE cluster: *Subbotina triangularis*, *S. triloculinodes*, *S. velasocoensis*, *S. cancellata*, *Parasubbotina pseudobulloides*, *P. variospira*, *P. varianta*, *Igorina tadjikistanensis*, *I. pusilla*, *Globanomalina compressa*, *G. chapmani*, *G. ehrenbergi*, *Acarinina strabocella*. Cluster (2) also includes species, which occur over the entire study interval (~62.5–61.5 Ma).

(3) Post-event cluster: *I. albeari*, *M. angulata*, *M. conicotruncata*, *M. oclusa*, *M. acutispira*, *M. aequa*, *M. apanthesma*, *G. cf. pseudomenardii*, *G. imitata*, *Parvularugoglobigerina alabamensis*, *Eoglobigerina spiralis*, *Chiloguembelina midwayensis*.

Table 5: Mean percentages per artificial cluster

Cluster	Walvis Ridge ODP Site 1261	SENR IODP Site U1407	Shatsky Rise ODP Site 1210	Qreiya 3, Egypt		
Paleolatitude	37° S (*)	33° N (*)	24° N (**)	9° N (**)		
(1) pre-event	4.1 %	5.5 %	18.5 %	9.3 %		
(2) LDE***	81.3 %	77.6 %	32.5 %	39 %		
(3) Post-event	14.6 %	16.9 %	49 %	51.7 %		
*	according	to	Kent	and	Irving,	2010
**	according	to	Torsvik	et	al.,	2012
***	during the event and/or during the entire observed record					

In the ternary diagram below (Figure 30), each point represents one sample and its composition according to the cluster as listed above. The most important testimony of this way of visualisation is to point out which site changed how much during the LDE in comparison to the other sites or how much the foraminiferal assemblages were influenced by the event.

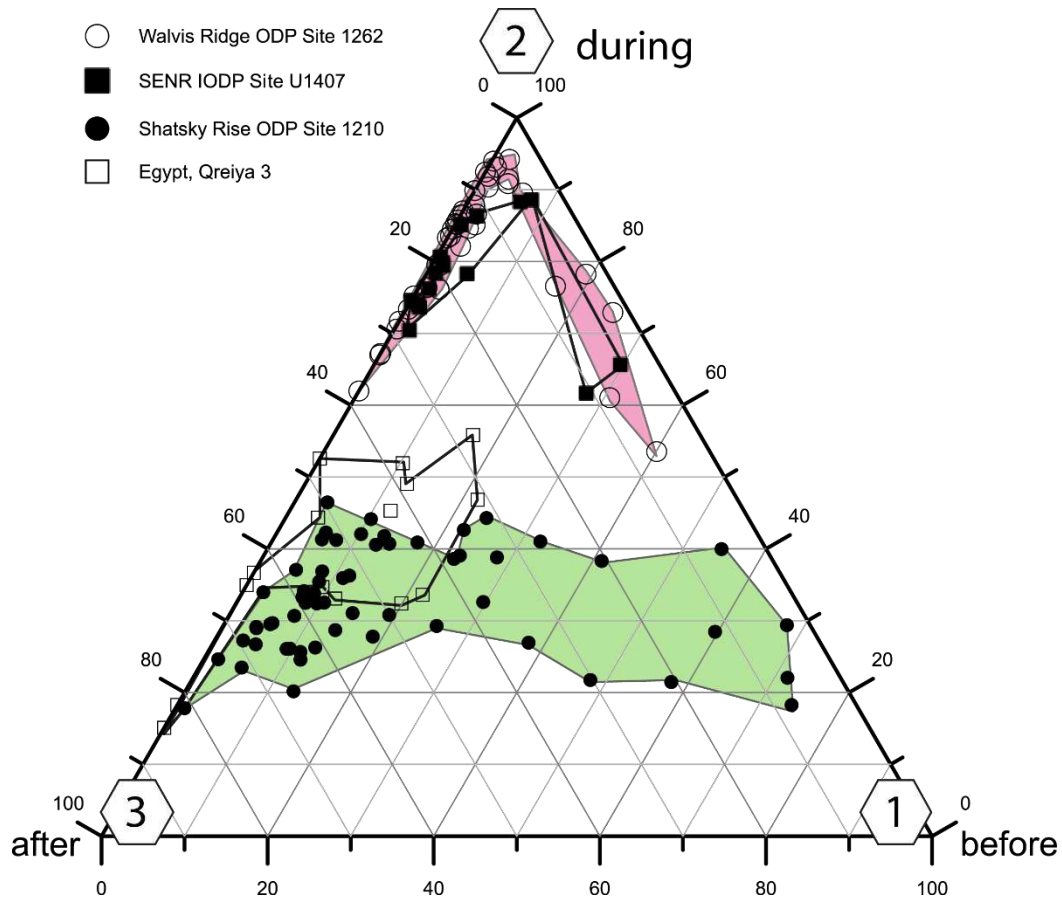


Figure 30: Ternary diagram for site comparison in aspects of assemblage. Species were grouped into three different clusters depending on the time interval in which they are most common. The clustering pattern was started on Walvis Ridge ODP Site 1262 and then applied to Shatsky Rise ODP Site 1210, SENR IODP Site U1407 and Qreiya 3 (Egypt). Each point in the plot represents a sample with its species composition. The positions are determined by the frequencies of abundance per cluster.

The four sites have in common to contain the smallest proportion in cluster (1). This could also be determined by the fact that the number of species which disappear or decrease before the LDE is lower compared to the number of species, which are less or little affected by the LDE (Figure 30).

There are mainly two distribution patterns among the sites: Samples from the Atlantic based sites Walvis Ridge and SENR are relatively congruent and concentrated on cluster (2) which could imply that the biotic reaction to the LDE was minor. Most samples mainly comprise specimens of species that are abundant throughout the observed interval and with little contribution of species that disappear and appear around the LDE (clusters (1) and (3)). Nevertheless, there are biotic reactions among surface dwellers to the LDE as already shown in the NMDS (Chapter III).

The Atlantic sites have in common to be situated at a similar paleolatitude during the LDE, which might have led to comparable conditions regarding ocean currents, upwelling or temperature. The recent northern and southern hemisphere show different climate systems in the same latitudes and are not directly comparable, however, the Paleocene temperature-latitude gradient was possibly smaller (Rea et al., 1990). A more restricted, smaller Atlantic basin compared to the more open Pacific and Tethys Ocean has possibly influenced the smaller LDE-related impact on planktic foraminifera due to vertical and horizontal circulation. As suggested

before (Ch. III), in contrast to Shatsky Rise 1210, the ocean stratification was not permanent in the Atlantic during the event.

Shatsky Rise was most likely situated in a very large ocean basin as Pacific and Tethyan oceans were largely one huge basin. These samples are most evenly distributed among the three defined endmembers, similar to the Egyptian Qreiya 3 data. The stronger faunal developments were probably caused by more extreme environmental changes than in the Atlantic, like the development of substantially enhanced surface water stratification and a permanent DCM during the LDE (Chs. II, III). The biotic changes at Site 1210 remained after the hyperthermal event on a lower level.

All samples from all four sites are dominated by species of subsurface planktic foraminifera. At Walvis Ridge Site 1262 (but also at Shatsky Rise Site 1210) warm water surface species (especially *I. albeari* and *M. angulata*) became more abundant during the two LDE phases.

For all four sites counts that the appearance of *I. albeari* and the decline of *Praemurica uncinata*, *P. inconstans* and *M. praeangulata* take place ~170 kyrs before the LDE, which hints towards a long-term development of oceanographic changes that were culminating at the LDE (Chapters II-IV). The enhanced surface ocean stratification as discussed for the oceanographic development of Shatsky Rise has its onset during that time as well (Jehle et al., 2015). Biotic reactions to the LDE are globally present, but not similar in between the different marine sites.

The faunal change below the LDE give one more hint towards the LDE onset below the remarkable negative CIEs, temperature changes and the globally corellatable XRF Fe and magnetic susceptibility peaks. Preceding environmental change is expressed by the FAD of *I. albeari* at all investigated sites, the  $\Delta\delta^{13}\text{C}$ ,  $\Delta\delta^{18}\text{O}$  and NMDS axis 1 changes at Shatsky Rise 1210 (Ch II) contemporary to that. Walvis Ridge 1262 shows these suspicious shifts for  $\Delta\delta^{13}\text{C}$  and the NMDS axis 1 (as an expression for faunal composition) shifts even earlier, however, the  $\Delta\delta^{18}\text{O}$  signal is rather uninformative. The LDE might have had an early onset, culminating into the hyperthermal event at 62.2 Ma.

## 4 Biostratigraphic implications

While investigating the planktic foraminiferal faunal changes during the time period before, during and after the LDE and connecting the first and last appearance datums (FAD, LAD) to biostratigraphic scales and astrochronology, it turned out that the new data disagrees with the established literature. The P3a/P3b Subzonal boundary is classically pinpointed to the LDE onset (~62.2 Ma), while here, the marker species for the P3a/b Subzone boundary *Igorina albeari* was consistently observed well below the LDE (~400 kyr, see Ch. IV). A reason for the discord is the rare abundance - but not absence - of the marker species *I. albeari* below the event, followed by a strong increase in numbers close to the onset of the LDE. Shipboard biostratigraphy mostly uses a low sample resolution of 9 m (one sample per core), which possibly led to overlooking early rare appearance of the marker (Bralower et al., 2002; Zachos et al., 2004). We conclude that the disappearance of *Praemurica* might represent a better age constrain than the somewhat diachronous appearance datum of *Igorina albeari* currently marking the base of the P3b Subzone. High resolution faunal analysis on several deep-sea sites

leave no doubt in the need for a revision of the biostratigraphy in terms of alternative marker species (Ch. IV).

## 5 Key results

The analysis of the four sites reveal the following key results:

- (1) The LDE left traces in both the surface ocean and the sea floor with different impact strengths.
- (2) A temperature rise of 2–4°C at the sea floor and the surface ocean was recorded with  $\delta^{18}\text{O}$  paleothermometry at Shatsky Rise, Walvis Ridge and Newfoundland.
- (3) A negative carbon isotope excursion (CIE) of 0.6–0.9 ‰ in planktic and benthic foraminiferal calcite accompanies the temperature anomaly at all sites and indicates a global perturbation of the carbon cycle.
- (4) At all deep-sea sites, the negative CIE shows a double-peak and implies a two-phase character of the event.
- (5) The negative CIE seems to be reflected in the  $\text{CaCO}_3$  and XRF Fe content at Shatsky Rise, Walvis Ridge and Newfoundland, but not within  $\delta^{18}\text{O}$  or the biotic response.
- (6) There is no complete recovery between the two phases.
- (7) Planktic foraminiferal fauna assemblage data shows different reactions in each ocean basin:
  - In the Pacific and Tethys Ocean, photosymbiotic surface dwelling species increased in abundance after the LDE but were slightly more affected by the event. The overall assemblage changes were stronger than in the Atlantic. A shallowing thermocline possibly improved the living conditions for subsurface dwellers.
  - At Walvis Ridge and Newfoundland, subsurface thermocline dwellers show a much stronger dominance during the observed record than surface dwellers and the overall biotic response to the event is smaller than at Shatsky Rise.
  - The Walvis Ridge faunal response implicates a development from temperate to subtropical conditions and back during the LDE.
  - Enhanced surface ocean stratification and a dominance of subsurface dwellers during the LDE was documented for the Pacific Ocean and linked to the development of a Deep Chlorophyll Maximum. The enhanced upper ocean stratification at Shatsky Rise 1210 sustained after the LDE.
  - Characteristic faunal changes (decline of *Praemurica uncinata*, *P. inconstans* and appearance of *I. albeari*) were initiated at least ~150 ky before the LDE, pointing towards ecological changes below the temperature rise, which were culminating during the LDE.

- (8) *Igorina albeari*, the biostratigraphic marker for the P3a/P3b planktic foraminiferal zone boundary was found below the assigned position, i.e. about 250-400 ky earlier than expected. The species shows a sudden rise in abundance with the onset of the LDE which is a possible reason for its original use as a biostratigraphic marker. *Praemurica inconstans* and *P. uncinata*, on the other hand, decrease below and finally disappear within the onset of the first negative CIE of the LDE. A revise of the late Danian biostratigraphy is suggested.



# References

- Agnini, C., Fornaciari, E., Raffi, I., Rio, D., Röhl, U. and Westerhold, T., 2007. High-resolution nannofossil biochronology of middle Paleocene to early Eocene at ODP Site 1262: Implications for calcareous nannoplankton evolution. *Marine Micropaleontology*. 64 (3-4), 215-248.
- Agnini, C., Macri, P., Backman, J., Brinkhuis, H., Fornaciari, E., Giusberti, L., Luciani, V., Rio, D., Sluijs, A. and Speranza, F., 2009. An early Eocene carbon cycle perturbation at similar to 52.5 Ma in the Southern Alps: Chronology and biotic response. *Paleoceanography*. 24, 10.1029/2008PA001649.
- Alegret, L., Ortiz, S., Arreguín-Rodríguez, G.J., Monechi, S., Millán, I. and Molina, E., 2016. Microfossil turnover across the uppermost Danian at Caravaca, Spain: Palaeoenvironmental inferences and identification of the latest Danian event. *Palaeogeography, Palaeoclimatology, Palaeoecology*. 463, 45-59.
- Allen, Dube, Solecki, Aragón-Durand and al., e., 2018. Global Warming of 1.5°C, an IPCC special report on the impacts of global warming of 1.5°C above preindustrial levels and related global greenhouse gas emission pathways, in the context of strengthening the global response to the threat of climate change, sustainable development, and efforts to eradicate poverty. IPCC. 15.
- Alley, R. and others, 2007. *Climate Change 2007: The Physical Science Basis. Summary for Policymakers. Contribution of Working Group I to the Fourth Assessment Report of the Intergovernmental panel on Climate Change. Agenda*, 6(07), 333
- Arenillas, I. and Molina, E., 1997. Análisis cuantitativo de los foraminíferos planctónicos del Paleoceno en Zumaya: implicaciones paleoambientales y eventos paleoceanográficos. *Revista Espanola de Paleontologia*. 12 (2) (ISSN 0213-6937), 207-232.
- Arenillas, I., Molina, E., Ortiz, S. and Schmitz, B., 2008. Foraminiferal and  $\delta^{13}\text{C}$  isotopic event-stratigraphy across the Danian-Selandian transition at Zumaya (northern Spain): chronostratigraphic implications. *Terra Nova*. 20 (1), 38-44.
- Arrhenius, G., 1950. Foraminifera and deep sea stratigraphy. *Science*. 111 (2881), 288.
- Arthur, M.A., 1979. North Atlantic Cretaceous black shales: the record at Site 398 and a brief comparison with other occurrences. *Initial Reports of the Deep Sea Drilling Project*. 47 (Part 2), 451e468.
- Aubry, M.P., Rodriguez, O., Bord, D., Godfrey, L., Schmitz, B. and Knox, R.W.O., 2012. The First Radiation of the Fasciculiths: Morphologic Adaptations of the Coccolithophores to Oligotrophy. *Austrian Journal of Earth Sciences*. 105 (1), 29-38.
- Banner, F., 1989. The nature of Globanomalina HAQUE. *The Journal of Foraminiferal Research*. 19 (3), 171-179.

- Barron, E.J. and Peterson, W.H., 1991. The Cenozoic Ocean Circulation Based on Ocean General-Circulation Model Results. *Palaeogeography, Palaeoclimatology, Palaeoecology*. 83 (1-3), 1-28.
- Be, A.W.H. and Tolderlund, D.S., 1971. Distribution and ecology of living planktonic foraminifera in surface waters of the Atlantic and Indian oceans. *The micropalaeontology of oceans*, p. 105-149, illus. (incl. sketch maps).
- Berger, W.H., 1970. Planktonic Foraminifera - Selective Solution and Lysocline. *Marine Geology*. 8 (2), 111-138.
- Berger, W.H., 1973. Deep-Sea Carbonates - Evidence for a Coccolith Lysocline. *Deep-Sea Research*. 20 (10), 917-921.
- Berger, W.H. and Parker, F.L., 1970. Diversity of planktonic foraminifera in deep-sea sediments. *Science*. 168 (3937), 1345-1347.
- Berggren, W.A., 1963. Problems of Paleocene stratigraphic correlation. *Inst. Fr. Petrole, Rev.* 18 (10), 1448-1457.
- Berggren, W.A., 1969. Cenozoic Chronostratigraphy, Planktonic Foraminiferal Zonation and Radiometric Time Scale. *Nature*. 224 (5224), 1072-&.
- Berggren, W.A., Kent, D.V., Aubry, M.P. and Hardenbol, J., 1995. Geochronology, time scales and global stratigraphic correlation. *SEPM Special Publication*, 54. SEPM (Society for Sedimentary Geology), Tulsa, 386 pp.
- Berggren, W.A., Kent, D.V., Swisher III, C.C. and Aubry, M.P., 1995. A revised Cenozoic geochronology and chronostratigraphy. *SEPM Special Publication*. 54, 129-212.
- Berggren, W.A. and Miller, K.G., 1988. Paleogene Tropical Planktonic Foraminiferal Biostratigraphy and Magnetobiochronology. *Micropaleontology*. 34 (4), 362-380.
- Berggren, W.A. and Norris, R.D., 1997. Biostratigraphy, Phylogeny and Systematics of Paleocene Trochospiral Planktic Foraminifera. *Micropaleontology*. 43, 119.
- Berggren, W.A. and Pearson, P.N., 2005. A revised tropical to subtropical paleogene planktonic foraminiferal zonation. *Journal of Foraminiferal Research*. 35 (4), 279-298.
- Bernaola, G., Baceta, J.I., Orue-Etxebarria, X., Alegret, L., Martin-Rubio, M., Arostegui, J. and Dinares-Turell, J., 2007. Evidence of an abrupt environmental disruption during the mid-Paleocene biotic event (Zumaia section, western Pyrenees). *Geological Society of America Bulletin*. 119 (7-8), 785-795.
- Bijma, J., Hemleben, C., Oberhansli, H. and Spindler, M., 1992. The Effects of Increased Water Fertility on Tropical Spinose Planktonic Foraminifers in Laboratory Cultures. *Journal of Foraminiferal Research*. 22 (3), 242-256.

- Birch, H., Coxall, H.K., Pearson, P.N., Kroon, D. and O'Regan, M., 2013. Planktonic foraminifera stable isotopes and water column structure: Disentangling ecological signals. *Marine Micropaleontology*. 101 (0), 127-145.
- Birch, H.S., Coxall, H.K. and Pearson, P.N., 2012. Evolutionary ecology of Early Paleocene planktonic foraminifera: size, depth habitat and symbiosis. *Paleobiology*. 38 (3), 374-390.
- Blow, W.H., 1979. *The Cainozoic Globigerinida; a Study of the Morphology, Taxonomy, Evolutionary Relationships and the Stratigraphical Distribution of some Globigerinida (mainly Globigerinacea)*, 1-3. E.J. Brill, Leiden, 1413 pp.
- Blunden, J., Hartfield, G. and Arndt, D., 2018. State of the Climate in 2017. *Bulletin of the American Meteorological Society*. 99 (8), Sxvi-Sxvi.
- Blunden, J. and Arndt, D.S., 2017. State of the Climate in 2016. *Bulletin of the American Meteorological Society*. 98 (8), Si-S280.
- Boersma, A. and Premoli Silva, I., 1991. Distribution of Paleogene Planktonic-Foraminifera - Analogies with the Recent. *Palaeogeography, Palaeoclimatology, Palaeoecology*. 83 (1-3), 29-47.
- Boersma, A. and Silva, I.P., 1983. Paleocene planktonic foraminiferal biogeography and the paleoceanography of the Atlantic Ocean. *Micropaleontology*, 355-381.
- Bohaty, S.M., Zachos, J.C., Florindo, F. and Delaney, M.L., 2009. Coupled greenhouse warming and deep-sea acidification in the middle Eocene. *Paleoceanography*. 24, 1-16.
- Bolli, H.M., 1957. The genera *Globigerina* and *Globorotaria* in Paleocene-Lower Eocene Lizard Spring Formation of Trinidad, BWI. *Bulletin of the United States National Museum*. 215, 61-81.
- Bond, G.C., Showers, W., Elliot, M., Evans, M., Lotti, R., Hajdas, I., Bonani, G. and Johnson, S., 2013. The North Atlantic's 1-2 Kyr Climate Rhythm: Relation to Heinrich Events, Dansgaard/Oeschger Cycles and the Little Ice Age, Mechanisms of Global Climate Change at Millennial Time Scales. 10.1029/GM112p0035.
- Bopp, L., Resplandy, L., Orr, J., Doney, S., Dunne, J., Gehlen, M., Halloran, P., Heinze, C., Ilyina, T., Séférian, R., Tjiputra, J. and Vichi, M., 2013. Multiple stressors of ocean ecosystems in the 21st century: Projections with CMIP5 models, 6225-6245.
- Bornemann, A., Norris, R.D., Friedrich, O., Beckmann, B., Schouten, S., Damsté, J.S.S., Vogel, J., Hofmann, P. and Wagner, T., 2008. Isotopic evidence for glaciation during the Cretaceous supergreenhouse. *Science*. 319 (5860), 189-192.
- Bornemann, A., Pirkenseer, C.M., Steurbaut, E. and Speijer, R.P., 2012. Early Paleogene  $\delta^{13}\text{C}$  and  $\delta^{18}\text{O}$  records based on marine ostracodes: implications for the upper Danian succession at Sidi Nasseur (Tunisia) and their application value in paleoceanography. *Austrian Journal of Earth Sciences* (1).

- Bornemann, A., Schulte, P., Sprong, J., Steurbaut, E., Youssef, M. and Speijer, R.P., 2009. Latest Danian carbon isotope anomaly and associated environmental change in the southern Tethys (Nile Basin, Egypt). *Journal of the Geological Society*. 166 (6), 1135-1142.
- Bowen, G.J. and Bowen, B.B., 2008. Mechanisms of PETM global change constrained by a new record from central Utah. *Geology*. 36 (5), 379-382.
- Bowen, G.J., Bralower, T.J., Delaney, M.L., Dickens, G.R., Kelly, D.C., Koch, P.L., Kump, L.R., Meng, J., Sloan, L.C., Thomas, E., Wing, S.L. and Zachos, J.C., 2006. Eocene hyperthermal event offers insight into greenhouse warming. *Eos*. 87 (17), 167-169.
- Boyd, C. and Gradmann, D., 2002. Impact of osmolytes on buoyancy of marine phytoplankton. *Marine Biology*. 141 (4), 605-618.
- Bradshaw, J.S., 1957. Ecology of living planktonic foraminifera in the North and Equatorial Pacific Ocean. 256 p.
- Bralower, T.J., 2002. Evidence of surface water oligotrophy during the Paleocene-Eocene thermal maximum: Nannofossil assemblage data from Ocean Drilling Program Site 690, Maud Rise, Weddell Sea. *Paleoceanography*. 17 (2), 10.1029/2001PA000662.
- Bralower, T.J., Premoli Silva, I. and Malone, M.J., 2002. Leg 198 summary. *Proceedings of the Ocean Drilling Program Initial Reports*. 198 (College Station, TX (Ocean Drilling Program)), 1–148. 10.2973/odp.proc.ir.198.2002.
- Bralower, T.J., Thomas, D.J., Zachos, J.C., Hirschmann, M.M., Röhl, U., Sigurdsson, H., Thomas, E. and Whitney, D.L., 1997. High-resolution records of the late Paleocene thermal maximum and circum-Caribbean volcanism: Is there a causal link? *Geology*. 25 (11), 963-966.
- Brönnimann, P. and Brown, N.K., 1958. Hedbergella, a new name for a Cretaceous planktonic foraminiferal genus. *Journal of the Washington Academy of Sciences*. 48 (1), 15-17.
- Brumsack, H.J., 2006. The trace metal content of recent organic carbon-rich sediments: Implications for Cretaceous black shale formation. *Palaeogeography, Palaeoclimatology, Palaeoecology*. 232 (2-4), 344-361.
- Buffett, B. and Archer, D., 2004. Global inventory of methane clathrate: sensitivity to changes in the deep ocean. *Earth and Planetary Science Letters*. 227 (3-4), 185-199.
- Burns, S.J., Fleitmann, D., Matter, A., Kramers, J. and Al-Subbary, A.A., 2003. Indian Ocean Climate and an Absolute Chronology over Dansgaard/Oeschger Events 9 to 13. *Science*. 301 (5638), 1365-1367.
- Cande, S.C. and Kent, D.V., 1995. Revised calibration of the geomagnetic polarity timescale for the Late Cretaceous and Cenozoic. *Journal of Geophysical Research, B, Solid Earth and Planets*. 100 (4), 6093-6095.

- Castradori, D., 1993. Calcareous Nannofossils and the Origin of Eastern Mediterranean Sapropels. *Paleoceanography*. 8 (4), 459-471. 10.1029/93pa00756.
- Clyde, W.C., Ting, S.Y., Snell, K.E., Bowen, G.J., Tong, Y.S., Koch, P.L., Li, Q. and Wang, Y.Q., 2010. New Paleomagnetic and Stable-Isotope Results from the Nanxiong Basin, China: Implications for the K/T Boundary and the Timing of Paleocene Mammalian Turnover. *Journal of Geology*. 118 (2), 131-143.
- Clyde, W.C., Tong, Y.S., Snell, K.E., Bowen, G.J., Ting, S.Y., Koch, P.L., Li, Q., Wang, Y.Q. and Meng, J., 2008. An integrated stratigraphic record from the Paleocene of the Chijiang Basin, Jiangxi Province (China): Implications for mammalian turnover and Asian block rotations. *Earth and Planetary Science Letters*. 269 (3-4), 553-563.
- Coccioni, R., Frontalini, F., Bancala, G., Fornaciari, E., Jovane, L. and Sprovieri, M., 2010. The Dan-C2 hyperthermal event at Gubbio (Italy): Global implications, environmental effects, and cause(s). *Earth and Planetary Science Letters*. 297 (1-2), 298-305. DOI 10.1016/j.epsl.2010.06.031.
- Cogné, J.-P. and Humler, E., 2006. Trends and rhythms in global seafloor generation rate. *Geochemistry, Geophysics, Geosystems*. 7 (3).
- Collinson, M., Steart, D., Handley, L., Pancost, R., Scott, A., Glasspool, I., Hooker, J. and Stott, A., 2006. Fire regimes and palaeoenvironments across the onset of the Palaeocene/Eocene thermal maximum, S. England, *Climate and Biota of the Early Paleogene, Bilbao, Volume of Abstracts*. 28.
- Corfield, R.M. and Granlund, A.H., 1988. Speciation and structural evolution in the Palaeocene *Morozovella* lineage (planktonic Foraminiferida). *Journal of Micropalaeontology*. 7 (1), 59-72.
- Corfield, R.M. and Cartlidge, J.E., 1991. Isotopic evidence for the depth stratification of fossil and Recent Globigerinina; a review. *Historical Biology*. 5 (1), 37-63.
- Courtillot, V., Besse, J., Vandamme, D., Montigny, R., Jaeger, J.-J. and Cappetta, H., 1986. Deccan flood basalts at the Cretaceous/Tertiary boundary? *Earth and Planetary Science Letters*. 80 (3), 361-374. [https://doi.org/10.1016/0012-821X\(86\)90118-4](https://doi.org/10.1016/0012-821X(86)90118-4).
- Coxall, H.K., D'Hondt, S. and Zachos, J.C., 2006. Pelagic evolution and environmental recovery after the Cretaceous-Paleogene mass extinction. *Geology*. 34 (4), 297-300.
- Criscione, J., Bord, D., Godfrey, L. and Aubry, M.-P., 2017. Inferred pseudo-cryptic speciation in the coccolithophore species *Braarudosphaera bigelowii* (Gran and Braarud) during the Early Paleocene (Danian). *Marine Micropaleontology*. 137 (Supplement C), 1-15.
- Crouch, E.M., Heilmann-Clausen, C., Brinkhuis, H., Morgans, H.E.G., Rogers, K.M., Egger, H. and Schmitz, B., 2001. Global dinoflagellate event associated with the late Paleocene thermal maximum. *Geology*. 29 (4), 315-318.

- Cullen, J.J., 1982. The Deep Chlorophyll Maximum - Comparing Vertical Profiles of Chlorophyll-A. *Canadian Journal of Fisheries and Aquatic Sciences*. 39 (5), 791-803.
- Cushman, J.A. and Stainforth, R.M., 1945. The Foraminifera of the Cipero marl formation of Trinidad, British West Indies. Cushman Lab. Foraminiferal Research Special Publications. 1491 p., illus., Apr. 21, 1945.
- Cushman, J., 1933. Some new foraminiferal genera. *Contributions from the Cushman Laboratory for Foraminiferal Research*. 9 (2), 33.
- Davidzon, R., 1976. Novyy paleogenovyy rod planktonnykh foraminifer. *Trudy Vsesoyuznogo Nauchno-issledovatel'skogo Geologorazvedochnogo Neftyanogo Instituta (VNIGNI), Tadzhijskoe Otdelenie*. 183, 197-199.
- Davis, S.J. and Caldeira, K., 2010. Consumption-based accounting of CO<sub>2</sub> emissions. *Proceedings of the National Academy of Sciences*. 107 (12), 5687-5692.
- DeConto, R.M., Galeotti, S., Pagani, M., Tracy, D., Schaefer, K., Zhang, T., Pollard, D. and Beerling, D.J., 2012. Past extreme warming events linked to massive carbon release from thawing permafrost. *Nature*. 484 (7392), 87-91.
- Deprez, A., Jehle, S., Bornemann, A. and Speijer, R.P., 2017. Differential response at the seafloor during Palaeocene and Eocene ocean warming events at Walvis Ridge, Atlantic Ocean (ODP Site 1262). *Terra Nova*. 29 (1), 71-76.
- Deprez, A., Jehle, S., Bornemann, A. and Speijer, R.P., 2017. Pronounced biotic and environmental change across the latest Danian warming event (LDE) at Shatsky Rise, Pacific Ocean (ODP Site 1210). *Marine Micropaleontology*. 137, 31-45.
- D'Hondt, S., 2005. Consequences of the Cretaceous/Paleogene mass extinction for marine ecosystems. *Annual Review of Ecology Evolution and Systematics*. 36, 295-317.
- D'Hondt, S. and Zachos, J.C., 1993. On stable isotopic variation and earliest Paleocene planktonic foraminifera. *Paleoceanography*. 8 (4), 527-547.
- D'Hondt, S. and Zachos, J.C., 1998. Cretaceous foraminifera and the evolutionary history of planktic photosymbiosis. *Paleobiology*. 24 (4), 512-523.
- D'Hondt, S., Zachos, J.C. and Schultz, G., 1994. Stable Isotopic Signals and Photosymbiosis in Late Paleocene Planktic Foraminifera. *Paleobiology*. 20 (3), 391-406.
- Dickens, G.R., 2011. Down the Rabbit Hole: toward appropriate discussion of methane release from gas hydrate systems during the Paleocene-Eocene thermal maximum and other past hyperthermal events. *Climate of the Past*. 7 (3), 831-846.
- Dickens, G.R., Castillo, M.M. and Walker, J.C.G., 1997. A blast of gas in the latest Paleocene: Simulating first-order effects of massive dissociation of oceanic methane hydrate. *Geology*. 25 (3), 259-262.

- Dickens, G.R., O'Neil, J.R., Rea, D.K. and Owen, R.M., 1995. Dissociation of oceanic methane hydrate as a cause of the carbon-isotope excursion at the end of the Paleocene. *Paleoceanography*. 10 (6), 965-971.
- Dinares-Turell, J., Baceta, J.I., Bemaola, G., Orue-Etxebarria, X. and Pujalte, V., 2007. Closing the Mid-Palaeocene gap: Toward a complete astronomically tuned Palaeocene Epoch and Selandian and Thanetian GSSPs at Zumaia (Basque Basin, W Pyrenees). *Earth and Planetary Science Letters*. 262 (3-4), 450-467.
- Dinares-Turell, J., Baceta, J.I., Pujalte, V., Orue-Etxebarria, X., Bernaola, G. and Lorito, S., 2003. Untangling the Palaeocene climatic rhythm: an astronomically calibrated Early Palaeocene magnetostratigraphy and biostratigraphy at Zumaia (Basque basin, northern Spain). *Earth and Planetary Science Letters*. 216 (4), 483-500.
- Dinares-Turell, J., Pujalte, V., Stoykova, K., Baceta, J.I. and Ivanov, M., 2012. The Palaeocene "top chron C27n" transient greenhouse episode: evidence from marine pelagic Atlantic and peri-Tethyan sections. *Terra Nova*. 24 (6), 477-486.
- Dinarès-Turell, J., Stoykova, K., Baceta, J.I., Ivanov, M. and Pujalte, V., 2010. High-resolution intra- and interbasinal correlation of the Danian-Selandian transition (Early Paleocene): The Bjala section (Bulgaria) and the Selandian GSSP at Zumaia (Spain). *Palaeogeography, Palaeoclimatology, Palaeoecology*. 297 (2), 511-533.
- Dinarès-Turell, J., Westerhold, T., Pujalte, V., Röhl, U. and Kroon, D., 2014. Astronomical calibration of the Danian stage (Early Paleocene) revisited: Settling chronologies of sedimentary records across the Atlantic and Pacific Oceans. *Earth and Planetary Science Letters*. 405 (0), 119-131.
- Dittert, N., Baumann, K.H., Bickert, T., Henrich, R., Huber, R., Kinkel, H. and Meggers, H., 1999. Carbonate Dissolution in the Deep-Sea: Methods, Quantification and Paleoceanographic Application. In: G. Fischer and G. Wefer (Editors), *Use of Proxies in Paleoceanography*. Springer Berlin Heidelberg, 255-284.
- Dittert, N. and Henrich, R., 2000. Carbonate dissolution in the South Atlantic Ocean: evidence from ultrastructure breakdown in *Globigerina bulloides*. *Deep-Sea Res Pt I*. 47 (4), 603-620.
- Donner, S.D., 2009. Coping with Commitment: Projected Thermal Stress on Coral Reefs under Different Future Scenarios. *PLoS ONE*. 4 (6), e5712.
- Douglas, R.G. and Savin, S.M., 1978. Oxygen isotopic evidence for the depth stratification of tertiary and cretaceous planktic foraminifera. *Marine Micropaleontology*. 3 (2), 175-196.
- Dunkley Jones, T., Lunt, D.J., Schmidt, D.N., Ridgwell, A., Sluijs, A., Valdes, P.J. and Maslin, M., 2013. Climate model and proxy data constraints on ocean warming across the Paleocene-Eocene Thermal Maximum. *Earth-Science Reviews*. 125 (Supplement C), 123-145. <https://doi.org/10.1016/j.earscirev.2013.07.004>.

- Dutton, A., Lohmann, K.C. and Leckie, R.M., 2005. Insights from the Paleogene tropical Pacific: Foraminiferal stable isotope and elemental results from Site 1209, Shatsky Rise. *Paleoceanography*. 20 (3), 10.1029/2004PA001098.
- Edgar, K.M., Anagnostou, E., Pearson, P.N. and Foster, G.L., 2015. Assessing the impact of diagenesis on  $\delta^{11}\text{B}$ ,  $\delta^{13}\text{C}$ ,  $\delta^{18}\text{O}$ , Sr/Ca and B/Ca values in fossil planktic foraminiferal calcite. *Geochimica Et Cosmochimica Acta*. 166, 189-209.
- Edgar, K.M., Pälike, H. and Wilson, P.A., 2013. Testing the impact of diagenesis on the  $\delta^{18}\text{O}$  and  $\delta^{13}\text{C}$  of benthic foraminiferal calcite from a sediment burial depth transect in the equatorial Pacific. *Paleoceanography*. 28 (3), 468-480.
- Eldholm, O. and Thomas, E., 1993. Environmental impact of volcanic margin formation. *Earth and Planetary Science Letters*. 117, 319-329.
- Emeis, K.C., Schulz, H., Struck, U., Rossignol-Strick, M., Erlenkeuser, H., Howell, M.W., Kroon, D., Mackensen, A., Ishizuka, S., Oba, T., Sakamoto, T. and Koizumi, I., 2003. Eastern Mediterranean surface water temperatures and  $\delta^{18}\text{O}$  composition during deposition of sapropels in the late Quaternary. *Paleoceanography*. 18 (1). 10.1029/2000pa000617.
- Emiliani, C., 1954. Depth habitats of some species of pelagic Foraminifera as indicated by oxygen isotope ratios. *Am. Jour. Sci.* 252 (3), 149-158.
- Emiliani, C., 1954. Temperatures of Pacific bottom waters and polar superficial waters during the Tertiary. *Science*. 119 (3103), 853-855.
- Emiliani, C., 1955. Pleistocene temperatures. *Journal of Geology*. 63 (6), 538-578.
- Emrich, K. and Vogel, J.C., 1970. Carbon Isotope Fractionation during Precipitation of Calcium Carbonate. *Earth and Planetary Science Letters*. 8 (5), 363-371.
- Erez, J. and Luz, B., 1983. Experimental Paleotemperature Equation for Planktonic-Foraminifera. *Geochimica Et Cosmochimica Acta*. 47 (6), 1025-1031.
- Farouk, S. and El-Sorogy, A., 2014. Danian/Selandian unconformity in the central and southern Western Desert of Egypt. *Journal of African Earth Sciences*. 103, 42-53.
- Fuqua, L.M., Bralower, T.J., Arthur, M.A. and Patzkowsky, M.E., 2008. Evolution of calcareous nannoplankton and the recovery of marine food webs after the Cretaceous-Paleocene mass extinction. *Palaios*. 23 (3-4), 185-194.
- Gobiet, A., Kotlarski, S., Beniston, M., Heinrich, G., Rajczak, J. and Stoffel, M., 2014. 21st century climate change in the European Alps- A review. *Science of The Total Environment*. 493, 1138-1151. 10.1016/j.scitotenv.2013.07.050.
- Gradstein, F.M., Ogg, J.G., Schmitz, M. and Ogg, G., 2012. *The geologic time scale 2012*. Elsevier



- Gulick, S., Morgan, J. and Mellett, C., 2016. Expedition 364 Scientific Prospectus: Chicxulub: drilling the K-Pg impact crater. International Ocean Discovery Program. sp. 364, 2332-1385.
- Guasti, E., 2005. Early Paleogene environmental turnover in the southern Tethys as recorded by foraminiferal and organic-walled dinoflagellate cyst assemblages, Universität Bremen, Bremen, 203 pp.
- Guasti, E., Speijer, R.P., Brinkhuis, H., Smit, J. and Steurbaut, E., 2006. Paleoenvironmental change at the Danian-Selandian transition in Tunisia: Foraminifera, organic-walled dinoflagellate cyst and calcareous nannofossil records. *Marine Micropaleontology*. 59 (3-4), 210-229.
- Gutjahr, M., Ridgwell, A., Sexton, P.F., Anagnostou, E., Pearson, P.N., Pälike, H., Norris, R.D., Thomas, E. and Foster, G.L., 2017. Very large release of mostly volcanic carbon during the Paleocene-Eocene Thermal Maximum. *Nature*. 548 (7669), 573-577.
- Hancock, H.J. and Dickens, G.R., 2006. Carbonate dissolution episodes in Paleocene and Eocene sediment, Shatsky Rise, west-central Pacific, Proceedings of the Ocean Drilling Program. Scientific Results. Texas A&M University, 1-24.
- Hancock, H.J.L., Dickens, G.R., Thomas, E. and Blake, K.L., 2007. Reappraisal of early Paleogene CCD curves: foraminiferal assemblages and stable carbon isotopes across the carbonate facies of Perth Abyssal Plain. *International Journal of Earth Sciences*. 96 (5), 925-946.
- Haq, B.U., 1981. Paleogene paleoceanography: Early Cenozoic oceans revisited. *Oceanologica Acta* (1981). SP, 71-82.
- Haque, A.F.M.M., 1956. The Foraminifera of the Ranikot and the Laki of the Nammal gorge, Salt Range. *Memoir of the Geological Survey of Pakistan, Palaeontologica Pakistanica*. 1, 300 pp.
- Hart, M.B., 2007. Late Cretaceous climates and foraminiferid distributions. *Geological Society Special Publication*, 235-250.
- Hay, W.W., DeConto, R.M., Wold, C.N., Wilson, K.M., Voigt, S., Schulz, M., Wold, A.R., Dullo, W.-C., Ronov, A.B. and Balukhovsky, A.N., 1999. Alternative global Cretaceous paleogeography. *Geological Society of America Special Paper*. 332, 1-47.
- Hedberg, H.D., 1976. *International stratigraphic guide. A guide to stratigraphic classification, terminology, and procedure*. John Wiley & Sons, New York.
- Hemleben, C., Spindler, M. and Anderson, O.R., 1989. *Modern planktonic foraminifera*. Springer, Berlin, 363 pp.
- Henderson, G.M., 2002. New oceanic proxies for paleoclimate. *Earth and Planetary Science Letters*. 203 (1), 1-13.

- Herbland, A. and Voituriez, B., 1979. Hydrological structure analysis for estimating the primary production in the tropical Atlantic Ocean. *Journal of Marine Research*. 37 (1), 87-101.
- Herman, A.B. and Spicer, R.A., 1996. Palaeobotanical evidence for a warm Cretaceous Arctic Ocean. *Nature*. 380 (6572), 330-333.
- Hilgen, F.J., Abels, H.A., Kuiper, K.F., Lourens, L.J. and Wolthers, M., 2015. Towards a stable astronomical time scale for the Paleocene: Aligning Shatsky Rise with the Zumaia–Walvis Ridge ODP Site 1262 composite. *Newsletters on Stratigraphy*. 48 (1), 91-110.
- Hipp, T., Etzelmüller, B., Farbrot, H., Schuler, T. and Westermann, S., 2012. Modelling borehole temperatures in Southern Norway - insights into permafrost dynamics during the 20th and 21st century. *The Cryosphere*. 6 (3), 553-571.
- Hoefs, J., 1997. *Stable isotope geochemistry*, 201. Springer
- Hoegh-Guldberg, O. and Bruno, J.F., 2010. The Impact of Climate Change on the World's Marine Ecosystems. *Science*. 328 (5985), 1523-1528.
- Houghton, J.T., Ding, Y., Griggs, D.J., Noguera, M., van der Linden, P.J., Dai, X., Maskell, K. and Johnson, C.A., 2001. *Climate change 2001: the scientific basis*. The Press Syndicate of the University of Cambridge
- Houston, R.M. and Huber, B.T., 1998. Evidence of photosymbiosis in fossil taxa? Ontogenetic stable isotope trends in some Late Cretaceous planktonic foraminifera. *Marine Micropaleontology*. 34 (1-2), 29-46.
- Huber, B.T., Hodell, D.A. and Hamilton, C.P., 1995. Middle-Late Cretaceous climate of the southern high latitudes: Stable isotopic evidence for minimal equator-to-pole thermal gradients. *Geological Society of America Bulletin*. 107 (10), 1164-1191.
- Huisman, J., Pham Thi, N.N., Karl, D.M. and Sommeijer, B., 2006. Reduced mixing generates oscillations and chaos in the oceanic deep chlorophyll maximum. *Nature*. 439 (7074), 322-325.
- Imbrie, J. and Kipp, N.G., 1971. A new micropaleontological method for quantitative paleoclimatology: Application to a late Pleistocene Caribbean core. *The Late Cenozoic Glacial Ages*, 71-181.
- Imbery, F., Friedrich, K., Haeseler, S., Koppe, C., Janssen, W. and Bissolli, P., 2018. Vorläufiger Rückblick auf den Sommer 2018-eine Bilanz extremer Wetterereignisse. *Deutscher Wetterdienst, Abteilung für Klimaüberwachung und Agrarmeteorologie*.
- Jehle, S., Bornemann, A., Deprez, A. and Speijer, R.P., 2015. The Impact of the Latest Danian Event on Planktic Foraminiferal Faunas at ODP Site 1210 (Shatsky Rise, Pacific Ocean). *PLoS ONE*. 10 (11), e0141644.

- Jiang, S.J., Bralower, T.J., Patzkowsky, M.E., Kump, L.R. and Schueth, J.D., 2010. Geographic controls on nannoplankton extinction across the Cretaceous/Palaeogene boundary. *Nature Geoscience*. 3 (4), 280-285.
- Katz, M.E., Cramer, B.S., Mountain, G.S., Katz, S. and Miller, K.G., 2001. Uncorking the bottle: What triggered the Paleocene/Eocene thermal maximum methane release? *Paleoceanography*. 16 (6), 549-562.
- Keller, G., 1988. Extinction, survivorship and evolution of planktic foraminifera across the Cretaceous/Tertiary boundary at El Kef, Tunisia. *Marine Micropaleontology*. 13 (3), 239-263.
- Kelly, D.C., Arnold, A.J. and Parker, W.C., 1996. Paedomorphosis and the origin of the Paleogene planktonic foraminiferal genus *Morozovella*. *Paleobiology*. 22 (2), 266-281.
- Kelly, D.C., Arnold, A.J. and Parker, W.C., 1999. The influence of heterochrony on the stratigraphic occurrence of *Morozovella angulata*. *Journal of Foraminiferal Research*. 29 (1), 58-68.
- Kendall, C. and Caldwell, E.A., 1998. *Fundamentals of isotope geochemistry, Isotope tracers in catchment hydrology*. Elsevier, 51-86.
- Kennett, J.P. and Stott, L.D., 1991. Abrupt deep-sea warming, palaeoceanographic changes and benthic extinctions at the end of the Paleocene. *Nature*. 353 (6341), 225-229.
- Kent, D.V. and Irving, E., 2010. Influence of inclination error in sedimentary rocks on the Triassic and Jurassic apparent pole wander path for North America and implications for Cordilleran tectonics. *Journal of Geophysical Research: Solid Earth*. 115 (B10).
- Killingley, J.S., 1983. Effects of diagenetic recrystallization on  $^{18}\text{O}/^{16}\text{O}$  values of deep-sea sediments. *Nature*. 301 (5901), 594-597.
- King, J.W. and Channell, J.E., 1991. Sedimentary magnetism, environmental magnetism, and magnetostratigraphy. *Rev Geophys*. 29 (S1), 358-370.
- Kirtland Turner, S. and Ridgwell, A., 2016. Development of a novel empirical framework for interpreting geological carbon isotope excursions, with implications for the rate of carbon injection across the PETM. *Earth and Planetary Science Letters*. 435, 1-13.
- Knox, R.W.O.B., 1996. Correlation of the early Paleogene in northwest Europe: An overview. *Geological Society Special Publication* (101), 1-11.
- Kroopnick, P., 1979. Isotopic fractionations during oxygen consumption and carbonate dissolution within the North Atlantic Deep Water. *Earth and Planetary Science Letters*. 49 (2), 485-498.
- Kroopnick, P., 1980. The Distribution of  $^{13}\text{C}$  in the Atlantic-Ocean. *Earth and Planetary Science Letters*. 49 (2), 469-484.

- Kroopnick, P.M., 1985. The distribution of  $^{13}\text{C}$  of  $\text{SCO}_2$  in the world oceans. *Deep-Sea Res.* 32 (1), 57-84.
- Kucera, M., 2007. Chapter Six Planktonic Foraminifera as Tracers of Past Oceanic Environments. *Dev. Mar. Geol.* 1, 213-262.
- Kucera, M. and Schönfeld, J., 2007. The origin of modern oceanic foraminiferal faunas and Neogene climate change. In: M. Williams, A.M. Haywood, F.J. Gregory and D.N. Schmidt (Editors), *Geological Society Special Publication*, 409-425.
- Kucera, M., Weinelt, M., Kiefer, T., Pflaumann, U., Hayes, A., Weinelt, M., Chen, M.-T., Mix, A.C., Barrows, T.T., Cortijo, E., Duprat, J., Juggins, S. and Waelbroeck, C., 2005. Reconstruction of sea-surface temperatures from assemblages of planktonic foraminifera: multi-technique approach based on geographically constrained calibration data sets and its application to glacial Atlantic and Pacific Oceans. *Quaternary Science Reviews.* 24 (7–9), 951-998. <http://dx.doi.org/10.1016/j.quascirev.2004.07.014>.
- Kurtz, A., Kump, L., Arthur, M., Zachos, J. and Paytan, A., 2003. Early Cenozoic decoupling of the global carbon and sulfur cycles. *Paleoceanography.* 18 (4).
- Larsen, L.M., Pedersen, A.K., Tegner, C., Duncan, R.A., Hald, N. and Larsen, J.G., 2016. Age of Tertiary volcanic rocks on the West Greenland continental margin: volcanic evolution and event correlation to other parts of the North Atlantic Igneous Province. *Geological Magazine.* 153 (3), 487-511.
- Larson, R.L., Steiner, M.B., Erba, E. and Lancelot, Y., 1992. Paleolatitudes and Tectonic Reconstructions of the Oldest Portion of the Pacific Plate: A Comparative Study, Larson, RL, Lancelot, Y., et al., *Proc. ODP, Sci. Results*, 615-631.
- Le Pichon, X., Sibuet, J.-C. and Francheteau, J., 1977. The fit of the continents around the North Atlantic Ocean— Contribution No. 470 of the Département Scientifique, Centre Océanologique de Bretagne. *Tectonophysics.* 38 (3-4), 169-209.
- Li, L.Q. and Keller, G., 1998. Maastrichtian climate, productivity and faunal turnovers in planktic foraminifera in south Atlantic DSDP sites 525A and 21. *Marine Micropaleontology.* 33 (1-2), 55-86.
- Littler, K., Röhl, U., Westerhold, T. and Zachos, J.C., 2014. A high-resolution benthic stable-isotope record for the South Atlantic: Implications for orbital-scale changes in Late Paleocene-Early Eocene climate and carbon cycling. *Earth and Planetary Science Letters.* 401, 18-30.
- Loeblich, A.R., Jr. and Tappan, H., 1987. *Foraminiferal Genera and their Classification*. Van Nostrand Reinhold, New York, 970 pp.
- Loeblich, A.R., Jr. and Tappan, H.N., 1957. Correlation of the Gulf and Atlantic Coastal Plain Paleocene and lower Eocene formations by means of planktonic Foraminifera. *Journal of Paleontology.* 1109-1137.

- Lourens, L.J., Sluijs, A., Kroon, D., Zachos, J.C., Thomas, E., Röhl, U., Bowles, J. and Raffi, I., 2005. Astronomical pacing of late Palaeocene to early Eocene global warming events. *Nature*. 435 (7045), 1083-7.
- Lund, S.P. and Karlin, R., 1990. Introduction to the Special Section on Physical and Biogeochemical Processes Responsible for the Magnetization of Sediments. *Journal of Geophysical Research: Solid Earth*. 95 (B4), 4353-4354.
- Lyell, C., 1830. *Principles of geology*. Murray, London. 3.
- Markwick, P., 2007. The palaeogeographic and palaeoclimatic significance of climate proxies for data-model comparisons. Deep-time perspectives on climate change: marrying the signal from computer models and biological proxies, 251-312.
- Masson-Delmotte, V., Schulz, M., Abe-Ouchi, A., Beer, J., Ganopolski, A., González Rouco, J.F., Jansen, E., Lambeck, K., Luterbacher, J., Naish, T., Osborn, T., Otto-Bliesner, B.L., Quinn, T.M., Ramesh, R., Rojas, M., Shao, X. and Timmermann, A., 2013. Information from Paleoclimate Archives, *Climate Change: The Physical Science Basis. Contribution of Working Group I to the Fifth Assessment Report of the Intergovernmental Panel on Climate Change*. Cambridge University Press, Cambridge, United Kingdom and New York, NY, USA, 383-464.
- McCarren, H., Thomas, E., Hasegawa, T., Röhl, U. and Zachos, J.C., 2008. Depth dependency of the Paleocene-Eocene carbon isotope excursion: Paired benthic and terrestrial biomarker records (Ocean Drilling Program Leg 208, Walvis Ridge). *Geochemistry Geophysics Geosystems*. 9 (10), 1-10.
- McGowran, B., 2005. Biostratigraphy and chronostratigraphic classification, *Biostratigraphy: Microfossils and Geological Time*. Cambridge University Press, Cambridge, 271-345.
- McInerney, F.A. and Wing, S.L., 2011. The Paleocene-Eocene Thermal Maximum: A Perturbation of Carbon Cycle, Climate, and Biosphere with Implications for the Future. *Annu Rev Earth Pl Sc*. 39 (1), 489-516.
- Molinos, J.G., Halpern, B.S., Schoeman, D.S., Brown, C.J., Kiessling, W., Moore, P.J., Pandolfi, J.M., Poloczanska, E.S., Richardson, A.J. and Burrows, M.T., 2016. Climate velocity and the future global redistribution of marine biodiversity. *Nature Climate Change*. 6 (1), 83.
- Monechi, S., Reale, V., Bernaola, G. and Balestra, B., 2012. Taxonomic review of early Paleocene fasciculiths. *Micropaleontology*. 58 (4), 351-365.
- Monechi, S., Reale, V., Bernaola, G. and Balestra, B., 2013. The Danian/Selandian boundary at Site 1262 (South Atlantic) and in the Tethyan region: Biomagnetostratigraphy, evolutionary trends in fasciculiths and environmental effects of the Latest Danian Event. *Marine Micropaleontology*. 98 (0), 28-40.

- Moore, E.A. and Kurtz, A.C., 2008. Black carbon in Paleocene-Eocene boundary sediments: A test of biomass combustion as the PETM trigger. *Palaeogeography, Palaeoclimatology, Palaeoecology*. 267 (1-2), 147-152.
- Müller, R.D., Sdrolias, M., Gaina, C., Steinberger, B. and Heine, C., 2008. Long-term sea-level fluctuations driven by ocean basin dynamics. *Science*. 319 (5868), 1357-1362.
- Murray, J., 1897. On the distribution of the pelagic foraminifera at the surface and on the floor of the ocean. *Nat. Sci.* 11 (65), 17-27.
- Neuer, S., Freudenthal, T., Davenport, R., Llinás, O. and Rueda, M.-J., 2002. Seasonality of surface water properties and particle flux along a productivity gradient off NW Africa. *Deep Sea Research Part II: Topical Studies in Oceanography*. 49 (17), 3561-3576.
- Nguyen, T.M.P., Petrizzo, M.R. and Speijer, R.P., 2009. Experimental dissolution of a fossil foraminiferal assemblage (Paleocene/Eocene Thermal Maximum, Dababiya, Egypt): Implications for paleoenvironmental reconstructions. *Marine Micropaleontology*. 73 (3), 241-258.
- Nguyen, T.M.P., Petrizzo, M.R., Stassen, P. and Speijer, R.P., 2011. Dissolution susceptibility of Paleocene–Eocene planktic foraminifera: Implications for palaeoceanographic reconstructions. *Marine Micropaleontology*. 81 (1-2), 1-21.  
10.1016/j.marmicro.2011.07.001.
- Nguyen, T.M.P. and Speijer, R.P., 2014. A new procedure to assess dissolution based on experiments on Pliocene–Quaternary foraminifera (ODP Leg 160, Eratosthenes Seamount, Eastern Mediterranean). *Marine Micropaleontology*. 106 (0), 22-39.
- Norris, R., Turner, S.K., Hull, P. and Ridgwell, A., 2013. Marine ecosystem responses to Cenozoic global change. *Science*. 341 (6145), 492-498.
- Norris, R., Wilson, P., Blum, P., Fehr, A., Agnini, C., Bornemann, A., Boulila, S., Bown, P., Cournede, C. and Friedrich, O., 2014. Expedition 342 Summary. Norris, RD, Wilson, PA, Blum, P., the Expedition. 342.
- Norris, R.D., 1991. Biased Extinction and Evolutionary Trends. *Paleobiology*. 17 (4), 388-399.
- Norris, R.D., 1996. Symbiosis as an evolutionary innovation in the radiation of Paleocene planktic foraminifera. *Paleobiology*. 22 (4), 461-480.
- Norris, R.D. and Wilson, P.A., 1998. Low-latitude sea-surface temperatures for the mid-Cretaceous and the evolution of planktic foraminifera. *Geology*. 26 (9), 823-826.
- Nunes, F. and Norris, R.D., 2006. Abrupt reversal in ocean overturning during the Palaeocene/Eocene warm period. *Nature*. 439 (7072), 60-63.
- Olsson, R.K., Hemleben, C., Berggren, W.A. and Chengjie, L., 1992. Wall texture classification of planktonic foraminifera genera in the Lower Danian. *Journal of Foraminiferal Research*. 22 (3), 195-213.

- Olsson, R.K., Hemleben, C., Berggren, W.A. and Huber, B.T., 1999. Atlas of Paleocene Planktonic Foraminifera. *Smithsonian Contributions to Paleobiology*, 85. Smithsonian Institution Press, Washington, D.C., 252 pp
- Ortiz, J.D., Mix, A.C. and Collier, R.W., 1995. Environmental-Control of Living Symbiotic and Asymbiotic Foraminifera of the California Current. *Paleoceanography*. 10 (6), 987-1009.
- Ortiz, J.D., Mix, A.C., Rugh, W., Watkins, J.M. and Collier, R.W., 1996. Deep-dwelling planktonic foraminifera of the northeastern Pacific Ocean reveal environmental control of oxygen and carbon isotopic disequilibria. *Geochimica Et Cosmochimica Acta*. 60 (22), 4509-4523.
- Pagani, M., Caldeira, K., Archer, D. and Zachos, J.C., 2006. An ancient carbon mystery. *Science*. 314 (5805), 1556.
- Pandolfi, J.M., Connolly, S.R., Marshall, D.J. and Cohen, A.L., 2011. Projecting coral reef futures under global warming and ocean acidification. *Science*. 333 (6041), 418-422.
- Pak, D.K. and Miller, K.G., 1992. Paleocene to Eocene benthic foraminiferal isotopes and assemblages: implications for deepwater circulation. *Paleoceanography*. 7 (4), 405-422.
- Pearson, P.N., 2012. Oxygen isotopes in foraminifera: Overview and Historical Review. *Reconstructing Earth's Deep-Time Climate—The State of the Art* in, 1-38.
- Pearson, P.N., Ditchfield, P.W., Singano, J., Harcourt-Brown, K.G., Nicholas, C.J., Olsson, R.K., Shackleton, N.J. and Hall, M.A., 2001. Warm tropical sea surface temperatures in the Late Cretaceous and Eocene epochs. *Nature*. 413 (6855), 481-7. 10.1038/35097000.
- Pearson, P.N., Evans, S.L. and Evans, J., 2014. Effect of diagenetic recrystallization on the strength of planktonic foraminifer tests under compression. *Journal of Micropalaeontology*. 10.1144/jmpaleo2013-032.
- Pearson, P.N., Olsson, R.K., Huber, B.T., Hemleben, C. and Berggren, W.A., 2006. Atlas of Eocene planktonic foraminifera. *Journal of Foraminiferal Research, Special Publication*. 41, 513.
- Pearson, P.N., Shackleton, N.J. and Hall, M.A., 1993. Stable isotope paleoecology of Middle Eocene planktonic foraminifera and multi-species isotope stratigraphy, DSDP Site 523, South Atlantic. *Journal of Foraminiferal Research*. 23 (2), 123-146.
- Pedersen, A.K., Larsen, L.M., Riisager, P. and Dueholm, K.S., 2002. Rates of volcanic deposition, facies changes and movements in a dynamic basin: the Nuussuaq Basin, West Greenland, around the C27n-C26r transition. *Geological Society, London, Special Publications*. 197 (1), 157-181.
- Pérez-Díaz, L. and Eagles, G., 2017. South Atlantic paleobathymetry since early Cretaceous. *Scientific Reports*. 7 (2), 11819.
- Petrizzo, M.R., 2005. An early late Paleocene event on Shatsky Rise, northwest Pacific Ocean (ODP Leg 198): Evidence from planktonic foraminiferal assemblages. *Proc. Ocean Drill. Program Sci. Res.* 198, 10.2973/odp.proc.sr.198.102.2005.

- Petrizzo, M.R., 2007. The onset of the Paleocene-Eocene Thermal Maximum (PETM) at Sites 1209 and 1210 (Shatsky Rise, Pacific Ocean) as recorded by planktonic foraminifera. *Marine Micropaleontology*. 63 (3-4), 187-200.
- Petrizzo, M.R., Leoni, G., Speijer, R.P., De Bernardi, B. and Felletti, F., 2008. Dissolution Susceptibility of Some Paleogene Planktonic Foraminifera from Odp Site 1209 (Shatsky Rise, Pacific Ocean). *Journal of Foraminiferal Research*. 38 (4), 357-371.
- Petrizzo, M.R., Premoli Silva, I. and Ferrari, P., 2005. Data report: Paleogene Planktonic Foraminifer Biostratigraphy, ODP Leg 198 Holes 1209A, 1210A, and 1211A (Shatsky Rise, Northwest Pacific Ocean). *Proceedings of the Ocean Drilling Program: Scientific Results*. 198.
- Plummer, H., 1926. *Foraminifera of the Midway formation in Texas*. University of Texas at Austin
- Pörtner, H., Karl, D., Boyd, P., Cheung, W., Lluh-Cota, S., Nojiri, Y. and Schmidt, D., 2014. Climate Change 2014: Impacts, Adaptation, and Vulnerability. Part A: Global and Sectoral Aspects. Contribution of Working Group II to the Fifth Assessment Report of the Intergovernmental Panel on Climate Change (eds Field CB et al.), 411-484.
- Premoli-Silva, I. and Bolli, H.M., 1973. Late Cretaceous to Eocene planktonic foraminifera and stratigraphy of the Leg 15 sites in the Caribbean Sea. Edgar, N. T., Saunders, J. B., Bolli, H. M., Boyce, R. E., Broecker, W. S., Donnelly, T. W., Gieskes, J. M., Hay, W. W., Horowitz, R. M., Maurrasse, F., Perez Nieto, H., Prell, W., Premoli Silva, I., Riedel, W. R., Schneidermann, N., Waterman, L. S., Kaneps, A. G., Herring, J. R. Initial reports of the Deep Sea Drilling Project, covering Leg 15 of the cruises of the drilling vessel Glomar Challenger, San Juan, Puerto Rico to Cristobal, Panama; December 1970-February 1971. *Scripps Inst. Oceanogr., Deep Sea Drilling Project, La Jolla, CA, United-States. Initial Reports of the Deep Sea Drilling Project*. 15. 499-547.
- Quillévéré, F., Aubry, M.P., Norris, R.D. and Berggren, W.A., 2002. Paleocene oceanography of the eastern subtropical Indian Ocean - An integrated magnetobiostratigraphic and stable isotope study of ODP Hole 761B (Wombat Plateau). *Palaeogeography, Palaeoclimatology, Palaeoecology*. 184 (3-4), 371-405.
- Quillévéré, F. and Norris, R.D., 2003. Ecological development of acarininids (planktonic foraminifera) and hydrographic evolution of Paleocene surface waters. In: S.L. Wing, P.D. Gingerich, B. Schmitz and E. Thomas (Editors), *Causes and Consequences of Globally Warm Climates in the Early Paleogene*. Geological Society of America Special Paper, 223-238.
- Quillevere, F., Norris, R.D., Kroon, D. and Wilson, P.A., 2008. Transient ocean warming and shifts in carbon reservoirs during the early Danian. *Earth and Planetary Science Letters*. 265 (3-4), 600-615.
- Quillévéré, F., Norris, R.D., Moussa, I. and Berggren, W.A., 2001. Role of photosymbiosis and biogeography in the diversification of early Paleogene acarininids (planktonic foraminifera). *Paleobiology*. 27 (2), 311-326.



- Raffi, I. and De Bernardi, B., 2008. Response of calcareous nannofossils to the Paleocene-Eocene Thermal Maximum: Observations on composition, preservation and calcification in sediments from ODP Site 1263 (Walvis Ridge -- SW Atlantic). *Marine Micropaleontology*. 69 (2), 119-138.
- Rahmstorf, S., 2003. Timing of abrupt climate change: A precise clock. *Geophys Res Lett*. 30 (10). doi:10.1029/2003GL017115.
- Railsback, L.B., Anderson, T.F., Ackerly, S.C. and Cisne, J.L., 1989. Paleoceanographic modeling of temperature-salinity profiles from stable isotopic data. *Paleoceanography*. 4 (5), 585-591.
- Randall, D.A., Wood, R.A., Bony, S., Colman, R., Fichefet, T., Fyfe, J., Kattsov, V., Pitman, A., Shukla, J. and Srinivasan, J., 2007. Climate models and their evaluation, *Climate change 2007: The physical science basis. Contribution of Working Group I to the Fourth Assessment Report of the IPCC (FAR)*. Cambridge University Press, 589-662.
- Rebotim, A., Voelker, A.H., Jonkers, L., Waniek, J.J., Meggers, H., Schiebel, R., Fraile, I., Schulz, M. and Kucera, M., 2017. Factors controlling the depth habitat of planktonic foraminifera in the subtropical eastern North Atlantic. *Biogeosciences* 14 (4), 827-859.
- Ridgwell, A. and Schmidt, D.N., 2010. Past constraints on the vulnerability of marine calcifiers to massive carbon dioxide release. *Nature Geoscience*. 3 (3), 196-200.
- Röhl, U., Westerhold, T., Bralower, T.J. and Zachos, J.C., 2007. On the duration of the Paleocene-Eocene thermal maximum (PETM). *Geochemistry, Geophysics, Geosystems*. 8 (12). 10.1029/2007GC001784.
- Röhl, U., Westerhold, T., Monechi, S., Thomas, E., Zachos, J.C. and Donner, B., 2005. The third and final early Eocene thermal maximum: Characteristics, timing, and mechanisms of the "X" event. *Geol. Soc. Am. Abstr. Programs*. 37 (7), 264.
- Rohling, E.J. and Cooke, S., 2003. Stable oxygen and carbon isotopes in foraminiferal carbonate shells, *Modern Foraminifera*. Springer Netherlands, Dordrecht, 239-258.
- Rohling, E.J. and Gieskes, W.W.C., 1989. Late Quaternary Changes in Mediterranean Intermediate Water Density and Formation Rate. *Paleoceanography*. 4 (5), 531-545.
- Rohling, E.J., Hopmans, E.C. and Damste, J.S.S., 2006. Water column dynamics during the last interglacial anoxic event in the Mediterranean (sapropel S5). *Paleoceanography*. 21 (2). 10.1029/2005pa001237.
- Rosenzweig, C., Elliott, J., Deryng, D., Ruane, A.C., Müller, C., Arneth, A., Boote, K.J., Folberth, C., Glotter, M., Khabarov, N., Neumann, K., Piontek, F., Pugh, T.A.M., Schmid, E., Stehfest, E., Yang, H. and Jones, J.W., 2014. Assessing agricultural risks of climate change in the 21st century in a global gridded crop model intercomparison. *Proceedings of the National Academy of Sciences*. 111 (9), 3268-3273.

- Rutherford, S., D'Hondt, S. and Prell, W., 1999. Environmental controls on the geographic distribution of zooplankton diversity. *Nature*. 400 (6746), 749-753.
- Sager, W.W., 2005. What built Shatsky Rise, a mantle plume or ridge tectonics? *Geological Society of America Special Papers*. 388, 721-733.
- Said, R., 1990. *The Geology of Egypt*. Balkema, Rotterdam, The Netherlands, 734 pp
- Saltzman, M.R. and Thomas, E., 2012. Carbon isotope stratigraphy, *The geologic time scale*. Elsevier, 207-232.
- Schiebel, R. and Hemleben, C., 2005. Modern planktic foraminifera. *Paläontologische Zeitschrift*. 79 (1), 135-148.
- Schmidt, D.N., Thierstein, H.R., Bollmann, J.r. and Schiebel, R., 2004. Abiotic forcing of plankton evolution in the Cenozoic. *Science*. 303 (5655), 207-210.
- Schmitz, B., Asaro, F., Molina, E., Monechi, S., vonSalis, K. and Speijer, R.P., 1997. High-resolution iridium,  $\delta^{13}C$ ,  $\delta^{18}O$ , foraminifera and nannofossil profiles across the latest Paleocene benthic extinction event at Zumaya, Spain. *Palaeogeography, Palaeoclimatology, Palaeoecology*. 133 (1-2), 49-68.
- Schmitz, B., Peucker-Ehrenbrink, B., Heilmann-Clausen, C., Å...berg, G., Asaro, F. and Lee, C.T.A., 2004. Basaltic explosive volcanism, but no comet impact, at the Paleocene-Eocene boundary: High-resolution chemical and isotopic records from Egypt, Spain and Denmark. *Earth and Planetary Science Letters*. 225 (1-2), 1-17.
- Schmitz, B., Pujalte, V., Molina, E., Monechi, S., Orue-Etxebarria, X., Speijer, R.P., Alegret, L., Apellaniz, E., Arenillas, I., Aubry, M.P., Baceta, J.I., Berggren, W.A., Bernaola, G., Caballero, F., Clemmensen, A., Dinares-Turell, J., Dupuis, C., Heilmann-Clausen, C., Hilario Orus, A., Knox, R., Martin-Rubio, M., Ortiz, S., Payros, A., Petrizzo, M.R., von Salis, K., Sprong, J., Steurbaut, E. and Thomsen, E., 2011. The Global Stratotype Sections and Points for the bases of the Selandian (Middle Paleocene) and Thanetian (Upper Paleocene) stages at Zumaia, Spain. *Episodes*. 34 (4), 220-243.
- Schmitz, B., Pujalte, V. and Nunez-Betelu, K., 2001. Climate and sea-level perturbations during the initial eocene thermal maximum: evidence from siliciclastic units in the Basque Basin (Ermua, Zumaia and Trabakua Pass), northern Spain. *Palaeogeogr. Palaeoclimatol. Palaeoecol.* 165 (3-4), 299-320.
- Schmuker, B., 2000. Recent planktic foraminifera in the Caribbean Sea: distribution, ecology and taphonomy, ETH Zurich
- Schmuker, B., 2000. The influence of shelf vicinity on the distribution of planktic foraminifera south of Puerto Rico. *Marine Geology*. 166 (1-4), 125-143.

- Schneider, L.J., Bralower, T.J., Kump, L.R. and Patzkowsky, M.E., 2013. Calcareous nanoplankton ecology and community change across the Paleocene-Eocene Thermal Maximum. *Paleobiology*. 39 (4), 628-647.
- Schott, W., 1935. Die Sedimente des äquatorialen Atlantischen Ozeans; I. Lieferung, B, Die Foraminiferen in dem äquatorialen Teil des Atlantischen Ozeans. *Deutsch. Atlantische Exped. "Meteor" (1925-7)*. Bd. 3, T. 3, p. 43-134, 40 figs. (sk. maps), 1935.
- Schrag, D.P., Depaolo, D.J. and Richter, F.M., 1995. Reconstructing Past Sea-Surface Temperatures - Correcting for Diagenesis of Bulk Marine Carbonate. *Geochimica Et Cosmochimica Acta*. 59 (11), 2265-2278.
- Schulte, P., Alegret, L., Arenillas, I., Arz, J.A., Barton, P.J., Bown, P.R., Bralower, T.J., Christeson, G.L., Claeys, P., Cockell, C.S., Collins, G.S., Deutsch, A., Goldin, T.J., Goto, K., Grajales-Nishimura, J.M., Grieve, R.A.F., Gulick, S.P.S., Johnson, K.R., Kiessling, W., Koeberl, C., Kring, D.A., MacLeod, K.G., Matsui, T., Melosh, J., Montanari, A., Morgan, J.V., Neal, C.R., Nichols, D.J., Norris, R.D., Pierazzo, E., Ravizza, G., Rebolledo-Vieyra, M., Reimold, W.U., Robin, E., Salge, T., Speijer, R.P., Sweet, A.R., Urrutia-Fucugauchi, J., Vajda, V., Whalen, M.T. and Willumsen, P.S., 2010. The Chicxulub Asteroid Impact and Mass Extinction at the Cretaceous-Paleogene Boundary. *Science*. 327 (5970), 1214-1218.
- Schulte, P., Schwark, L., Stassen, P., Kouwenhoven, T.J., Bornemann, A. and Speijer, R.P., 2013. Black shale formation during the Latest Danian Event and the Paleocene?Eocene Thermal Maximum in central Egypt: Two of a kind? *Palaeogeography, Palaeoclimatology, Palaeoecology*. 371, 9-25.
- Sen Gupta, B.K., 2002. *Modern Foraminifera*. Kluwer, Dordrecht, 371.
- Sexton, P.F., Norris, R.D., Wilson, P.A., Pälike, H., Westerhold, T., Röhl, U., Bolton, C.T. and Gibbs, S., 2011. Eocene global warming events driven by ventilation of oceanic dissolved organic carbon. *Nature*. 471 (7338), 349-353.
- Sexton, P.F., Wilson, P.A. and Pearson, P.N., 2006. Microstructural and geochemical perspectives on planktic foraminiferal preservation: "Glassy" versus "Frosty". *Geochemistry Geophysics Geosystems*. 7, 10.1029/2006GC001291.
- Shackleton, N., 1967. Oxygen isotope analyses and Pleistocene temperatures re-assessed. *Nature*. 215 (5096), 15-16.
- Shackleton, N., Corfield, R. and Hall, M., 1985. Stable isotope data and the ontogeny of Paleocene planktonic foraminifera. *The Journal of Foraminiferal Research*. 15 (4), 321-336.
- Shackleton, N.J., 1984. Oxygen isotope evidence for Cenozoic climatic change. *Brenchley, P. J. Fossils and climate*. Univ. Liverpool, Dep. Geol., Liverpool, United-Kingdom, 27-34.
- Shackleton, N.J. and Kennett, J.P., 1975. Paleotemperature history of the Cenozoic and the initiation of Antarctic glaciation; oxygen and carbon isotope analyses in DSDP sites 277, 279, and 281. *Deep Sea Drill. Proj.*, 743-755.

- Shannon, C.E. and Weaver, W., 1949. The mathematical theory of communication. University of Illinois Press, 19, 1-132 pp
- Sheehan, P.M., Coorough, P.J. and Fastovsky, D.E., 1996. Biotic selectivity during the K/ T and Late Ordovician extinction events. Special Paper - Geological Society of America. 307, 477-489.
- Silva, I.P. and Sliter, W.V., 1999. Cretaceous paleoceanography: evidence from planktonic foraminiferal evolution. Special Papers-Geological Society of America, 301-328.
- Sinton, C.W. and Duncan, R.A., 1998. <sup>40</sup>Ar-<sup>39</sup>Ar ages of lavas from the southeast Greenland Margin, ODP Leg 152 and the Rockall Plateau, DSDP Leg 81. Proceedings of the Ocean Drilling Program: Scientific Results. 152, 387-402.
- Sluijs, A., Bowen, G.J., Brinkhuis, H., Lourens, L.J. and Thomas, E., 2007. The Palaeocene-Eocene Thermal Maximum super greenhouse: Biotic and geochemical signatures, age models and mechanisms of global change. In: M. Williams, A.M. Haywood, F.J. Gregory and D.N. Schmidt (Editors), Deep-time perspectives on climate change - Marrying the signal from computer models and biological proxies. The Micropaleontological Society, Special Publication. Geological Society, London, 323-349.
- Sluijs, A., Brinkhuis, H., Schouten, S., Bohaty, S.M., John, C.M., Zachos, J.C., Reichart, G.J., Sinninghe Damste, J.S., Crouch, E.M. and Dickens, G.R., 2007. Environmental precursors to rapid light carbon injection at the Palaeocene/Eocene boundary. *Nature*. 450 (7173), 1218-21.
- Sluijs, A., Schouten, S., Pagani, M., Woltering, M., Brinkhuis, H., Damste, J.S.S., Dickens, G.R., Huber, M., Reichart, G.J., Stein, R., Matthiessen, J., Lourens, L.J., Pedentchouk, N., Backman, J., Moran, K. and Scientists, E., 2006. Subtropical arctic ocean temperatures during the Palaeocene/Eocene thermal maximum. *Nature*. 441 (7093), 610-613.
- Soldan, D.M. and Petrizzo, M.R., 2013. A new planktonic foraminifera species (*Igorina isabellae* n. sp.) from the late Paleocene of the Pacific Ocean. *Bollettino Della Societa Paleontologica Italiana*. 52 (2), 141-143.
- Soldan, D.M., Petrizzo, M.R., Silva, I.P. and Cau, A., 2011. Phylogenetic Relationships and Evolutionary History of the Paleogene Genus *Igorina* through Parsimony Analysis. *Journal of Foraminiferal Research*. 41 (3), 260-284.
- Soliman, M.F. and Obaidalla, N.A., 2010. Danian-Selandian transition at Gabal el-Qreiya section, Nile Valley (Egypt): lithostratigraphy, biostratigraphy, mineralogy and geochemistry. *Neues Jahrbuch für Geologie und Paläontologie - Abhandlungen* 258 (1), 1-30.
- Speijer, R.P., 2003. Danian-Selandian sea-level change and biotic excursion on the southern Tethyan margin (Egypt). In: S.L. Wing, P.D. Gingerich, B. Schmitz and E. Thomas (Editors), Causes and consequences of globally warm climates in the Early Paleogene. Geological Society of America Special Paper, 275-290.

- Speijer, R.P., Scheibner, C., Stassen, P. and Morsi, A.M.M., 2012. Response of Marine Ecosystems to Deep-Time Global Warming: A Synthesis of Biotic Patterns across the Paleocene-Eocene Thermal Maximum (PETM). *Austrian Journal of Earth Sciences*. 105 (1), 6-16.
- Speijer, R.P., Schmitz, B., Aubry, M.P. and Charisi, S.D., 1995. The latest Paleocene benthic extinction event: punctuated turnover in outer neritic foraminiferal faunas from Gebel Aweina, Egypt. *Israel Journal of Earth Sciences*. 44 (4), 207-222.
- Spero, H. and DeNiro, M., 1987. The influence of symbiont photosynthesis on the  $\delta^{18}\text{O}$  and  $\delta^{13}\text{C}$  values of planktonic foraminiferal shell calcite. *Symbiosis*. 4 (1-3), 213-228.
- Spero, H.J., Bijma, J., Lea, D.W. and Bemis, B.E., 1997. Effect of seawater carbonate concentration on foraminiferal carbon and oxygen isotopes. *Nature*. 390 (6659), 497-500.
- Spero, H.J. and Lea, D.W., 1993. Intraspecific Stable-Isotope Variability in the Planktic Foraminifera *Globigerinoides-Sacculifer* - Results from Laboratory Experiments. *Marine Micropaleontology*. 22 (3), 221-234.
- Spero, H.J., Lerche, I. and Williams, D.F., 1991. Opening the carbon isotope 'vital effect' black box, 2, quantitative model for interpreting foraminiferal carbon isotope data. *Paleoceanography*. 6 (6), 639-655.
- Sprong, J., Kouwenhoven, T.J., Bornemann, A., Dupuis, C., Speijer, R.P., Stassen, P. and Steurbaut, E., 2013. In search of the Latest Danian Event in a paleobathymetric transect off Kasserine Island, north-central Tunisia. *Palaeogeography, Palaeoclimatology, Palaeoecology*. 379, 1-16.
- Sprong, J., Kouwenhoven, T.J., Bornemann, A., Schulte, P., Stassen, P., Steurbaut, E., Youssef, M. and Speijer, R.P., 2012. Characterization of the Latest Danian Event by means of benthic foraminiferal assemblages along a depth transect at the southern Tethyan margin (Nile Basin, Egypt). *Marine Micropaleontology*. 86-87, 15-31.
- Sprong, J., Speijer, R.P. and Steurbaut, E., 2009. Biostratigraphy of the Danian/Selandian transition in the southern Tethys. Special reference to the Lowest Occurrence of planktic foraminifera *Igorina albeari*. *Geologica Acta*. 7 (1-2), 63-77.
- Sprong, J., Youssef, M.A., Bornemann, A., Schulte, P., Steurbaut, E., Stassen, P., Kouwenhoven, T.J. and Speijer, R.P., 2011. A multi-proxy record of the Latest Danian Event at Gebel Qreiya, Eastern Desert, Egypt. *Journal of Micropalaeontology*. 30 (2), 167-182.
- Stainforth, R.M., Lamb, J.L., Luterbacher, H., Beard, J.H. and Jeffords, R.M., 1975. Cenozoic planktonic foraminiferal zonation and characteristics of index forms. *Kansas University Paleontological Contributions*. 62, 425 pp.
- Stap, L., Lourens, L., van Dijk, A., Schouten, S. and Thomas, E., 2010. Coherent pattern and timing of the carbon isotope excursion and warming during Eocene Thermal Maximum 2 as recorded in planktic and benthic foraminifera. *Geochemistry Geophysics Geosystems*. 11. 10.1029/2010GC003097.

- Stap, L., Sluijs, A., Thomas, E. and Lourens, L., 2009. Patterns and magnitude of deep sea carbonate dissolution during Eocene Thermal Maximum 2 and H2, Walvis Ridge, southeastern Atlantic Ocean. *Paleoceanography*. 24. 10.1029/2008PA001655.
- Stassen, P., Dupuis, C., Steurbaut, E., Yans, J. and Speijer, R.P., 2012. Perturbation of a Tethyan coastal environment during the Paleocene-Eocene thermal maximum in Tunisia (Sidi Nasseur and Wadi Mezaz). *Palaeogeography, Palaeoclimatology, Palaeoecology*. 317, 66-92.
- Steffen, W., Rockström, J., Richardson, K., Lenton, T.M., Folke, C., Liverman, D., Summerhayes, C.P., Barnosky, A.D., Cornell, S.E., Crucifix, M., Donges, J.F., Fetzer, I., Lade, S.J., Scheffer, M., Winkelmann, R. and Schellnhuber, H.J., 2018. Trajectories of the Earth System in the Anthropocene. *Proceedings of the National Academy of Sciences*. 115 (33), 8252-8259. 10.1073/pnas.1810141115.
- Storme, J.-Y., Steurbaut, E., Devleeschouwer, X., Dupuis, C., Iacumin, P., Rochez, G. and Yans, J., 2014. Integrated bio-chemostratigraphical correlations and climatic evolution across the Danian-Selandian boundary at low latitudes. *Palaeogeography, Palaeoclimatology, Palaeoecology*. 414, 212-224.
- Steurbaut, E. and Sztrakos, K., 2008. Danian/Selandian boundary criteria and North Sea Basin-Tethys correlations based on calcareous nannofossil and foraminiferal trends in SW France. *Marine Micropaleontology*. 67 (1-2), 1-29.
- Thomas, D.J. and Bralower, T.J., 2005. Sedimentary trace element constraints on the role of North Atlantic Igneous Province volcanism in late Paleocene-early Eocene environmental change. *Marine Geology*. 217 (3-4), 233-254.
- Thomas, D.J., Bralower, T.J. and Zachos, J.C., 1999. New evidence for subtropical warming during the late Paleocene thermal maximum: Stable isotopes from Deep Sea Drilling Project Site 527, Walvis Ridge. *Paleoceanography*. 14 (5), 561-570.
- Thomas, E., 2003. Extinction and food at the sea floor: A high-resolution benthic foraminiferal record across the Initial Eocene Thermal Maximum, Southern Ocean Site 690. In: S.L. Wing, P.D. Gingerich, B. Schmitz and E. Thomas (Editors), *Causes and consequences of globally warm climates in the Early Paleogene*. Geological Society of America Special Paper, 319-332.
- Thomas, E. and Shackleton, N.J., 1996. The Paleocene-Eocene benthic foraminiferal extinction and stable isotope anomalies, Geological Society Special Publication, 401-441.
- Torsvik, T.H., Van der Voo, R., Preeden, U., Mac Niocaill, C., Steinberger, B., Doubrovine, P.V., van Hinsbergen, D.J.J., Domeier, M., Gaina, C., Tohver, E., Meert, J.G., McCausland, P.J.A. and Cocks, L.R.M., 2012. Phanerozoic polar wander, palaeogeography and dynamics. *Earth-Science Reviews*. 114 (3), 325-368.
- Toumarkine, M. and Luterbacher, H., 1985. Paleocene and Eocene planktic foraminifera. *Plankton stratigraphy*. 1, 87-154.

- Tripati, A. and Elderfield, H., 2005. Deep-sea temperature and circulation changes at the Paleocene-Eocene thermal maximum. *Science*. 308 (5730), 1894-1898.
- Tucholke, B. and Vogt, P., 1979. Western North Atlantic: Sedimentary evolution and aspects of tectonic history. Initial Rep. Deep Sea Drilling Project. 43, 791-825.
- Turner, A.G. and Annamalai, H., 2012. Climate change and the South Asian summer monsoon. *Nature Climate Change*. 2 (8), 587.
- Van Bael, R., Deprez, A., Stassen, P., Bornemann, A. and Speijer, R.P., 2015. Taphonomic impact of ultrasonic treatment on foraminifera from a deep-sea carbonate ooze. *Journal of Micropalaeontology*. 10.1144/jmpaleo2015-046.
- van Hinsbergen, D.J.J., de Groot, L.V., van Schaik, S.J., Spakman, W., Bijl, P.K., Sluijs, A., Langereis, C.G. and Brinkhuis, H., 2015. A Paleolatitude Calculator for Paleoclimate Studies. *PLoS ONE*. 10 (6), e0126946.
- Vandenbergh, N., Hilgen, F. and Speijer, R., 2012. The Paleogene Period. *The Geologic Time Scale 2012 2-Volume Set*. 2, 855.
- Varol, O., 1989. Palaeocene calcareous nannofossil biostratigraphy. In: J.A. Crux and S.E. Van Heck (Editors), *Nannofossils and their Applications*. Ellis Horwood, 267-310.
- Vaughan, A.P., 2007. Climate and geology- a Phanerozoic perspective. Deep-time perspectives on climate change: marrying the signal from computer models and biological proxies. *The Micropalaeontological Society, Special Publications*. The Geological Society, London, 5-60.
- Vincent, E. and Berger, W.H., 1981. Planktonic foraminifera and their use in paleoceanography. Emiliani, Cesare. *The oceanic lithosphere*. Univ. Miami, Dep. Geol., Miami, FL, United-States. 7, 1025-1119.
- Voigt, J., Hathorne, E.C., Frank, M. and Holbourn, A., 2016. Minimal influence of recrystallization on middle Miocene benthic foraminiferal stable isotope stratigraphy in the eastern equatorial Pacific. *Paleoceanography*. 31 (1), 98-114.
- Wade, B.S., Pearson, P.N., Berggren, W.A. and Palike, H., 2011. Review and revision of Cenozoic tropical planktonic foraminiferal biostratigraphy and calibration to the geomagnetic polarity and astronomical time scale. *Earth-Science Reviews*. 104 (1-3), 111-142.
- Wefer, G. and Berger, W.H., 1991. Isotope paleontology - growth and composition of extant calcareous species. *Marine Geology*. 100 (1-4), 207-248.
- Westerhold, T. and Röhl, U., 2005. Data report: Revised composite depth records for Shatsky Rise Sites 1209, 1210, and 1211. *Proceedings of the Ocean Drilling Program: Scientific Results*. 198.
- Westerhold, T., Röhl, U., Donner, B., McCarren, H.K. and Zachos, J.C., 2011. A complete high-resolution Paleocene benthic stable isotope record for the central Pacific (ODP Site 1209). *Paleoceanography*. 26. 10.1029/2010pa002092.

- Westerhold, T., Röhl, U., Raffi, I., Fornaciari, E., Monechi, S., Reale, V., Bowles, J. and Evans, H.F., 2008. Astronomical calibration of the Paleocene time. *Palaeogeogr. Palaeoclimatol. Palaeoecol.* 257 (4), 377-403.
- Williams, M., Haywood, A., Gregory, F.J. and Schmidt, D.N., 2007. Deep-time perspectives on climate change: an introduction. In: M. Williams, A. Haywood, F.J. Gregory and D.N. Schmidt (Editors), *Deep-Time Perspectives on Climate Change: Marrying the Signal from Computer Models and Biological Proxies*. The Micropaleontological Society, Special Publications. The Geological Society, London, 1-3.
- Yamaguchi, T., Bornemann, A., Matsui, H. and Nishi, H., 2017. Latest Cretaceous/Paleocene deep-sea ostracode fauna at IODP Site U1407 (western North Atlantic) with special reference to the Cretaceous/Paleogene boundary and the Latest Danian Event. *Marine Micropaleontology*. 135, 32-44.
- Yamaguchi, T. and Norris, R.D., 2015. No place to retreat: Heavy extinction and delayed recovery on a Pacific guyot during the Paleocene/Eocene Thermal Maximum. *Geology*. 43 (5), 443-446.
- Zachos, J.C., Dickens, G.R. and Zeebe, R.E., 2008. An early Cenozoic perspective on greenhouse warming and carbon-cycle dynamics. *Nature*. 451 (7176), 279-83.
- Zachos, J.C., Kroon, D., Blum, P., Bowles, J., Gaillot, P., Hasegawa, T., Hathorne, E.C., Hodell, D.A., Kelly, D.C., Jung, J.H., Keller, S.M., Lee, Y.S., Leuschner, D.C., Liu, Z., Lohmann, K.C., Lourens, L., Monechi, S., Nicolo, M., Raffi, I., Riesselman, C., Röhl, U., Schellenberg, S.A., Schmidt, D., Sluijs, A., Thomas, D. and Vallius, H., 2004. Leg 208 Summary. *Proceedings of the Ocean Drilling Program Initial Reports*. 208, 1-112.
- Zachos, J.C., McCarren, H., Murphy, B., Röhl, U. and Westerhold, T., 2010. Tempo and scale of late Paleocene and early Eocene carbon isotope cycles: Implications for the origin of hyperthermals. *Earth and Planetary Science Letters*. 299 (1-2), 242-249.
- Zachos, J.C., Röhl, U., Schellenberg, S.A., Sluijs, A., Hodell, D.A., Kelly, D.C., Thomas, E., Nicolo, M., Raffi, I., Lourens, L.J., McCarren, H. and Kroon, D., 2005. Rapid acidification of the ocean during the Paleocene-Eocene thermal maximum. *Science*. 308 (5728), 1611-5. [10.1126/science.1109004](https://doi.org/10.1126/science.1109004).
- Zachos, J.C., Stott, L.D. and Lohmann, K.C., 1994. Evolution of early Cenozoic marine temperatures. *Paleoceanography*. 9 (2), 353-387.
- Zachos, J.C., Arthur, M.A., Bralower, T.J. and Spero, H.J., 2002. Palaeoclimatology - Tropical temperatures in greenhouse episodes. *Nature*. 419 (6910), 897-898.
- Zeebe, R.E., Zachos, J.C. and Dickens, G.R., 2009. Carbon dioxide forcing alone insufficient to explain Palaeocene-Eocene Thermal Maximum warming. *Nature Geoscience*. 2 (8), 576-580.



# Appendix 1: Taxonomic notes

Planktic foraminifera species identification is based on Berggren and Norris (1997) and Olsson et al. (1999).

## ***Acarinina nitida***

Found at: Shatsky Rise ODP Site 1210

Citation: *Acarinina nitida* (Martin 1943)

Basionym: *Globigerina nitida*

Synonyms:

*Globigerina nitida* Martin, 1943: 115, pl. 7: fig. 1a-c

*Acarinina acarinata* Subbotina, 1953: 229, pl. 22: figs. 4, 5, 8, 10

— Shutsckaya, 1970b: 118, 228, pl. 27: fig. 13a-c

— Krasheninnikov and Hoskins, 1973: 116, pl. 1: figs. 1-3

*Globigerina stonei* Weiss, 1955: 18, pl. 5: figs. 16-18

*Globorotalia whitei* Weiss.—Bolli, 1957a: 79, pl. 19: figs. 10-12

*Globigerina* cf. *G. soldadoensis* Bronnimann.—Loeblich and Tappan, 1957a: 182, pl. 53: fig. 4a-c

*Globorotalia (Acarinina) acarinata acarinata* (Subbotina).— Blow 1979: 904, fig. 7

## ***Acarinina strabocella***

Found at: Egypt, Qreiya 3; South Eastern Newfoundland Ridge IODP Site U1407; Shatsky Rise ODP Site 1210; Walvis Ridge Site 1262

Citation: *Acarinina strabocella* (Loeblich and Tappan 1957)

Basionym: *Globorotalia strabocella*

Synonyms:

*Globorotalia angulata* (White) var. *praepentacamerata* Shutsckaya, 1956: 94, 95, pl. 3: fig. 3 *Globorotalia strabocella*.—Loeblich and Tappan, 1957a: 195, pl. 61: fig. 6a-c

*Globorotalia praepentacamerata* Shutsckaya.—Luterbacher, 1964: 665, pl. 40: fig. 45

*Acarinina praepentacamerata* (Shutsckaya).

—Shutsckaya, 1970b: 118-120, pl. 21: figs. 8, 10; pl. 22: fig. 2

—Stott and Kennett, 1990: 558, pl. 4: figs. 9, 10

—Huber, 1991b: 439, pl. 2: figs. 1, 2

*Globorotalia (Acarinina) strabocella* Loeblich and Tappan.—Jenkins, 1971: 84, pl. 4: figs. 102-104

*Acarinina praeangulata* (Blow).—Huber, 1991a: 439, pl. 1, figs. 6, 7

## ***Acarinina subsphaerica***

Found at: Shatsky Rise ODP Site 1210

Citation: *Acarinina subsphaerica* (Subbotina 1947)

Basionym: *Globigerina subsphaerica*

Synonyms:

*Globigerina subsphaerica* Subbotina, 1947: 108, pl. 5: figs. 23-28

1953: 59, pl. 2: fig. 15a-c

—Shutsckaya, 1956: 91, pl. 3: fig. 1

*Globoconusa quadripartitaformis* Khalilov, 1956: 249, pl. 5: fig. 3a-c

*Globigerina chascanona* Loeblich and Tappan, 1957a: 180, pl. 49: fig. 5a-c

*Globigerina spiralis* Bolli.—Loeblich and Tappan, 1957a: 182, pl. 47: fig. 3a-c, pl. 49: fig. 3a-c, pl. 51: figs. 6a-9c, pl. 53: fig. 3a-c

*Acarinina subsphaerica* (Subbotina)

—Shutsckaya, 1958: 89, pl. 2: figs. 12-14, pl. 3: figs. 1-3

1960: 249, pl. 2: fig. 8

1970b: 118-120, pl. 2: fig. 8a-c, pl. 6: fig. 3a-c, pl. 26: fig. 3a-c

*Acarinina falsospiralis* Davidzon and Morozova, 1964: 26, 28, pl. 1: fig. 5a-c

*Acarinina microsphaerica* Morozova in Morozova, Kozhevnikova, and Kuryleva, 1967: 195, pl. 6: figs. 3, 4

*Globorotalia (Acarinina) subsphaerica* (Subbotina).—Blow, 1979: 960, pl. 91: figs. 4-6, pl. 92: figs. 1-3

*Muricoglobigerina chascanona* (Loeblich and Tappan).—Blow, 1979: 1126, pl. 91: figs. 1, 2, pl. 92: fig. 3,

pl. 93: figs. 7-9, pl. 235: figs. 1-3, pl. 101: figs. 5, 6  
*Acarinina chascanona* (Loeblich and Tappan).—Huber, 1991b: 439, pl. 2: fig. 3

### ***Chiloguembelina crinita***

Found at: South Eastern Newfoundland Ridge IODP Site U1407

Citation: *Chiloguembelina crinita* (Glaessner 1937)

Basionym: *Guembelina crinite*

Synonyms:

*Chiloguembelina crinita* (Glaessner)

—Beckmann, 1957: 89, pl. 21: fig. 4

—Loeblich and Tappan, 1957: 178, pl. 49: fig. 1: pl. 51: figs. 1a-3, pl. 56: figs. 1a-b, pl. 60: fig. 6, pl. 62: fig. 1

—Olsson and others, 1999: 90, pl. 69: figs. 1-8

?*Chiloguembelina midwayensis subcylindrica* Beckmann, 1957: 92, pl. 21: figs. 2, 3

*Guembelina crinita* Glaessner, 1937: 383, pl. 4: fig. 34a, b

### ***Chiloguembelina midwayensis***

Found at: Egypt, Qreiya 3; South Eastern Newfoundland Ridge IODP Site U1407; Walvis Ridge Site 1262

Citation: *Chiloguembelina midwayensis* (Cushman 1940)

Basionym: *Guembelina midwayensis*

Synonyms:

*Guembelina midwayensis* Cushman, 1940: 65, pl. 11: fig. 15

—Cushman and Todd, 1946: 58, pl. 10: fig. 15

—Cushman, 1951: 37, pl. 11: figs. 7, 8

*Chiloguembelina midwayensis* (Cushman).

—Loeblich and Tappan, 1957a: 179, pl. 41: fig. 3, pl. 43: fig. 7a, b, pl. 45: fig. 9a, b

—D'Hondt, 1991:173, pl. 2: fig. 13, fig. 14

*Chiloguembelina midwayensis midwayensis* (Cushman).—Beckmann, 1957: 90, pl. 21: fig. 1a, b

*Chiloguembelina midwayensis strombiformis* Beckmann, 1957: 90, pl. 21: fig. 6a-c

### ***Chiloguembelina subtriangularis***

Found at: Shatsky Rise ODP Site 1210

Citation: *Chiloguembelina subtriangularis* Beckmann 1957

Basionym: *Chiloguembelina subtriangularis*

Synonyms:

*Chiloguembelina subtriangularis* Beckmann, 1957: 91, pl. 21: fig. 5a,b

—Said and Kerdany, 1961: 331, pl. 2: fig. 6

### ***Eoglobigerina spiralis***

Found at: South Eastern Newfoundland Ridge IODP Site U1407; Shatsky Rise ODP Site 1210; Walvis Ridge Site 1262

Citation: *Eoglobigerina spiralis* (Bolli 1957)

Basionym: *Globigerina spiralis*

Synonyms:

*Globigerina spiralis* Bolli, 1957a: 70, pl. 16: figs. 16-18.

—Bolli and Cita, 1960: 12, pl. 32: fig. 2a-c

—Hillebrandt, 1962: 130, pl. 11: figs. 14, 15

*Eoglobigerina spiralis* (Bolli).—Blow, 1979: 1222, pl. 79: figs. 5-9

*Igorina spiralis* (Bolli).—Huber, 1991c: 461, pl. 3: figs. 13-15

### ***Globanomalina chapmani***

Found at: Egypt, Qreiya 3; South Eastern Newfoundland Ridge IODP Site U1407; Shatsky Rise ODP Site 1210, Walvis Ridge Site 1262

Citation: *Globanomalina chapmani* (Parr 1938)

Basionym: *Globorotalia chapmani*

Synonyms:

- Globorotalia chapmani* Parr, 1938: 87, holotype: pl. 3: fig. 9a,b; topotype: pl. 3: fig. 8  
—McGowran, 1964:85, text-figs. 1-9  
—Berggren, Olsson, and Reyment, 1967: 277, text-figs. 1, 3: la-c, 4: l a - c , pl. 1: figs. 1-6  
—Pujol, 1983:657, pl. 3: fig. 3  
—Haig, Griffin, and Ujetz, 1993:275, pl. 1: figs. 1-6, pl. 2: figs. 1-23  
*Anomalina luxorensis* Nakkady, 1951: 691, pl. 90: figs. 39-41  
*Globorotalia membranacea* (Ehrenberg).—Subbotina, 1953: 205, pl. 16: fig. 12a-c  
*Globanomalina ovalis* var. *lakiensis* Haque, 1956: 149, pl. 14: fig. 2a-c  
*Globorotalia elongata* Glaessner.—Bolli, 1957a: 77, pl. 20: figs. 11-13  
*Globorotalia troelsenii* Loeblich and Tappan, 1957a: 196, pl. 60: fig. 4a-c, pl. 63: fig. 5a-c  
*Globorotalia (Globorotalia) ehrenbergi* Bolli.—Hillebrandt, 1962: 126, pl. 12: fig. 3a-c  
*Planorotalites chapmani* (Parr)  
—Nederbragt and Van Hinte, 1987: 586, pl. 2: figs. 3-10, pl. 3: figs. 4-6  
—Huber. 1991b: 440, pl. 6: figs. 19, 20

***Globanomalina compressa***

Found at: Egypt, Qreiya 3; South Eastern Newfoundland Ridge IODP Site U1407; Shatsky Rise ODP Site 1210; Walvis Ridge Site 1262

Citation: *Globanomalina compressa* (Plummer 1927)

Basionym: *Globigerina compressa*

Synonyms:

- Globigerina compressa* Plummer, 1927: 135, pl. 8: fig. 1 la-c  
*Globigerina compressa* var. *compressa* Plummer. —Subbotina, 1953: 63, pl. 2: figs. 2a-6c  
*Globorotalia compressa* (Plummer)  
—Bolli, 1957a:77, pl. 20: figs. 21-23 [lower Paleocene, Lizard Springs Fm., Trinidad]  
—Bolli and Cita, 1960:20, pl. 32: fig. 3a-c  
—Pujol, 1983: 656, pl. 2: figs. 3, 4  
*Globorotalia (Globorotalia) compressa* (Plummer).—Hillebrandt, 1962: 125, pl. 12: fig. la-c  
*Globorotalia (Turborotalia) compressa compressa* (Plummer).—Blow, 1979: 1062, pl. 75: figs. 10, 11, pl. 78: figs. 5-10, pl. 248: figs. 1-3 [topotype illustrations], pl. 254: figs. 1-3, pl. 257: figs. 5-7 *Planorotalites compressus* (Plummer).—Huber, 1991c:461, pl. 3: figs. 1, 2  
*Globanomalina compressa* (Plummer).—Berggren, 1992: 563, pl. 1: figs. 14-16

***Globanomalina ehrenbergi***

Found at: Egypt, Qreiya 3; South Eastern Newfoundland Ridge IODP Site U1407; Shatsky Rise ODP Site 1210; Walvis Ridge Site 1262

Citation: *Globanomalina ehrenbergi* (Bolli 1957)

Basionym: *Globorotalia ehrenbergi*

Synonyms:

- Globorotalia membranacea* (Ehrenberg).—Cushman and Bermudez, 1949: 34, pl. 6: figs. 16-18  
*Globorotalia ehrenbergi* Bolli, 1957a: 77, pl. 20: figs. 18-20  
*Globorotalia haunsbergensis* Gohrbandt, 1963: 53, pl. 6: figs. 10-12  
*Globorotalia (Turborotalia) haunsbergensis* Gohrbandt.—Blow, 1979: 1075, pl. 88: figs. 6, 8, fig.9

***Globanomalina imitata***

Found at: Egypt, Qreiya 3; South Eastern Newfoundland Ridge IODP Site U1407; Shatsky Rise ODP Site 1210; Walvis Ridge Site 1262

Citation: *Globanomalina imitata* (Subbotina 1953)

Basionym: *Globorotalia imitata*

Synonyms:

- Globorotalia imitata* Subbotina, 1953: 206, holotype: pl. 16: fig. 14a-c; paratype: pl. 16: figs. 15a-16c  
—Loeblich and Tappan, 1957a: 190, pl. 54: fig.8a-c, pl. 59: fig. 5a-c, pl. 63: fig. 3a-c  
—Olsson, 1960:46, pl. 9: figs. 7-9

***Globanomalina pseudomenardii / chapmani***

Found at: Walvis Ridge Site 1262

***Globanomalina cf. pseudomenardii***

Found at: South Eastern Newfoundland Ridge IODP Site U1407; Shatsky Rise ODP Site 1210; Walvis Ridge Site 1262

***Globanomalina pseudomenardii***

Found at: South Eastern Newfoundland Ridge IODP Site U1407; Shatsky Rise ODP Site 1210

Citation: *Globanomalina pseudomenardii* (Bolli 1957)

Basionym: *Globorotalia pseudomenardii*

Synonyms:

*Globorotalia membranacea* (Ehrenberg). —Subbotina, 1953: 205, pl. 16: fig. 13a-c

*Globorotalia pseudomenardii* Bolli, 1957a: 77, holotype: pl. 20: figs. 14-16; paratype: pl. 20: fig. 17

—Loeblich and Tappan, 1957a: 193, pl. 47: fig. 4a-c, pl. 49: fig. 6a-c, pl. 54: figs. 10a-13c, pl. 59: fig. 3a-c, pl. 60: fig. 8a-c, pl. 63: fig. 1a-c

—Bolli and Cita, 1960: 26, pl. 33: fig. 2a-c

*Globorotalia (Globorotalia) pseudomenardii* Bolli

—Hillebrandt, 1962: 126, pl. 12: figs. 5a-6b

—Blow, 1979: 892, pl. 89: figs. 1-5, pl. 94: figs. 1-5, pl. 108: figs. 4-7, pl. Ill: figs. 1-4, pl. 112 figs. 2, 3, 9, 10

*Planorotalites pseudomenardii* Bolli

—Nederbragt and Van Hinte, 1987: 587, pl. 1: figs. 1-16

—Nocchi et al., 1991: 269, pl. 1: figs. 7-9

***Igorina albeari***

Found at: Egypt, Qreiya 3; South Eastern Newfoundland Ridge IODP Site U1407; Shatsky Rise ODP Site 1210; Walvis Ridge Site 1262

Citation: *Igorina albeari* (Cushman and Bermudez 1949)

Basionym: *Globorotalia albeari*

Synonyms:

*Globorotalia albeari* Cushman and Bermudez, 1949: 33, pl. 6: figs. 13-15 —Cifelli and Belford, 1977: 100, pl. 1: figs. 4-6

*Globorotalia pusilla laevigata* Bolli, 1957a: 78, pl. 20: figs. 5-7

—Bolli and Cita, 1960: 27, pl. 32: fig. 6a-c

—Hillebrandt, 1962: 128, 129, pl. 11: fig. 17a-c

—McGowran, 1965: 63, pl. 6: fig. 4

*Globorotalia pseudoscitula* Glaessner

—Loeblich and Tappan, 1957a: 193, pl. 46: fig. 4a-c, pl. 53: fig. 5a-c, pl. 59: fig. 2a-c, pl. 63: fig. 6a-c

*Globorotalia (Globorotalia) albeari* Cushman and Bermudez. —Blow, 1979: 883, pl. 92: figs. 4, 8, 9, pl. 93: figs. 1-4

***Igorina pusilla***

Found at: Egypt, Qreiya 3; South Eastern Newfoundland Ridge IODP Site U1407; Shatsky Rise ODP Site 1210; Walvis Ridge Site 1262

Citation: *Igorina pusilla* (Bolli 1957)

Basionym: *Globorotalia pusilla pusilla* Bolli 1957

Synonyms:

*Globorotalia pusilla pusilla* Bolli, 1957a: 78, pl. 20: figs. 8-10 —Bolli and Cita, 1960: 388, 389, pl. 34: fig. 4a-c

*Planorotalites tauricus* Morozova, 1961: 16, pl. 2: fig. 3

*Globorotalia (Globorotalia ?) pusilla pusilla* Bolli. —Hillebrandt, 1962: 128, pl. 11: fig. 18a,b

*Globorotalia pusilla pusilla* (?) Bolli. —Shutskaya, 1970b: 218, pl. 22: fig. 3a-c

*Globorotalia pusilla* Bolli.—Pujol, 1983: 652, pl. 2: figs. 12, 13

*Morozovella pusilla pusilla* (Bolli).—Snyder and Waters, 1985:446, 449, 460, pl. 8: figs. 15-17  
*Planorotalites pusilla pusilla* (Bolli).—Toumarkine and Luterbacher, 1985:108, fig. 12:13a-c, fig. 12:14a-c

***Igorina cf. tadjikistanensis***

Found at: South Eastern Newfoundland Ridge IODP Site U1407

***Igorina tadjikistanensis***

Found at: South Eastern Newfoundland Ridge IODP Site U1407; Shatsky Rise ODP Site 1210; Walvis Ridge Site 1262

Citation: *Igorina tadjikistanensis* (Bykova 1953)

Basionym: *Globorotalia tadjikistanensis*

Synonyms:

*Globorotalia tadjikistanensis* Bykova, 1953: 86, pl. 3: fig. 5a-c

—Leonov and Alimarina, 1960: 53, pl. 7: figs. 1, 2, 3, 4, 7

—Luterbacher, 1964:52, text-fig. 52a-c

*Globorotalia convexa* Subbotina, 1953: 209, pl. 17: fig. 2a-c [holotype], fig. 3a-c

—Loeblich and Tappan, 1957a: 188, pl. 48: fig. 4a-c pl. 50: fig. 7a-c, pl. 53: figs. 6a-8c, pl. 57: figs. 5a-6c, pl. 63: fig. 4a-c

—Pujol, 1983:644, pl. 3: figs. 1, 2

*Truncorotaloides (Morozovella) convexus* (Subbotina).—McGowran, 1968: 192, pl. 2: figs. 11-14

*Globorotalia (Acarinina) convexa* Subbotina.—Jenkins, 1971: 81, pl. 3: figs. 79-83

—Blow, 1979: 920, pl. 85: figs. 2-7, pl. 88: figs. 3, 4, pl. 100: figs. 3, 5-9

*Globorotalia (Acarinina) convexa cf. convexa* Subbotina.—Blow, 1979:921, pl. 100: figs. 1, 2, 4

*Globorotalia (Morozovella) tadjikistanensis* Bykova.—Belford, 1984: 10, pl. 18: figs. 18-23

*Morozovella convexa* (Subbotina).—Stott and Kennett, 1990: 560, pl. 3 figs.5, 6

***Morozovella acuta***

Found at: Shatsky Rise ODP Site 1210

Citation: *Morozovella acuta* (Toulmin 1941)

Basionym: *Morozovella*

Synonyms:

*Globorotalia wilcoxensis* Cushman and Ponton var. *acuta* Toulmin, 1941: 608, pl. 82: figs. 6-8

—Cushman and Renz, 1942: 12, pl. 3: fig. 2a-c

—Cushman, 1944a: 48, 49, pl. 8: fig.5a, b

1944b: 15, pl. 2: fig. 16a, b

—Shifflett, 1948: 73, pl. 4: fig. 23a-c

*Globorotalia velascoensis* (Cushman) var. *parva* Rey, 1954: 209, pl. 12: fig. 1a, b

*Globorotalia acuta* Toulmin

—Loeblich and Tappan, 1957a: 185, pl. 47: fig. 5a-c, pl. 55: figs. 4a-5c, pl. 58: fig. 5a-c

—Aubert, 1962: 54, pl. 1: fig. 3a-c

—Luterbacher, 1964: 686-689, text-fig. 101a-c

*Globorotalia velascoensis parva* Rey

—Bolli and Cita, 1960: 392-393, pl. 35: fig. 5a-c

—Aubert, 1963: 54, pl. 1: fig. 2a-c

*Globorotalia velascoensis acuta* (Toulmin).—Shutskaya, 1970a: 119-120, pl. 27: fig. 11a - c, pl. 28: fig. 4a-c, pl. 29: fig. 9a-c

*Globorotalia (Morozovella) acuta* Toulmin.—Jenkins, 1971: 106, pl. 9: figs. 205-207

*Globorotalia (Morozovella) velascoensis parva* Rey.—Jenkins, 1971: 106, 107, pl. 9: figs. 211-213

—Blow, 1979: 1030, 1031, pl. 95: figs. 3-6

*Morozovella acuta* (Toulmin).—Toumarkine and Luterbacher, 1985: 111, text-fig. 14 (7, reillustration of holotype; 8, reillustration of Loeblich and Tappan, 1957a, pl. 55: fig. 4a-c)

### ***Morozovella acutispira***

Found at: Shatsky Rise ODP Site 1210; Walvis Ridge Site 1262

Citation: *Morozovella acutispira* (Bolli and Cita 1960)

Basionym: *Globorotalia acutispira*

Synonyms:

*Globorotalia californica* Smith, 1957: 190, pl. 28: figs. 22a-23c [homonym]

*Globorotalia acutispira* Bolli and Cita, 1960: 15, pl. 33: fig. 3a-c

*Globorotalia kolchidica* Morozova, 1961: 17, pl. 2: fig. 2a-c

*Globorotalia* sp. aff. *G. kolchidica* Morozova.—Luterbacher, 1964: 668, text-figs. 61, 62

*Globorotalia* sp. aff. *G. acutispira* Bolli and Cita. —Shutskaya, 1970b: 118-120, pl. 25: fig. 7a-c

*Globorotalia (Morozovella) oclusa acutispira* (Bolli and Cita).—Belford, 1984: 9, pl. 17: figs. 14-21

### ***Morozovella aequa***

Found at: Shatsky Rise ODP Site 1210; Walvis Ridge Site 1262

Citation: *Morozovella aequa* (Cushman and Renz 1942)

Basionym: *Globorotalia crassata aequa*

Synonyms:

*Globorotalia crassata* (Cushman) var. *aequa* Cushman and Renz, 1942: 12, pl. 3: fig. 3a-c

*Globorotalia lacerti* Cushman and Renz, 1946: 47, pl. 8: figs. 11, 12

*Globorotalia (Truncorotalia) crassata* (Cushman) var. *aequa* Cushman and Renz.—Cushman and Bermudez, 1949: 37, pl. 7: figs. 7-9

*Globorotalia praenartanensis* Shutskaya, 1956: 98, pl. 3: fig. 5a-c

—Luterbacher, 1964: 671, text-fig. 73a-c

*Globorotalia aequa* Cushman and Renz.

—Bolli, 1957a: 74, pl. 17: figs. 1-3, pl. 18: figs. 13-15

—Loeblich and Tappan, 1957a: 186, pl. 59: fig. 6a-c

—Bolli and Cita, 1960: 377, 378, pl. 33: fig. 5a-c

—Luterbacher, 1975b: 64, pl. 2: figs. 22-24, pl. 2: figs. 28-30

*Globorotalia angulata* (White).—Loeblich and Tappan, 1957a: 187, pl. 48: fig. 2a-c, pl. 58: fig. 2a-c

*Globorotalia (Truncorotalia) aequa aequa* (Cushman and Renz).

—Hillebrandt, 1962: 133, 134, pl. 13: fig. 1a-c

*Globorotalia aequa bullata* Jenkins, 1965: 1110, fig. 10, no. 87-91;

1971: 100, pl. 7: figs. 172-176

*Globorotalia loeblichii* El-Naggar, 1966: 218-220, pl. 23: fig. 1a-c

*Truncorotaloides (Morozovella) aequus* (Cushman and Renz).—McGowran, 1968: 190, pl. 1: figs. 3-12

*Globorotalia (Morozovella) aequa aequa* Cushman and Renz.—Jenkins, 1971: 100, pl. 7: figs. 167-169-171

—Blow, 1979: 975-977, pl. 96: figs. 4-9, pl. 218: figs. 1-6, pl. 99: fig. 5, pl. 102: figs. 6, 9, 10, pl. 103: fig. 1, pl. 211: figs. 3-5, pl. 118: figs. 8-10, pl. 211: figs. 1, 2

*Morozovella aequa* (Cushman and Renz).

—Berggren, 1971 b: 76, pl. 5: fig. 6

—Snyder and Waters, 1985: 446, pl. 7: figs. 5-7,

*Acarinina aequa* (Cushman and Renz). —Tjalsma, 1977: 508, pl. 3: fig. 13

*Globorotalia (Morozovella) aequa lacerti* (Cushman and Renz).—Blow, 1979: 977-979, pl. 138: figs. 1-3, pl. 115: fig. 6.

*Globorotalia (Morozovella) aequa tholiformis* Blow, 1979: 979-981, pl. 102: figs. 7, 8, pl. 119: figs. I, 2

[holotype], fig. 3, pl. 125: figs. 1, 2, pl. 127: figs. 8, 9, pl. 129: fig. 6, pl. 133: fig. 9

### ***Morozovella angulata***

Found at: Egypt, Qreiya 3; South Eastern Newfoundland Ridge IODP Site U1407; Shatsky Rise ODP Site 1210; Walvis Ridge Site 1262

Citation: *Morozovella angulata* (White 1928)

Basionym: *Globigerina angulata*

Synonyms:

*Globigerina angulata* White, 1928: 191, pl. 27: fig. 13.

*Globorotalia angulata* (White).—Glaessner, 1937b: 383, pl. 4: figs. 35a-c; ? 36a-c (? = *M. aequa*), fig. 37a-c

(*M. conicotruncata*),

—Bykova, 1953:82-86, text-figs. 7 a - 11 c.

—Shutskaya, 1956:92, 93, text-fig. 1, pl. 3: fig. 2a-c.

—Bolli, 1957a:74, pl. 17: figs. 7-9,

—Loeblich and Tappan, 1957a: 187, pl. 50: fig. 4a-c, pl. 64: fig. 5a-c.

—Bolli and Cita, 1960:376, 377, pl. 35: fig. 8a-c,

—Olsson, 1960:44, pl. 8: figs. 14-16.

—Toumarkine and Luterbacher, 1985:111, text-fig. 14: 5a-c [holotype reillustrated], text-fig. 14: 6a-c

*Globorotalia (Truncorotalia) angulata* (White).—Hillebrandt, 1962:131, 132, pl. 13: figs. 14a-15c,

*Truncorotaloides (Morozovella) angulatus* (White).—McGowran, 1968:190, pl. 1: figs. 13-18,

*Globorotalia (Morozovella) angulata* (White).—Blow, 1979:984, pl. 86: figs. 7-9

*Morozovella protocarina* Corfield, 1989:98, pl. 1: figs. 1-12

### ***Morozovella apantesma***

Found at: Egypt, Qreiya 3; South Eastern Newfoundland Ridge IODP Site U1407; Shatsky Rise ODP Site 1210; Walvis Ridge Site 1262

Citation: *Morozovella apantesma* (Loeblich and Tappan 1957)

Basionym: *Globorotalia apantesma*

Synonyms:

*Globorotalia apantesma* Loeblich and Tappan 1957a: 187, pl. 48: fig. 1a-c, pl. 58: fig. 4a-c (paratype), pl. 59: fig. 1a-c (holotype).

*Globorotalia (Morozovella) apantesma* Loeblich and Tappan.—Jenkins, 1971:102, pl. 8: figs. 186-188.

? *Globorotalia (Morozovella) apantesma* Loeblich and Tappan.—Blow, 1979: 988, pl. 251: fig. 2.

*Acarinina apantesma* (Loeblich and Tappan).—Huber, 1991b:446, pl. 4: figs. 1, 2.

### ***Morozovella occlusa***

Found at: Shatsky Rise ODP Site 1210; Walvis Ridge Site 1262

Citation: *Morozovella occlusa* (Loeblich and Tappan 1957)

Basionym: *Globorotalia occlusa*

Synonyms:

*Discorbina simulatilis* Schwager, 1883:120, pl. 29: fig. 15a-d,

*Globorotalia occlusa* Loeblich and Tappan, 1957a: 191, pl. 55: fig. 3a-c, pl. 64: fig. 3a-c

Luterbacher, 1964:690, text-figs. 112a-II 3c, text-fig. 114a-c.

*Globorotalia crosswicksensis* Olsson, 1960:47, pl. 10: figs. 7-9,

*Globorotalia (Truncorotalia) velascoensis occlusa* Loeblich and Tappan.—Hillebrandt, 1962:139, pl. 13: figs. 22-26

*Globorotalia (Morozovella) occlusa* Loeblich and Tappan.

—Jenkins, 1971: 106, pl. 9: figs. 208-210.

—Blow, 1979: 1007, pl. 90: figs. 7, 10, pl. 95: figs. 7-10, pl. 96: figs. 1-3, pl. 213: fig. 6. pl. 214: figs. 1-6, pl. 215: figs. 5, 6, pl. 103: figs. 4-6, pl. 108: figs. 9, 10, pl. 118: figs. 1-7.

—Belford, 1984:9, pl. 17: figs. 6-14.

*Globorotalia (Morozovella) occlusa cf. occlusa* Loeblich and Tappan.

—Blow, 1979: 1007, pl. 92: figs. 5, 6.

*Globorotalia (Morozovella) occlusa crosswicksensis* Olsson.—Blow, 1979: 1011, pl. 88: figs. 1, 2, pl. 213: figs. 1,2, pl. 90: figs. 3-6, 8, 9, pl. 213: figs. 3-5, pl. 215: figs. 1-4 .

*Morozovella simulatilis* (Schwager).—Snyder and Waters, 1985:470, pl. 9: figs. 7-9.

### ***Morozovella pasionensis***

Found at: Shatsky Rise ODP Site 1210

Citation: *Morozovella pasionensis* (Bermudez 1961)

Basionym: *Pseudogloborotalia pasionensis*

Synonyms:

*Pseudogloborotalia pasionensis* Bermudez, 1961: 1346, pl. 16: figs. 8a,b.

*Globorotalia pasionensis* (Bermudez).

—Luterbacher, 1964: 690, text-fig. 108a-c, text-figs. 109a-110c, text-fig. 11 la-c.  
—Samanta, 1970: 629, figs. 11, 12.  
*Globorotalia velascoensis caucasica* Glaessner.—El-Naggar, 1966: 242, pl. 19: fig. 6a-c.

### ***Morozovella praeangulata***

Found at: Egypt, Qreiya 3; South Eastern Newfoundland Ridge IODP Site U1407; Shatsky Rise ODP Site 1210; Walvis Ridge Site 1262

Citation: *Morozovella praeangulata* (Blow 1979)

Basionym: *Globorotalia (Acarinina) praeangulata*

Synonyms:

Transitional form between *Globorotalia uncinata* Bolli and *Globorotalia angulata* (White).—Bolli, 1957a: 74, pl. 17: figs. 10-12.

? *Acarinina quadratoseptata* Davidzon and Morozova, 1964: 28, 30, pl. 2: fig. 1a-c, figs. 2a-3c.

*Globorotalia (Acarinina) praeangulata* Blow, 1979: 942-944, pl. 82: figs. 5, 6, pl. 83: fig. 6, pl. 84: figs. 1, 7, pl. 212: figs. 1, 2 [holotype], fig. 8.

### ***Morozovella velascoensis***

Found at: Shatsky Rise ODP Site 1210

Citation: *Morozovella velascoensis* (Cushman 1925)

Basionym: *Pulvinulina velascoensis*

Synonyms:

*Pulvinulina velascoensis* Cushman, 1925:19, pl. 3: fig. 5a-c,

*Globorotalia velascoensis* (Cushman).

—White, 1928: 281, pl. 38: fig. 2a-c.

—Cushman and Renz, 1946: 47, pl. 8: figs. 13, 14,

—Subbotina, 1947: 123, pl. 7: figs. 9-11, pl. 9: figs. 21-23.

—Le Roy, 1953: 33, pl. 3: figs. 1-3.

—Haque, 1956: 181, pl. 24: fig. 2a-c,

—Bolli, 1957a: 76, pl. 20: figs. 1-4.

—Loeblich and Tappan, 1957a: 196, pl. 64: figs. 1a-2c,

—Bolli and Cita, 1960: 391, pl. 35: fig. 7a-c.

—Said and Kerdany, 1961: 330, pl. 1: fig. 10a-c.

—Shutskaya, 1970b: 118-120, pl. 23: fig. 3a-c, pl. 24: fig. 5a-c, pl. 25: fig. 5a-c, pl. 27: fig. 12a-c, pl. 29: fig. 8a-c.

—Luterbacher, 1975a: 726, pl. 1: fig. 8a,b.

—Pujol, 1983:644, pl. 3: fig. 9,

*Pseudogloborotalia velascoensis* (Cushman).

—Bermudez, 1961: 1349, pl. 16: fig. 1 la, b.

*Globorotalia (Truncorotalia) velascoensis velascoensis* (Cushman). Hillebrandt, 1962:169, pl. 13: figs. 16-21,

*Truncorotaloides (Morozovella) velascoensis* (Cushman).—McGowran, 1968:190, pl. 2: fig. 1 [Velasco Fm., Ebano, Mexico].

*Globorotalia (Morozovella) velascoensis velascoensis* (Cushman).

—Jenkins, 1971:107, pl. 9: figs. 214-216,

—Blow, 1979:1029, pl. 92: fig. 7, pl. 94: figs. 6-9, pl. 95: figs. 1, 2, pl. 216: figs. 1-8, pl. 217: figs. 1-6, pl. 99: figs. 3, 4.

*Morozovella velascoensis* (Cushman).—Toumarkine and Luterbacher, 1985:109, text-figs. 11, 12

### ***Morozovella conicotruncata***

Found at: Egypt, Qreiya 3; South Eastern Newfoundland Ridge IODP Site U1407; Shatsky Rise ODP Site 1210; Walvis Ridge Site 1262

Citation: *Morozovella conicotruncata* (Subbotina 1947)

Basionym: *Globorotalia conicotruncata*



Synonyms:

*Globorotalia conicotruncata* Subbotina, 1947: 115, pl. 4: figs. 11-13, pl. 9: figs. 9-11,  
—Luterbacher, 1964: 660, text-fig. 40, text-figs. 41, 42, text-figs. 46-49, text-fig. 51;  
1975a: 726, pl. 1: figs. 6, 7,

—Pujol. 1983:645, pl. 2: fig. 8,

*Acarinina conicotruncata* (Subbotina). —Subbotina, 1953:220. pl. 20: fig.5a,b, fig. 6a-c, fig. 7a-c, fig. 8a-c.

*Globorotalia angulata* (White) var. *kubanensis* Shutsкая, 1956: 93, pl. 3: fig. 4a-c.

*Globorotalia angulata abundocamerata* Bolli, 1957a: 74, pl. 17: figs. 4-6.

— Bolli and Cita, 1960:379, pl. 35: figs. 6a-c.

*Globorotalia (Truncorotalia) angulata* Hillebrandt, 1962: 131, pl. 13: figs. 14a-15c

*Globorotalia kubanensis* (Shutsкая). —Shutsкая, 1970b: 118-120, pl. 21: fig. 1a-c

*Morozovella conicotruncata* (White).

—Berggren, 1971b: 74, pl. 4: figs. 8-14.

—Snyder and Waters, 1985: 446, pl. 8: figs. 4, 5, 6

*Globorotalia (Morozovella) angulata conicotruncata* (White).—Blow, 1979:986, pl. 87: fig. 3

***Parasubbotina pseudobulloides/variata***

Found at: South Eastern Newfoundland Ridge IODP Site U1407

***Parasubbotina pseudobulloides+variospira***

Found at: Egypt, Qreiya 3; South Eastern Newfoundland Ridge IODP Site U1407; Shatsky Rise ODP Site 1210; Walvis Ridge Site 1262

***Parasubbotina variata***

Found at: Egypt, Qreiya 3; South Eastern Newfoundland Ridge IODP Site U1407, Walvis Ridge Site 1262

Citation: *Parasubbotina variata* (Subbotina 1953)

Basionym: *Globigerina variata*

Synonyms:

*Globigerina variata* Subbotina, 1953:63, holotype: pl. 3: fig.5a-c; paratypes: pl. 3: figs. 6a-7c, 10a-11c pl. 3: fig. 12a-c, pl. 4: figs. 1a-3c

*Globorotalia (Globorotalia) variata* (Subbotina).—Hillebrandt, 1962:125, pl. 12: figs. 10a-c, 11a,b

*Globorotalia (Turborotalia) quadrilocula* Blow, 1979:1109, holotype: pl. 87: fig. 7, paratypes: pl. 75: fig.8, pl. 78: figs. 2-4, pl. 83: fig. 3, pl. 87: fig.8.

*Subbotina variata* (Subbotina).—Berggren, 1992:563, pl. 1:fig.3

***Parasubbotina variospira***

Found at: Egypt, Qreiya 3; South Eastern Newfoundland Ridge IODP Site U1407; Shatsky Rise ODP Site 1210; Walvis Ridge Site 1262

Citation: *Parasubbotina variospira* (Belford 1984)

Basionym: *Globorotalia (Turborotalia) variospira*

Synonyms:

*Globorotalia (Turborotalia) variospira* Belford 1984:18, pl. 24: figs. 15-17, pl. 25: figs. 1-7.

*Morozovella variospira* (Belford).—Van Eijden and Smit, 1992: 113, text-fig. 26A-D, pl. 5: figs. 1-8

***Parvularugoglobigerina alabamensis***

Found at: Egypt, Qreiya 3; South Eastern Newfoundland Ridge IODP Site U1407; Shatsky Rise ODP Site 1210; Walvis Ridge Site 1262

Citation: *Parvularugoglobigerina alabamensis* (Liu and Olsson 1992)

Basionym: *Guembelitra alabamensis*

Synonyms:

*Guembelitra alabamensis* Liu and Olsson, 1992:341, pl. 2: figs. 1-7

### ***Praemurica inconstans***

Found at: Egypt, Qreiya 3; South Eastern Newfoundland Ridge IODP Site U1407; Shatsky Rise ODP Site 1210; Walvis Ridge Site 1262

Citation: *Praemurica inconstans* (Subbotina 1953)

Basionym: *Globigerina inconstans*

Synonyms:

*Globigerina inconstans* Subbotina, 1953:58, pl. 3: figs. 1, 2,—Berggren, 1965:291, text-fig. 9:3, 4.

*Globigerina schachdagica* Khalilov, 1956:246, pl. 1:fig.3.

*Acarinina praecursoria* Morozova, 1957:1111, text-fig. 1.

*Globorotalia trinidadensis* Bolli, 1957a:73, pl. 16: figs. 19-21 [holotype], figs. 22, 23,

Transitional form between *Globorotalia pseudobulloides* (Plummer) and *Globorotalia uncinata* Bolli.—  
Bolli, 1957a: 74, pl. 17: figs. 16-18

*Globorotalia (Acarinina) inconstans* (Subbotina).—Leonov and Alimarina, 1960, pl. 3: figs. 1-3, 5-8.

*Globorotalia scabrosa* Bermudez, 1961:1196, 1197, pl. 5: fig. 5.

*Globigerina scobinata* Bermudez 1961:1197, pl. 5: fig. 6.

*Globorotalia (Globorotalia) inconstans* (Subbotina).—Hillebrandt, 1962:130, pl. 12: figs. 7, 8.

*Globorotalia inconstans* (Subbotina).—Luterbacher, 1964:650: figs. 19-23.

*Globigerina arabica* El-Naggar, 1966:157, 158, pl. 18: fig. 6,

*Acarinina inconstans inconstans* (Subbotina). —Shutskaya, 1970b: 108, pl. 6: figs. 4, 5.

*Globorotalia (Turborotalia) inconstans* (Subbotina).

—Blow, 1979: 1080, pl. 71: figs. 6, 7, pl. 75: figs.4-7, pl. 76: figs. 3, 6, 7, fig.10, pl. 77: fig.1, pl. 81: figs. 1, 2, pl. 233: figs. 4, 5,

*Subbotina inconstans* (Subbotina).—Stott and Kennett, 1990: 559, pl. 2: figs.5, 6.

*Morozovella inconstans* (Subbotina).—Berggren, 1992: 564, pl. 1: figs. 12, 13

### ***Praemurica praecursoria***

Found at: South Eastern Newfoundland Ridge IODP Site U1407; Shatsky Rise ODP Site 1210

Citation: *Acarinina praecursoria* Morozova 1957

Type locality: Holotype from along the Khokodz River, in the northern Caucasus; and found also in the Crimea and along the Mangyshlak Peninsula; all in the USSR.

Type level: Danian *Holotype*

Repository: Moscow, Inst. of Geol. Sci. of the Academy of Sciences

Currently attributed to *Pr. inconstans*

### ***Praemurica uncinata***

Found at: Egypt, Qreiya 3; South Eastern Newfoundland Ridge IODP Site U1407; Shatsky Rise ODP Site 1210; Walvis Ridge Site 1262

Citation: *Praemurica uncinata* (Bolli 1957)

Basionym: *Globorotalia uncinata*

Synonyms:

*Globorotalia uncinata* Bolli, 1957a:74, pl. 17: figs. 13-15.

—Luterbacher, 1964:655, 657, fig. 30a-c, fig. 3 l a - c.

—Said and Sabry, 1964:385, 386, pl. 1: fig. 12a-c,

—Berggren, 1965:294, text-fig. 9 (5a-c),

—Toumarkine, 1978:692, 693, pl. 1: fig. 16,

—Pujol, 1983:645, 652, pl. 2: fig. 1.

*Acarinina indolensis* Morozova, 1959:1116, text-fig. 1

*Globorotalia uncinata uncinata* Bolli.—El-Naggar, 1966: 240, pl. 18: fig. la-c, pl. 19: fig. 2a-c.

*Acarinina inconstans uncinata* (Bolli). —Shutskaya, 1970a: 110, pl. 6: fig. la-c [holotype refigured], fig. 2a-c, fig. 3a-c; 1970b: 118-120, pl. 19: figs. 7a-c, lOa-c,

*Globorotalia (Acarinina) praecursoria praecursoria* ( Morozova).

—Blow, 1979:944-947, pl. 76: figs. 4, 8, 9, pl. 81: fig. 3, pl. 77: figs. 2-5, pl. 82: figs. 1-3, pl. 84:fig.2, pl. 85: fig. 9

*Morozovella uncinata* (Bolli).—Snyder and Waters, 1985:448,449, pl. 10: figs. 1, 2

***Praemurica uncinata inconstans***

Found at: Egypt, Qreiya 3; South Eastern Newfoundland Ridge IODP Site U1407

***Praemurica uncinata inconstans praecursoria***

Found at: South Eastern Newfoundland Ridge IODP Site U1407

***Subbotina cancellata***

Found at: Egypt, Qreiya 3; South Eastern Newfoundland Ridge IODP Site U1407; Shatsky Rise ODP Site 1210; Walvis Ridge Site 1262

Citation: *Subbotina cancellata* Blow 1979

Basionym: *Subbotina cancellata*

Synonyms:

? *Globigerina fringa* Subbotina, 1953:62, pl. 3: fig. 3.

*Subbotina triangularis cancellata* Blow, 1979:1284, holotype: pl. 80: fig. 7, paratypes: pl. 80: figs. 2-6, 8, 9, pl. 238: fig. 6

***Subbotina triangularis***

Found at: Egypt, Qreiya 3; South Eastern Newfoundland Ridge IODP Site U1407; Shatsky Rise ODP Site 1210; Walvis Ridge Site 1262

Citation: *Subbotina triangularis* (White 1928)

Basionym: *Globigerina triangularis*

Synonyms:

*Globigerina triangularis* White, 1928:195, pi. 28: fig. 1 a - c.

—Bolli, 1957a: 71, pl. 15: figs. 12-14.

—Shutskaya, 1970a: 104, pl. 3: fig. 5a-c;

1970b: 118, pi. 20: fig. 7a-c, p. 220, pi. 23: fig. 1a-c, p. 224, pl. 25: fig. 1a-c

*Globigerina inaequispira* Subbotina.—Loeblich and Tappan, 1957a: 181, pl. 52: figs. 1a-2c

*Globigerina triloculinoides* Plummer.—Loeblich and Tappan, 1957a: 183, pl. 62: fig. 3a-c

*Globigerina gerpegensis* Shutskaya, 1970a: 104, pl. 3: fig. 3a-c

*Globigerina pseudotriloba* Shutskaya, 1970a:85, pl. 2: fig. 7a-c

*Globigerina uruchaensis* Shutskaya, 1970a:87, pl. 2: fig. 6a-c

*Subbotina patagonica/triangularis* group Tjalsma, 1977:510, pl. 4: fig. 2, figs. 3-6.

*Subbotina triangularis triangularis* (White).—Blow, 1979:1281, pl. 91:figs.7, 9, pl. 98: fig. 6, pl. 107: figs. 8, 9

***Subbotina triloculinoides***

Found at: Egypt, Qreiya 3; South Eastern Newfoundland Ridge IODP Site U1407; Shatsky Rise ODP Site 1210; Walvis Ridge Site 1262

Citation: *Subbotina triloculinoides* (Plummer 1927)

Basionym: *Globigerina triloculinoides*

Synonyms:

*Globigerina triloculinoides* Plummer, 1926:134, pl. 8: fig. 10a-b.

—Bolli, 1957a:70, pl. 15: figs. 18-20,

—Loeblich and Tappan, 1957a: 183, pl. 40: fig. 4a-c, pl. 41: fig.2a-c, pl. 42: fig. 2a-c, pl. 43: fig.5a-c, pl. 43: figs. 8a, b, 9a-c, pl. 45:fig.3a-c.

—Bolli and Cita, 1960:13, pl.31: fig.1a-c,

—Berggren, 1962: 86, pl. 14: figs. 1a-2b.

—Hillebrandt, 1962: 119, pl. 11: fig. 1a-c.

—Shutskaya, 1970b: 118, pl. 18: fig. 1a-c, pl. 19: fig.3a-c, pl. 21: fig. 5a-c, pl. 23: fig. 12a-c *Globigerina pseudotriloba* White, 1928:194, pl. 27:fig.17a, b.

*Globigerina stainforthi* Bronnimann, 1952:23, pl. 3: figs. 10-12.

*Globigerina (Globigerina) microcellulosa* Morozova, 1961:14, pl. 1: fig. 11.

*Subbotina triloculinoides* (Plummer).

—Brotzen and Pozaryska, 1961: 160, text-fig. 2, pl. 4: fig.4,

—Belford, 1967:7, pl. 1: figs. 1-5 .

—Stott and Kennett, 1990:559, pl. 2: fig. 12.

*Subbotina triloculinoides triloculinoides* (Plummer).

—Blow, 1979:1287, pl. 74: fig. 6, pl.80: fig.1, pl. 98: fig.7, pl. 238:fig.5, pl. 248: figs. 9, 10, pl. 255: fig.9, pl. 257: fig. 9

### ***Subbotina velascoensis***

Found at: Egypt, Qreiya 3; South Eastern Newfoundland Ridge IODP Site U1407; Shatsky Rise ODP Site 1210; Walvis Ridge Site 1262

Citation: *Subbotina velascoensis* (Cushman 1925)

Basionym: *Globigerina velascoensis*

Synonyms:

*Globigerina velascoensis* Cushman, 1925:19, pl. 3: fig. 6a-c.

—White, 1928:196, pl. 28: fig. 2a,b.

—Bolli, 1957a:71, pl. 15: figs. 9-11.

—Bolli and Cita, 1960:374, pl. 34: fig. 8a-c.

—Hillebrandt, 1962:120, pl. 11: fig. 4a,b.

—Gohrbandt, 1963:47, pl. 2: figs. 1-3.

— Shutskaia, 1970a:94, pl. 4: figs. 3a-4c, 6a-c

*Globigerina velascoensis* Cushman var. *compressa* White, 1928:196, pl. 28: fig. 3a,b,

*Globigerina quadriloculinoides* Khalilov, 1956: 237, pl. 1: fig. 5a-c.

*Globigerina triloculinoides* Plummer *nana* Khalilov, 1956: 236, pl. 1: fig.4a-c

*Globorotalia tortiva* Bolli, 1957a: 78.

### ***Woodringina* sp.**

Found at: Walvis Ridge Site 1262

Citation: *Woodringina* Loeblich and Tappan, 1957

Rank: Genus

Type species: *Woodringina claytonensis* Loeblich and Tappan, 1957b.

Taxonomic discussion: Although *Woodringina* remains limited to the Paleocene, it is no longer monotypic. It was assigned to the subfamily *Guembeltriinae* by Loeblich and Tappan (1957b). Elevation of the subfamily *Guembeltriinae* to the family *Guembeltriidae* (El-Naggar, 1971; Blow, 1979; Loeblich and Tappan, 1988) removed it from the family *Heterohelicidae*. [Olsson et al. 1999]

## Appendix 2: Data Chapter II

Chapter 2 is a published paper: Jehle, S. et al., 2015. The Impact of the Latest Danian Event on Planktic Foraminiferal Faunas at ODP Site 1210 (Shatsky Rise, Pacific Ocean). PLoS ONE, 10, e0141644.

<https://doi.org/10.1371/journal.pone.0141644>

Supplementary data for Chapter 2 contains following data:

**Table 2.1** List of samples for ODP Site 1210. Used samples as well as excluded ones, please see reason for exclusion in Chapter 2 or the paper. Online repository:

<https://doi.org/10.1371/journal.pone.0141644.s001>

**Table 2.2** Planktic foraminifera assemblage census, raw count data. Online repository:

<https://doi.org/10.1371/journal.pone.0141644.s002>

**Table 2.3** Sediment parameters:

- CaCO<sub>3</sub> [wt%],
- fragmentation [%F],
- coarse fraction [%],
- proportion of planktic foraminifera [%],
- PFN [numbers per gram], PFAR [g/(kyr cm<sup>2</sup>)],
- sedimentation rate [cm/kyr]
- Shannon H' and taxa diversity.

Online repository: <https://doi.org/10.1371/journal.pone.0141644.s003>

**Table 2.4** Planktic foraminifera  $\delta^{13}\text{C}$ ,  $\delta^{18}\text{O}$ . Online repository:

<https://doi.org/10.1371/journal.pone.0141644.s004>

**Table 2.5** Benthic foraminifera  $\delta^{13}\text{C}$ ,  $\delta^{18}\text{O}$ .

Online repository: <https://doi.org/10.1371/journal.pone.0141644.s005>

used samples		NMDS				
core	section	top [cm]	bottom [cm]	depth [mbsf]	depth [rmc]	sample_id
.210-A-2	1	90.0	92.0	206.300	231.890	4
.210-A-2	1	100.0	102.0	206.400	231.990	5
.210-A-2	1	110.0	112.0	206.500	232.090	6
.210-A-2	1	120.0	122.0	206.600	232.190	7
.210-A-2	1	130.0	132.0	206.700	232.290	8
.210-A-2	2	10.0	12.0	207.000	232.590	10
.210-A-2	2	20.0	22.0	207.100	232.690	11
.210-A-2	2	35.0	37.0	207.25	232.84	12
.210-A-2	2	60.0	62.0	207.5	233.09	13
.210-A-2	2	70.0	72.0	207.600	233.190	14
.210-A-2	2	82.5	84.0	207.725	233.315	15
.210-A-2	2	87.0	88.5	207.770	233.360	16
.210-A-2	2	93.0	94.5	207.830	233.420	18
.210-A-2	2	97.5	99.0	207.875	233.465	19
.210-A-2	2	105.0	106.5	207.950	233.540	21
.210-A-2	2	106.5	108.0	207.965	233.555	22
.210-A-2	2	112.5	114.0	208.025	233.615	24
.210-A-2	2	117.0	118.5	208.070	233.660	25
.210-A-2	2	120.0	121.5	208.100	233.690	26
.210-A-2	2	123.0	124.5	208.130	233.720	27
.210-A-2	2	127.5	129.0	208.175	233.765	28
.210-A-2	2	132.0	133.5	208.220	233.810	29
.210-A-2	2	135.0	136.5	208.250	233.840	30
.210-A-2	2	138.0	139.5	208.280	233.870	31
.210-A-2	2	142.5	144.0	208.325	233.915	32
.210-A-2	2	147.0	148.5	208.370	233.960	33
.210-A-2	3	0.0	1.5	208.400	233.990	34
.210-A-2	3	3.0	4.5	208.430	234.020	35
.210-A-2	3	7.5	9.0	208.475	234.065	36
.210-A-2	3	12.0	13.5	208.520	234.110	37
.210-A-2	3	15.0	16.5	208.550	234.140	38
.210-A-2	3	18.0	19.5	208.580	234.170	39
.210-A-2	3	22.5	24.0	208.625	234.215	40
.210-A-2	3	27.0	28.5	208.670	234.260	41
.210-A-2	3	30.0	31.5	208.700	234.290	42
.210-A-2	3	33.0	34.5	208.730	234.320	43
.210-A-2	3	37.5	39.0	208.775	234.365	44
.210-A-2	3	40.5	42.0	208.805	234.395	45
.210-A-2	3	45.0	46.5	208.850	234.440	47
.210-A-2	3	48.0	49.5	208.880	234.470	48
.210-A-2	3	52.5	54.0	208.925	234.515	49
.210-A-2	3	57.0	58.5	208.970	234.560	50
.210-A-2	3	60.0	61.5	209.000	234.590	51
.210-A-2	3	63.0	64.5	209.030	234.620	52
.210-A-2	3	67.5	69.0	209.075	234.665	53
.210-A-2	3	72.0	73.5	209.120	234.710	54
.210-A-2	3	75.0	76.5	209.15	234.74	55
.210-A-2	3	80.0	81.5	209.200	234.790	56
.210-A-2	3	95.0	96.5	209.35	234.94	57
.210-A-2	3	105.0	106.5	209.450	235.040	58
.210-A-2	3	120.0	121.5	209.600	235.190	59
.210-A-2	3	145.0	146.5	209.850	235.440	60
.210-A-2	4	5.0	7.0	209.950	235.540	61
.210-A-2	4	20.0	22.0	210.100	235.690	62
.210-A-2	4	70.0	72.0	210.6	236.19	65
.210-A-2	4	80.0	82.0	210.7	236.29	66

.210-A-2	4	85.0	87.0	210.750	236.340	67
.210-A-2	4	95.0	97.0	210.85	236.44	68
.210-A-2	4	110.0	112.0	211	236.59	69

**excluded samples due to bad preservation**

core	section	top [cm]	bottom [cm]	depth [mbsf]	depth [rmcd]
.210-A-2	1	60.0	62.0	206.000	231.590
.210-A-2	1	85.0	87.0	206.250	231.840
.210-A-2	1	135.0	137.0	206.750	232.340
.210-A-2	2	90.0	91.5	207.800	233.39
.210-A-2	2	102.0	103.5	207.920	233.510
.210-A-2	2	108.0	109.5	207.980	233.57
.210-A-2	3	42.0	43.5	208.820	234.41
.210-A-2	4	45.0	47.0	210.350	232.940





209.20	234.79	1	1	3	3	3	22	33	80	2	138	15	21	15	56	2	35	57	4	61	9	2	25	8	<b>532</b>							
209.35	234.94	11			1		4	7	20	8	1	96	5	5	20	11	101	2	2	48	33	6	39	14	1	4	2	<b>404</b>				
209.45	235.04		1	8	3		5	14	104	1	155	1		22	2	121		1	29	16	6	22	1	9	9	4	3	<b>515</b>				
209.60	235.19	2	6	4	2		6	12	125	1	112			10	2	106		1	3	9	45	1	24	5	30	5	20	2	4	1	1	<b>509</b>
209.85	235.44	16	7	1				2	52	1	35	4		5	6	109		1	7	21	94	10	10	20	5	1	2		1	<b>390</b>		
209.95	235.54	21	1			3		1	32	6	1	26	2	3	1	1	219		6	7	81	1	9	1	11		1		3	<b>426</b>		
210.10	235.69	2	3				12	11	50	4	58	7		5	13	86		18	8	65	4	53	16	73	15	1	1	3	<b>436</b>			
210.60	236.19		3	1	6		3		1		13	1	2	8	3	114		11	10	70	2	27	9	38	2	1	2		1	<b>290</b>		
210.70	236.29	1			7		3		15		79			5	7	14	100		20	2	35		22	2	24	5	6		4	1	<b>328</b>	
210.75	236.34	7	4	2	1		1	2	20	4	1	63	3	2	18	4	109		19	9	112		17	17	34	2	13		1	3	<b>434</b>	
210.85	236.44	8	11		4		2		28		22	1		7	2	152		8	11	74	1	67	26	94	1	7	5	12	1	1	<b>451</b>	
211.00	236.59	16	7		2		1		10		11			13	3	162		1	25	7	123	3	57	19	79	3	4		2	3	<b>472</b>	

depth [rmcd]	depth [mbsf]	CaCO <sub>3</sub> [wt%]	fragmentation [%F]	coarse fraction [%]	% pl. Foraminifera	PFN [#lg]	PFAR [g/(kyr cm <sup>2</sup> )]	SR [cm/kyr]	Shannon H'	Taxa diversity
231.89	206.300	92.82	14.02	1.32	96.77	6527.0	-	0.3	2	20
231.99	206.400	91.25	13.58	3.15	98.74	6415.6	5017.5	0.6	2.07	18
232.09	206.500	90.68	14.80	3.48	98.82	5065.6	3961.7	0.6	1.85	16
232.19	206.600	95.00	12.73	6.97	99.14	17630.0	13788.1	0.6	2.16	20
232.29	206.700	93.69	6.21	5.04	98.64	14689.7	11488.5	0.6	2.33	20
232.59	207.000	94.21	12.76	5.58	98.91	13814.0	8524.6	0.5	1.87	15
232.69	207.100	94.34	6.68	4.13	98.88	12149.0	7497.1	0.5	2.37	20
232.84	207.250	94.42	6.67	5.31	98.75	13996.0	8636.9	0.5	2.08	17
233.09	207.500	95.70	12.98	2.55	98.39	5556.4	3227.2	0.5	2.03	18
233.19	207.600	94.88	12.11	1.64	97.56	4124.7	2395.6	0.5	2.05	18
233.32	207.725	95.31	4.68	4.28	99.12	9707.3	5638.0	0.5	2.14	16
233.36	207.770	93.65	14.11	1.23	98.04	3013.0	1750.0	0.5	2.24	18
233.42	207.830	93.48	4.44	4.48	99.42	8768.0	5092.5	0.5	2.35	19
233.47	207.875	95.03	13.16	1.90	98.94	3404.8	3721.1	0.5	1.65	14
233.54	207.950	92.87	10.79	3.12	98.67	6406.9	2720.8	0.5	1.84	16
233.56	207.965	93.65	11.84	2.00	99.08	4684.6	3448.3	0.5	2.28	22
233.62	208.025	93.03	9.64	2.27	98.38	5150.3	2991.3	0.5	1.76	15
233.66	208.070	93.00	8.51	3.31	99.09	7344.5	4265.7	0.5	2.24	23
233.69	208.100	94.93	8.47	6.61	99.60	13271.0	7707.8	0.5	1.75	16
233.72	208.130	94.88	10.81	4.10	99.23	9371.0	5442.7	0.5	2.11	18
233.77	208.175	92.80	10.68	3.40	99.04	7700.6	4472.5	0.5	2.02	16
233.81	208.220	93.04	9.85	2.16	98.62	5484.6	3185.5	0.5	1.97	18
233.84	208.250	94.39	5.93	5.46	99.33	9647.3	5603.2	0.5	2.26	20
233.87	208.280	93.76	9.66	2.85	98.95	6444.7	3743.1	0.5	1.82	14
233.92	208.325	93.61	2.91	2.28	99.02	3792.9	2202.9	0.5	2.2	18
233.96	208.370	92.50	0.58	2.23	99.37	5345.0	-	0.5	1.84	17
233.99	208.400	89.08	6.88	5.03	99.66	11780.0	-	0.4	2.12	15
234.02	208.430	84.75	9.09	2.46	99.58	6223.0	2863.8	0.4	1.88	17
234.07	208.475	91.26	2.81	6.61	99.52	14613.0	6724.9	0.4	2.18	18
234.11	208.520	94.22	10.22	2.05	98.98	4825.0	2220.5	0.4	1.64	13
234.14	208.550	93.90	4.16	5.93	99.73	13222.0	6084.8	0.4	2.08	16
234.17	208.580	92.94	5.12	5.17	99.77	7619.4	3506.4	0.4	1.86	16
234.22	208.625	94.67	1.29	13.43	99.58	33926.0	15612.7	0.4	2.21	19
234.26	208.670	95.17	2.30	10.87	99.74	26970.0	12411.6	0.4	2.05	18
234.29	208.700	93.64	5.82	7.43	99.85	16494.0	7590.5	0.4	2.17	18
234.32	208.730	92.82	3.29	6.30	99.87	17974.0	8271.6	0.4	2.14	20
234.37	208.775	91.71	5.03	7.86	99.60	15825.0	7282.7	0.4	2.24	20
234.40	208.805	87.02	9.56	1.23	98.85	2362.7	1115.2	0.4	1.98	17
234.44	208.850	84.32	8.17	3.47	99.14	8862.4	4183.1	0.4	2.35	20
234.47	208.880	91.41	13.40	2.52	98.98	5517.2	2604.1	0.4	2.05	21
234.52	208.925	91.44	1.70	9.00	99.68	17835.0	8418.1	0.4	2.25	19
234.56	208.970	94.47	5.24	3.63	99.37	6236.3	2943.5	0.4	2.16	21
234.59	209.000	94.04	3.23	8.88	99.77	22168.0	10463.3	0.4	2.24	20
234.62	209.030	94.18	3.87	3.28	99.16	7563.1	3569.8	0.4	2.14	18
234.67	209.075	94.66	5.13	9.26	99.53	20591.0	9719.0	0.4	2.26	21
234.71	209.120	94.83	0.92	6.66	99.75	14102.0	6656.1	0.4	2.47	21
234.74	209.150	94.42	5.61	7.33	99.58	15899.0	7504.3	0.4	2.34	22
234.79	209.200	94.27	2.21	10.08	99.88	21861.0	10576.4	0.4	2.38	21
234.94	209.350	93.86	6.91	6.70	99.37	12873.0	6228.0	0.4	2.27	20
235.04	209.450	94.26	3.74	2.82	99.35	5110.1	2472.3	0.4	1.97	18
235.19	209.600	94.59	0.20	4.58	99.00	9762.1	5644.4	0.5	2.11	21

depth [rmcd]	depth [mbsf]	CaCO <sub>3</sub> [wt%]	fragmentation [%F]	coarse fraction [%]	% pl. Foraminifera	PFN [# / g]	PFAR [g / (kyr cm <sup>2</sup> )]	SR [cm / kyr]	Shannon H'	Taxa diversity
235.44	209.850	94.43	8.45	8.15	99.64	13376.0	7734.0	0.5	2.13	19
235.54	209.950	92.41	8.78	2.59	98.71	4276.2	2432.7	0.5	1.66	19
235.69	210.100	93.06	13.49	1.97	97.47	4215.4	1370.3	0.3	2.42	21
236.19	210.600	93.03	6.15	4.69	98.94	10150.0	3299.6	0.3	1.9	18
236.29	210.700	93.67	13.46	4.60	98.91	8020.8	2607.4	0.3	2.08	17
236.34	210.750	94.53	5.45	4.88	99.37	10072.0	3274.2	0.3	2.2	21
236.44	210.850	93.73	3.63	8.00	99.70	21224.0	6899.5	0.3	2.16	19
236.59	211.000	94.31	8.88	3.25	99.18	8733.2	2839.0	0.3	1.94	17

Leg	Site	H	Cor	Sc	Top[cm]	PFN [#g]	depth [mbsf]	depth [rmcd]	$\delta^{13}\text{C}$ vs VPDB [‰]	$\delta^{18}\text{O}$ vs VPDB [‰]	species	size [ $\mu\text{m}$ ]
198	1210	A	23	1	70.0	72.0	206.100	231.69	2.954	-1.090	<i>M. angulata</i>	250-355
198	1210	A	23	1	90.0	92.0	206.300	231.89	2.857	-1.168	<i>M. angulata</i>	250-355
198	1210	A	23	1	100.0	102.0	206.400	231.99	2.943	-1.193	<i>M. angulata</i>	250-355
198	1210	A	23	1	105.0	107.0	206.450	232.04	3.032	-1.149	<i>M. angulata</i>	250-355
198	1210	A	23	1	110.0	112.0	206.500	232.09	3.265	-1.039	<i>M. angulata</i>	250-355
198	1210	A	23	1	120.0	122.0	206.600	232.19	3.101	-1.380	<i>M. angulata</i>	250-355
198	1210	A	23	1	130.0	132.0	206.700	232.29	3.024	-1.433	<i>M. angulata</i>	250-355
198	1210	A	23	2	0.0	2.0	206.900	232.49	2.826	-1.397	<i>M. angulata</i>	250-355
198	1210	A	23	2	10.0	12.0	207.000	232.59	3.130	-1.168	<i>M. angulata</i>	250-355
198	1210	A	23	2	20.0	22.0	207.100	232.69	2.842	-1.274	<i>M. angulata</i>	250-355
198	1210	A	23	2	35.0	37.0	207.25	232.84	2.919	-1.293	<i>M. angulata</i>	250-355
198	1210	A	23	2	50.0	52.0	207.400	232.99	2.856	-1.513	<i>M. angulata</i>	250-355
198	1210	A	23	2	60.0	62.0	207.5	233.09	3.214	-1.283	<i>M. angulata</i>	250-355
198	1210	A	23	2	70.0	72.0	207.600	233.19	2.856	-1.177	<i>M. angulata</i>	250-355
198	1210	A	23	2	82.5	84.0	207.725	233.32	2.828	-1.431	<i>M. angulata</i>	250-355
198	1210	A	23	2	87.0	88.5	207.770	233.36	3.171	-1.695	<i>M. angulata</i>	250-355
198	1210	A	23	2	93.0	94.5	207.830	233.42	2.859	-1.337	<i>M. angulata</i>	250-355
198	1210	A	23	2	97.5	99.0	207.875	233.47	2.802	-1.207	<i>M. angulata</i>	250-355
198	1210	A	23	2	105.0	106.5	207.950	233.54	3.117	-1.149	<i>M. angulata</i>	250-355
198	1210	A	23	2	106.5	108.0	207.965	233.56	3.293	-1.444	<i>M. angulata</i>	250-355
198	1210	A	23	2	108.0	109.5	207.980	233.57	2.890	-1.469	<i>M. angulata</i>	250-355
198	1210	A	23	2	112.5	114.0	208.025	233.62	3.160	-1.276	<i>M. angulata</i>	250-355
198	1210	A	23	2	117.0	118.5	208.070	233.66	3.121	-1.582	<i>M. angulata</i>	250-355
198	1210	A	23	2	120.0	121.5	208.100	233.69	3.076	-1.232	<i>M. angulata</i>	250-355
198	1210	A	23	2	123.0	124.5	208.130	233.72	3.091	-1.585	<i>M. angulata</i>	250-355
198	1210	A	23	2	127.5	129.0	208.175	233.77	2.997	-1.179	<i>M. angulata</i>	250-355
198	1210	A	23	2	132.0	133.5	208.220	233.81	3.200	-1.456	<i>M. angulata</i>	250-355
198	1210	A	23	2	135.0	136.5	208.250	233.84	3.187	-1.433	<i>M. angulata</i>	250-355
198	1210	A	23	2	138.0	139.5	208.280	233.87	3.151	-1.838	<i>M. angulata</i>	250-355
198	1210	A	23	2	142.5	144.0	208.325	233.92	2.827	-1.337	<i>M. angulata</i>	250-355
198	1210	A	23	2	147.0	148.5	208.370	233.96	2.719	-1.607	<i>M. angulata</i>	250-355
198	1210	A	23	3	0.0	1.5	208.400	233.99	2.882	-1.549	<i>M. angulata</i>	250-355
198	1210	A	23	3	3.0	4.5	208.430	234.02	3.099	-1.883	<i>M. angulata</i>	250-355
198	1210	A	23	3	7.5	9.0	208.475	234.07	2.999	-1.333	<i>M. angulata</i>	250-355
198	1210	A	23	3	12.0	13.5	208.520	234.11	2.951	-1.743	<i>M. angulata</i>	250-355
198	1210	A	23	3	15.0	16.5	208.550	234.14	2.941	-1.417	<i>M. angulata</i>	250-355
198	1210	A	23	3	18.0	19.5	208.580	234.17	2.656	-1.624	<i>M. angulata</i>	250-355
198	1210	A	23	3	22.5	24.0	208.625	234.22	3.097	-1.726	<i>M. angulata</i>	250-355
198	1210	A	23	3	27.0	28.5	208.670	234.26	3.031	-1.883	<i>M. angulata</i>	250-355
198	1210	A	23	3	30.0	31.5	208.700	234.29	2.895	-1.637	<i>M. angulata</i>	250-355
198	1210	A	23	3	33.0	34.5	208.730	234.32	2.575	-1.907	<i>M. angulata</i>	250-355
198	1210	A	23	3	37.5	39.0	208.775	234.37	2.736	-1.391	<i>M. angulata</i>	250-355
198	1210	A	23	3	40.5	42.0	208.805	234.40	2.611	-1.655	<i>M. angulata</i>	250-355
198	1210	A	23	3	45.0	46.5	208.850	234.44	2.707	-1.443	<i>M. angulata</i>	250-355
198	1210	A	23	3	48.0	49.5	208.880	234.47	2.975	-1.245	<i>M. angulata</i>	250-355
198	1210	A	23	3	52.5	54.0	208.925	234.52	3.042	-1.372	<i>M. angulata</i>	250-355
198	1210	A	23	3	57.0	58.5	208.970	234.56	2.627	-1.847	<i>M. angulata</i>	250-355
198	1210	A	23	3	60.0	61.5	209.000	234.59	2.827	-1.445	<i>M. angulata</i>	250-355
198	1210	A	23	3	63.0	64.5	209.030	234.62	2.948	-1.501	<i>M. angulata</i>	250-355
198	1210	A	23	3	67.5	69.0	209.075	234.67	3.121	-1.702	<i>M. angulata</i>	250-355
198	1210	A	23	3	72.0	73.5	209.120	234.71	3.293	-1.642	<i>M. angulata</i>	250-355

Leg	Site	H	Cor	Sc	Top[cm]	PFN [#g]	depth [mbsf]	depth [rmcd]	$\delta^{13}\text{C}$ vs VPDB [‰]	$\delta^{18}\text{O}$ vs VPDB [‰]	species	size [ $\mu\text{m}$ ]
198	1210	A	23	3	75.0	76.5	209.15	234.74	2.877	-1.543	<i>M. angulata</i>	250-355
198	1210	A	23	3	80.0	81.5	209.200	234.79	3.141	-1.627	<i>M. angulata</i>	250-355
198	1210	A	23	3	95.0	96.5	209.350	234.94	2.905	-1.308	<i>M. angulata</i>	250-355
198	1210	A	23	3	95.0	96.5	209.35	234.94	3.142	-1.546	<i>M. praeangulata</i>	250-355
198	1210	A	23	3	105.0	106.5	209.450	235.04	3.016	-1.383	<i>M. angulata</i>	250-355
198	1210	A	23	3	115.0	116.5	209.550	235.14	2.600	-1.276	<i>M. angulata</i>	250-355
198	1210	A	23	3	120.0	121.5	209.600	235.19	2.832	-1.255	<i>M. angulata</i>	250-355
198	1210	A	23	3	125.0	126.5	209.650	235.24	2.923	-1.718	<i>M. angulata</i>	250-355
198	1210	A	23	3	130.0	131.5	209.700	235.29	2.789	-1.322	<i>M. angulata</i>	250-355
198	1210	A	23	3	145.0	146.5	209.850	235.44	2.891	-1.489	<i>M. angulata</i>	250-355
198	1210	A	23	4	5.0	7.0	209.950	235.54	2.794	-1.380	<i>M. angulata</i>	250-355
198	1210	A	23	4	20.0	22.0	210.100	235.69	3.167	-1.360	<i>M. angulata</i>	250-355
198	1210	A	23	4	30.0	32.0	210.200	235.79	2.689	-1.199	<i>M. angulata</i>	250-355
198	1210	A	23	4	70.0	72.0	210.6	236.19	3.196	-1.465	<i>M. angulata</i>	250-355
198	1210	A	23	4	75.0	77.0	210.650	236.24	2.957	-1.635	<i>M. angulata</i>	250-355
198	1210	A	23	4	80.0	82.0	210.7	236.29	3.097	-1.249	<i>M. angulata</i>	250-355
198	1210	A	23	4	85.0	87.0	210.750	236.34	3.000	-1.104	<i>M. angulata</i>	250-355
198	1210	A	23	4	95.0	97.0	210.85	236.44	2.699	-1.172	<i>M. angulata</i>	250-355
198	1210	A	23	4	110.0	112.0	211	236.59	3.086	-1.709	<i>M. angulata</i>	250-355
198	1210	A	23	3	45.0	46.5	208.850	234.44	2.480	-1.216	<i>P. uncinata</i>	250-355
198	1210	A	23	3	52.5	54.0	208.925	234.52	2.876	-1.473	<i>P. uncinata</i>	250-355
198	1210	A	23	3	57.0	58.5	208.970	234.56	3.152	-1.402	<i>P. uncinata</i>	250-355
198	1210	A	23	3	63.0	64.5	209.030	234.62	3.010	-1.481	<i>P. uncinata</i>	250-355
198	1210	A	23	3	75.0	76.5	209.150	234.74	2.873	-1.223	<i>P. uncinata</i>	250-355
198	1210	A	23	3	95.0	96.5	209.350	234.94	3.021	-1.230	<i>P. uncinata</i>	250-355
198	1210	A	23	3	120.0	121.5	209.600	235.19	2.509	-1.326	<i>P. uncinata</i>	250-355
198	1210	A	23	3	130.0	131.5	209.700	235.29	2.432	-1.385	<i>P. uncinata</i>	250-355
198	1210	A	23	3	145.0	146.5	209.850	235.44	2.478	-1.209	<i>P. uncinata</i>	250-355
198	1210	A	23	4	70.0	72.0	210.600	236.19	2.612	-1.435	<i>P. uncinata</i>	250-355
198	1210	A	23	4	110.0	112.0	211	236.59	2.569	-1.295	<i>P. uncinata</i>	250-355
198	1210	A	23	2	70.0	72.0	207.600	233.19	1.495	-1.101	<i>P. varianta</i>	180-250
198	1210	A	23	2	120.0	121.5	208.100	233.69	2.105	-0.601	<i>P. varianta</i>	250-355
198	1210	A	23	3	52.5	54.0	208.925	234.52	1.948	-0.537	<i>P. varianta</i>	250-355
198	1210	A	23	3	75.0	76.5	209.150	234.74	1.920	-0.633	<i>P. varianta</i>	250-355
											<i>P. pseudobulloides/</i>	
198	1210	A	23	1	70.0	72.0	206.100	231.69	1.981	-0.071	<i>variospira</i>	250-355
											<i>P. pseudobulloides/</i>	
198	1210	A	23	1	90.0	92.0	206.300	231.89	2.209	-0.769	<i>variospira</i>	250-355
											<i>P. pseudobulloides/</i>	
198	1210	A	23	1	100.0	102.0	206.400	231.99	1.525	-0.300	<i>variospira</i>	250-355
											<i>P. pseudobulloides/</i>	
198	1210	A	23	1	105.0	107.0	206.450	232.04	1.623	-0.082	<i>variospira</i>	250-355
											<i>P. pseudobulloides/</i>	
198	1210	A	23	1	110.0	112.0	206.500	232.09	2.069	-0.006	<i>variospira</i>	250-355
											<i>P. pseudobulloides/</i>	
198	1210	A	23	1	120.0	122.0	206.600	232.19	2.123	-0.588	<i>variospira</i>	250-355
											<i>P. pseudobulloides/</i>	
198	1210	A	23	1	130.0	132.0	206.700	232.29	1.976	-0.337	<i>variospira</i>	250-355
											<i>P. pseudobulloides/</i>	
198	1210	A	23	2	0.0	2.0	206.900	232.49	1.677	-0.124	<i>variospira</i>	250-355
											<i>P. pseudobulloides/</i>	
198	1210	A	23	2	10.0	12.0	207.000	232.59	1.955	-0.365	<i>variospira</i>	250-355

Leg	Site	H	Cor	Sc	Top[cm]	PFN [#g]	depth [mbsf]	depth [rmcd]	$\delta^{13}\text{C}$ vs VPDB [‰]	$\delta^{18}\text{O}$ vs VPDB [‰]	species	size [ $\mu\text{m}$ ]
198	1210	A	23	2	20.0	22.0	207.100	232.69	2.097	-0.845	<i>P. pseudobulloides/</i> <i>variospira</i>	250-355
198	1210	A	23	2	35.0	37.0	207.250	232.84	1.648	-0.478	<i>P. pseudobulloides/</i> <i>variospira</i>	250-355
198	1210	A	23	2	50.0	52.0	207.400	232.99	1.668	-0.721	<i>P. pseudobulloides/</i> <i>variospira</i>	250-355
198	1210	A	23	2	60.0	62.0	207.500	233.09	2.059	-0.471	<i>P. pseudobulloides/</i> <i>variospira</i>	250-355
198	1210	A	23	2	70.0	72.0	207.600	233.19	2.030	-0.302	<i>P. pseudobulloides/</i> <i>variospira</i>	250-355
198	1210	A	23	2	82.5	84.0	207.725	233.32	1.823	-0.472	<i>P. pseudobulloides/</i> <i>variospira</i>	250-355
198	1210	A	23	2	87.0	88.5	207.770	233.36	1.893	-0.393	<i>P. pseudobulloides/</i> <i>variospira</i>	250-355
198	1210	A	23	2	93.0	94.5	207.830	233.42	1.961	-0.403	<i>P. pseudobulloides/</i> <i>variospira</i>	250-355
198	1210	A	23	2	97.5	99.0	207.875	233.47	1.941	-0.423	<i>P. pseudobulloides/</i> <i>variospira</i>	250-355
198	1210	A	23	2	105.0	106.5	207.950	233.54	1.857	-0.245	<i>P. pseudobulloides/</i> <i>variospira</i>	250-355
198	1210	A	23	2	106.5	108.0	207.965	233.56	1.828	-0.228	<i>P. pseudobulloides/</i> <i>variospira</i>	250-355
198	1210	A	23	2	112.5	114.0	208.025	233.62	1.841	0.067	<i>P. pseudobulloides/</i> <i>variospira</i>	250-355
198	1210	A	23	2	117.0	118.5	208.070	233.66	1.820	-0.751	<i>P. pseudobulloides/</i> <i>variospira</i>	250-355
198	1210	A	23	2	120.0	121.5	208.100	233.69	2.055	-0.462	<i>P. pseudobulloides/</i> <i>variospira</i>	250-355
198	1210	A	23	2	123.0	124.5	208.130	233.72	1.966	-0.610	<i>P. pseudobulloides/</i> <i>variospira</i>	180-250
198	1210	A	23	2	127.5	129.0	208.175	233.77	2.133	-0.828	<i>P. pseudobulloides/</i> <i>variospira</i>	250-355
198	1210	A	23	2	132.0	133.5	208.220	233.81	1.756	-0.698	<i>P. pseudobulloides/</i> <i>variospira</i>	180-250
198	1210	A	23	2	135.0	136.5	208.250	233.84	1.813	-0.775	<i>P. pseudobulloides/</i> <i>variospira</i>	250-355
198	1210	A	23	2	138.0	139.5	208.280	233.87	1.749	-0.557	<i>P. pseudobulloides/</i> <i>variospira</i>	180-250
198	1210	A	23	2	142.5	144.0	208.325	233.92	1.807	-0.343	<i>P. pseudobulloides/</i> <i>variospira</i>	250-355
198	1210	A	23	2	147.0	148.5	208.370	233.96	1.331	-0.769	<i>P. pseudobulloides/</i> <i>variospira</i>	250-355
198	1210	A	23	3	0.0	1.5	208.400	233.99	1.780	-0.501	<i>P. pseudobulloides/</i> <i>variospira</i>	250-355
198	1210	A	23	3	3.0	4.5	208.430	234.02	1.499	-0.573	<i>P. pseudobulloides/</i> <i>variospira</i>	250-355
198	1210	A	23	3	7.5	9.0	208.475	234.07	1.845	-0.542	<i>P. pseudobulloides/</i> <i>variospira</i>	250-355
198	1210	A	23	3	12.0	13.5	208.520	234.11	1.550	-0.759	<i>P. pseudobulloides/</i> <i>variospira</i>	180-250
198	1210	A	23	3	15.0	16.5	208.550	234.14	1.843	-0.571	<i>P. pseudobulloides/</i> <i>variospira</i>	250-355

Leg	Site	H	Cor	Sc	Top[cm]	PFN [#g]	depth [mbsf]	depth [rmcd]	$\delta^{13}\text{C}$ vs VPDB [‰]	$\delta^{18}\text{O}$ vs VPDB [‰]	species	size [ $\mu\text{m}$ ]
198	1210	A	23	3	18.0	19.5	208.580	234.17	1.148	-1.086	<i>P. pseudobulloides/</i> <i>variospira</i>	250-355
198	1210	A	23	3	22.5	24.0	208.625	234.22	1.360	-0.575	<i>P. pseudobulloides/</i> <i>variospira</i>	250-355
198	1210	A	23	3	27.0	28.5	208.670	234.26	1.265	-0.779	<i>P. pseudobulloides/</i> <i>variospira</i>	250-355
198	1210	A	23	3	30.0	31.5	208.700	234.29	1.502	-0.561	<i>P. pseudobulloides/</i> <i>variospira</i>	250-355
198	1210	A	23	3	33.0	34.5	208.730	234.32	1.508	-0.982	<i>P. pseudobulloides/</i> <i>variospira</i>	250-355
198	1210	A	23	3	37.5	39.0	208.775	234.37	1.694	-0.488	<i>P. pseudobulloides/</i> <i>variospira</i>	250-355
198	1210	A	23	3	40.5	42.0	208.805	234.40	1.464	-0.546	<i>P. pseudobulloides/</i> <i>variospira</i>	250-355
198	1210	A	23	3	45.0	46.5	208.850	234.44	1.588	-0.403	<i>P. pseudobulloides/</i> <i>variospira</i>	250-355
198	1210	A	23	3	48.0	49.5	208.880	234.47	1.888	-0.486	<i>P. pseudobulloides/</i> <i>variospira</i>	250-355
198	1210	A	23	3	52.5	54.0	208.925	234.52	1.857	-0.441	<i>P. pseudobulloides/</i> <i>variospira</i>	250-355
198	1210	A	23	3	57.0	58.5	208.970	234.56	1.819	-0.768	<i>P. pseudobulloides/</i> <i>variospira</i>	180-250
198	1210	A	23	3	60.0	61.5	209.000	234.59	1.886	-0.645	<i>P. pseudobulloides/</i> <i>variospira</i>	250-355
198	1210	A	23	3	63.0	64.5	209.030	234.62	2.065	-0.646	<i>P. pseudobulloides/</i> <i>variospira</i>	180-250
198	1210	A	23	3	67.5	69.0	209.075	234.67	2.014	-0.497	<i>P. pseudobulloides/</i> <i>variospira</i>	250-355
198	1210	A	23	3	72.0	73.5	209.120	234.71	1.986	-0.224	<i>P. pseudobulloides/</i> <i>variospira</i>	250-355
198	1210	A	23	3	75.0	76.5	209.150	234.74	1.810	-0.509	<i>P. pseudobulloides/</i> <i>variospira</i>	250-355
198	1210	A	23	3	80.0	81.5	209.200	234.79	1.872	-0.781	<i>P. pseudobulloides/</i> <i>variospira</i>	250-355
198	1210	A	23	3	95.0	96.5	209.350	234.94	1.934	-0.520	<i>P. pseudobulloides/</i> <i>variospira</i>	250-355
198	1210	A	23	3	105.0	106.5	209.450	235.04	2.071	-0.354	<i>P. pseudobulloides/</i> <i>variospira</i>	180-250
198	1210	A	23	3	120.0	121.5	209.600	235.19	1.884	-0.632	<i>P. pseudobulloides/</i> <i>variospira</i>	250-355
198	1210	A	23	3	125.0	126.5	209.650	235.24	1.867	-0.154	<i>P. pseudobulloides/</i> <i>variospira</i>	250-355
198	1210	A	23	3	130.0	131.5	209.700	235.29	2.298	-0.642	<i>P. pseudobulloides/</i> <i>variospira</i>	250-355
198	1210	A	23	3	145.0	146.5	209.850	235.44	2.720	-0.837	<i>P. pseudobulloides/</i> <i>variospira</i>	250-355
198	1210	A	23	4	5.0	7.0	209.950	235.54	2.131	-0.963	<i>P. pseudobulloides/</i> <i>variospira</i>	250-355
198	1210	A	23	4	20.0	22.0	210.100	235.69	2.758	-1.081	<i>P. pseudobulloides/</i> <i>variospira</i>	250-355
198	1210	A	23	4	30.0	32.0	210.200	235.79	2.432	-1.044	<i>P. pseudobulloides/</i> <i>variospira</i>	250-355

Leg	Site	H	Cor	Sc	Top[cm]	PFN [#/g]	depth [mbsf]	depth [rmcd]	$\delta^{13}\text{C}$ vs VPDB [‰]	$\delta^{18}\text{O}$ vs VPDB [‰]	species	size [ $\mu\text{m}$ ]
198	1210	A	23	4	60.0	62.0	210.500	236.09	2.090	-0.707	<i>P. pseudobulloides/</i> <i>variospira</i>	250-355
198	1210	A	23	4	70.0	72.0	210.600	236.19	2.184	-0.754	<i>P. pseudobulloides/</i> <i>variospira</i>	250-355
198	1210	A	23	4	75.0	77.0	210.650	236.24	2.702	-1.127	<i>P. pseudobulloides/</i> <i>variospira</i>	250-355
198	1210	A	23	4	80.0	82.0	210.700	236.29	2.207	-0.989	<i>P. pseudobulloides/</i> <i>variospira</i>	250-355
198	1210	A	23	4	85.0	87.0	210.750	236.34	2.598	-0.825	<i>P. pseudobulloides/</i> <i>variospira</i>	250-355
198	1210	A	23	4	95.0	97.0	210.850	236.44	2.315	-0.710	<i>P. pseudobulloides/</i> <i>variospira</i>	250-355
198	1210	A	23	1	90.0	92.0	206.300	231.89	2.129	-0.586	<i>A. strabocella</i>	250-355
198	1210	A	23	1	130.0	132.0	206.700	232.29	2.001	-0.037	<i>A. strabocella</i>	250-355
198	1210	A	23	3	105.0	106.5	209.450	235.04	2.352	-1.618	<i>A. strabocella</i>	250-355
198	1210	A	23	4	5.0	7.0	209.950	235.54	2.497	-1.112	<i>A. strabocella</i>	250-355
198	1210	A	23	2	35.0	37.0	207.25	232.84	1.667	-1.258	<i>G. chapmani</i>	250-355
198	1210	A	23	2	120.0	121.5	208.100	233.69	1.786	-1.166	<i>G. chapmani</i>	250-355
198	1210	A	23	2	35.0	37.0	207.250	232.84	1.776	-0.187	<i>G. imitata</i>	250-355
198	1210	A	23	2	90.0	91.5	207.800	233.39	1.867	-0.001	<i>G. imitata</i>	250-355
198	1210	A	23	1	90.0	92.0	206.300	231.89	2.565	-0.866	<i>I. albeari</i>	250-355
198	1210	A	23	1	130.0	132.0	206.700	232.29	2.823	-1.177	<i>I. albeari</i>	250-355
198	1210	A	23	2	35.0	37.0	207.25	232.84	2.943	-0.884	<i>I. albeari</i>	250-355
198	1210	A	23	2	142.5	144.0	208.325	233.92	2.689	-1.198	<i>I. albeari</i>	250-355
198	1210	A	23	3	37.5	39.0	208.775	234.37	2.423	-1.237	<i>I. albeari</i>	250-355
198	1210	A	23	3	80.0	81.5	209.200	234.79	2.665	-1.338	<i>I. albeari</i>	250-355
198	1210	A	23	4	20.0	22.0	210.100	235.69	2.769	-0.952	<i>I. albeari</i>	250-355
198	1210	A	23	4	85.0	87.0	210.750	236.34	2.702	-0.994	<i>I. albeari</i>	250-355
198	1210	A	23	1	90.0	92.0	206.300	231.89	3.217	-1.239	<i>M. conicotruncata</i>	250-355
198	1210	A	23	1	130.0	132.0	206.700	232.29	3.243	-1.277	<i>M. conicotruncata</i>	250-355
198	1210	A	23	2	35.0	37.0	207.25	232.84	3.343	-1.256	<i>M. conicotruncata</i>	250-355
198	1210	A	23	2	117.0	118.5	208.070	233.66	3.367	-1.248	<i>M. conicotruncata</i>	250-355
198	1210	A	23	2	142.5	144.0	208.325	233.92	2.885	-1.539	<i>M. conicotruncata</i>	250-355
198	1210	A	23	3	37.5	39.0	208.775	234.37	2.772	-1.549	<i>M. conicotruncata</i>	250-355
198	1210	A	23	3	80.0	81.5	209.200	234.79	3.020	-1.501	<i>M. conicotruncata</i>	250-355
198	1210	A	23	4	20.0	22.0	210.100	235.69	2.920	-1.131	<i>M. conicotruncata</i>	250-355
198	1210	A	23	4	85.0	87.0	210.750	236.34	3.102	-1.242	<i>M. conicotruncata</i>	250-355
198	1210	A	23	1	90.0	92.0	206.300	231.89	3.035	-1.357	<i>M. velascoensis</i>	250-355
198	1210	A	23	1	130.0	132.0	206.700	232.29	3.073	-1.585	<i>M. velascoensis</i>	250-355
198	1210	A	23	2	35.0	37.0	207.25	232.84	2.976	-1.248	<i>M. velascoensis</i>	250-355
198	1210	A	23	2	142.5	144.0	208.325	233.92	2.480	-1.514	<i>M. velascoensis</i>	250-355
198	1210	A	23	3	37.5	39.0	208.775	234.37	2.703	-1.458	<i>M. velascoensis</i>	250-355
198	1210	A	23	3	80.0	81.5	209.200	234.79	2.698	-1.171	<i>Pr. inconstans</i>	250-355
198	1210	A	23	4	20.0	22.0	210.100	235.69	2.884	-1.101	<i>Pr. inconstans</i>	250-355
198	1210	A	23	4	85.0	87.0	210.750	236.34	3.033	-1.371	<i>Pr. inconstans</i>	250-355
198	1210	A	23	3	80.0	81.5	209.200	234.79	3.025	-1.612	<i>Pr. praecursoria</i>	250-355
198	1210	A	23	4	20.0	22.0	210.100	235.69	2.710	-1.257	<i>Pr. praecursoria</i>	250-355
198	1210	A	23	4	85.0	87.0	210.750	236.34	2.583	-1.239	<i>Pr. praecursoria</i>	250-355



Leg	Site	H	Cor	Sc	Top [cm]	Bot [cm]	depth [mbsf]	depth [rmcd]	$\delta^{13}\text{C}$ vs. VPDB [‰]	$\delta^{18}\text{O}$ vs. VPDB [‰]	species	size [ $\mu\text{m}$ ]
198	###	A	23	1	70.0	72.0	206.100	231.69	0.770	0.130	<i>N. truempyi</i>	125-180
198	###	A	23	1	90.0	92.0	206.300	231.89	0.787	0.187	<i>N. truempyi</i>	125-180
198	###	A	23	1	100.0	102.0	206.400	231.99	0.772	0.259	<i>N. truempyi</i>	125-180
198	###	A	23	1	100.0	102.0	206.400	231.99	0.168	-0.062	<i>N. umbonifera</i>	125-180
198	###	A	23	1	105.0	107.0	206.450	232.04	0.624	0.051	<i>N. truempyi</i>	125-180
198	###	A	23	1	105.0	107.0	206.450	232.04	0.816	0.031	<i>N. truempyi</i>	125-180
198	###	A	23	1	105.0	107.0	206.450	232.04	0.785	-0.182	<i>N. umbonifera</i>	125-180
198	###	A	23	1	110.0	112.0	206.500	232.09	0.850	0.230	<i>N. truempyi</i>	125-180
198	###	A	23	1	120.0	122.0	206.600	232.19	0.780	-0.075	<i>N. truempyi</i>	125-180
198	###	A	23	1	130.0	132.0	206.700	232.29	0.734	0.073	<i>N. truempyi</i>	125-180
198	###	A	23	2	0.0	2.0	206.900	232.49	0.798	0.205	<i>N. truempyi</i>	125-180
198	###	A	23	2	10.0	12.0	207.000	232.59	0.550	0.130	<i>N. truempyi</i>	125-180
198	###	A	23	2	20.0	22.0	207.100	232.69	0.753	0.194	<i>N. truempyi</i>	125-180
198	###	A	23	2	35.0	37.0	207.250	232.84	0.810	0.120	<i>N. truempyi</i>	125-180
198	###	A	23	2	50.0	52.0	207.400	232.99	0.706	-0.077	<i>N. truempyi</i>	125-180
198	###	A	23	2	60.0	62.0	207.500	233.09	0.610	0.170	<i>N. truempyi</i>	125-180
198	###	A	23	2	70.0	72.0	207.600	233.19	0.774	0.195	<i>N. truempyi</i>	125-180
198	###	A	23	2	82.5	84.0	207.725	233.32	0.670	0.210	<i>N. truempyi</i>	125-180
198	###	A	23	2	82.5	84.0	207.725	233.32	0.840	0.200	<i>N. umbonifera</i>	125-180
198	###	A	23	2	87.0	88.5	207.770	233.36	0.666	0.155	<i>N. truempyi</i>	125-180
198	###	A	23	2	93.0	94.5	207.830	233.42	0.751	-0.049	<i>N. truempyi</i>	125-180
198	###	A	23	2	97.5	99.0	207.875	233.47	0.790	0.180	<i>N. truempyi</i>	125-180
198	###	A	23	2	105.0	106.5	207.950	233.54	0.650	-0.010	<i>N. truempyi</i>	125-180
198	###	A	23	2	106.5	108.0	207.965	233.56	0.755	0.120	<i>N. truempyi</i>	125-180
198	###	A	23	2	112.5	114.0	208.025	233.62	0.800	0.200	<i>N. umbonifera</i>	125-180
198	###	A	23	2	117.0	118.5	208.070	233.66	0.946	0.104	<i>N. truempyi</i>	125-180
198	###	A	23	2	120.0	121.5	208.100	233.69	0.620	0.060	<i>N. truempyi</i>	125-180
198	###	A	23	2	120.0	121.5	208.100	233.69	0.770	0.170	<i>N. umbonifera</i>	125-180
198	###	A	23	2	123.0	124.5	208.130	233.72	0.793	0.129	<i>N. truempyi</i>	125-180
198	###	A	23	2	127.5	129.0	208.175	233.77	0.700	0.100	<i>N. truempyi</i>	125-180
198	###	A	23	2	132.0	133.5	208.220	233.81	0.537	-0.047	<i>N. truempyi</i>	125-180
198	###	A	23	2	135.0	136.5	208.250	233.84	0.680	-0.080	<i>N. truempyi</i>	125-180
198	###	A	23	2	135.0	136.5	208.250	233.84	0.630	0.130	<i>N. umbonifera</i>	125-180
198	###	A	23	2	138.0	139.5	208.280	233.87	0.697	-0.101	<i>N. truempyi</i>	125-180
198	###	A	23	2	142.5	144.0	208.325	233.92	0.350	0.080	<i>N. truempyi</i>	125-180
198	###	A	23	2	147.0	148.5	208.370	233.96	0.156	-0.205	<i>N. truempyi</i>	125-180
198	###	A	23	3	0.0	1.5	208.400	233.99	0.680	0.130	<i>N. truempyi</i>	125-180
198	###	A	23	3	3.0	4.5	208.430	234.02	0.693	-0.043	<i>N. truempyi</i>	125-180
198	###	A	23	3	7.5	9.0	208.475	234.07	0.450	-0.190	<i>N. truempyi</i>	125-180
198	###	A	23	3	12.0	13.5	208.520	234.11	0.467	-0.141	<i>N. truempyi</i>	125-180
198	###	A	23	3	15.0	16.5	208.550	234.14	0.550	0.030	<i>N. truempyi</i>	125-180
198	###	A	23	3	18.0	19.5	208.580	234.17	0.544	0.065	<i>N. truempyi</i>	125-180
198	###	A	23	3	22.5	24.0	208.625	234.22	0.490	0.150	<i>N. truempyi</i> (2)	125-180
198	###	A	23	3	22.5	24.0	208.625	234.22	0.490	-0.050	<i>N. umbonifera</i>	125-180
198	###	A	23	3	27.0	28.5	208.670	234.26	0.442	0.140	<i>N. truempyi</i>	125-180
198	###	A	23	3	30.0	31.5	208.700	234.29	0.400	0.100	<i>N. truempyi</i>	125-180
198	###	A	23	3	30.0	31.5	208.700	234.29	0.460	0.000	<i>truempyi</i>	125-180
198	###	A	23	3	33.0	34.5	208.730	234.32	0.389	-0.083	<i>N. truempyi</i>	125-180
198	###	A	23	3	37.5	39.0	208.775	234.37	0.350	-0.020	<i>N. truempyi</i>	125-180

Leg	Site	H	Cor	Sc	Top [cm]	Bot [cm]	depth [mbsf]	depth [rmcd]	$\delta^{13}\text{C}$ vs. VPDB [‰]	$\delta^{18}\text{O}$ vs. VPDB [‰]	species	size [ $\mu\text{m}$ ]
198	###	A	23	3	40.5	42.0	208.805	234.40	0.310	-0.110	<i>N. truempyi</i>	125-180
198	###	A	23	3	45.0	46.5	208.850	234.44	0.230	0.060	<i>N. truempyi</i>	125-180
198	###	A	23	3	48.0	49.5	208.880	234.47	0.582	0.041	<i>N. truempyi</i>	125-180
198	###	A	23	3	52.5	54.0	208.925	234.52	0.680	0.190	<i>N. truempyi</i>	125-180
198	###	A	23	3	57.0	58.5	208.970	234.56	0.700	-0.040	<i>N. truempyi</i>	125-180
198	###	A	23	3	60.0	61.5	209.000	234.59	0.662	0.152	<i>N. truempyi</i>	125-180
198	###	A	23	3	63.0	64.5	209.030	234.62	0.870	0.220	<i>N. truempyi</i>	125-180
198	###	A	23	3	67.5	69.0	209.075	234.67	0.902	0.238	<i>N. truempyi</i>	125-180
198	###	A	23	3	72.0	73.5	209.120	234.71	0.810	0.190	<i>N. truempyi</i>	125-180
198	###	A	23	3	75.0	76.5	209.150	234.74	0.856	0.228	<i>N. truempyi</i>	125-180
198	###	A	23	3	80.0	81.5	209.200	234.79	0.830	0.350	<i>N. truempyi</i>	125-180
198	###	A	23	3	95.0	96.5	209.350	234.94	0.810	0.340	<i>N. truempyi</i>	125-180
198	###	A	23	3	105.0	106.5	209.450	235.04	0.884	0.195	<i>N. truempyi</i>	125-180
198	###	A	23	3	110.0	111.5	209.500	235.09	0.882	0.242	<i>N. truempyi</i>	125-180
198	###	A	23	3	120.0	121.5	209.600	235.19	0.790	0.230	<i>N. truempyi</i>	125-180
198	###	A	23	3	130.0	131.5	209.700	235.29	0.900	0.134	<i>N. truempyi</i>	125-180
198	###	A	23	3	145.0	146.5	209.850	235.44	0.730	0.190	<i>N. truempyi</i>	125-180
198	###	A	23	4	5.0	7.0	209.950	235.54	0.565	0.031	<i>N. truempyi</i>	125-180
198	###	A	23	4	10.0	12.0	210.000	235.59	0.679	0.023	<i>N. truempyi</i>	125-180
198	###	A	23	4	20.0	22.0	210.100	235.69	0.750	0.040	<i>N. truempyi</i>	125-180
198	###	A	23	4	30.0	32.0	210.200	235.79	0.713	-0.233	<i>N. truempyi</i>	125-180
198	###	A	23	4	60.0	62.0	210.500	236.09	0.890	-0.019	<i>N. truempyi</i>	125-180
198	###	A	23	4	70.0	72.0	210.600	236.19	0.720	0.190	<i>N. umbonifera</i>	125-180
198	###	A	23	4	80.0	82.0	210.700	236.29	0.600	0.030	<i>N. truempyi</i>	125-180
198	###	A	23	4	85.0	87.0	210.750	236.34	0.909	0.062	<i>N. truempyi</i>	125-180
198	###	A	23	4	95.0	97.0	210.850	236.44	0.930	-0.020	<i>N. truempyi</i>	125-180
											<i>N. umbonifera/</i>	
198	###	A	23	4	95.0	97.0	210.850	236.44	0.960	-0.010	<i>truempyi</i>	125-180
198	###	A	23	4	115.0	117.0	211.050	236.64	0.614	-0.440	<i>N. truempyi</i>	125-180

# Appendix 3: Data Chapter III

Supplementary data for Chapter 3 (Paleoceanographic changes across the Latest Danian Event in the South Atlantic Ocean and planktic foraminiferal response) contains following data:

**Table 3.1** List of samples ODP Site 1262 with planktic foraminifera assemblage census and raw count data.

**Table 3.2** Sediment parameters:

- $\text{CaCO}_3$  [wt%],
- fragmentation [%F],
- proportion of planktic foraminifera [%P],
- PFN [numbers per gram, PF/g]

**Table B.3**

- Planktic foraminifera  $\delta^{13}\text{C}$ ,  $\delta^{18}\text{O}$ .
- sedimentation rate [cm/kyr] as amended from Westerhold et al. (2008)

Site	H	c	sec	top	B	mcd [m]	CaCO <sub>3</sub> %
1262	B	20	2	50	52	191.230	79.83
1262	B	20	2	77.5	79.5	191.505	82.08
1262	B	20	2	98	100	191.710	83.75
1262	B	20	2	125.5	127.5	191.985	83.75
1262	B	20	2	146.5	148.5	192.195	82.92
1262	B	20	3	15	17	192.380	84.67
1262	B	20	3	36	38	192.590	85.50
1262	B	20	3	56	58	192.790	82.75
1262	B	20	3	77.5	79.5	193.005	80.25
1262	B	20	3	95.5	97.5	193.185	81.33
1262	B	20	3	119.5	121.5	193.425	83.00
1262	B	20	3	141	143	193.640	83.00
1262	B	20	4	2.5	4.5	193.755	83.83
1262	B	20	4	8.5	10.5	193.815	82.50
1262	B	20	4	11.5	13.5	193.845	81.67
1262	B	20	4	18	20	193.910	84.58
1262	B	20	4	21	23	193.940	84.67
1262	B	20	4	24	26	193.970	84.67
1262	B	20	4	27	29	194.000	84.67
1262	B	20	4	33	34	194.060	82.33
1262	B	20	4	36	38	194.090	82.67
1262	B	20	4	39	41	194.120	81.25
1262	B	20	4	42	44	194.150	83.75
1262	B	20	4	45	47	194.180	82.17
1262	B	20	4	48	50	194.210	82.92
1262	B	20	4	57	59	194.300	79.00
1262	B	20	4	60	62	194.330	79.67
1262	B	20	4	63	65	194.360	78.67
1262	B	20	4	66	68	194.390	82.42
1262	B	20	4	69	71	194.420	79.50
1262	B	20	4	75	77	194.480	73.83
1262	B	20	4	77.5	79.5	194.505	78.17
1262	B	20	4	80.5	82.5	194.535	76.75
1262	B	20	4	83.5	85.5	194.565	72.58
1262	B	20	4	87	89	194.565	71.42
1262	B	20	4	90	92	194.600	73.17
1262	B	20	4	96	98	194.630	81.08
1262	B	20	4	96	98	194.690	-
1262	B	20	4	101.5	103.5	194.745	79.75
1262	B	20	4	105	106.5	194.780	82.00
1262	B	20	4	107.5	109.5	194.805	81.58
1262	B	20	4	111	113	194.840	82.67
1262	B	20	4	116.5	118.5	194.895	84.67
1262	B	20	4	122.5	124.5	194.955	83.75
1262	B	20	4	126	128	194.990	81.83
1262	B	20	4	129	131	195.020	82.17
1262	B	20	4	132	134	195.050	82.83
1262	B	20	4	137.5	139.5	195.105	81.92
1262	B	20	4	141	143	195.140	78.25
1262	B	20	4	143.5	145.5	195.165	77.17
1262	B	20	4	147	149	195.200	77.33
1262	B	20	5	1	2	195.240	75.67
1262	B	20	5	6	8	195.290	68.75
1262	B	20	5	9	11	195.320	69.00
1262	B	20	5	12.5	14.5	195.355	71.33
1262	B	20	5	15	17	195.380	68.67
1262	B	20	5	18.5	20.5	195.415	69.25
1262	B	20	5	21.5	23.5	195.445	73.92
1262	B	20	5	27.5	29.5	195.505	71.50
1262	B	20	5	33.5	35.5	195.565	74.92
1262	B	20	5	36.5	38.5	195.595	76.33
1262	B	20	5	39.5	41.5	195.625	79.92
1262	B	20	5	45.5	47.5	195.685	82.17
1262	B	20	5	49	51	195.720	83.92
1262	B	20	5	55	57	195.780	81.58
1262	B	20	5	66	68	195.890	81.33
1262	B	20	5	78	80	196.010	79.67
1262	B	20	5	88	90	196.110	79.67
1262	B	20	5	104	106	196.270	79.92
1262	B	20	5	120	122	196.430	79.42
1262	B	20	5	140	144	196.630	78.33

Paleoceanographic changes across the  
Latest Danian Event in the South Atlantic Ocean  
and planktic foraminiferal response

1262	B	20	6	5	7	196.780	77.25
1262	B	20	6	25	27	196.980	82.00
1262	B	20	6	45	47	197.180	79.42
1262	B	20	6	65	67	197.380	78.17
1262	B	20	6	87	89	197.600	78.83
1262	B	20	6	107	109	197.800	79.42
1262	B	20	6	127	129	198.000	75.92
1262	B	20	6	147	149	198.200	70.08
1262	B	20	7	6	8	198.290	75.42
1262	B	20	7	25	27	198.480	73.83

SITE	H	C	SECTION	TOP	BOT	MBSF	MCD	SJ code	<i>Acarina</i> sp.	<i>A. strabocella</i>	<i>E. spiralis</i>	<i>C. midwayensis</i>	<i>Globanomalina</i> sp.	<i>G. compressa</i>	<i>G. ehrenbergi</i>	<i>G. imitata</i>	<i>G. pseudo/chapm</i>	<i>G. cf. pseudomenardi</i>	<i>G. chapmani</i>	<i>Igorina</i> sp.	<i>I. albeari</i>	<i>I. pusilla</i>	<i>I. tadsch.</i>	<i>Morozovella</i> sp.	<i>M. angulata</i>	<i>M. aequa</i>	<i>M. acutispira</i>	<i>M. apantesma</i>	<i>M. conicotruncata</i>	<i>M. occlusa</i>	<i>M. praeangulata</i>	<i>P. alabamensis</i>	<i>P. inconstans</i>	<i>P. uncinata</i>	<i>Parasubbotina</i> sp.	<i>P. pseudobulloides</i>	<i>P. varianta</i>	<i>P. variospira</i>	<i>Subbotina</i> sp.	<i>S. cancellata</i>	<i>S. triangularis</i>	<i>s. triloculinoides</i>	<i>S. velascoensis</i>	<i>Woodringa</i> sp.	indet			
1262	B	20	2	50	52	174	191.23	SJ 361							2			1	16	48	3		2	74	4		2	22						1	7	45	47	4	38	1	72	11						
1262	B	20	2	147	148.5	175	192.2	SJ 365		5			2		6	8		5	48	51	12		1	81	10		3	26			1					9	72	50	6	74	1	85	11					
1262	B	20	3	56	58	175	192.79	SJ 368		2		1	1		2	1		1	30	25	12				4										8	48	33	2	48	4	68	9	2					
1262	B	20	4	2.5	4.5	176	193.76	SJ 373		3					3	2			30	8	2				69										9	46	44	8	56	1	57	13	1					
1262	B	20	4	21	23	177	193.94	SJ 377		4			2		10	5			25	6	2		1	26	1									1	10	68	58	7	48		78	14						
1262	B	20	4	36	38	177	194.09	SJ 381		1					10	3			12	14	6				22	4								1	10	62	52	5	71	4	65	18						
1262	B	20	4	42	44	177	194.15	SJ 383		1		1	1		2	3			13	12	3				19	4								1	10	57	48	7	93	4	93	15	1					
1262	B	20	4	48	50	177	194.21	SJ 385		5					4	1			9	1	14	4			12									1	10	52	38	10	63	3	83	20	1					
1262	B	20	4	60	62	177	194.33	SJ 387		2			2		8	3			24	51	14				1	33	3							2	11	50	44	6	59	6	74	21	1					
1262	B	20	4	66	68	177	194.39	SJ 389		5		1	1		4				20	26	5				2	35	5							3	13	47	49	3	49	2	60	13						
1262	B	20	4	75	77	177	194.48	SJ 391		3				1	2	4			19	32	17				3	49	3							2	17	56	57	6	55	2	42	10						
1262	B	20	4	81	82.5	177	194.54	SJ 393	2	10		1		1	1	1			21	23	19				2	19								2	13	51	55	4	38	3	42	11						
1262	B	20	4	87	89	177	194.6	SJ 395		12		1			5	3			25	14	14				1	33								1	20	73	85	11	95	2	83	16						
1262	B	20	4	96	98	177	194.69	SJ 397		6					4	6			38	10	8				15									1	22	55	64	7	63	4	62	13						
1262	B	20	4	102	103.5	177	194.75	SJ 399		3					9	5			31	13	6				28									2	21	52	76	3	66	3	74	13	1					
1262	B	20	4	108	109.5	177	194.81	SJ 401		4		1			9	8			48	2	2				11										26	78	93	4	84	1	63	9	2					
1262	B	20	4	117	118.5	178	194.9	SJ 403		6		4			18	1			27	8	22				1	15								2	23	59	76	4	76	6	84	16	1					
1262	B	20	4	126	128	178	194.99	SJ 405		1		1	3		9	2			27	10	39				7									13	36	58	4	48		75	18							
1262	B	20	4	132	134	178	195.05	SJ 407							8	4			38	26	18				1	20								2	22	56	72	1	63	3	48	14						
1262	B	20	4	141	143	178	195.14	SJ 409							8	2			22	28	27				16										22	65	84	4	57	1	52	8						
1262	B	20	4	147	149	178	195.2	SJ 411				1			5	3			30	24	20				24									1	1	26	66	83	2	64	2	50	13					
1262	B	20	5	6	8	178	195.29	SJ 413							2	6			32	24	5				23									1	39	12	50	56	1	58	39	12						
1262	B	20	5	9	11	178	195.32	SJ 414					1		3	4			14	13	42	1			27									6	7	17	56	80	7	69	77	9	1					
1262	B	20	5	15	17	178	195.38	SJ 416		4		2	2		2	1		1	14	23	34				1	30								8	6	3	1	19	45	59	13	59	2	69	20	1		
1262	B	20	5	19	20.5	178	195.42	SJ 417		3			1			1			16	26	22				2	46								5	2	2	1	21	39	59	5	59	4	74	15			
1262	B	20	5	28	29.5	178	195.51	SJ 419								5			9	41	5				29									5	3	21	56	79	9	54	5	43	26					
1262	B	20	5	34	35.5	178	195.57	SJ 420			1		1		5	6			33	14	17				1	30								7	7	1	1	15	32	73	11	83	5	72	17			
1262	B	20	5	37	38.5	178	195.6	SJ 421			2	1			2	7	2		19	18	2				2	27								1	16	6	8	4	2	21	41	72	8	67	2	41	22	1
1262	B	20	5	40	41.5	178	195.63	SJ 422							4	10			23	1	11				2	16		1	1	5			3	4	5	4	7	31	68	2	50	2	73	9	3			
1262	B	20	5	49	51	178	195.72	SJ 424				2	2		1	1			11	5	4				8									4	2	18	45	62	3	59		80	10					
1262	B	20	5	55	57	178	195.78	SJ 425		1	1				9	11			19	5	8				6									1	2	23	62	103	5	54	2	75	18					
1262	B	20	5	66	68	179	195.89	SJ 426		4					2	3	10		29	1	3				7									3	7	3	8	31	67	73	6	64	1	91	13			
1262	B	20	5	78	80	179	196.01	SJ 427					1	3	4	3			15	4	1				3									11	8	2	3	2	19	56	115	5	82	1	50	14		
1262	B	20	5	120	122	179	196.43	SJ 430				1		7	7	13			32			5	1		2									5	1	4	39	53	85	2	80	1	94	18	1			
1262	B	20	5	140	144	179	196.63	SJ 431			1		1		1	6			4	4	4				1									4	15	3	3	1	24	31	75	2	76	5	64	31		
1262	B	20	6	25	27	180	196.98	SJ 433		8		1	2	11	6	6			16			3			1	2								32	2	8	43	22	66	67	4	61	1	61	12			
1262	B	20	6	45	47	180	197.18	SJ 434					1	4	1	2			8			7			6									54	1	5	55	21	49	64	8	65	1	85	18			
1262	B	20	6	65	67	180	197.38	SJ 435			4		4	1	1	15						1			7									38	10	52	11	28	62	2	66	1	21	6				
1262	B	20	6	127	129	181	198	SJ 438	18	2		2	7	6	8	4			24		9			2	10									32	6	13	29	2	26	56	72	7	53	58	10	4		
1262	B	20	7	25	27	181	198.48	SJ 441				1		1		2	1		4		13			1	12									47	1	7	65	6	18	21	36	13	29	1	22	1	3	

Site	H	c	sec	top	B	mcd [m]	CaCO3%	SJ code	F [%]	P [%]	PF/g	CF > 63µm	mcd [m]	SR [cm/kyr]
1262	B	20	2	50	52	191.230	79.83	SJ 361	3.148	99.751	6708.156	7.940	189.5	0.832
1262	B	20	2	147	149	192.195	82.92	SJ 365	2.911	99.299	5747.684	6.602	190.03	0.832
1262	B	20	3	56	58	192.790	82.75	SJ 368	5.405	98.746	5932.902	5.277	190.53	0.832
1262	B	20	4	2.5	4.5	193.755	83.83	SJ 373	4.000	99.756	7598.926	6.293	190.98	0.832
1262	B	20	4	21	23	193.940	84.67	SJ 377	1.750	98.992	5073.909	6.146	191.505	0.820
1262	B	20	4	36	38	194.090	82.67	SJ 381	2.344	100.000	4386.536	6.084	191.985	0.820
1262	B	20	4	42	44	194.150	83.75	SJ 383	4.286	98.289	5664.465	6.605	192.38	0.878
1262	B	20	4	48	50	194.210	82.92	SJ 385	2.500	99.433	6124.736	6.723	192.79	0.878
1262	B	20	4	60	62	194.330	79.67	SJ 387	2.381	98.904	5043.509	6.839	193.185	0.878
1262	B	20	4	66	68	194.390	82.42	SJ 389	1.617	98.118	6154.454	7.208	193.64	0.878
1262	B	20	4	75	77	194.480	73.83	SJ 391	1.675	99.516	4519.199	6.544	193.815	0.878
1262	B	20	4	80.5	82.5	194.535	76.75	SJ 393	4.735	99.708	7987.957	6.408	193.91	0.878
1262	B	20	4	87	89	194.565	71.42	SJ 394	2.330	99.016	4387.325	5.585	193.97	0.878
1262	B	20	4	96	98	194.630	81.08	SJ 396	1.530	98.720	4954.300	6.380	194.06	0.878
1262	B	20	4	102	104	194.745	79.75	SJ 399	1.435	99.277	3822.557	5.145	194.12	0.878
1262	B	20	4	108	110	194.805	81.58	SJ 401	3.017	98.039	4119.582	5.026	194.18	0.878
1262	B	20	4	117	119	194.895	84.67	SJ 403	0.871	99.129	4096.216	4.910	194.3	0.878
1262	B	20	4	126	128	194.990	81.83	SJ 405	2.139	99.457	3893.488	5.431	194.36	0.878
1262	B	20	4	132	134	195.050	82.83	SJ 407	1.942	98.297	2397.737	5.739	194.42	0.878
1262	B	20	4	141	143	195.140	78.25	SJ 409	1.923	99.512	1814.354	5.876	194.505	0.878
1262	B	20	4	147	149	195.200	77.33	SJ 411	3.348	98.633	3488.419	5.075	194.565	0.827
1262	B	20	5	6	8	195.290	68.75	SJ 413	4.211	99.183	5761.702	2.871	194.63	0.827
1262	B	20	5	9	11	195.320	69.00	SJ 414	4.185	98.416	2768.772	3.827	194.72	0.827
1262	B	20	5	15	17	195.380	68.67	SJ 416	8.114	96.544	1679.096	2.703	194.78	0.827
1262	B	20	5	18.5	20.5	195.415	69.25	SJ 417	5.841	98.775	2649.790	2.876	194.84	0.827
1262	B	20	5	27.5	29.5	195.505	71.50	SJ 419	15.449	92.255	301.508	0.567	194.955	0.827
1262	B	20	5	33.5	35.5	195.565	74.92	SJ 420	9.244	95.154	469.501	1.068	195.02	0.827
1262	B	20	5	36.5	38.5	195.595	76.33	SJ 421	4.136	98.254	1507.426	2.317	195.105	0.827
1262	B	20	5	39.5	41.5	195.625	79.92	SJ 422	4.830	98.529	2595.485	3.176	195.165	0.827
1262	B	20	5	49	51	195.720	83.92	SJ 424	4.154	97.289	2261.459	4.143	195.24	0.827
1262	B	20	5	55	57	195.780	81.58	SJ 425	2.864	99.755	3281.710	3.708	195.32	0.827
1262	B	20	5	66	68	195.890	81.33	SJ 426	5.543	99.070	6942.174	3.669	195.38	0.827
1262	B	20	5	78	80	196.010	79.67	SJ 427	2.663	98.529	3055.219	3.747	195.445	0.827
1262	B	20	5	120	122	196.430	79.42	SJ 430	7.771	97.619	3865.542	3.027	195.565	0.827
1262	B	20	5	140	144	196.630	78.33	SJ 431	6.069	98.072	2156.146	3.434	195.625	0.827
1262	B	20	6	25	27	196.980	82.00	SJ 433	5.022	99.542	2159.479	2.944	195.72	0.827
1262	B	20	6	45	47	197.180	79.42	SJ 434	9.000	98.270	2288.950	3.210	195.89	0.827
1262	B	20	6	65	67	197.380	78.17	SJ 435	3.790	98.800	1707.910	2.720	196.11	0.827
1262	B	20	6	127	129	198.000	75.92	SJ 438	10.291	98.089	6161.974	4.142	196.43	0.827
1262	B	20	7	25	27	198.480	73.83	SJ 441	14.246	98.397	1935.764	2.889	196.78	0.827
													197.18	0.827
													197.6	0.827
													198	0.827
													198.29	0.827

SR...sedimentation rate  
(Westerhold et al., 2008)

SITE	H	C	SEC	TOP	BOT	MCD	SJ code	Species	$\delta^{13}\text{C}$ vs VPDB [‰]	$\delta^{18}\text{O}$ vs VPDB [‰]
1262	B	20	2	50	52	191.23	SJ 361	M. angulata	3.284	-1.147
1262	B	20	2	50	52	191.23	SJ 361	P. pseudobulloides/variopsira	1.861	-0.413
1262	B	20	2	146.5	148.5	192.195	SJ 365	P. pseudobulloides/variopsira	2.038	-0.237
1262	B	20	2	146.5	148.5	192.195	SJ 365	M. angulata	3.366	-1.041
1262	B	20	3	56	58	192.79	SJ 368	M. Praeangulata	3.229	-0.892
1262	B	20	3	56	58	192.79	SJ 368	M. Angulata	2.946	-1.112
1262	B	20	3	56	58	192.79	SJ 368	P. variospira	2.063	-0.163
1262	B	20	4	2.5	4.5	193.755	SJ 373	M. angulata	3.465	-0.977
1262	B	20	4	2.5	4.5	193.755	SJ 373	P. pseudobulloides/variopsira	2.099	-0.234
1262	B	20	4	21	23	193.94	SJ 377	M. angulata	3.712	-0.769
1262	B	20	4	21	23	193.94	SJ 377	P. pseudobulloides/variopsira	2.055	-0.210
1262	B	20	4	36	38	194.09	SJ 381	M. angulata	3.305	-0.696
1262	B	20	4	36	38	194.09	SJ 381	P. pseudobulloides/variopsira	1.936	-0.328
1262	B	20	4	42	44	194.15	SJ 383	M. angulata	3.101	-0.714
1262	B	20	4	42	44	194.15	SJ 383	P. pseudobulloides/variopsira	2.062	-0.170
1262	B	20	4	45	47	194.18	SJ 184	M. angulata	3.463	-0.769
1262	B	20	4	45	47	194.18	SJ 184	P. pseudobulloides/variopsira	2.040	-0.273
1262	B	20	4	48	50	194.21	SJ 385	M. angulata	3.145	-0.960
1262	B	20	4	48	50	194.21	SJ 385	P. pseudobulloides/variopsira	2.298	0.298
1262	B	20	4	60	62	194.33	SJ 387	M. angulata	3.044	-1.105
1262	B	20	4	60	62	194.33	SJ 387	P. pseudobulloides/variopsira	1.840	-0.373
1262	B	20	4	66	68	194.39	SJ 389	M. angulata	3.002	-1.255
1262	B	20	4	66	68	194.39	SJ 389	P. pseudobulloides/variopsira	1.772	-0.341
1262	B	20	4	75	77	194.48	SJ 391	M.angulata	3.051	-1.286
1262	B	20	4	75	77	194.48	SJ 391	P. pseudobulloides/variopsira	1.600	-0.474
1262	B	20	4	80.5	82.5	194.535	SJ 393	M. Praeangulata	2.507	-1.339
1262	B	20	4	80.5	82.5	194.535	SJ 393	M. Angulata	2.661	-0.917
1262	B	20	4	80.5	82.5	194.535	SJ 393	P. variospira	1.456	-0.223
1262	B	20	4	87	89	194.6	SJ 395	M. angulata	2.867	-1.213
1262	B	20	4	87	89	194.6	SJ 395	P. pseudobulloides/variopsira	1.834	-0.326
1262	B	20	4	96	98	194.69	SJ 397	M. angulata	3.185	-1.263
1262	B	20	4	96	98	194.69	SJ 397	P. pseudobulloides/variopsira	2.085	-0.306
1262	B	20	4	101.5	103.5	194.745	SJ 399	M. angulata	3.039	-1.114
1262	B	20	4	101.5	103.5	194.745	SJ 399	P. pseudobulloides/variopsira	1.949	-0.219
1262	B	20	4	105	106.5	194.780	SJ 400	M. angulata	3.328	-0.970
1262	B	20	4	105	106.5	194.780	SJ 400	P. pseudobulloides/variopsira	2.059	-0.252
1262	B	20	4	107.5	109.5	194.805	SJ 401	M. angulata	2.947	-0.757
1262	B	20	4	107.5	109.5	194.805	SJ 401	P. pseudobulloides/variopsira	1.993	-0.278
1262	B	20	4	116.5	118.5	194.895	SJ 403	M. angulata	3.094	-1.360
1262	B	20	4	116.5	118.5	194.895	SJ 403	P.pseudobulloides	1.969	-0.230
1262	B	20	4	122.5	124.5	194.955	SJ 404	M. angulata	2.793	-1.269
1262	B	20	4	122.5	124.5	194.955	SJ 404	P.pseudobulloides	1.878	-0.055
1262	B	20	4	126	128	194.99	SJ 405	M.angulata	3.173	-1.204
1262	B	20	4	126	128	194.99	SJ 405	P.pseudobulloides	1.910	-0.523
1262	B	20	4	132	134	195.05	SJ 407	M.angulata	3.367	-0.742
1262	B	20	4	132	134	195.05	SJ 407	P.pseudobulloides	1.921	-0.262
1262	B	20	4	137.5	139.5	195.105	SJ 408	M. angulata	3.250	-1.113
1262	B	20	4	137.5	139.5	195.105	SJ 408	P. pseudobulloides/variopsira	1.734	-0.402
1262	B	20	4	141	143	195.14	SJ 409	M.angulata	3.002	-0.870
1262	B	20	4	141	143	195.14	SJ 409	P.pseudobulloides	1.698	-0.282
1262	B	20	4	147	149	195.2	SJ 411	M.angulata	3.060	-1.045
1262	B	20	4	147	149	195.2	SJ 411	P.pseudobulloides	1.973	-0.131
1262	B	20	5	6	8	195.29	SJ 413	M. Praeangulata	2.871	-1.414
1262	B	20	5	6	8	195.29	SJ 413	M. Angulata	3.283	-0.821
1262	B	20	5	6	8	195.29	SJ 413	P. variospira	2.007	-0.327
1262	B	20	5	9	11	195.32	SJ 414	M.(prae)angulata	2.785	-1.157
1262	B	20	5	9	11	195.32	SJ 414	P.pseudobulloides	1.917	-0.092
1262	B	20	5	15	17	195.38	SJ 416	M.angulata	3.025	-1.126
1262	B	20	5	15	17	195.38	SJ 416	P.pseudobulloides	2.054	-0.159
1262	B	20	5	18.5	20.5	195.415	SJ 417	M. angulata	2.575	-1.087
1262	B	20	5	18.5	20.5	195.415	SJ 417	P. pseudobulloides/variopsira	1.969	-0.268
1262	B	20	5	21.5	23.5	195.445	SJ 418	M.angulata	2.949	-1.060
1262	B	20	5	21.5	23.5	195.445	SJ 418	P.pseudobulloides	1.998	-0.071
1262	B	20	5	27.5	29.5	195.505	SJ 419	M. angulata	2.709	-0.842
1262	B	20	5	27.5	29.5	195.505	SJ 419	P. pseudobulloides/variopsira	1.991	-0.014
1262	B	20	5	33.5	35.5	195.565	SJ 420	M.(prae)angulata	3.321	-0.715
1262	B	20	5	33.5	35.5	195.565	SJ 420	P.pseudobulloides	2.158	-0.211



1262	B	20	5	36.5	38.5	195.595	SJ 421	M. praeangulata	2.760	-0.362
1262	B	20	5	36.5	38.5	195.595	SJ 421	M. angulata	3.036	-0.684
1262	B	20	5	36.5	38.5	195.595	SJ 421	P. pseudobulloides/variopsira	2.132	0.161
1262	B	20	5	39.5	41.5	195.625	SJ 422	M.angulata	3.164	-0.642
1262	B	20	5	39.5	41.5	195.625	SJ 422	P.pseudobulloides	2.175	-0.144
1262	B	20	5	49	51	195.72	SJ 424	M. Praeangulata	2.936	-0.777
1262	B	20	5	49	51	195.72	SJ 424	M.angulata	3.553	-0.903
1262	B	20	5	49	51	195.72	SJ 424	P. pseudobulloides/variopsira	2.176	-0.008
1262	B	20	5	55	57	195.78	SJ 425	M. angulata	3.182	-0.603
1262	B	20	5	55	57	195.78	SJ 425	P. pseudobulloides/variopsira	2.100	0.077
1262	B	20	5	66	68	195.89	SJ 426	M.angulata	3.518	-0.739
1262	B	20	5	66	68	195.89	SJ 426	P. pseudobulloides/variopsira	2.195	0.053
1262	B	20	5	78	80	196.01	SJ 427	M. angulata	3.290	-0.853
1262	B	20	5	78	80	196.01	SJ 427	P. pseudobulloides/variopsira	2.337	0.100
1262	B	20	5	120	122	196.43	SJ 430	M. angulata	2.797	-0.617
1262	B	20	5	120	122	196.43	SJ 430	P. pseudobulloides/variopsira	2.322	0.216
1262	B	20	5	140	144	196.63	SJ 431	M. angulata	2.864	-0.717
1262	B	20	5	140	144	196.63	SJ 431	P. pseudobulloides/variopsira	2.130	0.061
1262	B	20	6	5	7	196.780	SJ 432	M. praeangulata	2.843	-0.328
1262	B	20	6	5	7	196.780	SJ 432	P. pseudobulloides/variopsira	2.205	0.315
1262	B	20	6	25	27	196.98	SJ 433	M. praeangulata	2.895	-0.440
1262	B	20	6	25	27	196.98	SJ 433	P. pseudobulloides/variopsira	2.258	-0.075
1262	B	20	6	45	47	197.18	SJ 434	M. praeangulata	2.427	-0.194
1262	B	20	6	45	47	197.18	SJ 434	M. angulata	2.793	-1.269
1262	B	20	6	45	47	197.18	SJ 434	P. variopsira	2.434	0.164
1262	B	20	6	45	47	197.18	SJ 434	P.pseudobulloides	1.960	-0.191
1262	B	20	6	45	47	197.18	SJ 434	P.pseudobulloides	1.878	-0.055
1262	B	20	6	65	67	197.38	SJ 435	M. praeangulata	2.696	-0.465
1262	B	20	6	65	67	197.38	SJ 435	P. pseudobulloides/variopsira	2.106	0.081
1262	B	20	6	127	129	198	SJ 438	M. Praeangulata	2.703	-0.784
1262	B	20	6	127	129	198	SJ 438	M. Angulata	2.831	-0.820
1262	B	20	6	127	129	198	SJ 438	P. variopsira	2.072	0.061
1262	B	20	7	25	27	198.48	SJ 441	M. praeangulata	2.694	-0.660
1262	B	20	7	25	27	198.48	SJ 441	M. angulata	2.563	-0.860
1262	B	20	7	25	27	198.48	SJ 441	P. pseudobulloides/variopsira	2.135	0.108

## Appendix 4: Data Chapter IV

Supplementary data for Chapter 4 (Mid-Paleocene planktic foraminifera biostratigraphy – lessons from the appearance of *Igorina albeari* and the Latest Danian Event) contains following data:

**Table 4.1** List of used samples: IODP Site U1407

Planktic foraminifera assemblage census, raw count data: *Igorina albeari*, *Praemurica uncinata*, *P. inconstans*, *Globanomalina pseudomenardii*

Bulk rock  $\delta^{13}\text{C}$ ,  $\delta^{18}\text{O}$ .

**Table 4.2** Qreiya 3

Planktic foraminifera assemblage census, raw count data: *Igorina albeari*, *Praemurica uncinata*, *P. inconstans*

Benthic foraminifera  $\delta^{13}\text{C}$ ,  $\delta^{18}\text{O}$ .

---

site	H	c	sec	T	B	CSF-A	CCSF	<i>Globanomalina pseudomenardii</i>	<i>Globanomalina</i> cf. <i>pseudomenardii</i>	<i>Igorina albeari</i>	<i>Praemurica inconstans</i>	<i>Praemurica praecursoria</i>	<i>Praemurica uncinata</i>
1407	A	22	2	110.0	112.0	176.90	207.05	2	7	26			
1407	A	22	3	5.0	7.0	177.35	207.50	8	8	9			
1407	A	22	3	65.0	67.0	177.95	208.10			29			
1407	A	22	3	95.0	97.0	178.25	208.40	5		23			
1407	A	22	3	125.0	127.0	178.55	208.70		4	27			
1407	A	22	4	10	12	178.9	209.05		2	22			
1407	A	22	4	71	73	179.51	209.66		5	17			
1407	A	22	4	135	137	180.15	210.3			34			
1407	A	22	5	25.0	27.0	180.55	210.70			9	8		2
1407	A	22	5	45	47	180.75	210.9			6			
1407	A	22	5	67.5	69.5	180.98	211.13			4			
1407	A	22	5	78	80	181.08	211.23			7	5		
1407	A	22	5	101	103	181.31	211.46			6	3		2
1407	A	22	5	140	142	181.7	211.85			1	3		3
1407	C	20	3	139.0	141.0	179.39	212.77		5		29	2	83
1407	C	20	4	82	84	180.32	213.7				23	12	91

<b>site</b>	<b>H</b>	<b>c</b>	<b>sec</b>	<b>T</b>	<b>B</b>	<b>CSF-A</b>	<b>CCSF</b>	<b>bulk rock δ<sup>13</sup>C vs VPDB</b>	<b>bulk rock δ<sup>18</sup>O vs VPDB</b>
1407	A	22	2	110.0	112.0	176.90	207.05	1.366	-0.337
1407	A	22	3	5.0	7.0	177.35	207.50	1.303	-0.504
1407	A	22	3	65.0	67.0	177.95	208.10	1.223	-0.423
1407	A	22	3	125.0	127.0	178.55	208.70	1.283	-1.213
1407	A	22	4	71	73	179.51	209.66	1.003	-0.945
1407	A	22	4	135	137	180.15	210.3	0.505	-1.162
1407	A	22	5	25.0	27.0	180.55	210.70	1.024	-0.894
1407	A	22	5	45	47	180.75	210.9	1.204	-0.975
1407	A	22	5	72.0	74.0	181.02	211.17	1.456	-0.918
1407	A	22	5	78	80	181.08	211.23	1.336	-0.807
1407	A	22	5	100.5	102.5	181.305	211.455	1.348	-0.978
1407	A	22	5	110.0	112.0	181.40	211.55	1.405	-0.931
1407	A	22	5	122	124	181.52	211.67	1.378	-0.841
1407	A	22	5	130	132	181.6	211.75	1.432	-0.907
1407	A	22	5	140	142	181.7	211.85	1.458	-0.690
1407	C	20	3	139.0	141.0	179.39	212.77	1.340	-0.703
1407	C	20	4	82	84	180.32	213.7	1.391	-0.757

---

depth [m]	<i>I. albeari</i>	<i>P. inconstans</i>	<i>P. uncinata</i>	depth [m]	$\delta^{13}\text{C}$	$\delta^{18}\text{O}$
12.05	23			15.4	0.19	-1.79
11.35	136			13.9	0.27	-2.11
10.15	35			13.7	-0.85	-2.33
9.50	23			13.2	-0.72	-1.84
8.80	21			12.8	-0.46	-2.21
8.50	10	2		12.3	-0.54	-1.95
8.35	1	3	3	12.1	-0.57	-2.09
8.04	5	2	6	11.8	-0.05	-1.74
7.50		3	7	11.6	-0.36	-2.04
7.00		1	5	11.3	-0.44	-2.05
6.50	2	2	5	11.1	0.05	-1.07
6.05	2		2	9.92	-0.91	-1.38
5.55	4	3	4	9.92	-0.77	-1.54
5.05	7	4		9.45	-0.48	-1.56
4.60		6	8	9.21	-1.06	-1.54
				8.5	-0.9	-2.24
				8.42	-0.43	-1.59
				8.35	-1.28	-1.74
				8.32	-0.97	-1.9
				8	-0.94	-2.24
				7.5	0	-1.56
				7	-0.01	-1.47
				6.28	-0.65	-1.37
				5.55	-0.29	-1.94
				5.31	-0.29	-2.09
				4.34	-0.11	-2.38
				4.34	-0.16	-2.32
				4.34	-0.48	-2.28
				2.41	0.44	-1.45
				2.17	-0.17	-1.43
				1.69	-0.26	-1.89
				1.45	-0.28	-1.55
				0.97	-0.22	-1.51
				0.72	-0.18	-1.99
				0.24	-0.14	-2.47
				0	-0.18	-1.72
				0	-0.36	-1.81

# Appendix 5: Data Chapter V

Supplementary data for Chapter V (Synthesis) contains following data:

## **Table 5.1**

Planktic foraminifera assemblage census IODP Site U1407

## **Table 5.2**

Planktic foraminifera assemblage census Qreiya 3



depth (m)	<i>A. strabocella</i>	<i>C. midwayensis</i>	<i>G. chapmani</i>	<i>G. compressa</i>	<i>G. ehrenbergi</i>	<i>G. imitata</i>	<i>I. albeari</i>	<i>I. pusilla</i>	<i>M. angulata</i>	<i>M. apanthesma</i>	<i>M. conicotruncata</i>	<i>M. praeangulata</i>	<i>P. alabamensis</i>	<i>P. pseudobulloides</i>	<i>P. varianta</i>	<i>P. variospira</i>	<i>P. inconstans</i>	<i>P. uncinata</i>	<i>S. cancellata</i>	<i>S. triangularis</i>	<i>S. triloculinoides</i>	<i>S. velascoensis</i>	<i>Globanomalina</i> spp.	<i>Morozovella</i> spp.	<i>Parasubbotina</i> spp.	<i>Praemurica</i> spp.	<i>Subbotina</i> spp.	<i>Morozovella</i> small	<i>Parasubbotina</i> small	<i>Subbotina</i> small	Indet
12.05	1	1	6			1	23	370	9					1	27	1				1	23						4	3			
11.35	1	1	9				136	1 172		1				7	20					1	27	2	1	3	6						1
10.15			11			2	35	191	23					9	54	4			5	3	22	1		3	5	5					
9.50	3	3	8		5	2	23	104	2					15	46	2			3	7	46	3		4	5	1			4		
8.80	1	2			1	3	21	1 97						12	13	1			1	4	29		2	7	5	7	1				4
8.50			11			2	10	121	4		6			7	44	4	2		33	6		5		4	5	8					1
8.35	1	2			2	5	1	35				1	1	6	6	1	3	3						60	13	2	8				3
8.04	10	2	8		3	3	5	1 83	2			10		8	23	2	2	6	3	13	20	2		1	27	6	1				5
7.50					2	1		3 102				23		8	22	3	3	7	1	8	22	1		2	4	1					1
7.00	3	1		2	3			2 88				12		33	37	1	1	5	4	9	26			5	7	6					
6.50	3			8	1	1	2	156				64		7	43		2	5		8	47	3		5	1	7					
6.05	20			1	7	2	1 130					19		4	27	3		2	2	15	10	3		1	98		7	2			
5.55	10	3		9	1	4	4	293				49		19	80	4	3	4		15	38	1		6		9	3				2
5.05	8			7	3	7		109				75		10	77	2	4			20	41	13	3	6	5	9	6			1	
4.60	3	1		7	4			92				31		14	81	2	6	8		19	69		1	5	8	16					3



# Curriculum Vitae

## Work experience

10/2017 – now	G.U.B. Ingenieur AG, dep. “Soil and contaminated sites” in Leipzig/Zwickau <i>Project engineer</i> (Environmental remediation, Building dismantling)
11/2016 – 09-2017	Huber Beyer Umweltconsult GmbH, Leipzig <i>Project engineer</i> (Survey of contaminated soil and buildings, monitoring of sanitation after mining renaturation)
01/2013– 12/2015	Institute for Geophysics and Geology, University of Leipzig Scientific employee for marine micropaleontology
05–09/2012	Pollems GmbH, Berlin, Civil engineering company for groundwater lowering. <i>Project engineer</i> (Planning and monitoring of urban water management during civil engineering projects)
03/2012	Umweltzentrum Tübingen, NGO for education for sustainable development. <i>Referee (internship)</i>
2006 –2011	Institute for Geoscience, Eberhard-Karls-Universität Tübingen <i>Student assistant</i> (Micropaleontological preparation and analysis, geophysical measurements, co-organisation/assistance of conferences/meetings)
09 – 10/2009	British Geological Survey (BGS) in Keyworth <i>Internship: Biostratigraphy on Late Cretaceous foraminifera of the Isle of Wight</i>

---

## Education

2011	Graduation as Dipl. Geol.
2005 –2011	Diploma programme in Geosciences at the University of Tübingen, specialisation on marine micropaleontology.
2005	High School Graduation (Abitur) at Zinzendorf Gymnasium in 78126 Königfeld.

---

## Meeting participation

Dec 2015	AGU Fall Meeting, San Francisco, poster presentation.
Apr 2015	EGU General Assembly, Vienna, oral presentation.
Mar 2015	IODP/ ICDP Colloquium, Bonn, poster presentation.
Sept 2014	GeoFrankfurt, oral presentation.
June 2014	CBEP Ferrara, poster presentation.
Mar 2014	IODP/ ICDP Colloquium 2014, Erlangen, poster presentation.
Nov 2013	TMS Conference 2013, The National History Museum, London, poster presentation.
Mar 2013	IODP/ ICDP Colloquium 2013, Freiberg, poster presentation.
Dec 2011	StEvE: Students in Evolution and Ecology, Tübingen, poster presentation.
July 2011	Quenstedt Annual Celebration, Tübingen, poster presentation.

- June 2011 TMS The Foraminifera and Nannofossil Groups Joint Meeting 2011, Krakow, poster presentation.
- Sep 2010 FORAMS 2010: International Symposium on Foraminifera, Bonn, poster presentation.
- Sep 2009 UK Archaeological Sciences UKAS, Biennial Conference 2009, hosted by NERC Isotope Geosciences Laboratory and the Department of Archaeology, University of Nottingham at The BGS, Keyworth, attendance.
- 

## Award

- Nov 2013 TMS Conference 2013, The National History Museum, London: Best poster award.
- 

## Workshop participation

- July 2014 USSP Urbino Summerschool Paleoclimate at University of Urbino: Past Global Change Reconstruction and Modelling Techniques
- Mar 2014 GESEP SCHOOL 2014: Initial Drill-Core Processing, Analyses and Archiving: “Hands-on introduction to initial core handling and measurements: from drilling to core repository”
- Aug 2013 Early Paleogene Workshop Leuven: talk
- 

## Publications

### Paper

- 2017 Deprez, A., Jehle, S., Bornemann, A. and Speijer, R.P., 2017. Pronounced biotic and environmental change across the latest Danian warming event (LDE) at Shatsky Rise, Pacific Ocean (ODP Site 1210). *Marine Micropaleontology*. 137, 31-45.
- 2017 Deprez, A., Jehle, S., Bornemann, A., & Speijer, R. P. (2017). Differential response at the seafloor during Palaeocene and Eocene ocean warming events at Walvis Ridge, Atlantic Ocean (ODP Site 1262). *Terra Nova*, 29(1), 71-76.
- 2015 Jehle S., Bornemann A., Deprez A., Speijer, R.P., 2015. The Impact of the Latest Danian Event on Planktic Foraminiferal Faunas at ODP Site 1210 (Shatsky Rise, Pacific Ocean). – *PLoS ONE* 10(11): e0141644. doi:10.1371/journal.pone.0141644
- 2011 Hopson, P., Farrant, A., Wilkinson, I., Woods, M., Kender, S. and Jehle, S., 2011. The lithostratigraphy and biostratigraphy of the Chalk Group (Upper Coniacian to Upper Campanian) at Scratchell’s Bay and Alum Bay, Isle of Wight. – *UK Proceedings of the Geologists’ Association*, 122, 850 - 861.
- 

### Talks

- 2015 Jehle S., Bornemann A., Deprez A., Speijer, R.P., 2015. Planktic foraminiferal response to the Latest Danian Event in the Pacific Ocean (ODP Site 1210). EGU General assembly Vienna
- 2014 Jehle S., Bornemann A., Deprez A., Speijer, R.P., 2014. A paleoenvironmental reconstruction of the Latest Danian Event at ODP Site 1210 (Shatsky Rise, Pacific Ocean). *GeoFrankfurt, SDGG Vol. 85*, p.25
-

---

## Poster

- 2015      Jehle S., Bornemann A., Deprez A., Lagel F., Speijer, R.P., 2015. Planktic foraminiferal response to the “Latest Danian Event” (62.15 Ma) on an almost global scale – results from Shatsky Rise, Walvis Ridge and Newfoundland. AGU Fall meeting San Francisco.
- Jehle S., Bornemann A., Deprez A., Speijer, R.P., 2015. The Paleoenvironmental impact of the Latest Danian Event and response of planktic foraminifera at ODP Site 1210 (Shatsky Rise, Pacific Ocean). IODP/ICDP colloquium Bonn, p.66.
- 2014      Jehle S., Bornemann A., Deprez A., Speijer, R.P., 2014. Paleooceanographic reconstruction of the Latest Danian Event at ODP Site 1210 (Shatsky Rise, Pacific Ocean). Rend. Online Soc. Geol. It., Vol. 31(Climatic and Biotic Events of the Paleogene, Ferrara), pp. 120 (doi: 10.3301/ROL.2014.77)
- Jehle, S., Bornemann, A., Deprez, A., Speijer, R.P., 2014. The impact of the Latest Danian Event on planktic foraminifera faunas at ODP Site 1210 (Shatsky Rise, Pacific Ocean). IODP colloquium Erlangen, p. 69-71.
- 2013      Jehle, S., Bornemann, A., Deprez, A., Speijer, R.P., 2013. Transient paleooceanographic events of Danian-Selandian age: first micropaleontological results for the Latest Danian Event at Shatsky Rise. IODP/ICDP colloquium Freiberg, p 103.
- Jehle, S., Bornemann, A., Deprez, A., Speijer, R.P., 2013. Planktic foraminiferal response to the Latest Danian Event at ODP Site 1210 (Shatsky Rise). The Micropaleontological Society meeting, London.
- 

## Theses

- 2011      Jehle, S., 2011. The effect of Monsoon climate on the flux of planktic foraminifera in sediment traps off the Sunda Shelf in the South China Sea. Diploma thesis, Micropaleontology, University of Tubingen: 1-117.
- 2010      Jehle, S., 2010. Test morphologies of benthic foraminifera of industrially polluted sediments of the harbour area of Mumbai, India. Student research thesis, Micropaleontology, University of Tubingen: 1-60. (in German)
-